

MICROCOPY RESOLUTION TEST CHART  
NATIONAL BUREAU OF STANDARDS-1963-A

20222.1-EG-CF

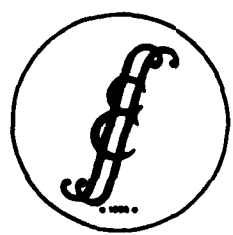
DTIC FILE COPY AD A138155

# ABSTRACTS

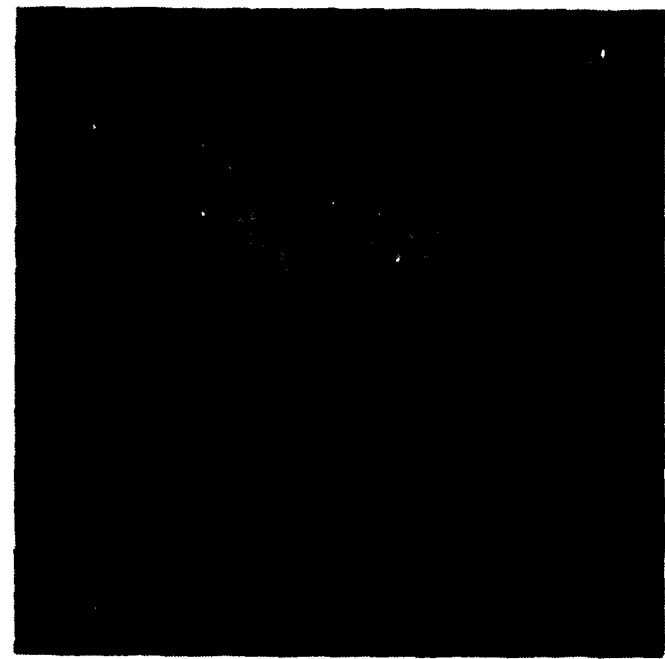
- 20th Annual Meeting -  
Society of Engineering  
Science, Incorporated

August 22, 23 and 24, 1983

University of Delaware  
Newark, Delaware 19711 USA



DTIC  
COLLECTED  
1983



This document has been approved  
for public release and sale; its  
distribution is unlimited.

84 02 14 112

Unclassified

SECURITY CLASSIFICATION OF THIS PAGE (When Data Entered)

REPORT DOCUMENTATION PAGE		READ INSTRUCTIONS BEFORE COMPLETING FORM
1. REPORT NUMBER 20222.1-EG	2. GOVT ACCESSION NO. <b>AD-A138155</b>	3. RECIPIENT'S CATALOG NUMBER
4. TITLE (and Subtitle) Abstracts of the 20th Annual Meeting- Society of Engineering Science, Inc.	5. TYPE OF REPORT & PERIOD COVERED 30 Apr 83 - 30 Sep 83 Final Report	
	6. PERFORMING ORG. REPORT NUMBER	
7. AUTHOR(s) Minoru Taya	8. CONTRACT OR GRANT NUMBER(s) JAAG29-83-M-0258	
9. PERFORMING ORGANIZATION NAME AND ADDRESS University of Delaware Newark, DE 19711	10. PROGRAM ELEMENT, PROJECT, TASK AREA & WORK UNIT NUMBERS N/A	
11. CONTROLLING OFFICE NAME AND ADDRESS U. S. Army Research Office Post Office Box 12211 Research Triangle Park, NC 27709	12. REPORT DATE Sep 83	
	13. NUMBER OF PAGES	
14. MONITORING AGENCY NAME & ADDRESS (if different from Controlling Office)	15. SECURITY CLASS. (of this report)  Unclassified	
	15a. DECLASSIFICATION/DOWNGRADING SCHEDULE	
16. DISTRIBUTION STATEMENT (of this Report)  Approved for public release; distribution unlimited.		
17. DISTRIBUTION STATEMENT (of the abstract entered in Block 20, if different from Report)		
18. SUPPLEMENTARY NOTES  The view, opinions, and/or findings contained in this report are those of the author(s) and should not be construed as an official Department of the Army position, policy, or decision, unless so designated by other documentation		
19. KEY WORDS (Continue on reverse side if necessary and identify by block number) Applied Mechanics Materials Applied Mathematics Thermodynamics		
20. ABSTRACT (Continue on reverse side if necessary and identify by block number) Abstracts of the Twentieth Annual Meeting of the Society of Engineering Science at the U of Delaware on Aug 22,23, and 24, 1983. Thirty eight technical sessions were scheduled during the three days of the meeting. Special efforts were made to provide a spectrum of Technical sessions balanced between topics in the thermal sciences, applied mechanics, materials science, and applied mathematics. Multiple sessions were organized on phase transitions, bio-mechanics heat transfer, geomechanics, fracture mechanics, composite materials, and numerical methods.		

ABSTRACTS

20th ANNUAL MEETING

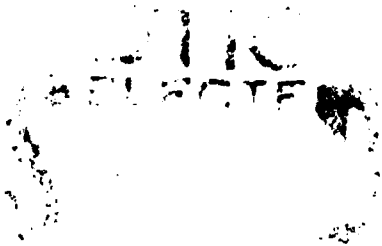
SOCIETY OF ENGINEERING SCIENCE

AUGUST 22, 23 AND 24, 1983

UNIVERSITY OF DELAWARE

NEWARK, DELAWARE

Accession For	
NTIS GRA&I	<input checked="" type="checkbox"/>
DTIC TAB	<input type="checkbox"/>
Unannounced	<input type="checkbox"/>
Justification	
By _____	
Distribution/	
Availability Codes	
Dist	Avail and/or Special
A-1	



This document has been approved  
for public release and sale  
distribution is unlimited

## PREFACE

The Twentieth Annual Meeting of the Society of Engineering Science is a special conference for the University of Delaware. It is the first meeting of a national engineering society at the University. Coincidentally, Dr. E. A. Trabant, President of the University, was one of the early members of SES and, early on, worked to shape its programs and future growth.

Thirty eight technical sessions are scheduled during the three days of the Meeting, as well as Keynote Lectures by D. C. Drucker, the 1983 Prager Medalist, and R. B. Bird, the 1983 Eringen Medalist. Special efforts have been made to provide a spectrum of technical sessions balanced between topics in the thermal sciences, applied mechanics, materials science and applied mathematics. Multiple sessions have been organized on phase transitions, biomechanics, heat transfer, geomechanics, fracture mechanics, composite materials, and numerical methods. We hope that this menu will appeal to a large cross section of the SES membership, as well as to the general engineering and scientific communities.

Partial financial support of the Annual Meeting has been provided by several industries, agencies of the Federal Government, and the University. A list of these supporters is given in the Preliminary Program. To all of them, we are extremely grateful. We also express our appreciation for the staff support given by the Department of Mechanical and Aerospace Engineering through the many long months of planning and the final period of active preparation.

Newark  
August, 1983

Frank A. Kulacki  
Minoru Taya  
Co-Chairmen

ORGANIZATION OF THE 20TH ANNUAL MEETING

Local Organizing Committee

T.-W. Chou  
H. B. Kingsbury  
F. A. Kulacki, Co-Chairman  
E. E. Michaelides  
R. B. Pipes  
I. Stakgold  
M. Taya, Co-Chairman

Session Organizers

E. Aifantis (Michigan Technological University)  
R. Asaro (Brown)  
W. Aung (National Science Foundation)  
C. W. Bert (Oklahoma)  
C. F. Carey (University of Texas at Austin)  
M. M. Chen (University of Illinois at Urbana)  
H. Cheng (Northwestern)  
T.-W. Chou (Delaware)  
M. Comninou (Michigan)  
Y. Jaluria (Rutgers)  
F. A. Kulacki (Delaware)  
D. Y. S. Lou (University of Texas at Arlington)  
L. E. Malvern (Florida)  
E. E. Michaelides (Delaware)  
G. Moss (U.S. Army Ballistic Research Laboratory)  
T. Mura (Northwestern)  
S. Nemat-Nasser (Northwestern)  
S. L. Passman (Sandia National Laboratories)  
R. B. Pipes (Delaware)  
T. Porsching (Pittsburgh)  
J. N. Reddy (Virginia Polytechnic & State University)  
A. B. Schultz (University of Illinois at Chicago)  
C. T. Sun (Purdue)  
M. Taya (Delaware)  
J. R. Vinson (Delaware)  
C. Y. Yang (Delaware)  
U. Yuceoglu (Florida International)

TABLE OF CONTENTS

	Page
Preface.....	i
Organization of the 20th Annual Meeting.....	ii
AMS-1 Heat and Fluid Flow in Materials Processing.....	1
AMS-2 Recent Advances in Materials Science.....	9
BIO-1 Musculoskeletal Biomechanics.....	19
BIO-2 Thermo-Fluid Biomechanics.....	28
CM-1 Micromechanical Modeling of Failure in Composite Materials.....	33
CM-2 Layered Composites.....	43
CM-3 Impact in Composites.....	51
CM-4 General Topics in Composite Materials.....	58
DSN-1 Recent Advances in Mechanical Design.....	64
DYN-1 Dynamics and Vibrations.....	72
ESM-1 Elasticity and Structural Mechanics-1: Elasticity.....	81
ESM-2 Elasticity and Structural Mechanics-2: General Topics...	90
FM-1 Second Order Fluids.....	103
FM-2 Topics in Fluid Mechanics: Stability and Turbulence.....	110
FR-1 General Topics in Fracture Mechanics.....	123
FR-2 Contact Problems with Friction.....	133
FR-3 Lubricated Contact Problems.....	141
GEO-1 Geomechanics-1.....	149
GEO-2 Geomechanics-2.....	158
GEO-3 Geomechanics-3.....	166

	Page
HST-1 High Strain Rate Deformation of Solids-1.....	176
HST-2 High Strain Rate Deformation of Solids-2.....	181
HST-3 High Strain Rate Deformation of Solids-3.. ..	187
HT-1 Heat Transfer in Porous Media-Experimental Aspects.....	196
HT-2 Heat Transfer in Porous Media-Theoretical Aspects.....	210
HT-3 Mixed Convection Heat Transfer.....	218
HT-4 General Topics in Heat and Mass Transfer.....	233
NM-1 Numerical Fluid Dynamics.....	242
NM-2 Recent Developments in Computational Methods.....	254
NM-3 Vector and Micro-Computers in Computational Mechanics...	265
PHT-1/PHT-2 Symposium on Phase Transformations.....	270
PL-1 Plasticity-1.....	280
PL-2 Plasticity-2.....	290
TPF-1 Two-Phase Flow-1.....	299
TPF-2 Two-Phase Flow-2.....	308
WP-1 Wave Propagation-1.....	315
WP-2 Wave Propagation-2.....	326
Author Index.....	333

NUMERICAL SIMULATION OF STRONGLY NON-ISOTHERMAL  
COMPRESSION MOLDING FLOWS

by

C.-C. Lee and C. L. Tucker III  
Department of Mechanical and Industrial Engineering  
1206 W. Green Street  
University of Illinois at Urbana-Champaign  
Urbana, IL 61801

Compression molding is an important processing technique for polymers and composite materials. Usually, a thermosetting molding compound is squeezed between heated dies; the squeezing flow fills the mold, and heat from the mold initiates the curing reaction. There is considerable interest in simulating this process for non-trivial geometries for the purpose of optimizing the design and manufacture of parts.

Previous simulations used the fact that the parts are all thin compared to their lateral dimensions, resulting in the Generalized Hele-Shaw model [1-3]. This is a non-Newtonian non-isothermal lubrication model, in which shear stresses across the thin dimension dominate the flow.

Experiments [2,3] have shown that the Generalized Hele-Shaw model is adequate for sufficiently thin parts, but not for thicker parts. This transition occurs sooner than might be expected, since thicker parts experience large temperature gradients during squeezing, and thus have large viscosity gradients. Several different calculations were performed to explore the effects of rheology and heat transfer on mold filling for cases where the Generalized Hele-Shaw model is not valid.

A two-dimensional finite element model was first developed to investigate how the transverse viscosity gradient affects the velocity profiles. It was found that as the viscosity gradient is increased, a bulge shaped velocity profile develops, with the material near the mold (less viscous) flowing preferentially to that in the core region (more viscous). These results are very similar to previous work on the axisymmetric case [4].

Using a three-dimensional finite element model with stratified viscosities and an approximate flow-front advancement scheme, the filling pattern was calculated for a rectangular charge. It was seen that as the viscosity gradient increases, the charge shape changes more slowly. The simulation was compared with experimental data and the correct trend was verified.

From the calculated velocity profiles, it can be seen that under nonisothermal conditions, a thin layer adjacent to the hot wall would serve as a lubricant, and the material in the central region essentially undergoes biaxial extension, and thus the pressure distribution would be more even than that for isothermal cases.

In order to know how severe the nonisothermality is in the real compression molding process, a conduction-convection heat transfer analysis was performed. The transient temperature distribution was determined as a function of charge dimension, mold temperature and mold closing speed.

The heat transfer analysis along with a relation between viscosity and temperature was then incorporated into the flow simulation to see how operating conditions affect the filling pattern.

#### REFERENCES

1. Heiber, C. A. and S. F. Shen, "A Finite Element/Finite Difference Simulation of the Injection Mold Filling Process," J. Non-Newtonian Fl. Mech., 7, 1980, pp. 1-32.
2. Tucker, C. L. and F. Folgar, "A Model of Compression Mold Filling," Polym. Eng. Sci., 23, 1983, pp. 69-74.
3. Lee, C.-C., F. Folgar and C. L. Tucker, "Simulation of Compression Molding for Fiber Reinforced Thermosetting Polymers," Polymer Processing, N. P. Suh and C. L. Tucker, Eds., ASME, New York, 1982, pp. 41-65.
4. Lee, S. J., M. M. Denn, M. J. Crochet and A. B. Metzner, "Compressive Flow Between Parallel Disks: I. Newtonian Fluid with a Transverse Viscosity Gradient," J. Non-Newtonian Fl. Mech., 10, 1982, pp. 3-30.

Heat Flow, Fluid flow and Solidification  
Phenomena in Weld Pools

by

Gregory Oreper and Julian Szekely  
Department of Materials Science and Engineering  
and Center for Materials Processing  
Massachusetts Institute of Technology  
Cambridge, Massachusetts 02139

Through the simultaneous statement of the axisymmetric form of Maxwell's equations, the Navier-Stokes equations, and the differential thermal energy balance equation, a mathematical formulation has been presented to describe the transient development of the fluid flow field, the temperature field and the melt - solid interface, in a liquid pool, generated by a spatially variable heat flux and current falling on an initially solid block. Full mathematical statement of the problem was developed in [1,2]. This physical situation is a somewhat idealized representation of the TIG welding process. In the formulation allowance has been made for the electromagnetic, buoyancy and surface tension forces and the resultant equations were solved numerically.

It was found that both the convective flow field and the temperature field were markedly affected by the nature of the heat flux, and the current distribution on the free surface. Furthermore, surface tension gradients at the free surface, caused either by temperature gradients, or by an inhomogeneous impurity distribution could also play a very important, sometimes dominant role in affecting the flow.

In the absence of surface tension effects a broadly distributed heat flux and corresponding current distribution caused a situation, where the fluid flow field was affected by both buoyancy and electromagnetic forces; however in these systems the fluid flow did not play a significant role in the heat transfer process. Indeed the shape of the weldpool could have been predicted by considering thermal conduction only.

In contrast for a sharply focussed heat flux and current strong electromagnetically driven flows resulted, which played an important role in determining the shape of the weldpool. This is illustrated in Fig. 1, where the pool shape drawn with the full line represented the pool shape computed for electromagnetically and buoyancy driven flow, while the broken line designates the pool shape computed by allowing for conduction, and chain line for buoyancy driven flows only.

Calculations were also carried out examining the effect of surface tension driven flows, and Fig. 2 shows an example how these phenomena may give rise to quite high velocities,

and may produce quite deep penetration of the weldpool.

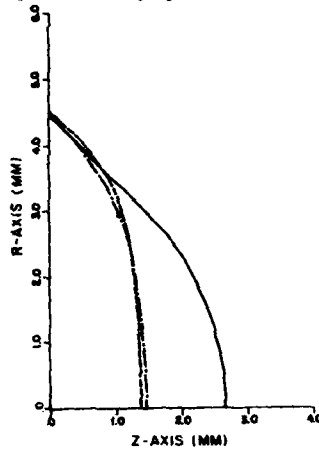


Fig. 1 Shape of weldpools after 8 sec of welding.

Finally, calculations have been carried out also, examining the solidification of the molten phase contained in the weldpool, once the application of the heat source has been discontinued. It has been found that for these cases the velocity field will be dominated by buoyancy driven flows, and that solidification would in general occur from circulating liquid mass.

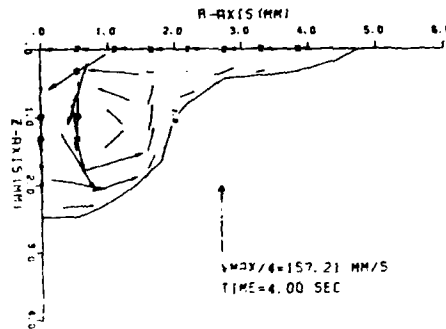


Fig. 2 Shape of the weld and velocity field for combined buoyancy, electromagnetically and surface tension driven flow.

#### References:

1. Oreper, G.M. and Szekely, J., "Heat and Fluid Flow Phenomena in Weldpools," J. Fluid Mechanics, in press.
2. Oreper, G.M., Eaqr, T.W. and Szekely, J., "Convection in Arc Weldpools," Welding Journal, in press.

SIMULATION OF HEAT TRANSFER AND FLUID FLOW IN THE  
SOLIDIFICATION OF ALLOYS

Harold D. Brody and Robert A. Stoehr  
Metallurgical and Materials Engineering  
University of Pittsburgh  
Pittsburgh, Pennsylvania 15261

At some stage of their processing history most metal and alloy products undergo a solidification step. This solidification step may be one that takes the alloy to an intermediate shape and condition or may be one performed near the end of the processing chain resulting in the (near) final configuration and condition. Examples of the former include ingotmaking, continuous casting, powder atomization, vacuum arc remelting and electroslag remelting. Examples of the latter include sand casting, investment casting, die casting, laser glazing, welding, and brazing. The metallurgical structure and soundness achieved in the primary processing steps have a strong influence on the success of the later processing steps, e.g. ability to roll an ingot without edge cracking; and the final metallurgical structure has a strong influence on the products performance in service through control of the properties, e.g. fatigue strength, corrosion resistance, thermal conductivity, etc. It is important to control solidification processing operations in order to control metallurgical structure, soundness and properties. The conditions of heat transfer and fluid flow during solidification processing are subject to control and as a result can be used to control the success of the process.

Modeling of heat transfer and fluid flow in solidification processes applied to alloys has been carried out to improve our understanding of the basic phenomena involved and to be used as design tools. Heat transfer analyses have been carried out extensively. Fluid flow analyses have been applied on a more limited scale. There are substantial opportunities to make contributions by developing fluid flow analyses of solidification processes. For the most part, analyses have not treated heat and fluid flow in a coupled manner. Both research and process design would be significantly advanced by development of practical analyses of coupled phenomena in alloy solidification. An important adjunct to developing analyses is determination of materials properties at high homologous temperatures for input to the mathematical (computer) models.

Several examples will be given of heat transfer and fluid flow models that have been applied to practical solidification processes. Finite difference and finite element techniques have been successfully applied to these complex problems. Underlying relations will be discussed and indication will be made of areas fertile for further analytical development.

## Fluid Flow in Laser Melted Pool

C. Chan, J. Mazumder, and M. M. Chen  
Department of Mechanical Engineering  
1206 West Green Street  
University of Illinois at Urbana-Champaign  
Urbana, IL 61801

The laser surface alloying (LSA) has been of interest for some time, its potential has not yet been fully explored. It is because the process of LSA is not well understood. The heat transfer process has been studied mainly by using a conduction model. Convective heat transfer has not been investigated. Moreover, fluid flow within the molten region has been neglected, although several authors [1-7] acknowledged its existence and influence during LSA.

Most of the work on fluid flow has been qualitative [1-5], except the analysis by Anthony and Cline [6]. They did the first quantitative work [6]. They proposed that the fluid flow is driven by the surface tension gradient on the surface. The model that they considered is essentially a one-dimensional case. The flow field thus obtained is not coupled to the heat transfer process. Hence, no additional information can be obtained about the heat transfer process.

Recently, Chande and Mazumder [7] observed that an effective diffusivity of  $10^6$  cm<sup>2</sup>/sec is required to explain, experimentally obtained uniform solute redistribution during LSA, on the basis of molecular diffusion. The implication, as pointed out by Chande and Mazumder [7], is that the fluid flow within the molten pool plays a significant role in the mechanism of solute redistribution and hence also in the heat transfer process. The understanding of convective heat transfer and fluid flow is therefore crucial in understanding the process of LSA.

In this paper, the convective heat transfer and fluid flow is analyzed. Transient two dimensional model for surface tension driven fluid flow in laser melted pool is developed. The model describes the transient behavior of the heat transfer process of a stationary band source. Some semi-quantitative understanding of scanning can be obtained by a coordinate transformation. Four dimensionless parameters arising from the general 3-D mathematical formulation are Reynolds number (Re), Prandtl number (Pr), Surface tension number (S), and the melting temperature ( $T_{melt}$ ). Each of these would govern the characteristics of the problem and each has its own physical interpretation (see reference [9] for detail discussion). It is important to point out that in the case of band source, Re and S can be grouped into one parameter--their product. Numerical solution, using the program SOLA by

Hirt's [8], is obtained for two different Prandtl number 0.1 and 0.02, while the remaining parameters are the same for both cases, namely,  $S = 55,000$ ,  $Re = 12.5$ , and  $T_{melt} = 0.05$ . They correspond to steel and aluminum respectively.

Numerical results of velocity field at  $t^* = 0.5$ , of the two cases are presented in Figs. 1 and 2. Recirculating flow is clearly demonstrated. The magnitude of the recirculating flow velocity is one to two orders of magnitude higher than that of the scanning speed in both cases. Consequently, the heat transfer process is convection dominated. This also explains the highly disperse and uniform distribution of solute within the molten region.

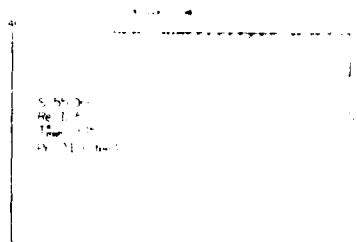


Fig. 1 Velocity Field in Molten Pool at  $t^* = 0.5$  for Steel

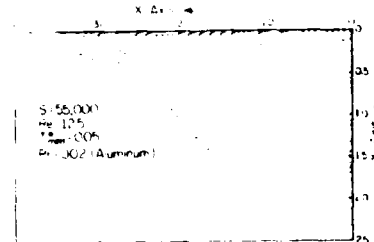


Fig. 2 Velocity Field in Molten Pool at  $t^* = 0.5$  for Aluminum

#### REFERENCES

1. Gnanamuthu, D. S., "Applications of Lasers in Materials Processing," E. A. Metzower, ed., pp. 177-289, ASM, 1979.
2. Moore, P. M., and L. S. Weiman, *SPIE*, Vol. 198, p. 120, 1979.
3. Weiman, L. S., J. H. Devault, and P. Moore, *Applications of Lasers in Materials Processing*, E. A. Metzower, ed., pp. 245-259, 1979.
4. Draper, C. W., *Proc. Conf. of Lasers in Metallurgy*, Chicago, Ill., K. Mukherji and J. Mazumder, eds., AIME, 1981.
5. Weiman, L. S., and J. H. Devault, *AIP Conference Proc.* No. 50, *Symp. on Laser Solid Interactions and Laser Processing*, Boston, Mass., p. 239, 1978.
6. Anthony, T. R., and H. F. Cline, *J. Appl. Phys.*, Vol. 48, No. 9, pp. 3888-3894, 1977.
7. Chande, T., and J. Mazumder, *Appl. Phys. Letter*, Vol. 41, No. 1, p. 42, 1982.
8. Hirt, C. W., B. D. Nichols, and N. C. Romero, "A Numerical Solution Algorithm for Transient Fluid Flows," UC-34 and UC-79d, April 1975.
9. Chan, C., J. Mazumder, and M. M. Chen, to appear in *Applications of Lasers in Materials Processing*, E. A. Metzower, ed., ASM, 1983.

## Finite Element Analysis of Axisymmetric Forging

C. I. Weng\* and C. T. Ho\*

Department of Mechanical Engineering  
National Cheng Kung University  
Tainan, Taiwan, R.O.C.

## Abstract

The finite element method is used to analyze the forging problem of an axially symmetric body. The punching load as well as the distribution of pressure and strain rate are computed from the computer code developed in this paper. The validity of the code is verified by applying it to an ideally-plastic material with no friction between the die and material. It is shown that both the gross deformation rate and friction play a very important role in affecting the characteristics of forging. When the deformation rate is large, the nearly-rigid region is small, the strain rate is more uniform, and hence bulging is little. However, the punching load is increased as the flow stress is increased by increasing the strain rate of material. It is also shown that punching load increases abruptly when the material flows and is in contact with the sidewall of die, and that the strain rate is low and the pressure is high in the flow-restricted regions.

\* Professor

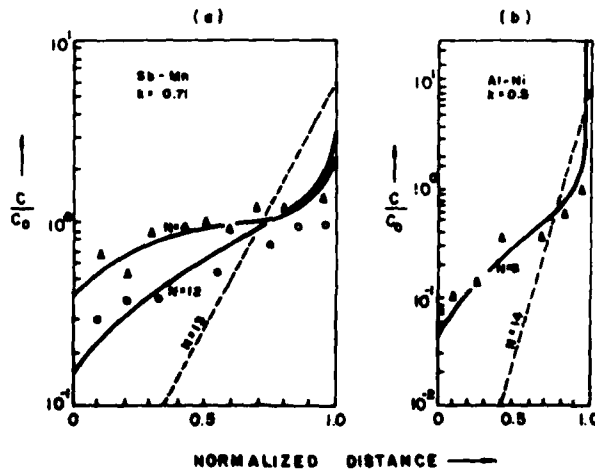
\* Lecturer

## PURIFICATION OF METALS BY ZONE MELTING-AN OPTIMIZATION

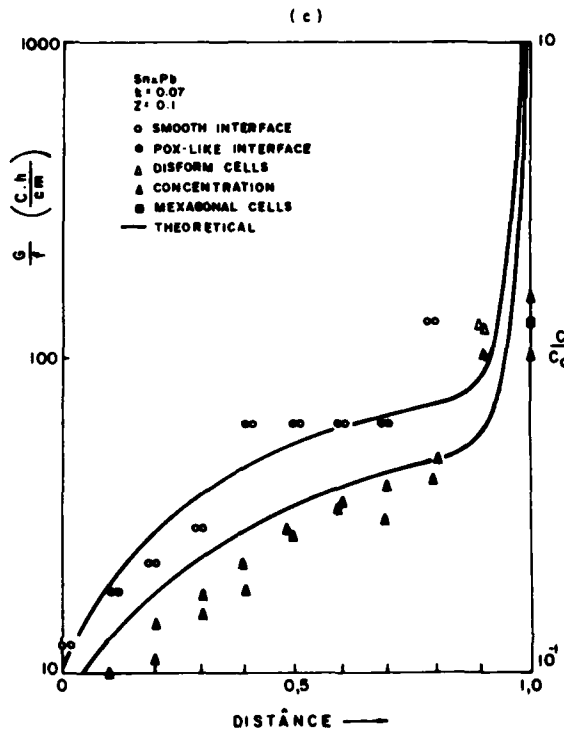
by

R. Bertazzoli and A. Garcia  
 Department of Mechanical Engineering  
 State University of Campinas - UNICAMP/FEC/DEM  
 13100 - CAMPINAS - SAO PAULO - BRAZIL

An experimental set-up, which permits controlled purification of metals by zone melting was developed. Some experiments were carried-out with aluminium and antimony, where samples were submitted to different passes of the liquid zone (from 1 to 12). The resulting experimental concentration profiles were determined by atomic absorption spectroscopy and compared with theoretical predictions furnished by a multipass finite difference technique. Figures (a) and (b) present some of these results, where theoretical and experimental normalized concentration profiles ( $C/C_0$ ) along the samples are compared, showing a good agreement. The number of passes necessary to attain the ultimate distribution were also calculated and are presented in the above mentioned figures. Traditionally the zone melting process is carried-out with constant rate of displacement of the liquid zone. Under this condition interface stability will be overestimated in some sections of the sample. This work presents a solid/liquid interface stability criterion which permits to get a maximum purification efficiency by varying the liquid zone speed with position along the sample. The maximum speed in each point will depend on the calculated



Solute concentration profiles of (a) manganese in antimony after four and twelve passes and (b) nickel in aluminum after eight passes. ( $C$  = concentration,  $C_0$  = initial concentration,  $x$  = position in the sample and  $L$  = length of the sample).



Microstructure and concentration profile obtained in zone melting with variable rate of displacement of liquid zone.

solute concentration and thermal gradient ahead the interface. Experimental evidence was obtained through the observation of the resulting microstructure and concentration profiles (Figure c). The results obtained permits to conclude that the stability criterion emerges as an useful tool in the optimization of the zone refining process.

APPLICATION OF THE FINITE ELEMENT METHOD  
TO STUDY CRYSTAL GROWTH

by

Birbal Singh  
Oil Sands Research Department  
Alberta Research Council  
11315 - 87 Avenue  
Edmonton, Alberta, Canada

and  
Robert R. Gilpin<sup>1</sup>  
Mechanical Engineering Department  
University of Alberta  
Edmonton, Alberta, Canada

This paper presents an investigation of the applicability of the finite element method to the study of crystal growth transport processes. The finite element method was chosen because a review of past analytical research in the area of crystal growth theory indicated that analytical techniques may have reached the limit of their usefulness and further progress in the area may require the exploitation of numerical methods.

To demonstrate its applicability, the method has been used to analyze the problems such as, the stability of cylindrical and spherical particles growing in supercooled liquid, dendritic growth, and the evolution of dendritic shape with time. Quantitative comparisons of the results obtained by this approach, other theories and experimental data indicate that the method can be successfully used to study a variety of problems in the area of crystal growth.

The method has also been used to obtain a time invariant shape of a dendrite growing in a supercooled liquid. The results indicate that the time invariant shape of a dendrite is close to a paraboloid but not exactly a paraboloid of revolution. It is also found that the velocity of growth of a dendrite with time invariant shape is closer to that predicted by the Langer-Krumbhaar stability criterion than to that predicted by the often used maximum velocity principle.

These results on the applicability of the finite element method to crystal growth problems are encouraging. However, certain concerns still remain regarding calculation of surface curvatures and separation of numerical instabilities from physical instabilities. If these concerns and problems can be overcome, a number of interesting applications of the finite element method to the study of crystal growth phenomena are possible.

-----  
<sup>1</sup>Now deceased.

GRAIN REFINEMENT OF COMMERCIAL ALUMINUM BY NIOBIUM AND ZIRCONIUM ADDITIONS TO THE MELT.

by

M.H. Robert and N.L. Cupini  
 Department of Mechanical Engineering  
 Campinas State University  
 13.100 - Campinas - SP - Brazil.

Taking the "peritectic theory" [1 3] as a very reasonable one to explain the mechanism of grain refinement of Aluminum by Titanium additions, it is investigated in this work the efficiency of Niobium and Zirconium as grain refiners of Aluminum, since these elements also present peritectic reactions with liquid Aluminum, like Titanium does.

For this purpose, Nb and Zr were added to liquid Al in different amounts and two different ways: master alloys and halogen salts of easy dissociation ( $K_2NbF_7$ ,  $K_2ZrF_6$ ). In order to compare the effects with the traditional Ti, this element also was utilized, in the same conditions.

Figure 1 shows the variation of grain diameter with increasing amount of added element, for both ways of inoculation.

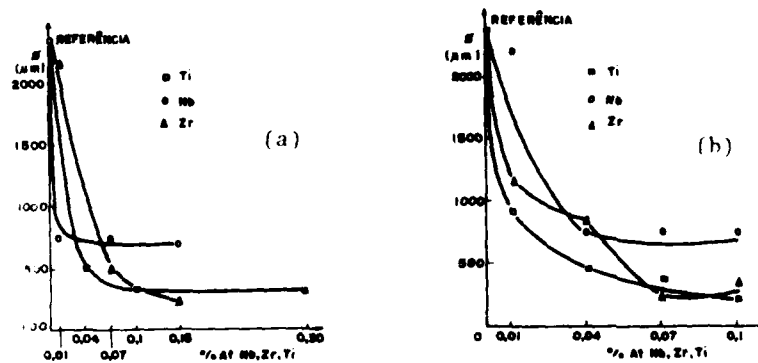


Fig.1 - Average grain diameter in function of Ti,Zr,Nb amount for Aluminum. (a) master alloy way of inoculation; (b) salts inoculation.

It can be observed in both cases that Ti and Zr have similar results, while Nb though acts as refiner, doesn't present so high efficiency. The explanation for these behaviours is that reactions in Nb/Al system are lower than in Zr/Al and Ti/Al systems.

Related to master alloy inoculation way, it was observed [4] that NbAl<sub>3</sub> particles (introduced via master alloy) which probably acts as nucleant for Al via peritectic reaction, have high stability in this liquid, with high tendency to agglomerate even at low amount added; while TiAl<sub>3</sub> particles quickly dissolve, at low amount, or maintain in

suspension as isolated particles.  $ZrAl_3$  particles have an intermediate behaviour between Niobium and Zirconium.

Related to salt additions, the worst behaviour of Nb was attributed also to the lower kinetics of this system when compared with the others elements analysed (more severe conditions are required for  $K_2NbF_7$  dissociation and  $NbAl_3$  formation).

Conclusions: Both methods of additions seemed to be adequate to introduce Nb and Zr to the liquid, the difference being the dimensions and distribution of remained  $NbAl_3$  and  $ZrAl_3$  particles in the resultant structure. In the case of master alloys inoculations, the particles are bigger and more agglomerate than in the salts inoculations case, the presence of discrete particles of  $NbAl_3$  and, in some cases,  $ZrAl_3$  in the final structure, while Ti was completely dissolved in the Al matrix, show that the grain refinement process by Nb and Zr additions via master alloys is more interesting in relation to Ti additions, for some specific purposes, for instance, like electrical conductors fabrication [5]. High efficiency of Ti in promoting grain refinement even at low amount (lower than solubility limit of  $TiAl_3$  in liquid Al) was attributed to the presence of "Ohno's separation theory" mechanism.

References:

- [1] Bäckerud, L. - Jernkont. Ann., 1971, vol. 155.
- [2] Maxwell, I; Helawell, A. - Metall.Trans., june 72, vol.3, p.1487.
- [3] Cornish, A.J. - Metal Science, 1975, vol.9, p.477.
- [4] Clyne, T.W.; Robert, M.H. - Metal Tech., May 80, p.177.
- [5] Robert, M.H.; Cupini, N.L. - Proceedings of "XXXVI Congresso Anual da ABM", Brasil, july 1981. vol. 3, p.415.
- [6] Ohno, A. - "The Solidification of Metals" - Chijin Shokan, Co, Ltd, Tokyo, Japan, 1976, p.62.

A UNIFIED FRACTURE KINETICS  
REPRESENTATION OF THE THREE  
REGIONS OF STRESS CORROSION  
CRACKING

by

A.S. Krausz\* and K. Krausz

\*Department of Mechanical Engineering  
University of Ottawa, Ottawa, Ontario  
K1N 6N5  
Canada

The data obtained in environment assisted crack propagation experiments are often presented in the log velocity-stress intensity factor (or crack extension force) coordinate system. It has been shown that the complex processes of thermally activated stress corrosion cracking (SCC) can be described by a relation that was derived from kinetics analysis and fracture mechanics, that is, from fracture kinetics considerations and is of the form

$$v = \frac{1}{k_I^{-1} + k_{II}^{-1}} + k_{III}$$

where  $k_I$ ,  $k_{II}$  and  $k_{III}$  are the rate constants associated with Regions I, II and III of SCC; each, by itself, being a very involved expression. It will be shown that for certain conditions the above description of the three regions can be well simplified by the velocity relation

$$v = \lambda k = \lambda \frac{kT}{h} \exp \left( - \frac{\Delta G}{kT} \right),$$

where  $\lambda$  is the (atomic) distance travelled by the crack during activation and  $\Delta G$  is the thermal energy that makes the crack propagate. A representation of the velocity as the function of  $\Delta G$  results in a diagram in which the experimental points are distributed along a single straight line. The good agreement between the relation and the values that were obtained for different materials, tested in various environments and temperatures, will be presented. The advantages of the simple relation will be discussed. It will be shown how the single-line representation facilitates the use of the available SCC data for design and test engineering purposes.

## SURFACE FATIGUE CHARACTERISTICS OF TRANSMISSION GEARS

by

R. KRISHNAMURTHY and R. NATARAJAN

Production Engineering Section  
Mechanical Engineering Department  
Indian Institute of Technology  
Madras 600 036, INDIA.

Fatigue tests were carried out on spur gears in a recirculation power type test rig to understand the influence of hunting tooth, surface finish and surface treatment on fatigue characteristics. The study includes involute recording, metallographic studies and Scanning electron microscopy. The study forms part of the tests being carried out for finding techniques to enhance the performance characteristics of even low/medium strength steel gears. Some of the original data obtained forms part of the present paper.

During service, gears are subjected to both static and dynamic load. The dynamic load could be influenced by the mesh stiffness of the contacting tooth pair, which is significantly affected by transmitted load and composite tooth profile imperfections. The composite tooth profile imperfection depends upon the mating teeth imperfections. Thus introducing a slight modification in the geometric ratio (i.e. by changing the pinion/wheel number of teeth by + 1 tooth) would considerably minimise the frequency of occurrence of maximum error teeth meshing. This enhances the fatigue characteristics of gears as shown in Fig.1.

Apart from hunting tooth design, suitable surface treatments were carried out on gear flanks and were tested. With suitable surface treatments like Tufftriding, it is possible to enhance the fatigue performance of even low strength steel gears (Fig.2). This would be a very useful data for application involving light/medium contact stresses.

SEM pictures, Fig.3 of fatigue surfaces and wear debris collected during tests clearly show that fatigue failure is associated with delamination. The occurrence of spherical wear debris indicates that the pitting cracking is influenced by hydraulic wedge formed by the oil entering the cracks. The formation of the oil wedge in the pitting crack depends upon the ability of the oil to fill up the crack. This is mostly related to the oil viscosity. There exists an optimum viscosity for which fatigue crack propagation is minimum.

## References:

1. Kasuba, R., et al. An extended model in Dynamic load in spur gears, Trans. ASME, Vol.103, April 1981, p.398.

2. Scott, D., et al. Spherical Debris - Rolling contact fatigue, Wear 24, 1973, p.235-42.

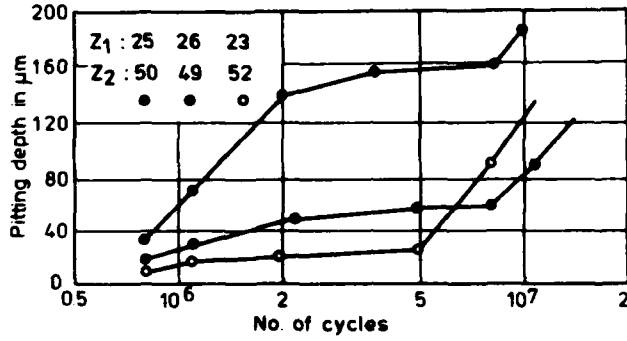


Fig. 1 Influence of hunting tooth on durability

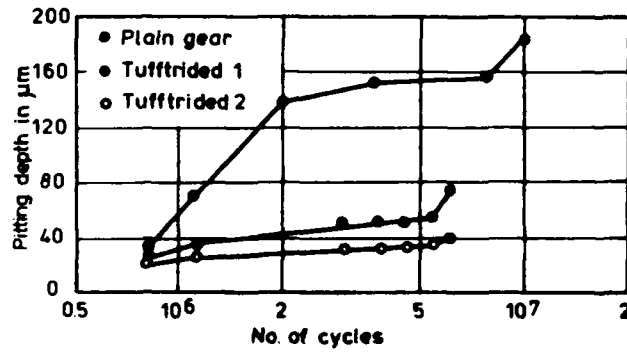


Fig. 2 Influence of tufftriding on durability

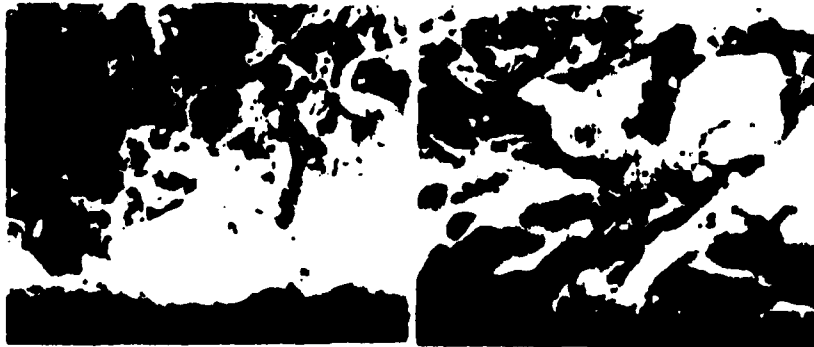


Fig. 3 SEM pictures of wear debris

A Micromechanical Derivation of the  
Differential Equations of Interfacial Statics  
III. Line Tension

by

M. Adler\* and H. Brenner  
Department of Chemical Engineering  
Massachusetts Institute of Technology  
Cambridge, MA 02139

A continuum-mechanical theory of line-excess tension and adsorption is developed, quantitatively relating such phenomena directly to the density-gradient intermolecular forces existing in the neighborhood of the three-phase contact line. This purely mechanical (i.e. nonthermodynamic) theory is rigorously derived via singular perturbation methods, utilizing a small parameter expansion involving the ratio of the microscopic length scale over which the density-gradient forces act to an appropriate macroscale associated with the macroscopic physical attributes (depth, interfacial curvature, lens radius, etc.) of the bulk phases. "Slender-body" theory serves as the geometrical basis of the perturbation scheme, with the body axis oriented along the contact line. In the sense of the theory of matched asymptotic expansions, the scheme automatically derives the proper pair of macroscopic "boundary conditions" at the common intersection of the phases, along the contact line. Specifically, these boundary conditions link together the "outer" or macroscopic stress fields existing within the three bulk phases, and along the three interfaces separating these bulk phases.

Of the two boundary conditions thereby derived by the matching of inner and outer expansions, the condition normal to the contact line is found to be identical to the so-called "generalized Neumann force balance" of Buff and Saltsburg (1), involving a line tension. The second condition, tangent to the contact line, and arising from line tensions gradients, appears to be new. In non-equilibrium circumstances (where this line-tension gradient is not balanced by a line-excess external stress) it represents a potential source of lineal Marangoni flow phenomena, analogous to classical areal phenomena existing at interfaces.

(1) Buff, F.P. and Saltsburg, H., J. Chem. Phys., 26, 23, 1957.

\* Permanent address: Laboratoire d'Aérothermique, 4<sup>ter</sup>  
Route des Gardes, 92190-Meudon,  
France

ON GEOMETRICAL ACCURACY IN PRECISE METAL FORMING\*  
by

Nguyen L. Dung  
Dept. of Mechanical Engineering, McMaster University,  
Hamilton, Ontario, Canada L8S 4L7

C. Westerling and O. Mahrenholtz  
Institute of Mechanics, University of Hannover  
Appelstr. 11, 3000 Hannover, F.R. Germany

In industrial metal forming, the high quality of the product depends on the grade of shape accuracy. There are five main factors which influence the accuracy of the formed parts: raw piece, forming procedure, tool, forming machine and tribology. These factors have mutual effect on each other, so that the study of shape accuracy is quite complicated and complex.

In this paper, we try to investigate this problem by analyzing the material flow and behaviour, the contact stresses, and the forming load during the forming processes with the finite element method. This will allow the study of the mutual effect between tool and formed part, and from that the shape accuracy.

The applied finite element method [1], based on Markov's variational principle for rigid-plastic material, includes the consideration of friction on the interface between tool and formed part. The friction affects the material flow and the material behaviour due to the temperature rise on the interface. Numerical results are shown for forging processes.

Reference:

- [1] Dung, N.L., Newerla, A., Marten, J.: FARM Finite Element Analysis of Rigid-Plastic Metal Forming - User's Manual. Institute of Mechanics, University of Hannover, 1982.

---

\* Supported by the "Deutsche Forschungsgemeinschaft DFG",  
F.R. Germany

## STRUCTURAL MECHANICS OF THE HUMAN KNEE

Edward S. Grood, Ph.D  
 Ramesh D. Kandadal, M.S  
 Mohamed S. Hefzy, Ph.D

Giannestras Biomechanics Laboratory  
 Department of Orthopaedic Surgery  
 University of Cincinnati Medical Center

INTRODUCTION: The purpose of this paper is to present a closed form analytical model based on finite element approach for the contribution of ligamentous and capsular structures to the coupled stiffness characteristics of the human knee and the experimental validation for that model.

THE MODEL: The system of characteristic equations for the knee joint in the set of local coordinate systems (located in tibia and femur) expressed in matrix form is:

$$\begin{bmatrix} Q_T \\ Q_F \end{bmatrix} = \begin{bmatrix} K_{11} & K_{12} \\ K_{21} & K_{22} \end{bmatrix} \begin{bmatrix} q_T \\ q_F \end{bmatrix} \quad (1)$$

where  $K_{11}$  are 6x6 stiffness submatrices. Equation (1) is the characteristic equation for the equivalent beam element model of the knee where  $q_T$  and  $q_F$  are tibial and femoral displacement vectors respectively.  $Q_T$  and  $Q_F$  are tibial and femoral load vectors due to the given displacements. In our analysis the tibia is considered to be fixed and displacements are applied to the femur. In addition  $K_{22}$  can be expressed in terms of  $K_{12}$  using relative rotational orientation and translation between femur and tibia. This reduces the unknowns to just  $K_{12}$ . It is assumed that ligaments support only tension and that there is a unique relationship between the tensile force  $T$  and length  $L$  of the ligament.

In the simplified equation (1), the stiffness matrix can be partitioned into four quadrants  $S_1, S_2, S_3$  and  $S_4$ , each of which is a submatrix of partial differentials of the joint load with respect to joint displacement. For a single ligament, the force acting on it is given by the product of the tensile force  $T$  and the direction cosines  $l_i$  of the ligament. Using chain differentiation, we obtain

$$S_{1ij} = \partial F_i / \partial x_{jF} = dT/dL l_i l_j + T/L (\delta_{ij} - l_i l_j) \quad (2)$$

where  $\delta_{ij}$  is the Kronecker delta. Note that there are two contributing factors - one due to axial stiffness of the ligament and other due to change in its orientation. On further analysis, it was found that the other quadrants can be expressed as a function of  $S_{1ij}$ . A significant observation is that of the 36 elements in the stiffness matrix for the entire joint only six are independent.

The problem of ligaments wrapping around bone surface is treated as a geometric nonlinearity [2]. All bone sur-

faces where a ligament can change directions are described by lines of auxiliary nodes. The ligament can change direction freely at these nodes under the assumption that the bending and shear stiffness are small. The length  $L$  of the ligament is the sum of the lengths of the straight line segments. If  $s_1$  are the local position coordinates along nodal lines, for a given joint position and minimum length  $L$ , the partial derivative of the length  $L$  with respect to  $s_1$  is equal to zero. From this solutions for  $s_1$  can be obtained.

**STRUCTURAL PROPERTIES:** For the analytical model outlined above to be validated we require load-length data on all ligamentous structures. This data is obtained experimentally. The test fixtures incorporate a dynamometer to measure the three force components and three moment components of the total reaction load on the joint. Controlled displacements are applied to the joint and the three dimensional load components and the applied displacements are measured by a minicomputer using an analog to digital converter and stored on magnetic disk. The tests are repeated after a ligament is cut. The difference between the joint loads before cutting and after cutting is the load carried by the ligament. This data provides load-displacement characteristics of each structure sectioned.

At the end of all load displacement testing, all insertion sites on the femur and tibia are marked. These along with some lines of auxiliary nodes are measured and stored on magnetic disk. Straight line lengths are computed using this data and the transformation between the femur and the tibia. The characteristics of the controlled displacement allows computation of the length at any point during the displacement. The combination of the load displacement and the length displacement data on a ligament provides load length characteristics of each ligament:

**DISCUSSION:** The load length data determined, as outlined above is used as the basis to predict joint load displacement characteristics for a different displacement. This prediction is compared with experimental data. Thus the model can be validated. Ligament load and length patterns during axial tibial rotation are currently being experimentally measured. The controlled displacement technique outlined above is a powerful approach for determining three dimensional function of ligaments. The load length data reduced from such tests is independent of the cutting sequence of the ligaments.

**ACKNOWLEDGEMENTS:** This work was supported by the National Institute of Arthritis, Diabetes, Digestive & Kidney Diseases R01 AM21172.

**REFERENCES:** 1. Grood, E.S., and Hefzy, M.S., (1981) J. of Biomechanical Eng., 104: 330-337. (2) Hefzy, M.S., and Grood, E.S., (1983) J. of Biomechanical Eng., May.

Biomechanical Studies of the Progression  
of Idiopathic Scoliosis

by

Albert B. Schultz  
University of Illinois at Chicago  
Box 4348  
Chicago, IL 60680

From a biomechanical viewpoint, progression of the lateral curves of scoliosis can be thought of as a lateral buckling of the deformable column the human spine constitutes. Lateral buckling tendencies will be more pronounced if the spine is abnormally slender (perhaps due to genetic influences), or has an abnormally high flexibility (perhaps due to hormonal or other biochemical influences), or is subject to abnormal forces and moments (perhaps due to neuromuscular influences).

Studies of spine slenderness in healthy children and children with moderate degrees of idiopathic scoliosis show that the spines of girls are significantly more slender than the spines of boys. This may explain in part why scoliosis progresses so much more often in girls. Nevertheless, pronounced differences in spine slenderness do not seem to exist between healthy girls and girls with idiopathic scoliosis.

Studies of spine flexibility indicate that structurally normal girls are somewhat more flexible than girls with mild idiopathic scoliosis. So, factors in addition to or other than spine slenderness and spine flexibility apparently have important roles in determining whether an idiopathic lateral curve in the spine will become more severe.

Studies of the strengths of the major trunk muscles show that the maximum voluntary strengths of these muscles are the same in girls with structurally normal spines as in girls with moderate degrees of idiopathic scoliosis. Still other studies of myoelectric activity in the trunk muscles show that asymmetric trunk muscles myoelectric activity occurs in girls with structurally normal spines as well as girls who have mild scoliosis. Substantial asymmetries in myoelectric activities seem to result from rather than be involved in creating lateral curves in the spine.

Biomechanical model analyses of the actions of the trunk muscles suggest that neuromuscular influences can cause scoliosis to progress. These studies indicate that the malfunctions responsible for progression are not intrinsic to the trunk muscles themselves, but seem to arise because of disorders in the neural systems which maintain upright postures of the trunk.

Based on present evidence, two hypotheses seem reasonable as to the biomechanical aspects of the progression of idiopathic scoliosis. First, progression impends when the neuromuscular system fails to provide adequate asymmetry of trunk muscle contraction forces, so that the motion segments must provide through passive tilt resistances the lateral moments necessary for equilibrium. Second, progression occurs when those tilts increase and become semi-permanent in long-term response to the nearly constant lateral moments.

## PERFORMANCE OF TOTAL JOINT REPLACEMENTS

by

Timothy M. Wright, Ph.D.  
Department of Biomechanics  
The Hospital for Special Surgery  
(affiliated with New York Hospital and  
Cornell University Medical College)  
535 East 70 Street  
New York, New York 10021

The replacement of diseased or damaged joints in the human body with prosthetic devices is a proven treatment for the relief of pain and the restoration of function. Joint replacement surgery is not without complications, however, many of which involve mechanical failure of the prosthetic components. It is important to examine such failures carefully to understand the problem and to hopefully arrive at solutions for improving performance.

One failure problem which has received considerable attention is the fatigue fracture of metallic femoral components in total hip replacement. Such fractures form a significant portion of total hip complications, particularly in heavy, active individuals. Examination of failed components reveals numerous variables which may adversely affect the fatigue performance, including surgical technique, design variables and material defects. Recent changes in component design and the manufacturing processes used in component production should result in significant reductions in the number of fractures seen in the future.

Another as yet unresolved problem concerns the mechanical performance of polyethylene components in total joint replacements. Ultra high molecular weight polyethylene is used extensively in total joints to provide a low friction articulation with polished metal surfaces and, consequently, to transfer significant loads across the joint. In performing these functions, polyethylene components often experience considerable wear and permanent deformation. Fracture of polyethylene components can also occur. Examination of worn and failed components together with experimental and analytical studies of the contact problem in total joints have revealed that clinical factors (such as patient weight) play a significant role and that the polyethylene experiences stresses in the range of its yield stress even under modest approximations of the applied loads occurring in-vivo. Though some solutions to improve the performance of polyethylene components have been proposed, they are not without compromise. Until sufficient clinical success is demonstrated, it must be assumed that problems in component performance will continue.

Analysis of Structural Failure in a Biological Tissue

by

M. G. Sharma  
 Pennsylvania State University  
 University Park, Pennsylvania

During mechanical harvesting, storage, and transportation fruits generally experience boundary forces that may cause structural damage in the form of bruises, punctures, and cracks. An estimation of a threshold value of force that is necessary to bring about damage in a given fruit is very important from the point of view of the design of harvesting and handling systems.

The paper is concerned with an experimental investigation for the development of general rheological constitutive relations and failure criteria for apple cortex tissue. Furthermore, stress and deformation analyses in the whole fruit under a concentrated boundary loading have been performed using the developed constitutive relations and the critical regions of stresses and strains have been determined. Based upon the results, a mechanism of structural failure based upon excessive plastic deformation has been advanced.

As part of the experimental investigation, torsional creep and creep recovery experiments were conducted on cylindrical samples using a specially developed multi-axial creep apparatus (see Fig. 1). Typical data from torsional creep experiments is shown in Fig. 2. Based upon the data, the following nonlinear viscoelastic constitutive relation was obtained

$$\gamma = \int_0^t J_1(t-t_1) \frac{d\tau}{dt_1} dt_1 + \int_0^t \int_0^t J_2(t-t_1, t-t_2) \frac{d\tau}{dt_1} \frac{d\tau}{dt_2} dt_1 dt_2$$

where,  $\gamma$  = shear strain

$\tau$  = shear stress (psi)

$$J_1(t) = (4.07 + 0.0265t + 0.0071t^2) 10^{-3}$$

$$J_2(t, t) = 1.95 \times 10^{-4} + 7.5 \times 10^{-7} t$$

$t$  = time (min.)

Dilatational creep response of the tissue was also studied by subjecting cylindrical samples to various magnitudes of hydrostatic stress. Typical data obtained from these tests is shown in Fig. 3. General rheological constitutive relations were developed by combining the constitutive relations for shear and dilatational deformations. In addition, uniaxial tension, compression and torsion combined with compression creep tests were also conducted as part of this study and the yield curves were obtained in the principal stress coordinates as shown in Fig. 4. The results indicate that the structural failure though yielding can be characterized by the Prager-Drucker yield criterion.

The developed constitutive relations were linearized and then used in conjunction with the yield criterion to predict stresses and strains within an apple fruit subjected to a contact loading from a spherical indenter. It has been found that at the critical region of yielding as predicted by the model, the tissue damage through cell rupture occurred and browning started. This has been corroborated by the microstructural examination of the tissue.

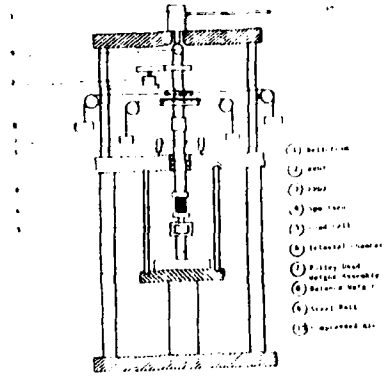


Fig. 1. Schematic diagram of the differential test apparatus.

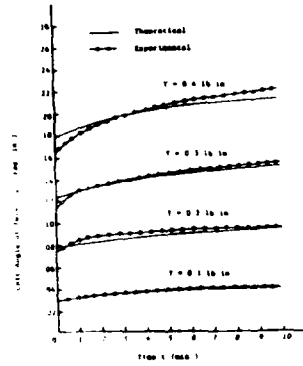


Fig. 2. Volt-Ampere of Total Torque Time Curves Obtained from Torqueless Cross-Flow in Apolo System.

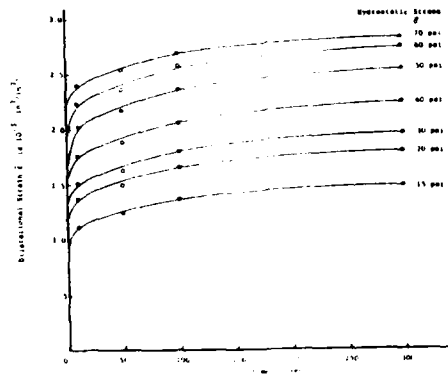


Fig. 3. Rotational Speed versus Time Curves for the Apolo System.

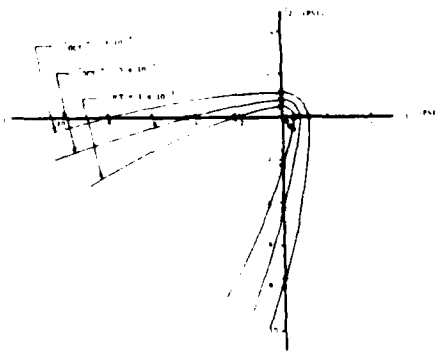


Fig. 4. Torque versus Time Curves for the Apolo System.

## BIOMECHANICS OF ARTICULAR CARTILAGE

by

P.A. Torzilli  
Biomechanics Department  
The Hospital for Special Surgery  
Affiliated with  
Cornell University Medical Center-New York Hospital  
New York, New York 10021

Articular cartilage is a unique biological tissue covering the bony ends of articulating joints. It is a smooth and almost frictionless bearing material which exhibits lubricating properties superior to that developed by man. Structurally, the tissue is a biphasic, viscoelastic, porous material composed of approximately 80 percent water. The movement of this interstitial water through the tissue and across the articular surface governs the tissue's mechanical response to applied loads. This provides the mechanism responsible for lubrication of the articular surfaces, and provides for the nutrition of the cartilage cells and the removal of metabolic waste products. Changes in the tissue's ultrastructure and in the loading configuration can drastically alter the normal physiological function of the tissue through altered fluid movement.

Using radioisotope tracer methods [1], solute and water concentration-depth profiles within the tissue have been determined for "unloaded" diffusion and transport in loaded tissue. Transient diffusion was studied using a one-dimensional non-linear regression model to determine the diffusion coefficient and equilibrium partition coefficient. The diffusion coefficient was found to decrease with transport time indicating a concentration-dependent response. In addition, partition coefficients were less than unity. This signifies that regions exist within the tissue which are not readily accessible to solute and water exchange.

Transport in mechanically loaded tissue was found to be enhanced only when the articular surface was completely uncovered. This allowed surface recovery (expansion) and concomitant fluid imbibition. With the removal of the dense fibrous articular surface greater fluid transport was evidenced. It is believed the articular surface plays a major role in controlling fluid movement and tissue mechanical deformation.

---

[1] Torzilli, P.A., Rose, D.E. and Dethmers, D.A., "Equilibrium Water Partition in Articular Cartilage," Biorheology, 19, 1982, pp. 519-537.

This work was supported by NIH Grants AM19849 and AM28151, and the Clark Foundation.

**SHEAR-DEPENDENT TERMS IN THE STRAIN  
ENERGY DENSITY FUNCTION OF THE ARTERIAL TISSUE**

by

R.N. Vaishnav, J. Vossoughi, M.P. Vaishnav

School of Engineering and Architecture  
The Catholic University of America  
Washington, D.C. 20064

The tissue of the large arteries can be characterized as a curvilinearly orthotropic, incompressible material capable of undergoing large deformations (1). Its mechanical response under "physiological" loading consisting of an intravascular pressure and a longitudinal tethering force has been characterized previously (2,3,4). However, for certain applications, such as vehicle crash dynamics and flow through the aortic arch, it is important to characterize the tissue response for more complex loadings. Such characterization requires inclusion of shear-dependent terms in the formulation. We therefore present here a form of strain energy density function which can be used to characterize the elastic response of the arterial tissue for loading more complex than physiological loading.

The appropriate set of invariants for curvilinear orthotropy is  $(a, b, c, d^2, e^2, f^2, def)$ , where  $a - f$  are the physical components of the Green-St. Venant strain tensor referred to the natural cylindrical coordinate system of an arterial segment assumed to be circularly cylindrical and stress-free. Specifically,  $a, b$  and  $c$  denote the radial, circumferential and longitudinal strain components, and  $d, e$ , and  $f$  denote the shearing strain components. For an incompressible material, one of the invariants can be eliminated in favor of the rest. To be consistent with our prior work, we choose to eliminate "a" in favor of the others. Accordingly, as a starting point for characterization of the arterial tissue we postulate the following specific polynomial form of  $W$ :

$$\begin{aligned}
 W = & C_1 b^2 + C_2 bc + C_3 c^2 + C_4 b^3 + C_5 b^2 c + C_6 bc^2 + C_7 c^3 \\
 & + C_8 d^2 + C_9 e^2 + C_{10} f^2 + C_{11} def + C_{12} bd^2 + C_{13} be^2 \\
 & + C_{14} bf^2 + C_{15} bdef + C_{16} cd^2 + C_{17} ce^2 + C_{18} cf^2 + C_{19} cdef \\
 & + C_{20} d^4 + C_{21} e^4 + C_{22} f^4 + C_{23} d^2 e^2 f^2 + C_{24} d^2 e^2 + C_{25} e^2 f^2 \\
 & + C_{26} d^2 f^2 + C_{27} d^3 ef + C_{28} de^3 f + C_{29} def^3 \quad (1)
 \end{aligned}$$

In Eq. (1),  $C_1 - C_{29}$  are material parameters to be determined using experiments involving various combinations of the strains  $b, c, d, e$ , and  $f$  over a physiologically significant range. The coefficients  $C_8$  to  $C_{29}$  are new and provide for the dependence of  $W$  on  $d, e$  and  $f$ , as well as the interactions of  $b$  and  $c$  with  $d, e$ , and  $f$ . Equation (1) represents, within the framework of hyperelasticity, a minimal consistent polynomial form for  $W$  which contains all the basic non-linearities and interactions of interest.

In conclusion, we have presented a rational starting point for the strain energy density function for the arterial tissue for applications beyond those involving physiological loading only.

#### References

- (1) Patel, D.J. and R.N. Vaishnav. Basic Hemodynamics and Its Role in Disease Processes. University Park Press, Baltimore, MD, 1981, 504p.
- (2) Vaishnav, R.N., J.T. Young, J.S. Janicki, and D.J. Patel. Nonlinear anisotropic elastic properties of the canine aorta. Biophysical J., 12, 1972, pp. 1008-1027.
- (3) Vaishnav, R.N., J.T. Young, and D.J. Patel. Distribution of stresses and of strain-energy density through the wall thickness in a canine aortic segment. Circ. Res. 32, 1973, pp. 577-583.
- (4) Young, J.T., R.N. Vaishnav, and D.J. Patel. Nonlinear anisotropic viscoelastic properties of canine arterial segments. J. Biomechanics, 10, 1977, pp. 549-559.

METHODOLOGY AND RESULTS OF USING ENGINEERING  
EQUIPMENT IN THE ANALYSIS OF BRAIN WAVES

by

Drs. Karel Montor & Bruce Johnson, and Mrs. Ann Lambert  
United States Naval Academy, Annapolis, Maryland 21402

During the summer of 1976, at the United States Naval Academy, 1227 members of the class that graduated in May 1980 were neurologically tested with their brain waves collected on an instrumentation recorder and analyzed using fast fourier transform, cross-correlation, and cross-spectrum analyzers. A "waterfall" display was also employed to enable presentation of multiple FFTs as they developed over time.

One-hundred and ninety-two different items of data were collected on each student including: college board scores, academic grades, performance grades, conduct grades, along with psychological and motivational profile ratings. Special analyses were made to determine the relationship between the foregoing factors and other recorded items of information including the effect of smoking on academic performance, the relationship of various blood factors to other measured parameters, and the interpretation of post-graduation performance as related to recorded variables.

Both individual and group studies will be discussed that enabled post-accident explanation of contributing factors. A review of personality/motivational shifts will provide insight as to changing national changes from the 1971 to 1981 time period. In addition a special report will identify significant differences in psychological and motivational profiles between (a) those who graduated with distinction and those who did not, (b) those who were selected to be Honor Set Strippers and those who were not.

Differences found between men and women will be reported including those related to SMA-12 blood analysis and those determined by both neurological and psychological testing.

Differences between low and high grade point average groups will be reported. As an example of findings the following was found with regard to those who smoke vs. those who do not. The smokers had lower SAT verbal scores; lower levels in the blood of protein, urea nitrogen, and bilirubin; slower neurological processing speed in the right hemisphere; lower academic, conduct, and military performance grades; as well as the finding that physical education grades were lower during the smokers last five semesters at the Academy. An analysis of the psychological/motivational profile scores indicates that the smokers are: more assertive, more happy go lucky, less conscientious, more venturesome, more tenderminded, more suspicious of others, more extroverted; and were not as close with their parents. These latter factors were measured by tests developed by the Institute for Personality and Ability Testing. A loanable video tape describing repeatable type measurement procedures and equipment configurations has been prepared describing this seven year effort. Computer analysis programs will also be shared with other institutions.

In Vitro Flow Visualization Experiments  
with Prosthetic Mitral Valves

by

J. R. Shanebrook, S. R. Bussolari, and J. M. Rinaldo  
Mechanical Engineering Department  
Union College  
Schenectady, New York 12308

An in vitro flow visualization system for observing the left ventricular flow patterns generated by prosthetic mitral valves has been developed. The system employs a left ventricular test chamber consisting of stationary and moving parts that are similar to those employed by Davila et al.<sup>1</sup> However, instead of a post-mortem heart, the stationary atrial and left ventricular test chambers are machined from rectangular blocks of plexiglas according to specifications reported by Wieting.<sup>2</sup> The moving portion of the left ventricular test chamber is a cam-operated piston that moves vertically inside the stationary ventricular chamber. The piston is also machined from plexiglas and its upper surface, simulating the bottom of the ventricle, is "cupped" in the shape of half an ellipsoid.

For flow visualization purposes, a system similar to that of Wieting<sup>2</sup> was utilized except the tracer particles were formed from a white ion exchange resin and an aqueous solution of sodium bromide as described by Miller et al.<sup>3</sup> The blood analog fluid (glycerine and distilled water) with neutrally buoyant tracer particles then provided an excellent medium for visualizing the flow patterns in the left ventricular test chamber.

Left ventricular flow patterns for three different prosthetic mitral valves, now employed in clinical applications, were recorded at a pulse rate of 100 cycles per minute and a stroke volume of 85 cc. Comparing the three valves tested, it was apparent that the Björk-Shiley tilting disc valve has superior left ventricular flow patterns compared to the other two valves tested. The left ventricular vortex generated during diastole, as shown in Figure 1, should produce desirable hemodynamic functions similar to those of the natural valve. The systolic left ventricular flow pattern is also advantageous in that an orderly flow pattern of separate inflow and outflow tracts is established by the valve as shown in Figure 2. Finally, it is noted that these properties of the Björk-Shiley valve also make it an attractive selection for the inlet valve of an artificial ventricle especially regarding the natural cleansing action of the diastolic ventricular vortex. By optimizing the shape of the artificial ventricle it may be possible to take full advantage of this vortex and substantially alleviate the tendency for blood thrombi to form within the ventricle.

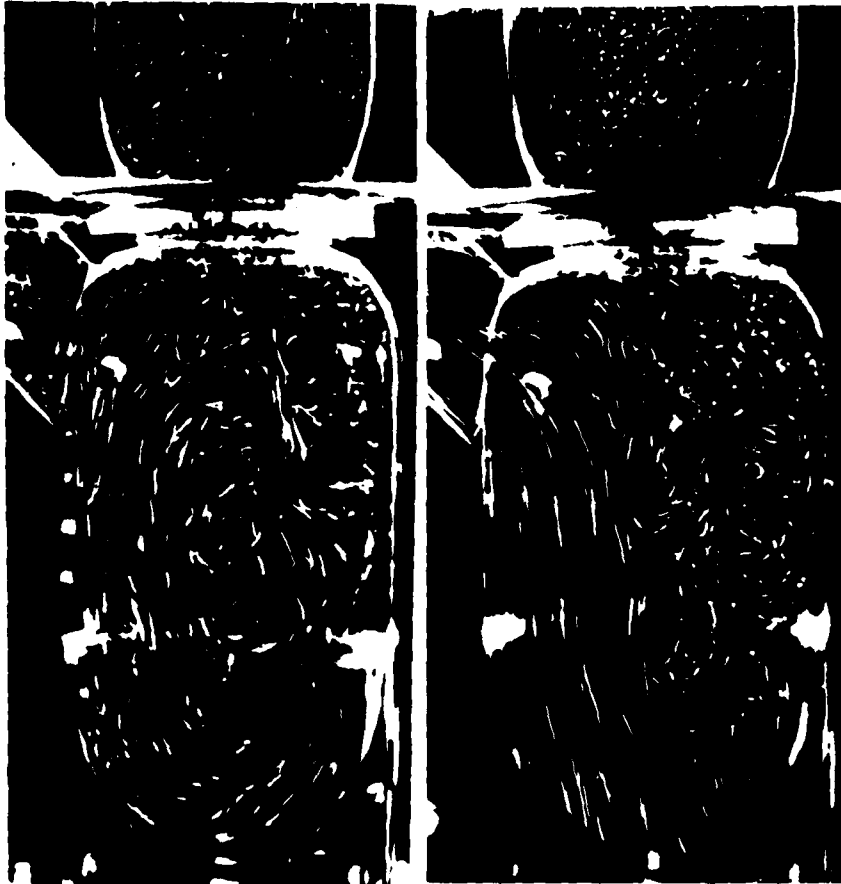


Figure 1.  
Björk-Shiley tilting  
disc valve during diastole.

Figure 2.  
Björk-Shiley tilting  
disc valve during systole.

#### References

1. Davila, J. C., Trout, R. G., Sunner, J. E., and Glover, R. P., "A Simple Mechanical Pulse Duplicator for Cinematography of Cardiac Valves in Action," Annals of Surgery, 143, 1956, pp. 544-551.
2. Wieting, D. W., "Dynamic Flow Characteristics of Heart Valves," Ph.D. dissertation, The University of Texas at Austin, 1969.
3. Miller, V. J., Bussolari, S. R., and Shanebrook, J. R., "Flow Visualization with Blood Analog Fluid," J. Biomechanics, 9, 1976, pp. 663-664.

INFLUENCE OF MALARIA ON THE ERYTHROCYTE  
SEDIMENTATION PROFILES AS DETERMINED IN  
PRESENCE OF INHOMOGENEOUS MAGNETIC FIELD

Megha Singh and K. Paul Joseph  
Biomedical Engineering Division  
Indian Institute of Technology  
Madras - 600 036, INDIA

The effect of magnetic field on the erythrocytes has been well established and has been used to determine the hepatic iron stores in the body (1,2), and change in the erythrocyte sedimentation in the CNS blood vessels of the rabbit (3). It is reported that under the influence of magnetic field the erythrocytes undergo shape alteration and orient to a preferred direction along the principal axes where the change in susceptibility with respect to the surrounding medium has its smallest value (4). Paul, et al (5) have shown that the application of the high gradient magnetic field affects the sedimentation of the erythrocytes but the detailed distribution of the erythrocytes during this process, below the cell-free layer of plasma, could not be determined. Recently we have developed a method to determine the erythrocyte distribution in the form of erythrocyte sedimentation profiles (concentration of the erythrocytes at the various points along the height and width of sample holder) of normal blood (6) and have also shown that these profiles show significant variations depending on the clinical status of the patient (7).

To determine the erythrocyte sedimentation profiles (ESP), in presence of inhomogeneous magnetic field, two identical magnets were coaxially held by mutual attraction sandwiching the glass chamber. The magnets were located in such a way that the top layer of the blood sample coincided with the center of the magnets. The chamber with magnets was positioned vertically on a specially designed platform on the upright of an optical bench. On the same platform another sample holder, without magnets, shielded from the magnetic field, was also placed.

The blood samples of the normal and malaria patient were obtained by venepuncture with sodium citrate as an anticoagulant (1,4) and filled in the chambers. The focussed light of the He-Ne laser was divided into two beams of equal intensity and were allowed to pass through the sample holders. The transmitted intensity was detected by two photodetector-amplifier assemblies, and were electronically subtracted to obtain the net change in ESP due to the presence of magnetic field.

The results indicate that initially the differential output at various points is zero but tends to change with the increase of sedimentation duration. The mobility of the malarial erythrocyte, at various locations, of the chamber, at different sedimentation durations, is significantly different from that of the normal blood.

The mechanism of this variation could be attributed to the influence of the malarial parasite on the erythrocyte hemoglobin which influence its sedimentation tendency in the presence of magnetic field.

## References:

1. Bauman, J.H. and Hoffman, R.W., "Magnetic susceptibility meter for in vivo estimation of hepatic iron stores," IEEE Trans. Biomed. Eng., 1967, pp. 239-243.
2. Baumann, J.R. and Harris, J.W., "Estimation of hepatic iron stores by in vivo measurement of magnetic susceptibility," J. Lab. Clin. Med., 70, 1967, pp. 246-257.
3. Likhachev, A.I. "Changes in the erythrocyte sedimentation rate of rabbit due to exposure of the central nervous system to a constant magnetic field," Biological Effects of Magnetic Fields, Barnothy, M.F., Ed., vol. 2, Plenum, New York, 1964, p. 137.
4. Gill, S.J., Malone, C.P. and Downing, "magnetic susceptibility measurement of single small particles," Rev. Sci. Instrum., 31, 1960, pp. 1299-1303.
5. Paul, F., Roath, S. and Melville, D., "Differential cell separation using a high gradient magnetic field," Br. J. Haematol., 38, 1978, pp. 273-280.
6. Singh, M., Meyyappan, A., Ramachandran, N., and Sivaram, B.M., "Erythrocyte distribution profiles as determined by He-Ne laser light," Med. Biol. Eng. Comput., 18, 1980, pp. 391-395.
7. Singh, M. and Joseph, K.P. "Erythrocyte sedimentation profiles under gravitational field as determined by He-Ne laser; IV. Effects of various diseases," Clinical Hemorheology, to be published.

EFFECTS OF CURING STRESS ON INTRALAMINAR  
CRACKING IN GRAPHITE-EPOXY LAMINATES

by

A. S. D. Wang  
Drexel University  
Philadelphia, PA 19104

In this paper, the effects of curing (thermal) stress on the formation mechanisms of intralaminar cracks in resin-based composite laminates are investigated. The curing stress which is considered here, is caused primarily by the thermal cooling in the laminate fabrication process. By itself, the residual curing stress may not cause sub-laminate damage; but it can couple with mechanical stresses, when the laminate takes up external loads, so as to produce premature internal failures.

It will be shown in this investigation that in the formation and propagation mechanisms of intralaminar cracks such as transverse cracking (crack along fibers that are transverse to the loading), or fiber-splitting (crack along fibers that are parallel to the loading), the effect of the residual curing stress can be the predominant factor.

In this paper, the initiation and propagation mechanisms of transverse crack in [0/90]<sub>s</sub> type laminates are analyzed using the energy release rate criterion of the classical fracture mechanics. The analytical results are then correlated with experiments in which a series of graphite-epoxy laminates are tested under a wide range of temperature conditions. It will be shown that, although the thermal stress and the mechanical stress are additive, their effects on both crack initiation and propagation are coupled together in a quadratic form. Thus, in a certain case, the thermal coupling effect contribution to crack formation can be as much as 70%.

FATIGUE DAMAGE AND CRACK GROWTH  
IN RANDOM SHORT-FIBER REINFORCED COMPOSITES

by

S. S. Wang  
Department of Theoretical and Applied Mechanics  
University of Illinois  
Urbana, IL 61801

A study on damage accumulation, cyclic degradation and crack growth in a random short-fiber SMC composite subjected to fatigue loading is presented. Fatigue damage mechanisms in various forms of microcracking are examined. The transient nature of the nonlinear monotonic (or the first cycle) stress-strain behavior is investigated first. Subsequent property degradation and hysteresis dissipation are examined. Contrary to the behavior of certain homogeneous metals and polymers, a cyclic stable state is not reached in general; cyclic softening is always observed in this class of materials. Fatigue damage initiation and growth are homogeneous and isotropic in general. A parameter is introduced to define the degree of the homogeneous damage in the random short-fiber composites. A power-law relationship among the rate of damage evolution, loading variables, and cyclic history is established. The homogeneous fatigue damage decreases rapidly with the loading cycle due to combined effects of rapid depletion of microcrack initiation sites and various crack arrest mechanisms in the composite. In conjunction with the development of the present damage theory, nonhomogeneous damage in the form of macroscopic crack growth in the short-fiber composite is studied. A theoretical model is established to account for the interaction between homogeneous damage and nonhomogeneous crack growth. Fatigue crack growth rate in this class of materials is predicted to have a power-law-relationship with crack-tip stress intensity but possesses a much higher exponent than that in the homogeneous material.

A PROBABILISTIC THEORY FOR THE STRENGTH OF  
DISCONTINUOUS FIBRE COMPOSITES

by

Fuminori Hikami and Tsu-Wei Chou  
Department of Mechanical and Aerospace Engineering  
University of Delaware  
Newark, Delaware 19711

The strength of discontinuous fiber reinforced composites is often reduced due to local stress concentrations at large fiber-end-gaps. A theoretical prediction of the strength of unidirectional fiber composites is performed based upon a probabilistic model of the fiber configuration. This work further develops the concepts of Bader, Chou and Quigley [1], and Fukuda and Chou [2]. A limiting case of the present analysis shows good agreement with the theoretical results of Smith [3]. Emphases are placed on the effect of matrix stress transfer properties including matrix plasticity. For matrix deforming elastically, the strength as compared to rule-of-mixtures prediction for continuous fiber composites with identical fiber volume fraction, is reduced as the composite size ( $N$ ) increases. The reduction is shown to be proportional to  $(\ln N)^{-P}$ , with the exponent  $P$  being between 0.5 and 1 for two dimensional composites and between 0.25 and 0.5 for three dimensional composites. For matrix deforming plastically, the local stress concentrations are reduced. Based upon the analytical expression of local load shearing rule for plastic matrix [4,5], the composite strength is shown to approach the modified rule of mixture of Kelly and Tyson as the matrix yield stress decreases [Fig. 1].

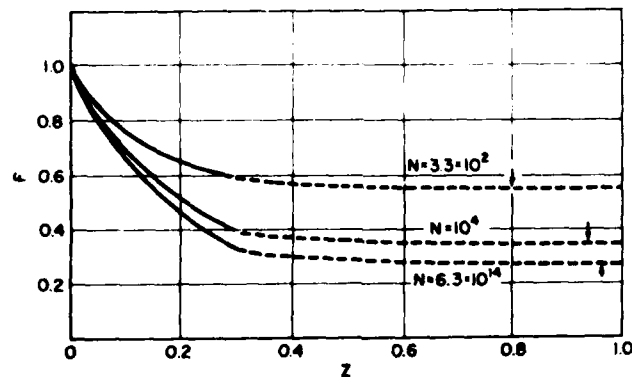


Fig. 1. Strength ratio,  $F$ , to the value predicted by the rule of mixture vs. normalized matrix yielding stress,  $z$ . Arrows indicate the onset of matrix plastic deformation.  $N$  is the total number of fibers.

References

1. Bader, M. G., Chou, T. W., and Quigley, J., New Developments and Applications in Composites, edited by D. Wilsdorf (The Metallurgical Society-American Institute of Mining Metallurgy and Petroleum Engineering, New York, 1979).
2. Fukuda, H. and Chou, T. W., "A Probabilistic Theory for the Strength of Short Fibre Composites," J. Mater. Sci., 16, 1981, pp. 1088-1096.
3. Smith, R. L., "A Model for Chopped Fibre Composites," submitted for publication to Stoch. Proc. & Appl.
4. Hikami, F. and Chou, T. W., "Explicit Crack Problem Solutions of Unidirectional Composites Part I: Elastic Stress Concentration," submitted for publication to ASME J. of Applied Mechanics.
5. Hikami, F., Chou, T. W. and Hsiao, G. C., "Explicit Crack Problem Solutions of Unidirectional Composites Part II: Effect of Crack Tip Damage," submitted for publication to ASME J. of Applied Mechanics.

## Plasticity of Laminated Composites

BY

S. Nomura  
Department of Mechanical Engineering  
University of Texas at Arlington  
Arlington, Texas 76019

This paper studies plastic behavior of metal composite materials, especially layered composites.

The treatment of plastic behavior of composites is more complicated than that of elastic behavior because unlike in elasticity, the governing equations in plasticity are non-linear and path-dependent. Non-homogeneous stress distribution in composites also contributes to the difficulty of plasticity of composite materials. However, metal composites are attractive advanced materials in their high yield strength, high temperature performance, high stiffness/density ratios.

A considerable effort has been devoted to the study of overall yield criterion of metal composites. This problem is essentially equivalent to estimating a local stress field in the composite.

Our objective here is work-hardening phenomena of a layered composite material consisting of two different types of layers stacking either randomly or periodically. Each layer is isotropic and homogeneous, and deforms either elastically or elastic-perfectly-plastically.

We make use of a statistical approach which was employed for the effective elastic modulus of short-fiber composites by the authors [1]. In that analysis, each field quantity such as stress, strain, displacement, or elastic modulus was decomposed into a volumetric average part and a fluctuating part, and they are subsequently substituted into the stress equilibrium equation. This operation yields the partial differential equation with respect to the fluctuating displacement field that calls for the introduction of the elastic Green function. The solution for the local stress field was expressed by Neumann type infinite series. In the analysis of short-fiber composites, several assumptions such as statistical homogeneity or ergodicity enabled the integral operator to be evaluated up to certain degrees.

In the presence of plastic strains inside the composite, it can be shown that by considering the additional plastic strain term in the constitutive equation, a stress field expression similar to the pure elastic deformation can be derived formally that involves both the external (average) stress and the plastic strain. It is further shown that if statistical properties of the composite are homogeneous and depend only on the major axis,

each term in the infinite series can be evaluated exactly up to arbitrary orders. The infinite series can thus be summed up and the local stress and strain fields of layered composites are obtained in closed forms as functions of material properties, externally applied stresses (average stresses), and plastic strains. It should be noted that the plastic strain inside the composite is still unknown quantity.

To determine this plastic strain, the von-Mises yield criterion is adopted. By substituting the local stress expression that contains the average stress and plastic strains into the von-Mises yield criterion, the plastic strain can be expressed as a function of the external (average) stress, thus, the local stress field and strain field are completely determined at each stage of the loading. Therefore, overall stress-strain curves are obtained for any loading histories.

The overall stress-strain curves for three different kinds of loadings are presented, namely, the tensile loading, the transverse shear loading, and the longitudinal shear loading. By comparing the longitudinal shear loading with the transverse shear loading, it is shown that the hardening rate for the transverse shear loading is more enhanced than that for the longitudinal shear loading. The convergence of the series is also discussed.

Reference:

- [1] Nomura, S., "Statistical Aspects of Heterogeneous Materials", Proceedings of the Fourth International Conference on Composite Materials, pp.1083-1089 (1982).

## The Effective Behavior of Inelastic Composites

by

Jacob Aboudi  
Department of Solid Mechanics,  
Materials and Structures  
Tel-Aviv University  
Ramat-Aviv 69978, Israel

The average behavior of unidirectional fiber-reinforced composites, whose constituents are anisotropic in the elastic region and viscoplastic in the inelastic region, is determined. Effective stress-effective strain curves are presented for various types of loading. In the special case of perfectly elastic phases, the effective moduli of the composite are obtained. Several comparisons between the effective behavior of the composite, as predicted by the present theory and by other analytical, numerical and experimental approaches, are given.

References

1. Aboudi, J., "A Continuum Theory for Fiber-Reinforced Elastic-Viscoelastic Composites," Int. J. Engng. Sci., 20, 1982, pp. 605-621.
2. Aboudi, J., "Effective Constitutive Equations for Fiber-Reinforced Viscoplastic Composites Exhibiting Anisotropic Hardening," Int. J. Engng. Sci., 21, 1983, in press.
3. Aboudi, J., "The Effective Behavior of Inelastic Composites," submitted for publication in Int. J. Engng. Sci..

RELIABILITY-BASED DESIGN PRINCIPLE OF COMPOSITE MATERIALS  
WITH FAILURE PROBABILITY AS A STATISTIC

Hiroshi ISHIKAWA\*, Toshio TANIMOTO\*\* and Hitoshi KIMURA\*

\*Dept. of Information Science, Kagawa University,  
Takamatsu 760 JAPAN

\*\*Dept. of Mechanical Engineering, Doshisha University,  
Kyoto 602 JAPAN

### 1. INTRODUCTION

The present paper first deals with the statistical modelling of the failure probability under service loading in the sense that the failure probability can be evaluated only through the limited number of experimental data, which would, of course, vary from sample to sample. It then investigates how to determine the reliability-based design safe lives of composite materials.

### 2. STATISTICAL MODELLING OF FAILURE PROBABILITY UNDER SERVICE LOADING

Let  $Z_n = \sum_{i=1}^n (S_i/s_0)^b$  be a normalized damage accumulated during  $n$  cycles of, in general, random loading with arbitrary distribution  $R(s) = P\{S_i < s\}$ , where  $S_i$  and  $s_0$  are applied  $i$ -th and normalization stress levels, respectively. With  $Z_c$  being the critical value of  $Z_n$ , and for  $n \gg 1$ , the distribution of  $Z_n$  can be well approximated by a normal distribution by virtue of central limit theorem, and then the distribution function  $F_N(n)$  of fatigue life  $N$  can be derived in the following form:

$$F_N(n) = P\{N < n\} = P\{Z_n > Z_c\} = \int_{-\infty}^{\infty} F_{Z_c}(z_c) \cdot \frac{1}{\sqrt{2\pi n\nu}} \exp\left[-\frac{(z_c - n\lambda)^2}{2n\nu^2}\right] dz_c$$

$$= F_{Z_c}(n\lambda) + (n\nu^2/2) F_{Z_c}''(n\lambda) + O(1/n^2) \approx F_{Z_c}(n\lambda) \quad (1)$$

$$\text{where } \lambda = E\{Z_n\}/n = \int_0^{\infty} (s/s_0)^b dR(s) \quad (2)$$

$$\nu^2 = V\{Z_n\}/n = (1/s_0^{2b}) \left[ \int_0^{\infty} s^{2b} dR(s) - \left( \int_0^{\infty} s^b dR(s) \right)^2 \right]. \quad (3)$$

Assuming that  $Z_c$  follows a log-normal distribution independently of  $Z_n$ , the failure probability  $P$  can be given as

$$P \approx F_N(n) \approx F_{Z_c}(n\lambda) = P\{Z_c < n\lambda\} = P\{(\ln Z_c - \mu)/\sigma < (\ln(n\lambda) - \mu)/\sigma\}$$

$$= \begin{cases} \Phi\{(\ln(n\lambda) - \mu)/\sigma\} & \text{for } n\lambda > 0 \\ 0 & \text{otherwise} \end{cases} \quad (4)$$

where  $\Phi[\cdot]$  is the standard normal distribution function and  $\mu = E[\ln Z_c]$ ,  $\sigma^2 = V[\ln Z_c]$ .

Since the true value of  $\mu$  and  $\sigma$  are usually unknown, they need to be replaced, for instance, by their maximum likelihood estimates  $\hat{\mu}$  and  $\hat{\sigma}$  from a sample of size  $k$ , thus  $P$  by  $\hat{P}$ , all being random variables. The distribution function  $H(p)$  of the statistical failure probability  $\hat{P} = \Phi\{(\ln(n\lambda) - \hat{\mu})/\hat{\sigma}\}$  thus constructed can be derived:

$$H(p) = P\{\hat{P} \leq p\} = P\{\Phi\{(\ln(n\lambda) - \hat{\mu})/\hat{\sigma}\} < p\}$$

$$\begin{aligned}
 &= 1 - \int_0^{\infty} (1/\Gamma(\frac{k-1}{2})) \phi \left[ \frac{\sqrt{k}}{\sigma} \{ \ln(n\lambda) - \mu \} - \phi^{-1}(p) \sqrt{2w} \right] w^{(k-3)/2} e^{-w} dw \\
 &= 1 - (1/\Gamma(\frac{k-1}{2})) \int_0^{\infty} \phi \left[ \sqrt{k}x - \phi^{-1}(p) \sqrt{2w} \right] w^{(k-3)/2} e^{-w} dw
 \end{aligned}
 \tag{5}$$

where  $x = \{ \ln(n\lambda) - \mu \} / \sigma$ . (6)

3. RELIABILITY-BASED FATIGUE-PROOF DESIGN PRINCIPLE

H(p) thus defined is now utilized for the reliability-based fatigue-proof design of composite materials, whose principle requires that the decision of the failure probability being less than allowable value  $p_H$  during design life be correct with a pre-specified level of reliability H. In other words, fatigue-proof design has to be made so as to obtain as large value of  $n\lambda$  as possible under the condition that sample size k, reliability level H and allowable value of failure probability  $p_H$  are all given.

4. RELIABILITY-BASED DESIGN SAFE LIVES OF COMPOSITE MATERIALS

The statistical fatigue life data of satin woven glass cloth FRP were obtained experimentally under rotating bending of constant amplitude with not less than twenty replication tests at each stress level. Then they were analyzed to clarify the statistical properties of FRP as shown in Fig.1. By using the result for  $S=110$  MPa, as an example, we can determine the reliability-based design safe life — the value of  $n\lambda = E[Z_n]$  — so as to leave the failure probability less than a certain value, say,  $p_H \approx 5 \times 10^{-4}$  with a given reliability level of, for instance,  $H=90\%$ . First we get  $x = -3.8$  for  $p_H = 5 \times 10^{-4}$  and  $H=90\%$  from Fig.2, and then maximum likelihood estimates of  $\hat{\mu} = 10.842$  and  $\hat{\sigma} = 0.104$  from experimental data. Hence,  $n\lambda = \exp[\hat{\mu} + x\hat{\sigma}] = \exp[10.842 - 3.8 \times 0.104] = 3.44 \times 10^4$ . By adopting this value of  $n\lambda$ , we can conclude, with reliability level of 90%, that the probability of failure during lifetime would be less than  $5 \times 10^{-4}$ .

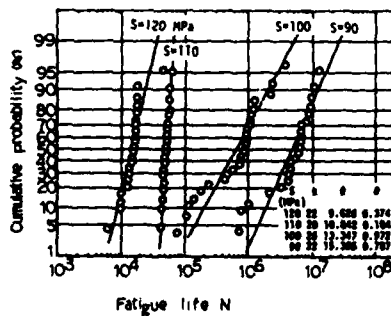


Fig.1 Fatigue life distributions

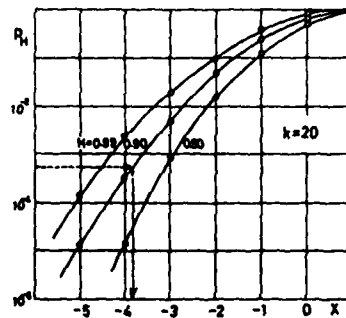


Fig.2 Relationship between allowable failure probability  $p_H$  and parameter  $x$  for given values of reliability level H

EFFECTIVE ELASTIC MODULI OF AN ISOTROPIC,  
TWO-PHASE COMPOSITE

by

C. R. Chiang and G. J. Weng  
Department of Mechanics and Materials Science  
Rutgers University  
New Brunswick, New Jersey 08903

A theoretical approach to determine the effective elastic moduli of an isotropic, two-phase composite is presented. The overall elastic response of the composite is modeled by an assumed global physical system. The underlying principle of the present method combines the spirit of self-consistent formulation [1,2] and the concept of polarization stress and strain [3,4]. In contrast to the classically adopted constant polarization stress in each phase, a non-uniform polarization field is assumed. The analysis was carried out for both traction and displacement prescribed processes. By consideration of strain energy of the composite and an optimization process, bounds and unique solutions for the effective moduli of the composite are obtained in terms of those of the constituent phases and their volume fractions. Numerical results of both bulk and shear moduli, using the unique solutions, were found to lie between the tight Hashin-Shtrikman bounds and close to the self-consistent estimates. This result was also shown to be in good accord with Richard's experimental data [5].

References

1. Hill, R., "A Self-Consistent Mechanics of Composite Materials," J. Mech. Phys. Solids, 13, 1965, pp. 213-222.
2. Budiansky, B., "On the Elastic Moduli of Some Heterogeneous Materials," J. Mech. Phys. Solids, 13, 1965, pp. 223-227.
3. Hashin, Z., and Shtrikman, S., "A Variational Approach to the Theory of the Elastic Behavior of Multiphase Materials," J. Mech. Phys. Solids, 11, 1963, pp. 127-140.
4. Walpole, L. J., "On Bounds for the Overall Elastic Moduli of Inhomogeneous Systems I," J. Mech. Phys. Solids, 14, 1966, pp. 151-162.
5. Richard, T. G., "The Mechanical Behavior of a Solid Microsphere Filled Composite," J. Comp. Mat., 9, 1975, pp. 108-113.

DYNAMIC INSTABILITY OF SUDDENLY HEATED,  
THICK, COMPOSITE SHELLS

H. Ray

Department of Mechanical and Aerospace Engineering  
Rutgers University, New Brunswick, NJ 08903

and

C.W. Bert

School of Aerospace, Mechanical and Nuclear Engineering  
University of Oklahoma, Norman, OK 73019

Critical structural applications involving rapidly heated shell-type structures include missile/spacecraft re-entry vehicles and inertially-confined fusion reactors. Parametric instability due to nonlinear energy exchange between the unstable axisymmetric mode and unstable flexural modes was first investigated for suddenly applied, axisymmetric pressure loading by Goodier and McIvor [1]. The thermal-loading analog of this problem was attacked by Ray and Lovell [2] and later extended to the case of a laminated composite shell by Ray [3].

The present analysis is an extension of the work of Ray [3] to include two additional effects of particular importance in the case of composite shells: (1) transverse-shear deformation, using a thick-shell generalization [4] of the Sanders shell theory, and (2) damping action. Analyses of both the short-term and long-term responses are presented. The effects of various parameters on the shell response are presented in graphical form.

References

- [1] Goodier, J.N. and McIvor, I.K., "The Elastic Cylindrical Shell Under Nearly Uniform Radial Impulse," J. Appl. Mech. 31, 1964, pp. 259-266.
- [2] Ray, H. and Lovell, E.G., "Dynamic Instability of Suddenly Heated Cylindrical Shells," Nuc. Eng. Des. 61, 1980, pp. 237-243.
- [3] Ray, H., "Dynamic Instability of Suddenly Heated Angle-Ply Laminated Composite Cylindrical Shells," Computers & Structures 16, 1983, pp. 119-124.
- [4] Hsu, Y.S., Reddy, J.N., and Bert, C.W., "Thermoelasticity of Circular Cylindrical Shells Laminated of Bimodulus Composite Materials," J. Thermal Stresses 4, 1981, pp. 155-177.

## TRANSVERSE SHEAR EFFECTS IN BIMODULAR COMPOSITE LAMINATES

by

Charles W. Bert and Faramarz Gordaninejad  
 School of Aerospace, Mechanical & Nuclear Engineering  
 University of Oklahoma, Norman, OK 73019

A closed-form solution for the Timoshenko-type shear correction coefficient ( $K^2$ ) governing the deflection of bimodular composite laminates in cylindrical bending is presented. The bending-stress distribution for a laminate constructed of bimodular materials (defined below) is used in the two-dimensional equilibrium equation to obtain the transverse shear-stress distribution. This distribution is used to obtain expressions for the shear correction coefficient (based on equivalent shear strain energy) and the maximum dimensionless transverse shear stress ( $\tau_{xz}$ )<sub>max</sub>.

Materials which have different moduli in tension and in compression are called bimodular materials. Rock, concrete, cord-rubber, paperboard, and certain biological tissues are examples of such materials. Even aramid-fiber, polymer-matrix composites exhibit some bimodularity. The analysis of laminated bimodular material is more complicated than unimodular material (ordinary material) due to the dependency of the material stiffness on the material properties, which indeed depend on the state of stress (i.e., tensile or compressive) in the laminate.

Although transverse shear deformations have been considered in recent analyses of bimodular laminates, there has been no effort to include the effect of bimodularity on  $K^2$ . Here a straight-forward approach analogous to that used in elementary shear theory for single-layer ordinary materials is employed. It may be considered to be a generalization of the work of Bert [1] from ordinary-material laminates to bimodular-material laminates.

In the case of single-layer bimodular material, it is interesting to note that both  $K^2$  and ( $\tau_{xz}$ )<sub>max</sub> are unaffected by the bimodular ratio  $E^c/E^t$  ( $c$ =compression and  $t$ =tension). However, this does not imply that the distribution of shear stress is the same for unimodular and bimodular materials.

In bending of a two-layer bimodular laminate, since one of the two layers is always in compression (or tension), only three of the four elastic moduli belonging to these layers are pertinent. The  $K^2$  coefficient varies drastically with the ratio of the shear moduli of the two layers ( $G_1/G_2$ ), whereas it changes only a little for a wide range of  $E_2^c/E_2^t$  (for  $E_1^c/E_2^c=1$ ), as shown in Fig. 1 (subscripts 1 and 2 denote the layer numbers). However,  $K^2$  for two-layer unimodular laminates increases rapidly from 50% to 98% of the classical value (5/6) as the elastic-modulus ratio  $E_1/E_2$  varies from 0 to 0.25 (see Fig. 2).

Three-layer bimodular laminates, which have facings (top and bottom layers, denoted as layers 1 and 3, respectively) made of the same materials, are also considered. For the case in which  $E_1^c/E_2^c=1$ , the effect of bimodular ratio  $E_3^t/E_2^c$  on  $h_t/h$  (defined in Fig. 1) for different ratios of  $E_2^t/E_2^c$  (1/2, 1, and 2) is shown in Table 1. In all cases which were

discussed above, the laminates are assumed to be made of equal-thickness layers and the effect of the sign of the longitudinal normal strain on shear moduli is ignored (i.e.,  $G^c/G^t=1$ ).

In brief, for two- and three-layer laminates, both  $K^2$  and  $(\bar{\epsilon}_{xz})_{max}$  depend upon the bimodular ratios and transverse shear moduli ratios. According to the results presented, in some cases  $K^2$  is considerably less than the classical 5/6.

[1] C.W. Bert, "Simplified Analysis of Static Shear Factors for Beams of Nonhomogeneous Cross Section," *Journal of Composite Materials*, Vol. 7 (1973), p. 525.

Table 1. Effect of Bimodular Ratios on Neutral-Surface Location for Three-Layer Bimodular Laminates ( $h_1/h_2=h_3/h_2=1$ ,  $E_1^c/E_2^c=E_3^c/E_2^c=1$ )

$E_3^t/E_2^c$	$h_t/h$		
	$E_2^t/E_2^c=1/2$	$E_2^t/E_2^c=1$	$E_2^t/E_2^c=2$
0	0.724	0.833	0.609
1/4	0.643	0.722	0.573
1/2	0.586	0.633	0.541
3/4	0.542	0.561	0.513
1	0.508	0.500	0.488
2	0.418	0.333	0.414
5	0.310	0.119	0.309
8	0.267	0.033	0.266
10	0.250	0	0.249

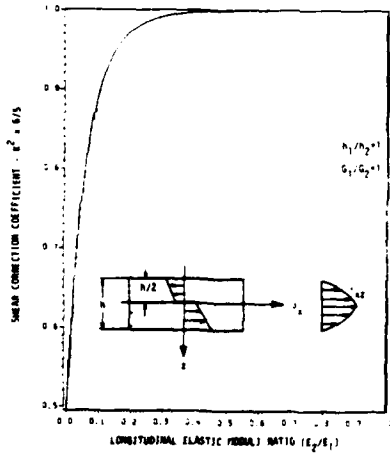


Fig. 2

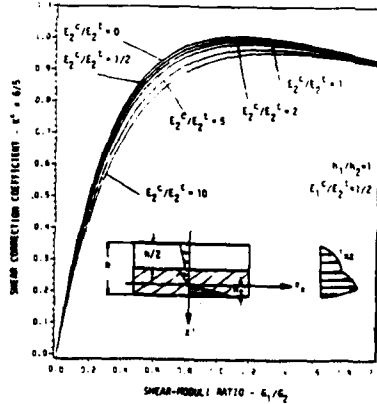


Fig. 1

LONGITUDINALLY STIFFENED COMPOSITE  
MULTI-LAYER CYLINDRICAL SHELLS (AND RINGS)  
UNDER INTERNAL PRESSURE

D.P. Updike  
Lehigh University  
Bethlehem, PA 18015

U. Yuceoglu  
Florida Int'l University  
Miami, FL 33199

In relatively long, multi-layer, composite, circular cylindrical shells (and also in short rings) subjected to high internal pressure it is observed that individual shell layers may crack or fracture in longitudinal direction. These long cracks are primarily due to large hoop stresses in circumferential direction.

A complete analysis of this problem is rather complicated because of the yielding across the thickness near the longitudinal crack regions. In this paper, an approximate analysis of the problem is presented. For this purpose, in a two-layer composite cylindrical shell, the inner shell layer is assumed fractured completely across the thickness in longitudinal direction while the outer shell remains intact. After then, the inner shell layers are considered as "longitudinal stiffeners" attached to the outer shell through an adhesive layer (1). The problem is formulated as a B.V.P. within the restrictions of a tenth order shear theory of shells. The system of first order partial differential equations are solved by a numerical scheme (2).

Numerical results for some practical problems are presented. Also the extension of the problem to more complicated problems such as fiber layer reinforced, multi-layer, long cylindrical shells and short rings are discussed in detail. Further extension of the problem to non-linear cases are considered.

References

- (1) Updike, D. P. and Yuceoglu, U., "Comparison of Continuum and Mechanical Spring Models for Adhesive Layer in Bonded Joints" "1981 Advances in Aerospace Structures and Materials" edited by S.S. Wang and W. J. Renton, Pp. 75-83, November 1982
- (2) Yuceoglu, U. and Updike, D.P., "On The Analysis of Adhesive Joints in Fiber-Reinforced Composite Plates and Shells", "1982 Advances in Aerospace Structures, Materials and Dynamics" edited by R.M. Laurenson and U. Yuceoglu, Pp. 19-24, on ASME Publication, November 1982

On Some Dynamic Problems  
in Layered Elastic-Viscoelastic Beams

by

Richard B. Hetnarski  
Department of Mechanical Engineering  
Rochester Institute of Technology  
Rochester, NY 14623

Vibration modes of layered beams are studied. The beams under consideration consist of an elastic main (central) element, two viscoelastic layers (one on each side of the main element), and elastic outside layers which serve as constraining layers for the viscoelastic material. The purpose of inclusion of viscoelastic layers is to increase internal damping of vibrations of the layered beams compared with purely elastic beams.

In the considered model, the main elastic element is assumed to exhibit no internal damping, with only normal stresses appearing in it. Viscoelastic layers are assumed to exhibit only shear stresses. As for the behavior of the outside (constraining) layers, two different approaches are considered.

1. It is assumed that the outside layers have zero normal strain during bending of the beam. This simplifying assumption allows one to derive a fourth order differential equation governing the motion. An appropriate set of boundary conditions is obtained from the energy approach.

2. Normal strain is allowed in the outside layers. This case is much more difficult for theoretical treatment. The obtained governing equation in this case is of the sixth order. A set of boundary conditions for this case is received by analogy with case 1.

A detailed analysis is shown for the cantilever beams. The discussion of results obtained in case 1 and case 2 is presented.

References

1. DiTaranto, R. A., Theory of Vibratory Bending for Elastic and Viscoelastic Layered Finite-Length Beams, Journal of Applied Mechanics, 1965, pp. 881-886.
2. Abgasiere, J. A., and Grootenhuis, P., Flexural Vibration of Symmetrical Multi-Layer Beams with Viscoelastic Damping, J. Mech. Eng. Science, vol. 10, No. 3, 1968, pp. 269-281.
3. Mead, D. J. and Markus, S., The Forced Vibration of a Three-Layer Damped Sandwich Beam with Arbitrary Boundary Conditions, J. Sound Vib., vol. 10, No. 2, 1969, pp. 163-175.

STATISTICAL FATIGUE AND RESIDUAL STRENGTH DEGRADATION  
MODEL FOR GLASS/POLYESTER LAMINATES

BY

Toshio TANIMOTO\* and Hiroshi ISHIKAWA\*\*

\* Department of Mechanical Engineering, Doshisha University,  
Kyoto 602 JAPAN

\*\* Department of Information Science, Kagawa University,  
Takamatsu 760 JAPAN

1. INTRODUCTION

A new residual strength degradation model for composite materials has been proposed in this paper based upon the assumption that the residual strength, as a random variable, decreases monotonically in exponential form with increasing number of stress cycles. An experimental test program on the plain woven glass cloth laminated FRP has been conducted to generate statistical meaningful data. Fatigue tests were carried out under repeated tension and compression loadings. Then the tensile strength was measured to examine the change of properties in the material at a given fraction of the fatigue life.

2. THEORETICAL DERIVATION

(1) Residual Strength Degradation Model

The ultimate strength,  $R(0)$ , residual strength,  $R(n)$ , and fatigue life,  $N$ , as well, should be treated as a random variable. And therefore hereinafter, the random variable is represented using Gothic letters.

Assuming that the degradation process of residual strength is represented by the following rate equation, then

$$dR(n)/dn = -f(s) \cdot R(n) \quad (1)$$

in which  $f(s)$  is a function of cyclic stress  $s$ .

By integrating of Equation (1) from 0 to  $n$  cycles

$$R(n) = R(0) \cdot \exp[-f(s) \cdot n] \quad (2)$$

(2) Statistical Distribution of Ultimate Strength and Residual Strength

It is reasonable to assume that the statistical distribution of the ultimate strength of virgin material,  $R(0)$ , follows a two-parameter Weibull distribution, giving such a distribution function that

$$F_{R(0)}(x) = P[R(0) \leq x] = 1 - \exp[-(x/\beta)^\alpha] \quad (3)$$

in which  $\alpha$  is the shape parameter and  $\beta$  is the scale parameter.

Similarly, the distribution function of residual strength  $R(n)$  is given in the following form with the aid of Equation (2).

$$F_{R(n)}(x) = P[R(n) \leq x] = P[R(0) \cdot \exp(-f(s)n) \leq x] \\ = 1 - \exp[-(x/\beta^*(s))^\alpha] \quad (4)$$

Where  $\beta^*(s) = \beta \exp(-f(s) \cdot n) \quad (5)$

(3) Statistical Distribution of Fatigue Life

$$F_{N_f}(n) = P[N_f \leq n] = P[R(n) \leq s] = 1 - \exp[-(s/\beta^*(s))^\alpha] \\ = 1 - \exp[-e^{f(s)n} (s/\beta)^\alpha] \quad (6)$$

Where  $f(s) = af(s)$ ,  $n(s) = -\frac{\ln(s/B)}{f(s)}$  (7)

It is quite interesting to note that the statistical distribution of fatigue life has been derived based upon the proposed model to be a well-known double exponential distribution.

(4) Extended Model

Present model might be easily extended to reflect the engineering reality for the other kinds of composites and different loading conditions.

The degradation process in such cases is given by

$$R(n) = R(0) \cdot \exp[-f(s) \cdot n^c] \quad (8)$$

in which  $c$  is a constant to be determined.

Equation (8) returns to the original model when  $c=1$ .

3. EXPERIMENTAL VERIFICATION

Figure 1 shows the residual strength distribution at the cycle ratio of 0.6 under perfectly reversed loading with stress amplitude of 80 MPa. The theoretical prediction using Equation (4) is drawn as a solid line and experimental data as circles. The correlation between test data and theoretical prediction is reasonable.

Comparison between experimental data and predicted results of residual strength were made for the various cyclic stress levels. An example of the result is shown in Figure 2 for 80 MPa. Again, good correlation between test data and theoretical predictions was obtained. Prediction by the extended model was performed for  $c=1$ . Thus, it will be possible to make a conservative estimation, as is often desired in the practical design, by the adequate adjustment of constant  $c$ .

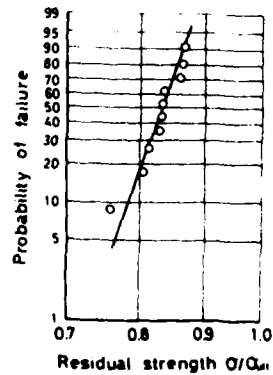


Fig.1. Distribution of residual strength.

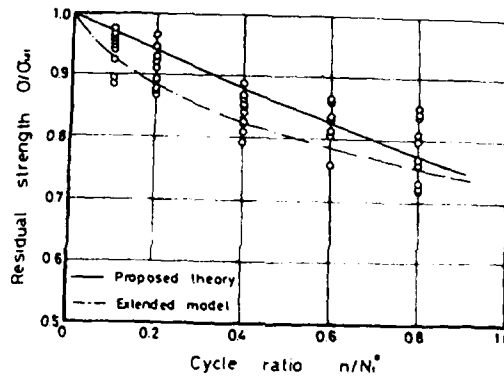


Fig.2. Degradation process of residual strength.

Effect of Stress Singularities on  
the Delamination of Laminated Composites

by

F. Delale  
Drexel University  
Department of Mechanical Engineering and Mechanics  
Philadelphia, PA. 19104

ABSTRACT

In the recent past, research in anisotropic materials in general and in layered composite materials in particular has attracted a great deal of interest. The reasons for this are the ever-increasing use of composites in many structures and the fact that the failure resistance of composites can be improved considerably without adding to the weight of the structure. In layered composite structures, one of the most important design problems is the initiation and propagation of the so-called "delamination surface". From the study of bonded isotropic materials it is known that, the stresses near a free edge have a weak power singularity and under certain loading conditions, the normal stress can be tensile, thus enhancing the possibility of delamination failure. It is clear that the severity of the power of singularity may have a decisive bearing upon the initiation and propagation of delamination surfaces. Treated as single layers, the constituents of layered composites are in general highly anisotropic. Therefore, one needs the general solution of bonded anisotropic materials. In this paper, the general problem of stress singularities occurring near the free edge of two bonded anisotropic materials is investigated. After formulating the problem of two bonded anisotropic wedges, the stress singularity near the free edge of two bonded layers, at the tip of a crack between two materials and in the vicinity of a broken layer is obtained by simply varying the wedge angles. It is shown that, the power of singularity depends on the elastic constants of the adjacent layers. Several examples occurring in real layered composites are studied in some detail. It is also shown that, unlike the isotropic case the power of singularity at the tip of a crack between two materials can be real.

Effect of Initial Stresses on the Impact  
Behavior of Graphite-Epoxy Laminates

by

B.V. Sankar and C.T. Sun  
School of Aeronautics and Astronautics  
Purdue University  
West Lafayette, Indiana 47907

In spite of their high strength and high stiffness, laminated composites are susceptible to foreign object impact damage. Some of the reasons for their poor impact strength are lack of through the thickness reinforcement, brittle matrix, and manufacturing defects which may occur during the curing process. The strength degradation may become severe if the structure is under preload at the time of impact. The present study is concerned with the low velocity impact damage in graphite-epoxy laminates subjected to initial tensile stresses.

Graphite-epoxy laminates were fabricated using 3M SP313 graphite-epoxy prepregs. The layup was  $[0_2/90_2/0_2/90_2/0_2]_s$ . The preload was applied using a pneumatic cylinder capable of exerting a load up to 20,000 N. Impact tests were conducted with a compressed air gun and a 12.7mm diameter steel ball as the projectile. Delamination area was determined by an ultrasonic C-scanning system. The residual strength was measured by performing tensile and bending tests on the impacted specimens as well as on the virgin specimens.

Finite elements were employed to study the effect of initial stresses on the impact response. Contact force and bending strain histories were calculated with a plate finite element program [1]. The numerical solution was compared with the experimental results. A two dimensional finite element which can account for the effects of initial stresses was also developed to evaluate the interlaminar stresses which are needed in developing an impact damage model.

The results show that the laminate plate theories are sufficient to predict the contact force history and the bending stresses. But from the two dimensional analysis it is found that in the vicinity of the impact point, the maximum interlaminar shear stress does not occur at the centre of the laminate, but at a point closer to the impact point. In the examples used in the present study, the maximum shear stress is in the  $90^\circ$  layer at a point about half the plate thickness away from the impact point. The effects of initial stresses on the impact force and stresses in the plate are shown in Figures 1 and 2. From Fig. 1 it may be seen that the increase in the maximum impact force and duration is only minimal for the case of low velocity impacts (about 25 m/s). Same conclusions apply to shear and bending stresses also (Fig. 2). The initial stresses are expected to play a significant role during high velocity impacts when their effect will be felt through the large deflections and large rotations of the impacted structure.

Reference

1. Chen, J.K. and Sun, C.T., "Impact Response of Buckled Composite Laminates", ASCE EMD Speciality Conference, Purdue University, May 1983.

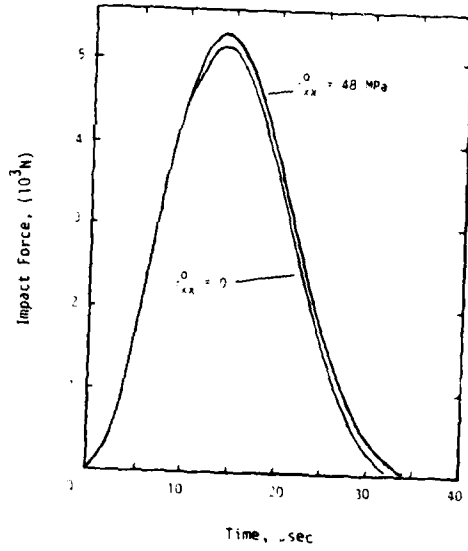


Fig. 1. Impact Force History, (Velocity = 25.4 m/s)

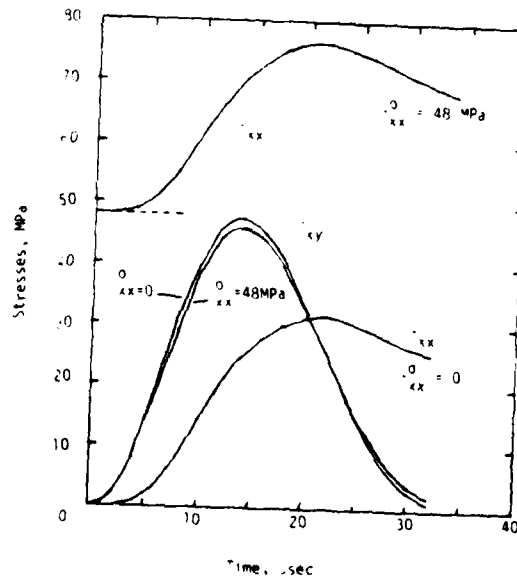


Fig. 2. Effect of Initial Stress on Bending and Shear Stresses.

by

L.W. Gause and Richard E. Llorens  
Aircraft and Crew Systems Technology Directorate  
Naval Air Development Center  
Warminster, Pennsylvania 18974

A finite element solution which predicts the strains in clamped orthotropic plates which arise as a consequence of relatively low speed (0 to 30 m/s), hard object, transverse normal impact was developed. Previous analysis of impact on both beams and simply-supported orthotropic plates showed that an undamped theoretical solution of the vibrating system, suitably corrected for damping, correlates available experimental data. This work extends those results to the analysis of the practically important problem of a clamped plate.

The technique developed represents the solution of the following physical problem. A mass of small dimensions, possessing unit velocity, is directed at a plate which is initially at rest. During impact, the impactor transfers its momentum to the region of the plate with which it is in contact. This information establishes initial conditions for the vibrating system. The plate and impactor remain in contact during the remainder of the first quarter of the first cycle of motion.

Although the present task may be completed utilizing existing general purpose finite element programs, i.e., NASTRAN, a stand-alone program was written specifically for this problem. Most solutions of the eigenvalue problem obtained using general purpose finite element programs are costly in terms of CPU and I/O time. Thus, it was an objective of this study that the resulting software considerably reduce the computer resources employed in the solution of the low velocity impact problem.

The program developed in this study possesses three operational modules: 1) a pre-processor estimates the magnitudes of the first two eigenvalues of the system, 2) a finite element program, which employs a bending element, determines the first two eigenvalues and eigenvectors of a clamped plate, and 3) a post-processor transforms the conclusions of the finite element program to a solution of the impact problem.

Observe that the pre-processor was formulated on the basis of the energy method, i.e., assuming a shape function, which satisfied the boundary conditions of the problem, the kinetic and potential energies of the system were calculated. This information was employed to generate estimates of the first two natural frequencies of the vibrating system. Generally, the resulting values of the first frequencies were approximately ten percent too large. Additionally, the average of the second frequencies was approximately twenty-five percent too large. Numerical estimates of the frequencies utilized in the finite element program were adjusted according to these observations. The fine numerical performance of the finite element solution may be ascribed to these frequency estimates.

The finite element program was constructed to provide a bending solution of the impact problem. Employing symmetry, only one quarter of the plate was analyzed. This quarter of the physical system was

subdivided into a set of ten by ten finite elements. In view of its numerical simplicity and the rapidity with which it may be performed, the inverse power method was employed to determine the eigenvalues and eigenvectors of the vibrating clamped plate. The program performs all operations in the core of the computer. Thus, the only I/O operations executed during the operation of the program are the input data and solution output transfers. Stiffness and coupled mass matrices are partitioned and stored, in core, in a minimum form. Approximately thirty-six thousand words of storage are required to contain the needed portions of the approximately three hundred by three hundred array employed to compute the eigenvectors.

Note that the post-processor is constructed to determine a modal solution of the impact event. In view of the linearity of the analysis, a unit input velocity is adopted in determining the solution of the impact problem. Further, this solution is empirically corrected for damping by employing the conclusions of damped beam theory. The program computes the strain in two perpendicular directions during the first quarter cycle of plate motion. Values of the maximum strain at the center of the plate are ascertained during this time period.

This numerical procedure determines a complete solution of the vibrational problem in slightly over four seconds of CPU time on a CDC 6600 Series Computer. The identical problem calculated on the same computer system but employing NASTRAN required slightly over thirty-four seconds of CPU time. Thus, the present program has produced a significant reduction in computer utilization.

Applying this analysis to impact tests on clamped thick plates, i.e., 48 and 52 ply, which are representative of panels on naval aircraft, it was discovered that the correspondence between theory and experiment was quite good. Additionally, values of damping obtained for the present experiments coincide with the damping constants determined for simply supported plate tests. In the case of the thin plate series, i.e., 24 ply, the correlation was not good. It appears that another physical mechanism is operative during the thin plate experimental investigation. Of the possible omissions, the effects of in-plane stretching represent the most likely variable which is needed to improve the correlation.

Resonant Scattering of Waves in Random  
Particulate Composites

by

Vikram K. Kinra  
Aerospace Engineering Department  
Texas A&M University  
College Station, Texas 77843

Scattering of longitudinal waves in three different random particulate composites has been studied experimentally: lead spheres/epoxy, glass spheres/epoxy, and steel spheres/PMMA. The phase velocity of longitudinal waves,  $\langle C_1 \rangle$ , and their absorption were measured at low, medium and high frequencies:  $0.15 < \omega < 5.0 \text{ MHz}$  or  $0.25 \leq k_1 a \leq 8$ , where  $a$  is the inclusion radius and  $k_1$  is the longitudinal wave number in the matrix. A wide range of volume fraction of inclusions was studied, namely  $5 < \bar{C} < 50\%$  nominal. At low frequencies,  $k_1 a < 1$ , the data were found to be in very good agreement with static analyses, e.g. [1]. At high frequencies,  $k_1 a \gg 1$ , the results were found to be drastically different: the velocity takes a finite positive jump across a well defined cut-off frequency,  $\omega_c$ ; and it appears to attain a frequency independent limit at high frequencies (optical limit). Very recently, these results have been simulated at low concentrations by a rather elementary but very effective theoretical model [3].

Moon and Mow [2] carried out an approximate analysis of the problem. They postulated the existence of an acoustical branch and an optical branch separated by a cut-off frequency. Our data exhibits both these branches. We have also studied explicitly the phenomenon of resonant scattering. The amplitude of the signal received through a specimen was measured as a function of frequency; sharp minimum indicated the resonance. Excellent agreement was noted between the measured and the predicted values of the cut-off frequency over a wide range of  $\bar{C}$ .

References

- [1]. Z. Hashin and S. Shtrikman, J. Mech. Phys. Solids, 11, p. 127.
- [2]. F. C. Moon and C. C. Mow, Rand Corporation Rep. RM-6139-PR, Rand, Santa Monica, CA (1970).
- [3]. C. M. Sayers and R. L. Smith, AERE-R 10722, AERE Harwell, Oxfordshire, England.

## Impact and Fatigue of Graphite/Epoxy Laminates

by

William G. Patterson and Minoru Taya  
Department of Mechanical and  
Aerospace Engineering  
University of Delaware  
Newark, Delaware  
19711

The widespread use of composite materials such as graphite/epoxies, particularly in aerospace applications, has been widely discussed. One apparent shortcoming of these materials has been found in their lack of resistance to foreign object damage, especially impact.

In this study, 8 ply laminates supported by aluminum honeycomb sections were impacted using an ETI 300 instrumented drop-weight impact system; and then either tension fatigued, or examined ultrasonically and microscopically.

Hercules AS4/3501-6 graphite/epoxy prepreg was used to lay up three laminates: (0)<sub>8</sub>, (+45)<sub>2</sub>, and (0/+45/90). Cured panels were end-tabbed and cut into coupons 1/2 inch wide by 9 inches long. The specimens were then set on honeycomb sections 1/2 inch wide by 1 1/4 inches thick, and impacted. The drop-weight had a total weight of 5 1/2 pounds, and a cylindrical indenter of 1/8 inch radius. Specimens were impacted across their full width.

Data obtained from these experiments includes impact load/time and energy/time traces from the ETI 300, residual static and fatigue strength, ultrasonic C-scans and SEM photographs of as-impacted specimens, and fractographs of failed specimens.

The analysis of the data includes comparing the residual strength properties of the different stacking sequences by relating them to several impact parameters. These parameters include NDE data obtained from the C-scans, and the energy absorbed by the specimens during impact.

THE EFFECT OF MATRIX PROPERTIES AND FIBER PROPERTIES  
ON IMPACT FAILURE MECHANICS

W. Elber  
NASA Langley Research Center  
Hampton, Virginia 23665

Abstract of Paper Proposed for the  
20th Annual Meeting of the Society of Engineering Science, Inc.  
August 22-24, 1983  
Newark, Delaware

The low-velocity impact problem in graphite/epoxy composite sheets must be solved before large amounts of that material can be used in commercial aircraft. Many of the low-velocity impacts that affect aircraft parts occur during normal ground operations and maintenance. Service equipment and tools have masses above 1 kg, and at velocities of less than 3 m/s can impact structural parts with energies higher than composites can endure without degradation of stiffness or strength. Because of the point load characteristics of impacts from rigid bodies, most of the problems involve large local deformations in the elastic regime, and the penetration failure is usually purely a stretched membrane problem. From a computational view, it is prohibitive to model large deformations, as well as stiffness changes during failure, together with time-dependent mechanics.

In this study, simple solutions have therefore been developed for those large-mass, low-velocity impacts which can be modeled as quasi-static events. Static test data and impact data have shown that the fiber properties control the impact energy which can be absorbed before penetration. Matrix shear strength and peel resistance control the extent of delamination. Comparison of results from tough matrix and brittle matrix composites have shown that although tough matrices reduce the extent of delamination, they lead to more fiber damage in the contact area.

These results have led to the conclusion that both tougher fibers and tougher matrices are required to significantly raise the impact resistance of graphite fiber composites.

APPLICATION OF STRESS-GENERATED HEAT IN COMPOSITES  
TO THERMOGRAPHIC NDI

by

Philip V. McLaughlin, Jr., and Mukesh G. Mirchandani\*  
Department of Mechanical Engineering  
Villanova University  
Villanova, PA 19085

This paper evaluates the use of cyclic stressing of fiber composite materials as a means of generating detectable heat in flawed regions of composite structures for flaw detection purposes.

A combined analytical/experimental investigation is conducted which enables the viscoelastic heat generated in polymeric matrix composites to be predicted from applied peak loads and loading frequency. Elastic stresses in the matrix of unidirectional fiber composites are calculated using the composite cylinder assemblage of Hashin and Rosen. Tests show that the peak stresses under viscoelastic cyclic loading do not differ significantly from those predicted from an elastic analysis. Therefore, the elastic stress distribution is used in conjunction with a three-parameter linear viscoelastic matrix model to derive the following equation for energy dissipation rate density,  $\dot{D}$  (heat energy generated per unit composite volume per unit time):

$$\dot{D} = \omega^2 S_{ij}^0 S_{ij}^0 / [2\pi(A+B\omega^2)] \quad (1)$$

Where  $\omega$  is cyclic loading frequency,  $S_{ij}^0 S_{ij}^0$  is the volume averaged second invariant of the matrix stress deviator and A and B are viscoelastic material constants. The constants A and B were determined empirically from cyclic tests of unidirectional glass/epoxy and graphite/epoxy materials.

The energy dissipation rate density is used in conjunction with finite element stress analysis and finite difference heat transfer analysis of  $[0/\pm 45/90]$  glass/ and graphite/epoxy laminates to predict the surface temperatures in the vicinity of flaws. Cyclic tension tests are conducted on these same laminates, and surface temperatures are measured with an infrared camera. Good agreement is obtained between analysis and test.

---

\* Professor and Graduate Research Assistant, respectively

The heat generation analysis is then used to investigate the effects of stress amplitude and cyclic frequency upon surface temperatures of glass/epoxy and graphite/epoxy specimens. It is demonstrated that, for these laminates, heat generated near flaws due to matrix viscoelasticity is insufficient to cause surface temperature differences which would allow flaw detection by infrared thermography. It is also shown that large amounts of heat can be generated near flaws if considerable damage and/or frictional rubbing of crack surfaces occurs during testing.

It is concluded that infrared measurement of stress-generated heat near flaws is not a viable method of flaw detection unless friction between flaw surfaces is the primary generation mode. It is postulated that frictional heat is generated during the "vibrothermography" delamination detection method of Reifsnider, Henneke and Stynchcomb.

## Observations on the Fracture of Fibrous Composites

by

Bruce A. Yost  
Dr. R. Byron PipesCenter for Composite Materials  
University of Delaware  
Newark, DE 19711

The fracture behavior of several composite material systems subjected to uniaxial tensile loads at ambient temperatures and containing through cracks 0.635 cm (0.250 in) to 2.54 cm (1.00 in) in length, was examined. The crack growth patterns and failure mode of each material system were recorded in a series of photographs and comparisons were made. Two distinct crack growth patterns and failure modes were observed, depending upon the orientation and length of the fibers. The notched strength data indicate that each material system exhibits a region of notch insensitivity, beyond which notched strength decreases with increasing crack size. Moreover, the fracture behavior of one of the randomly oriented, short fiber systems was further examined at low temperatures, i.e.  $-73^{\circ}\text{C}$  ( $-100^{\circ}\text{F}$ ) and  $-129^{\circ}\text{C}$  ( $-200^{\circ}\text{F}$ ). These results indicate that the notch insensitivity of this particular material system increases with decreasing temperature. Several of these specimens exhibited both a tensile and a compressive failure mode.

"An Integral Optical Method for Determining Stress Intensity Factors"

by

C. W. Smith, J. S. Epstein and O. Olasebikan  
Department of Engineering Science and Mechanics  
Virginia Polytechnic Institute and State University  
Blacksburg, Virginia 24061

The determination of stress intensity factor distributions during the sub-critical flaw growth regime preceding service fracture usually involves complex geometries since cracks usually start in regions of high stress near reinforced junctures of structural members. Moreover, flaw growth may be non-self-similar and non-planar with the flaw shape at any given stage of growth not known a-priori. In order to construct appropriate numerical models for such situations, one needs to know flaw shapes and the relative contribution of the various boundaries other than crack surfaces.

For over a decade, the first author and his associates have been working towards the development of an experimental optical modeling technique for predicting flaw shapes and corresponding stress intensity distributions for complex three dimensional cracked body problems. The first stage of the development involved a photoelastic model for Mode I problems [1] and this method was then extended to mixed mode problems [2].

In its current state [3][4], the method involves the use of frozen stress photoelasticity and high sensitivity Moire interferometry to obtain optical data at intervals along the border of real cracks grown under service load conditions. These data are then converted into independent stress intensity factor estimates through the use of simple algorithms.

After briefly reviewing the method as it is currently applied, and delineating the restrictions and limitations of the method, this paper will focus upon some features pertaining to three dimensional continuum effects in near tip structural mechanics not previously measured. In particular, the region surrounding the point of right angle intersection of a crack with a free boundary will be discussed in some detail.

#### References

- [1] Smith, C. W., "Use of Three Dimensional Photoelasticity and Progress in Related Areas", Experimental Techniques in Fracture Mechanics, 2, A. S. Kobayashi, Ed., SESA Monograph, Iowa State Press, Chapter 7, pp. 3-58, 1975.
- [2] Smith, C. W., "Use of Photoelasticity in Fracture Mechanics", Mechanics of Fracture, 7, G. C. Sih, Ed., Martinus-Nijhoff, Chapter 2, pp. 163-187, 1981.
- [3] Smith, C. W., "Use of Optical Methods in Stress Analysis of Three Dimensional Cracked Body Problems", Journal of Optical Engineering, Vol. 21, No. 4, pp. 696-703, July/Aug. 1982.
- [4] Smith, C. W. and Epstein, J. S., "Observations from Modelling of Sub-Critical Flaw Growth by Optical Methods" (In Press), Proc. of NSF Workshop on Damage and Fracture, Nov. 1982.

ON THE ANALYSIS OF THICK WALLED COMPOSITE MATERIAL  
CYLINDRICAL SHELLS

by

T. L. Waltz  
Hercules, Inc.

J. R. Vinson  
University of Delaware

Methods of analysis are developed for very thick cylindrical, specially orthotropic shells. In the radial direction, all dependent variables are placed in terms of Legendre polynomials, or closely related functions, which have desirable properties. The present theory is an elasticity theory solution, does not employ any shell theory assumptions, and is approximate only in that the infinite series of Legendre polynomials and the closely related functions are truncated.

The theory is developed starting with the elasticity equations in a circular cylindrical coordinate system. All assumptions are given and discussed. Explicit solutions are given for the following axially symmetric problems:

1. A semi-infinite shell with transverse shear stresses acting along the edge.

2. A semi-infinite shell acted upon by axial in-plane edge stresses which are directly proportional vectorially to the distance from the shell middle surface (i.e. analogous to a stress couple).

3. A semi-infinite shell acted upon by axial in-plane edge stresses which do not cause bending (i.e., analogous to an in-plane stress resultant).

4. A shell of infinite length subjected to a constant lateral distributed loading on either the inner or outer lateral shell surface or both.

5. A shell of infinite length subjected to a lateral distributed load varying linearly in the axial direction.

It is found that the stress loadings of the first three problems above can be integrated across the shell thickness, such that the loadings are transverse shear resultants, stress couples, and in-plane stress resultants, identical to those of classical shell theory. The solutions of the first two problems therefore provide the edge load solution form of the homogeneous equations for a shell of finite length. The third solution accounts for axial loads in a finite length shell, such as those introduced in pressure vessels by closures. Solutions four and five provide the particular solutions for the cylindrical shell being under internal and external uniform pressure, and under a hydraulic heat, respectively. Hence, these five solutions provide a complete elastic analysis of very thick walled pressure vessels of a specifically orthotropic material subjected to hydraulic and/or pneumatic loading. The solutions are also applicable to thin walled shells as well.

The analytical results can be easily programmed for digital calculation of the stress and deformations of pressure vessels of specific geometry, material, and loading.

## CRACK-GROWTH RESISTANCE OF LAMINATED HYBRID COMPOSITES

S.K. Chaturvedi and C.T. Sun  
Department of Engineering Sciences  
University of Florida, Gainesville, FL 32611

It is generally recognized that a structural composite element having particular fibers and matrix along with a kind of lamination may not provide us with all the advantages that may be necessary and desirable for high performance applications. The hybridization, in such cases, seems to offer unlimited possibilities that can be considered in achieving a more favorable balance between advantages and disadvantages inherent in any composite material system.

The present work is aimed at characterizing the crack-growth behavior of hybrid composites having two different stacking sequences, namely;  $[C/1/2R/C/1/2R/C]$  and  $[R/C/1/2R/C/1/2R/C/R]$  to be designated here as material A and material B, respectively. The letter C in these hybrids represents a 50% weight fraction continuous fiber composite (glass-polyester) layer while the R represents a 50% weight fraction randomly oriented chopped fiber composite (glass-polyester) layer. The standard compact tension specimens having notches oriented along and perpendicular to the fiber direction of the C layers to be designated, respectively, as A-0, B-0, and A-90, B-90 with the a/w (notch length/specimen width) ratios as 0.3, 0.4, 0.5, 0.6 and 0.7 were chosen. The fracture-resistance of the specimens A-0 and B-0, for which a self-similar crack-growth was observed, was calculated using the K-calibration technique, and also the method that uses the load  $P_{max}$  at which incipient crack-growth occurs.

For the specimens A-90 and B-90 where the observed crack-growth was in the direction perpendicular to the notch direction, i.e., a non-self-similar crack-growth, the theory of linear elastic fracture mechanics cannot be applied. The flexural strength is purported to be an adequate parameter for crack-growth characterization of such cases.

Based upon the numerical results, it is observed that the fracture resistance of A-0 and B-0 specimens is significantly greater than the pure 0-degree layered composite, but only relatively lower than the pure chopped fiber composite. This fracture resistance does not appear to be sensitive to the stacking sequence for these composites. For the A-90 and B-90 specimens the fracture resistance (the flexural strength) is found to be close to their transverse tensile strengths. Finally, a rule-of-mixture relationship based upon the crack-energy release rates of the C layers and R layers is proposed to predict the fracture toughness of such hybrids. Further, it is asserted that the similar theories based upon the critical stress intensity factors proposed in the literature appear to be misleading.

1. Sun, C.T. and Sierakowski, R.L., "Fracture Characterization of Composites With Chopped Fiberglass Reinforcement," SAMPE Quarterly, p. 15, July 1980.
2. Chaturvedi, S.K. and Sun, C.T., "Fracture Toughness of Laminated Hybrid Composites," Presented in a Research Workshop on "Advancements in Hybrid Composite Materials", Sponsored by Army Research Office, Nov. 9-10, 1982, Palm Beach, Florida.

by

Ferdinand Freudenstein  
Department of Mechanical Engineering  
220 Mudd Building  
Columbia University  
New York, NY 10027

The computer-aided design of mechanisms and mechanical systems has made extraordinary progress in design analysis and optimization. Computer-aided approaches in the creative design of mechanisms, on the other hand, are still in the research stage. Such approaches can be expected to make their appearance within the next three to five years.

Creative design begins with a consideration of the kinematic structure of mechanisms (i.e.: the nature of the joint connection between links) and includes precise definitions of the terms kinematic pairs, links, mechanisms, independent loops and degree-of-freedom. Next we consider the abstract representation of the kinematic structure of mechanisms (1965+) in terms of linear graphs in which vertices correspond to links and kinematic pairs to labeled edges. The advantages of such a representation are summarized (network properties directly applicable to mechanisms, unique identification of mechanisms etc.).

The mathematical representation of kinematic structure leads directly to a discussion of a systematic method for the creation of mechanisms according to the separation of structure and function. This approach represents a combination of theory and engineering judgement and involves a systematic, unbiased search through the kinematic structures of potentially useful mechanisms satisfying the given motion requirements.

Current capabilities of this approach are illustrated by means of the following examples:

- \*Creation of multi-link mechanisms, including plane linkages and constant-velocity shaft couplings.

- \*Development of a variable-stroke internal-combustion-engine mechanism.

- \*Concept evaluation: application to the analysis of a mechanical patent.

Next we explore some current research areas, including the following:

- \*A new classification scheme for mechanical patents, its potential for cross-indexing and determining novelty; possibility of the development of a reference atlas of mechanisms along the lines of kinematic structure.

- \*Partial automation of the creative design process. This involves the computer-aided determination of the kinematic structure of mechanisms fulfilling given motion requirements. Such a development requires certain theoretical developments involving the special properties of the graphs of mechanisms and algorithms for their enumeration. The latter may involve further developments of the classical results of Whitney, Weinberg and others and/or heuristic approaches.

\*Development of a unified design procedure in which creative design is part of an integrated computer-aided design procedure which includes kinematic, dynamic and stress analysis, optimization and other CAD/CAM capabilities. Eventually one can envisage developments - which may be a generation away - such as the inclusion of logical, hydraulic, pneumatic and electrical design in a single interactive computer-aided design system.

Concluding remarks will explore the ultimate limits and capabilities of such approaches and relate these to some remarkable exceptional cases in the areas of kinematic art and molecular biology.

Automated Dynamic Analysis of Mechanisms  
with Flexible Links

by

Burton Paul  
Asa Whitney Professor of Dynamical Engineering  
Department of Mechanical Engineering  
and Applied Mechanics  
University of Pennsylvania  
Philadelphia PA 19104

This paper is focussed on the development of analytical and numerical methods for the dynamics and kinematics of linkage machinery--methods which are suitable for automatic formulation and solution of the differential equations of motion.

The methods proposed use a set of redundant coordinates termed Lagrangian coordinates as well as the classical (independent) generalized coordinates. The Lagrangian coordinates are shown to be especially well-suited to problems involving closed loops of links, and make it extremely convenient for users to pose constraint relationships of a most general type--both holonomic and nonholonomic. In addition, the topology of the vector network inherent in any linkage mechanism is exploited to find the equations of constraint due to loop closure, in a systematic readily programmable procedure.

The procedure used to automatically formulate and numerically integrate the differential equations of motion for the general dynamics problem is based on the d'Alembert-Lagrange generalization of the method of virtual work. The order of the system of differential equations is kept low by automatically eliminating Lagrangian coordinates associated with loop closures, but the very general constraints (of unknown structure) imposed by users (e.g. the simulation of nonlinear feedback) are treated by the method of Lagrange Multipliers.

Based upon these concepts, programs have been developed for the automatic formulation and solution of planar kinematic chains with arbitrary forces applied. Arbitrary constraints--in addition to those inherent in loop closure, and the common forms of joint construction (hinges, sliders, gears, and cams)--are readily input by users, and are properly processed internally.

Examples are given of how the simulation proceeds for various systems with rigid links. It is also shown how it is possible to model flexible links so that the same computer programs can perform dynamic analyses of the highly nonlinear vibrations of flexible link mechanisms--without restriction to small rotations or to small departures from the unstrained state.

## A Designer's Perception of Computer-Aided Design

by

Warren P. Seering  
Department of Mechanical Engineering  
Massachusetts Institute of Technology  
77 Massachusetts Avenue  
Cambridge, MA 02139

Computer-Aided Design is an area which is receiving a great deal of attention currently. Yet in most cases, work being done could more correctly be categorized as computer-aided analysis or computer-aided drafting. And for these applications, existing systems are very valuable. But existing hardware and software systems are generally not set up to be of great value to the conceptual designer.

This task will center on the needs of the mechanical designer and on the configuration of several computer-aided design systems proposed by the author to more effectively meet these needs. A brief history of computer-aided design in the United States will be followed by a discussion of current trends and of possible alternatives.

OPTIMIZATION OF HIGH SPEED LINKAGES

by

Ting W. Lee  
Associate Professor  
Department of Mechanical and Aerospace Engineering  
Rutgers University  
New Brunswick, New Jersey 08903

This paper presents an analytical and computer-aided procedure on the optimum design of linkages for high speed operation. The subject is treated in two parts. Part I concerns the development of an optimality criterion on the dynamic balancing of linkages, involving an analytical formulation using both the Lagrangian as well as the Newtonian approach. The major emphasis is on the development of a criterion which is capable of providing for a trade-off on the minimization among various quantities such as input torque, force and moment, as well as being efficient in its numerical evaluation. In Part II, a unit computer package for the design of high-speed linkage is described. The effects of the design parameters on the linkage performance are then investigated and design guidelines are presented. The computational procedure involves the utilization of an effective optimization algorithm, namely the HOT code (Heuristic Optimization Technique of Lee and Freudenstein [1]), on the minimization of an objective function involving the dynamic balancing criterion developed in Part I and a high-speed performance criterion proposed by Funabashi and Freudenstein [2]. Using this procedure, the design model is demonstrated, in examples, to offer better dynamic performance than the models designed through conventional techniques.

There are several remarks worth mentioning and perhaps these may be considered a contribution. Firstly, a novel approach to the balancing problem is presented. It includes the presentation of a new and direct criterion for optimum balancing and an analytical formulation which is numerically very efficient to evaluate. Secondly, the HOT code is used and it efficiently reaches a solution. Both these reasons, it is believed, have contributed to an approach which will facilitate considerably the computation in the search for an optimum solution on the design of high speed linkage. Furthermore, in this paper, definitions of shaking force, shaking moment, input torque and the associated optimization problem are clearly made in order to provide the practicing engineer with a better understanding of the subject.

References

1. Lee, T. W. and Freudenstein, F., "Heuristic Combinatorial Optimization in the Kinematic Design of Mechanisms, Parts 1 & 2," ASME Journal of Engineering for Industry, Vol. 98, No. 4, Nov. 1976, pp. 1277-1284.

2. Funabashi, H. and Freudenstein, F., "Performance Criteria for High-Speed Crank-and-Rocker Linkages, Part I: Plane Crank-and-Rocker Linkages," ASME Journal of Mechanical Design, Jan. 1979, pp. 20-25.

**KINSYN and Micro KINSYN™  
User-Friendly Computer Systems for Linkage Design**

by

Roger E. Kaufman  
Professor of Mechanical Engineering  
The George Washington University  
Washington, DC 20052

and

Murali Raju Dandu  
Member of Technical Staff  
KINTECH, Inc.

KINSYN was the first interactive computer system developed for the synthesis of linkage mechanisms. When it was first introduced (circa 1970) it ran on an 8K IBM 1130 and cost about \$50.00/hour for computer time. Now, four KINSYN generations later, a Micro KINSYN™ system has been developed which runs circles around the old IBM version and costs practically nothing per hour to run. It runs on an Apple II™ computer. Many people have one at home and think of it as a machine for playing video games. Can a machine that plays Space Invaders be taken seriously as a computer??

This live demonstration of Micro KINSYN™ will show that so-called 'personal' computers are far from toys. They can perform some very serious number crunching and can be extremely cost-effective tools for computer-aided design. In many engineering applications, modern personal computers can out run the large machines of a decade ago. While they may not have the inherent CPU speed of a mainframe system, they can often provide the same- or better- turnaround time. From the point of view of the user sitting at the display thinking, a little Apple may be a much more effective companion than an expensive mainframe hooked up at the end of a phone line.

Micro KINSYN™ is a hardware/software system for the synthesis and analysis of linkage mechanisms. It allows one to quickly and easily design four-bar linkages capable of exactly meeting specified performance requirements.

One of the main features of Micro KINSYN™ is its 'user friendly' dialogue. The system is almost self teaching. It allows a user with little or no specialized training in either kinematics or computers to quickly and effectively design mechanisms using sophisticated kinematic theories. Due to the specialized hardware developed for Micro KINSYN™, communication with the machine takes place by a natural, graphical dialogue. Control dials light up to prompt the user when they can be used and mnemonic menus prompt the user when typed input is required. On-line help is always available, simply by typing 'H' at the keyboard. The dialogue has been carefully structured to utilize the strengths of the available hardware while recognizing its limitations.

While most of this system is coded in Pascal, a large section needed to be implemented in hardware in order to achieve the necessary power and speed in a microcomputer-based system. The overall system includes an Apple II™, a printer, two disk drives, a specialized Micro KINSYN™ circuit board that plugs into the Apple, a Micro KINSYN™ control box that connects to this circuit board, and the necessary software on floppy diskettes. Much of

Micro KINSYN™ is coded in assembly language and burned into eproms on the special circuit board.

If time permits, after the demonstration of the Micro KINSYN™ system, the latest implementation of the full version of KINSYN will be discussed. This runs on a Vax 11/780 computer using a Megatek display. It treats a much wider class of problems than does the micro version and is undoubtedly the most powerful mechanism synthesis system available today. Many complex problems require this added flexibility and power which can only be achieved through the use of large computers and high-performance displays. At the same time, however, the majority of four-bar linkage synthesis problems can be handled very nicely on a well-designed "personal" computer system. For those linkage synthesis problems, Micro KINSYN™, is probably the most cost-effective tool in existence.

## Dynamic Stability of High Order Linear Systems

by

Maurice I. Young  
 Department of Mechanical and Aerospace Engineering  
 University of Delaware  
 Newark, Delaware 19711  
 U.S.A.

The dynamic stability of a linear system with a large number of degrees of freedom can be examined effectively by considering the influence of the many system parameters on the purely imaginary eigenvalues<sup>1</sup> of the 2Nth order dynamic matrix  $D \equiv B^{-1}A$ , given the matrix differential equation  $A\dot{x} + Bx = 0$ , where  $x = \bar{x}e^{\lambda t}$  and  $D\bar{x} = \lambda^{-1}\bar{x}$ . This approach quickly yields the boundary of system dynamic stability as an explicit function of the systems parameters, provided the system characteristic equation can be determined for the boundary case when  $\lambda = j\omega$ , where  $j^2 = -1$ . This can be done in a straightforward manner employing the principal minor determinants of  $D$ .<sup>2</sup> This yields the stability boundary

$$(j\omega)^{-2N} - A_1(j\omega)^{-(2N-1)} + \dots + (-1)^i A_i(j\omega)^{-(2N-i)} + \dots + (-1)^{-2N} A_{2N} = 0,$$

where  $A_i$  is given by the sum of all  $i$ -rowed principal minor determinants of  $D$ . Since both the real and imaginary parts of the foregoing equation must be satisfied simultaneously, the stability boundary follows at once as

$$\begin{aligned} &\omega^{-2N} + A_2(j)^2 \omega^{-(2N-2)} + \dots + A_2(j)^2 \omega^{-2} + A_{2N} \\ &= A_1(j)^{(2N-2)} \omega^{-(2N-1)} + A_3(j)^{(2N-4)} \omega^{-(2N-3)} + \dots + \\ &+ A(j)^4 \omega^{-3} + A(j)^2 \omega^{-1} \\ &\quad 2N-3 \quad \quad 2N-1 \end{aligned}$$

A detailed numerical example of the procedure is presented which illustrates the calculation of critical parameter values and the frequency of oscillation at the stability boundary. An approximative method for rapid estimates of stability is also discussed. This employs the principal minor determinants of first and second order only.

1. Wiberg, Donald T., State Space and Linear Systems, McGraw-Hill Book Company, 1971, pp. 69-98.
2. Ayres, Frank, Jr., Matrices, McGraw-Hill Book Company, 1962, pp. 151-152.

SURVIVAL PROBABILITY OF NON-LINEAR OSCILLATORS SUBJECTED  
TO BROAD-BAND RANDOM DISTURBANCES

by

P. D. Spanos  
Engineering Mechanics  
University of Texas  
Austin, TX 78712

A method is presented for determining the survival probability of the response amplitude of a class of lightly damped non-linear oscillators which are subjected to a stationary broad-band random disturbance. The method is based on modeling the response amplitude by a Markovian process. This modeling leads to a backward Kolmogorov equation which is satisfied by the survival probability. For the case of a linear oscillator, the solution of this equation has been determined in the literature by using the technique of separation of variables. This technique leads to a boundary value problem, the eigenfunctions of which are a set of orthogonal confluent hypergeometric functions. The associated eigenvalues corresponding to typical values of the barrier have already been presented in the literatures [1]. The orthogonality of this particular class of hypergeometric functions and the availability of the associated eigenvalues, is the basis of developing approximate methods of solving the backward Kolmogorov equation which governs the survival probability of the non-linear oscillators. Specifically, formulae for application of the Galerkin technique and of a perturbation technique are developed [2]. As an example of application of the Galerkin technique, the response of the well known Van der Pol oscillator subjected to white noise is considered. Based on digital data generated by Monte Carlo studies regarding the survival probability of the oscillator and the first-passage time probability density, it is shown that a Galerkin solution with ten (10) basis-functions is quite adequate. Furthermore, it is seen that for small values of the coefficient of the non-linear term of the Van der Pol oscillator, the survival probability of the response amplitude is a close approximation of the survival probability, with respect to a D-type barrier, of the oscillator response itself. However, it is found that the quality of this approximation deteriorates as the strength of the non-linear term increases.

## REFERENCES

- [1]. Spanos, P-T. D., "Numerics for Common First-Passage Problems." Journal of the Engineering Mechanics Division, American Society of Civil Engineers, Vol. 108, No. EMS, 1982, pp. 864-881.
- [2]. Spanos, P-T. D., "Survival Probability of Non-Linear Oscillators Subjected to Broad-Band Random Disturbances," International Journal of Non-Linear Mechanics, Vol. 17, No. 5/6, 1982, pp. 303-317.

CONSERVATION LAWS FOR SOME SEPARABLE  
GYROSCOPIC DYNAMICAL SYSTEMS (\*)

Leon Y. Bahar & Harry G. Kwatny  
Department of Mechanical Engineering & Mechanics  
Drexel University  
Philadelphia, PA 19104

ABSTRACT

Until recently, the main approach to the study of conservation laws for non-conservative dynamical systems was largely based on group-theoretic methods leading to various generalizations of Noether's Theorem. In a series of papers, the authors developed a method based on the inverse problem of variational calculus, which generates conservation laws in the form of first integrals or constants of the motion in a more direct manner. This makes the new methodology more accessible to a wider audience of engineers, whose interest in problems such as system stability requires advance knowledge of such conservation laws. Typical results of this effort will be found in [1].

In a recent paper, Vujanović [2] used a geometric approach to develop conservation laws for non-conservative dynamical systems. The present investigation shows that it is often simpler to exploit certain properties inherent to the system in arriving at conservation laws. For the sake of specificity, this paper concentrates on a typical problem treated in [2], that of the Foucault pendulum which is now viewed as a special case of a gyroscopic system. By exploiting the separability and commutativity properties of a dynamical system, as defined in [1], which are automatically satisfied in this instance, it is shown that the governing equations of motion can be uncoupled, thus yielding three time-independent and one time-dependent integrals. The Vujanović invariants which appear to be complicated at first glance [2] are shown to be linear combinations of the conservation laws expressed in the original coupled variables. The paper concludes by embedding the results obtained into the inverse problem of Lagrangian dynamics.

(\*) To appear in Solid Mechanics Archives.

REFERENCES

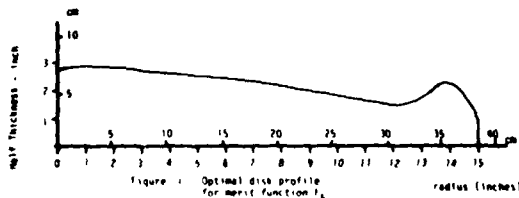
1. Bahar, L.Y., and Kwatny, H.G., "Some Remarks on the Derivability of Linear Nonconservative Systems from a Lagrangian," Hadronic Journal, Vol. 3, No. 4, June 1980, pp. 1264-1280.
2. Vujanović, B.D. "A Geometrical Approach to the Conservation Laws of Non-Conservative Dynamical Systems," Tensor (New Series), Vol. 32, No. 3, 1978, pp. 357-365.

Optimal Design of Rotating Disk  
with Temperature Gradient

L. W. Hu and X. C. Pan  
The Pennsylvania State University

For turbine wheels, it is generally recognized that the so-called 'constant strength' profile is the best design for a solid disk of uniform temperature. It can be shown that such a 'constant strength' stress state does not exist for disks with temperature gradient. Therefore, the quest for the ideal design must be restated: what is the best profile for a rotating disk under given operating conditions with stress field of desired characteristics? Namely, the profile design is reduced to a problem of optimization with multiple variables.

To this end, an optimization scheme is developed on the basis of Zheng's Method\* in searching for the global minimum. By taking the thickness of the disk at a number of points along the radius of the disk as variables, a procedure for design is established to minimize a merit function which is formulated by incorporating the desired characteristics of the stress field with specified bounds on the thickness of the disk. The feasibility and the practicality of the method are demonstrated by applying it to five numerical examples. For a computation time limited to 100 seconds with an IBM 370 system, each case yields excellent results. For example, consider a solid disk of outside diameter of 30 in. made of a steel with  $E = 29 \times 10^6$  psi,  $\nu = 0.3$  and  $\rho = 7.2 \times 10^{-4}$  lb-mass/in<sup>3</sup>. Operating velocity is 6000 RPM with temperature at the center = 300°F and temperature at outer boundary = 960°F. It is specified that the thickness of the disk cannot exceed 6 in. nor can be less than 2 in. For a given "dead" rim load, to minimize the shear stress at the outer boundary as well as to keep the normal stress as low as possible, we obtain the optimal profile as shown in Fig. 1. The corresponding stress field is shown in Fig. 2.



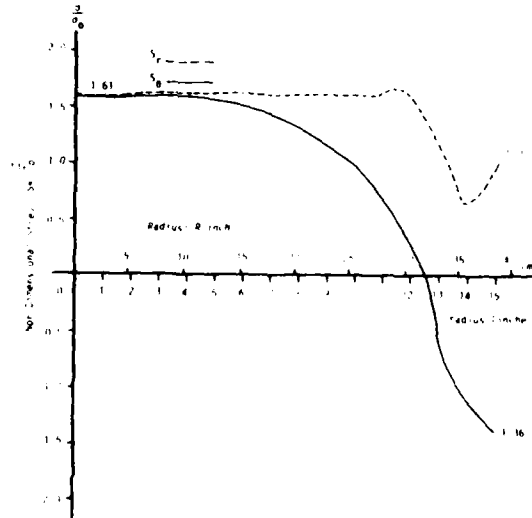


Figure 1. The optimal profile for a rotating disk.

In conclusion, the paper shows that an optimal profile of a rotating disk with temperature gradient for given design specifications can be obtained. The method presented proves to be both practical at trivial cost and theoretically sound as established in the reference cited.

\*Q. Zheng, B. Z. Jiang & S. L. Zhuang: A Method for Finding Global Extremum", ACTA Mathematica Applicatae Sinica, Vol. 1, No. 2, pp. 161-174, 1978.

Nonlinear Vibrations of a Rubber Support System  
Constrained by a Fixed Surface

by

Millard F. Beatty  
Department of Engineering Mechanics  
University of Kentucky  
Lexington, KY 40506

The finite amplitude, free nonlinear oscillation of a mass attached to a neo-Hookean, rubber spring support and constrained to move on a smooth plane surface is solved exactly. The solution is obtained for both compression and suspension supports in terms of the beta and lambda-functions defined in [1]. The periodic times for all cases are thus derived in terms of the tabulated Heuman lambda-function [2]; and the physical conclusions are described graphically.

References

- [1] Beatty, M.F., Finite amplitude oscillations of a simple rubber support system. Arch. Rational Mech. Anal. (in press).
- [2] Heuman, C., Tables of complete elliptic integrals. J. Math. & Phys. 20 (1941), 127-206. Errata. Ibid., 336.

## CRITICALLY DAMPED DYNAMIC SYSTEMS

D. J. Inman  
 Department of Mechanical & Aerospace Engineering  
 State University of New York at Buffalo  
 Buffalo, New York 14260

I. Orabi  
 Department of Mechanical & Industrial Engineering  
 Clarkson College  
 Potsdam, New York 13676

Recently several authors [1,2] have extended the single degree of freedom concept of critical damping to lumped parameter systems with  $n$ -degrees of freedom. This work compares those definitions and derives a new method of calculating the critical damping condition. The method is more efficient than those given previously and insures that each mode is critically damped. The computational savings results because the method proposed here does not require the calculation of eigenvectors or derivatives as the other methods do. A four degree of freedom example is given to indicate the effectiveness of the result.

The systems considered are those successfully modeled by the vector differential equation

$$M\ddot{x} + D\dot{x} + Kx = 0 \quad (1)$$

where  $M$ ,  $D$  and  $K$  are real symmetric  $n \times n$  positive definite matrices and  $x$  is a  $n$ -vector of generalized displacements. The over dot indicates differentiation with respect to time. Such systems are shown to be critically damped in each mode if

$$D = \sum_{j=0}^{n-1} \beta_j K^j$$

where  $\beta_j = \sum_{i=0}^{n-1} \omega_j^{i+1}$ . The positive real numbers  $\omega_j$  are the eigenvalues of the matrix  $K$ .

- [1] Beskos, D.E. and Boley, B.A., "Critical Damping in Linear Discrete Dynamic Systems," Journal of Applied Mechanics, Vol. 47, No. 3, 1980, pp. 627-630.
- [2] Inman, D.J. and Andry, A.N., Jr., "Some Results on the Nature of Eigenvalues of Discrete Damped Linear Systems," Journal of Applied Mechanics, Vol. 47, No. 4, 1980, pp. 927-930.

Random Vibration Solutions for the  
Reservoir-Dam-Earthquake Problem

by  
C. Y. Yang  
Civil Engineering Department  
University of Delaware  
Newark, DE 19711

The response of reservoir-dam systems to a deterministic or prescribed ground motion has been investigated successfully first by Westergaard [1] as early as 1933. However, the more realistic problem in which the earthquake generated ground motion is treated as a random process has not been solved even in the simplest case where the process is assumed to be stationary with a white power spectral density until 1981 by Yang and Chairito [2].

In this paper new analytic and approximate solutions are presented for the random response and the probability of barrier crossing for reservoir dam systems subjected to stationary and nonstationary excitations.

Statement of the Problem and Non-random Solution

The dam-reservoir system is assumed to be one-dimensional with a vertical earthquake excitation. The fluid is assumed to be compressible but the viscosity and surface wave effects are negligible. The non-random solution for the hydrodynamic pressure on the dam was obtained by Rosenblueth [3] in the form of a unit impulse response function  $h(y, t)$ . For the idealized case of a rigid reservoir base,  $h(y, \cdot)$  is undamped and periodic with a period of  $4H/c$ . For the more realistic case of a deformable reservoir base,  $h_p(t)$  is damped periodic. Taking advantage of the periodicity and symmetry of the impulse response  $h_p(y, t)$  for the hydrodynamic pressure, the corresponding solutions for the shear force  $h_f(y, t)$  and overturning moment  $h_M(y, t)$  can be determined.

Stationary Random Solutions

When the vertical earthquake excitation is idealized to be a Gaussian stationary random process with zero mean and uniform spectral density  $S_0$ , the stationary mean square shear force and overturning moment respectively are obtained analytically in closed forms. For the shear force

$$E[F^2(y)] = \sigma_P^2(y) = \frac{1+\alpha}{3(1-\alpha)} \pi S_0 \rho^2 c H^3 \left(1 - \frac{y}{H}\right)^3$$

On the basis of the classical failure criterion of barrier crossing and the crucial assumption of a Poisson random crossing events, closed form solutions for the reliability functions are obtained. For the shear force,

$$R_s(y, t) = \exp \left\{ - \frac{2\sqrt{3}}{\pi^2} \frac{\omega_1 t}{1 - (y/H)} \exp \left[ - \frac{a^2(y)}{2 \left(1 - (y/H)\right)^3 \sigma_P^2(0)} \right] \right\}$$

Nonstationary Random Solutions

The transient solutions for the shear force  $F(y, t)$  and overturning moment  $M(y, t)$  are obtained analytically in a series form. For the shear force

$$E[F^2(y,t)] = \sigma_F^2(y,t) = \frac{g_0^2 (1+\alpha)^2 c^2 H^3}{3} \left(1 - \frac{y}{H}\right)^3 \sum_{n=1}^N \alpha^{2(n-1)}$$

where  $N = t/(2H/c)$

Using this transient mean square response  $\sigma_F^2(y,t)$  an approximate reliability solution can be determined from the same approach as in the stationary case.

#### Conclusions

For dam-reservoir systems subjected to random vertical earthquake excitation which is modeled by a stationary random process, closed form solution for mean square response of shear forces and overturning moments and for reliability probabilities are obtained. The simple analytic results, although highly idealized because of the assumptions made in their derivations, are believed useful as a guide for practical applications and for more realistic future investigations, taking into account such important effect as the non-rigid dam and fluid interaction [1].

#### Acknowledgment

The work has been supported in part by funds provided by the National Science Foundation Grant No. CEE-8208840 with the University of Delaware.

#### References

- [1] Westergaard, H. M. "Water Pressures on Dams During Earthquakes." Transactions ASCE, Vol. 98, paper 1835- 1933, pp. 418-471.
- [2] Yang, C. Y. and V. Chiarito "Random Hydrodynamic Forces on Dams From Earthquakes" Journal of the Engineering Mechanics Division, ASCE, Vol. 107, No. EM 1, Feb, 1981, pp. 117-129.
- [3] Newmark, N. M. and E. Rosenblueth "Fundamentals of Earthquake Engineering" Prentice Hall, 1971.

## An Expression of Strain Energy Involving Couple Stresses In Solids

by

Surinder K. Lakhanpal  
 Department of Civil Engineering  
 Union College  
 Schenectady, New York 12308

Throughout the literature, the concept of load transfer is based on linear stresses. However, the material behavior is better defined when load transfer is considered to be by couple stresses, in addition to linear stresses. The strain energy expression is an important tool for the study of material. With this in mind, the expression with couple stresses included is developed.

The theory of elasticity describes analytically the nature of the displacements and the corresponding stress field in a continuous elastic body subjected to known forces. In a perfectly elastic body the deformations disappear when the forces are removed. The deformations may be of any magnitude but the theory is simplified to a great extent when only small deformations are considered and assumed to produce no rigid motion of the system. The theory, based on small deformations, required for the development of the energy expression is available in [1, 2, 3, 4, 5].

The energy absorbed in a body due to the work done by external forces acting on the body is called the strain energy. If the body behaves elastically and the small amount of energy lost in the form of heat is ignored, the strain energy can be recovered when the body is returned to its original position. The strain energy expression is developed as follows.

The expression for the work done by the normal stress components, symmetric shear components, moment (couple stress) components, anti-symmetric shear components and the body forces acting at a generic point in an elastic continuum is developed. The equations of equilibrium and kinematic relationships are used to simplify the expression in the following form:

$$\begin{aligned} & \frac{1}{2} [\sigma_{xx}\epsilon_{xx} + \sigma_{yy}\epsilon_{yy} + \sigma_{zz}\epsilon_{zz} + \frac{1}{2}(\sigma_{xy} + \sigma_{yx})\epsilon_{xy} + \frac{1}{2}(\sigma_{yz} + \sigma_{zy})\epsilon_{yz} \\ & + \frac{1}{2}(\sigma_{zx} + \sigma_{xz})\epsilon_{zx} + (\sigma_{yz} - \sigma_{zy})\omega_x + (\sigma_{zx} - \sigma_{xz})\omega_y + (\sigma_{xy} - \sigma_{yx})\omega_z \\ & + \mu_{yx} \frac{\partial \omega_x}{\partial y} + \mu_{zx} \frac{\partial \omega_x}{\partial z} + \mu_{zy} \frac{\partial \omega_y}{\partial z} + \mu_{xy} \frac{\partial \omega_y}{\partial x} + \mu_{xz} \frac{\partial \omega_z}{\partial x} + \mu_{yz} \frac{\partial \omega_z}{\partial y}] dx dy dz \end{aligned}$$

When the couple stress effect is omitted,

$$\mu_{yx} = \mu_{zx} = \mu_{zy} = \mu_{xy} = \mu_{xz} = \mu_{yz} = 0$$

and

$$\sigma_{yz} = \sigma_{zy}, \sigma_{zx} = \sigma_{xz}, \sigma_{xy} = \sigma_{yx}$$

The energy expression reduces to the form:

$$\frac{1}{2} [\sigma_{xx}^e \epsilon_{xx} + \sigma_{yy}^e \epsilon_{yy} + \sigma_{zz}^e \epsilon_{zz} + \sigma_{yz}^e \epsilon_{yz} + \sigma_{xy}^e \epsilon_{xy} + \sigma_{xz}^e \epsilon_{xz}] dx dy dz$$

which is the standard strain energy expression encountered in conventional linear elastic analysis [2].

#### Notations

- $dx, dy, dz$  . . . . . Finite lengths along  $x, y,$  and  $z$  axes, respectively.
- $x, y, z$  . . . . . Set of right hand coordinate axes.
- $\frac{\partial}{\partial x}, \frac{\partial}{\partial y}, \frac{\partial}{\partial z}$  . . . . . Partial derivatives with respect to  $x, y,$  and  $z,$  respectively.
- $(\epsilon_{xx}, \dots, \epsilon_{xy}, \dots)$  . . . . . Strain components at a generic point.
- $(\sigma_{xx}, \dots, \sigma_{xy}, \dots)$  . . . . . Stress components at a generic point.
- $(\mu_{yx}, \dots)$  . . . . . Couple stress components at a generic point.
- $\omega_x, \omega_y, \omega_z$  . . . . . Components of rotation about  $x, y,$  and  $z$  axes, respectively.

#### References

1. Love, A.E.H., "A Treatise on the Mathematical Theory of Elasticity," Dover Publications, Inc., New York, New York, 1944.
2. Timoshenko, S., and Goodier, J.N., "Theory of Elasticity," McGraw-Hill Book Company, New York, 2nd Edition, 1951.
3. Lakhinskii, S.G., "Theory of Elasticity of an Anisotropic Elastic Body," Holden-Day, Inc., San Francisco, 1963.
4. Mindlin, R.D., "Influence of Couple-Stresses on Stress Concentrations," Experimental Mechanics, January, 1963, pp. 1-7.
5. Lakhanpal, Surinder Kumar, "A Model of Couple Stress Effect Upon the Transverse Stiffness of a Fiber-Reinforced Material," Ph.D. dissertation, Vanderbilt University, May, 1974.

Pressure Induced Radial Diffusion of a Fluid  
Through a Thick Walled Highly Elastic Cylinder

by

A.S. Wineman and M. Gandhi  
Department of Mechanical Engineering  
and Applied Mechanics  
The University of Michigan  
Ann Arbor, Michigan 48109

and

D.R. Rajagopal  
Department of Mechanical Engineering  
University of Pittsburgh  
Pittsburgh, PA 15261

We consider the problem of the radial diffusion of a fluid through a highly elastic thick walled cylinder due to pressure differences at the inner and outer surfaces. The interaction between the fluid diffusion and large solid deformation is accounted for by formulating the problem in the context of the theory of mixtures.

The constitutive equation for the partial stresses and diffusive body force incorporate an expression for the specific internal energy function which is suggested by the kinetic theory of rubber elasticity. The difficulty of specifying the boundary condition for such a problem is resolved by using a relation between surface traction and deformation when the mixture is in a saturated state.

Results of numerical solution of the governing equations include a radial mass flux-pressure difference relation and the influence of axial stretch on this relation.

HELICAL SHEAR OF AN ELASTIC, CIRCULAR TUBE  
WITH NON-CONVEX STORED ENERGY

BY

R. L. Fosdick  
Dept. of Aero. Engr. & Mechanics  
University of Minnesota  
Minneapolis, MN 55455

G. P. Mac Sithigh  
Dept. of Engineering Mechanics  
University of Missouri-Rolla  
Rolla, MO 65401

The problem of helical shear for a tube composed of a homogeneous, isotropic, incompressible, finitely elastic material was first considered by Rivlin. It was further studied by Ogden, Chadwick, and Haddon. A recent paper of Abeyaratne examines the sub-case of circumferential twist for a material whose stored energy function is non-convex. This paper analyses the full helical shear problem for such a material.

We formulate it as a minimization problem which generates the following system of Euler-Lagrange equations;

$$\begin{aligned} R^3 \mu(k^2) w'(R) &= A \\ R \mu(k^2) u'(R) &= B \end{aligned} \quad (1)$$

with the boundary conditions  $u(a) = w(a) = 0$ ;  $u(b) = U_0$ ,  $w(b) = \Omega_0$ . Here  $\mu(\cdot)$  is a material function related to the shear stress  $\tau(\cdot)$  by  $\tau(k) = k \mu(k^2)$ ,  $u(\cdot)$  is the axial shear,  $w(\cdot)$  the circumferential twist, and the function  $k(\cdot)$  is given by

$$k^2(R) = (R w'(R))^2 + (u'(R))^2. \quad (2)$$

The minimization problem reduces to that of finding values of the constants  $A$ ,  $B$ , and a piecewise  $C^1$  solution of (1) for these values such that (i)  $k(R)$  is a point of convexity of the stored energy function for each  $R$ ; (ii) the boundary conditions are satisfied.

We solve this novel inversion problem for all values of  $(\Omega_0, U_0)$ . Our result includes that of Abeyaratne as the special case  $B = U_0 = 0$ .

Stresses in and Around Double Confocal Spheroids Embedded  
in Infinite Media

by

Yozo Mikata

Minoru Taya

Department of Mechanical and Aerospace Engineering  
University of Delaware  
Newark, Delaware 19711

In order to solve the state of stress in a coated short fiber composite, the coated short fiber is modelled as double concentric spheroids embedded in infinite elastic media. When the composite system is subjected to uniform temperature rise  $T$ , the residual thermal stress is induced in and around the coating zone. We compute the amount of the residual stresses in and around the coated short fiber to discuss the possibility of the circumferential cracks in the coating zone. The method of analysis is based on the classical three-function approach initiated by Boussinesq in the three domains, the fiber, coating zone and infinite media.

APPROXIMATIONS FOR ELASTIC LAYERS AND A THREE-DIMENSIONAL  
ELASTICITY SOLUTION FOR A SIMPLY SUPPORTED RECTANGULAR PLATE

by

Mark Levinson

Department of Mechanical Engineering  
University of Maine at Orono  
Orono, Maine 04469, U.S.A.

Two classes of problems for elastic layers, those for thick plates and for foundations, usually have been treated separately. Recent work [1,2] has shown that both may be treated in a unified manner. In [1] a theory of thick elastic plates is given which accounts for transverse normal stresses and strains as well as transverse shear deformations with warping while [2] provides a generalization of the Vlasov-Jones foundation model [3,4] which allows for displacements in planes parallel to the foundation surface. Both theories are based on the assumed, approximate displacement field

$$u = -g(z)\partial W(x,y)/\partial x, \quad v = -g(z)\partial W(x,y)/\partial y, \quad (1)$$

and

$$w = f(z)W(x,y)$$

where  $W(x,y)$  is the transverse deflection of a suitable reference surface and  $f(z)$  and  $g(z)$  are "shape functions" which provide the  $z$  (thickness) dependence of the displacement components.

Substitution of equations (1) into the strain energy expression for an isotropic, linearly elastic medium, together with the use of the principle of stationary potential energy, provides the governing differential equations for the elastic layer as well as boundary conditions for  $f$  and  $g$  on the faces of the layer and for  $W$  on the edges of the layer. The differential equations are

$$k_3 \nabla^4 W + (k_4 - k_2) \nabla^2 W + k_1 W = P(x,y)$$

$$I_1 \frac{d^2 f}{dz^2} + (I_3 - I_2) \frac{dg}{dz} - I_3 f = 0, \quad (2)$$

and

$$I_3 \frac{d^2 g}{dz^2} - (I_3 - I_2) \frac{df}{dz} - I_4 g = 0.$$

The peculiar feature of equations (2) is that the  $k_j$  are functionals (definite integrals) of  $f$  and  $g$  while the  $I_j$  are functionals of  $W$ .

This unusual nonlinear system of equations would not seem amenable to exact analysis. Therefore an iterative method of approximation, which in some cases may be applied analytically, is proposed. More generally, the method may

be implemented numerically and the key to such implementation will be generalized plate bending finite elements such as the one recently given in [5]. A simple example is given, a problem of the cylindrical bending of a thick plate, in which the iterative method of solution is found to converge to the corresponding elasticity solution [6] in a single cycle of iteration.

Because of this somewhat surprising result, it was decided to investigate the question of whether any three-dimensional elasticity problems have solutions corresponding to assumptions [1]. Substitution of these kinematic assumptions into the Navier equations of linear elasticity and subsequent inverse satisfaction of boundary conditions leads to a three-dimensional, linear elastostatic solution of the problem of rectangular plate which is simply supported on all four edges [7]. As the plate thickness approaches zero the new solution approaches the classical Navier solution of the plate problem, i.e. the Navier solution is the limiting case of the elasticity solution. Furthermore, it is similarly possible to find the elasticity solution of the free vibration problem of the simply supported, rectangular plate.

The above-mentioned result provides a heuristic basis, previously lacking, for the novel theory of plates of arbitrary planform and edge support given in [1].

#### REFERENCES

1. M. Levinson, "A Novel Theory of Thick, Elastic Plates," Int. J. Mech. Sci., in press.
2. M. Levinson, "The Generalized Vlasov-Jones Foundation Model: A Foundation of Grade 4," Int. J. Mech. Sci., in press.
3. V.Z. Vlasov and N.N. Leont'ev, Beams, Plates and Shells on Elastic Foundations, Israel Program for Scientific Translations, Tel Aviv, 1966.
4. R. Jones and J. Zenophontos, "The Vlasov Foundation Model," Int. J. Mech. Sci., 19, 317, 1977.
5. B. El Sharnouby and M. Levinson, "A Triangular, Conforming Element for the Foundation of Grade 4," Mech. Res. Comm., 9, 391, 1982.
6. R.W. Little, Elasticity, Prentice-Hall, Inc., Englewood Cliffs, 1973.
7. M. Levinson, "The Simply Supported Rectangular Plate: An Exact, Three Dimensional, Linear Elasticity Solution," UMOME Report 83-1, Orono, February 1983.

## THERMAL BUCKLING OF CONCRETE PAVEMENTS

by

Arnold D. Kerr  
 Department of Civil Engineering  
 University of Delaware  
 Newark, Delaware 19711

Presentation discusses the recently developed analyses for the thermal lift-off buckling of concrete pavements, by Kerr and Dallis [1] and Kerr and Shade [2]. The aim of these studies was to provide analyses for concrete pavement blowups, which are caused by axial compression forces, often induced into the pavement by a rise in temperature and moisture. Since a moisture increase (or drop) in the concrete slab may be expressed by an equivalent temperature rise (or drop), only temperature changes were considered.

The used analytical model is shown in Fig. 1. A uniform temperature increase induces, due to constrained expansions, a uniform axial force  $N_t$ . When the force is sufficiently large the pavement may buckle out vertically. Then in the lift-off region, part of the constrained expansions are released. This results in a reduction of the axial force in the lift-off region to  $\tilde{N}_t$ . In the adjoining regions, due to the resistance  $r(x)$  to axial displacements, the constrained expansions vary; so does the axial force  $\tilde{N}_t < N_t$ , as shown in Fig. 1.

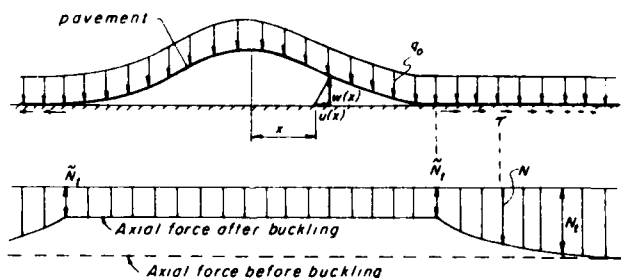


FIG. 1. BUCKLED PAVEMENT AND CORRESPONDING AXIAL FORCE DISTRIBUTION

The lift-off phenomenon is geometrically non-linear. For the analyses, it was stipulated that the pavement is subjected to a uniform temperature change  $T_0$  above "neutral" (at which the axial forces are zero) and a uniformly distributed pavement weight  $q$ . Because the vertical deflections in the adjoining regions are very small, it was assumed that the base is rigid. Furthermore, it was assumed that prior and during buckling the response of the concrete pavement is elastic.

According to tests, the axial shearing resistance in the contact area of pavement and base is non-linear. In [1] this response was described by a bi-linear approximation. In [2] it was represented by the non-linear relation  $r = r_0 \tanh[\mu u(x)]$ , where  $u(x)$  is the axial displacement and  $(r_0, \mu)$  are coefficients determined from fitting the test data. Although, the shearing resistance is mainly non-elastic, the assumed representations are justified, because during buckling the axial displacements are monotonically increasing.

The reinforced concrete pavement was replaced by a beam of rectangular cross section. To account for plate action, the bending stiffness was increased to  $EI/(1-\nu^2)$ , in the numerical evaluations.

The respective formulations were derived using variational calculus for variable matching points. The obtained non-linear formulations, consisting of differential equations and matching conditions, were then solved *exactly* and in *closed form*. The analytical solutions were numerically evaluated for a wide range of pavement parameters and presented as graphs [1,2].

A typical result is shown in Fig. 2. Note, that the analyses yield the post-buckling deflection shapes and the corresponding distribution of axial forces. From the nature of post-buckling equilibrium branches and their stability, it follows that the "safe range" of temperature and moisture increases to prevent pavement buckling may be determined solely from the post-buckling equilibrium branches. It is

$$0 < T_0 < T_L$$

where  $T_L$  is the temperature increase that corresponds to the horizontal tangent of a branch II.

According to Fig. 2 for a pavement with  $h = 20$  cm, the safe temperature increase to prevent buckling by lift-off is  $T_L = 50^\circ\text{C}$ . This means, that for a temperature increase of less than  $50^\circ\text{C}$  above "neutral", the pavement is safe against buckling by lift-off. For a temperature increase  $T_0 = 60^\circ\text{C}$  above "neutral", there exists three equilibrium configurations and when buckling does occur the pavement moves to the stable equilibrium configuration ③. Note the corresponding drop of the axial force  $N_t$  in the lift-off region.

Additional graphs [1,2] identify a number of important pavement parameters and show their effect on the safe temperature increase.

#### ACKNOWLEDGMENT

This research was supported by the National Science Foundation, Washington, DC, Grant CME8001928.

#### REFERENCES

- [1] Kerr, A. D. and Dallis, Jr., W. A. "Blowup of Concrete Pavements", University of Delaware, Department of Civil Engineering Report, CE-81-20, April 1981.
- [2] Kerr, A. D. and Shade, P. J. "Analysis of Concrete Pavement Blow-ups", University of Delaware, Department of Civil Engineering Report, CE-82-26, April, 1982.

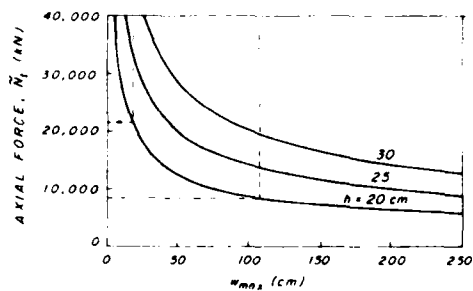
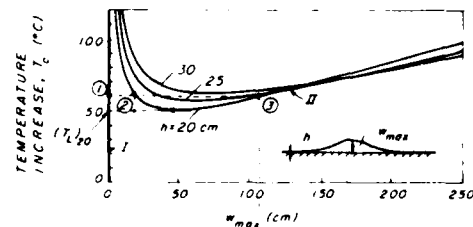


FIG. 2. EQUILIBRIUM BRANCHES AND AXIAL FORCE  $N_t$ .

AD A138 155

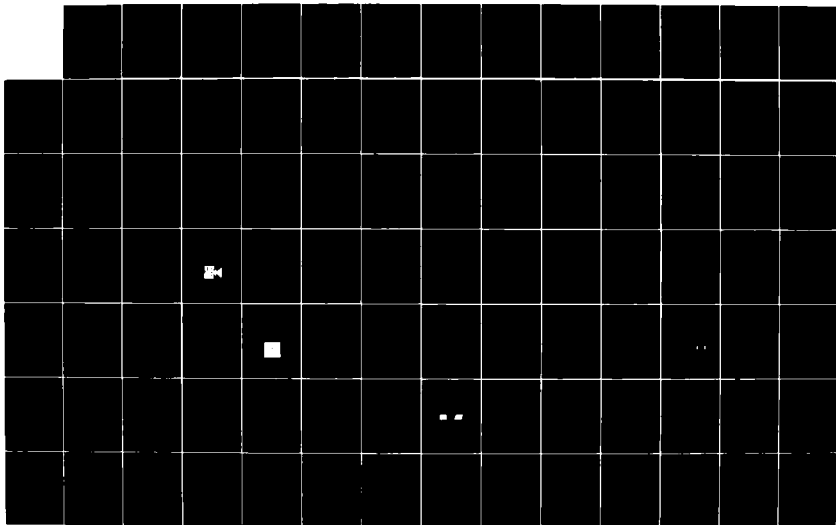
ABSTRACTS OF THE ANNUAL MEETING OF THE SOCIETY OF  
ENGINEERING SCIENCE INC. (U) DELAWARE UNIV NEWARK  
M TAYA SEP 83 ARO-20222.1-EG-CF DAAG29-83-M-0258

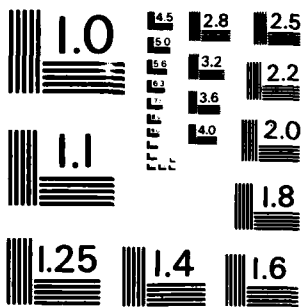
2/4

UNCLASSIFIED

F/G 5/1

NI





MICROCOPY RESOLUTION TEST CHART  
NATIONAL BUREAU OF STANDARDS-1963-A

The reinforced concrete pavement was replaced by a beam of rectangular cross section. To account for plate action, the bending stiffness was increased to  $EI/(1-\nu^2)$ , in the numerical evaluations.

The respective formulations were derived using variational calculus for variable matching points. The obtained non-linear formulations, consisting of differential equations and matching conditions, were then solved *exactly* and in *closed form*. The analytical solutions were numerically evaluated for a wide range of pavement parameters and presented as graphs [1,2].

A typical result is shown in Fig. 2. Note, that the analyses yield the post-buckling deflection shapes and the corresponding distribution of axial forces. From the nature of post-buckling equilibrium branches and their stability, it follows that the "safe range" of temperature and moisture increases to prevent pavement buckling may be determined solely from the post-buckling equilibrium branches. It is

$$0 < T_0 < T_L$$

where  $T_L$  is the temperature increase that corresponds to the horizontal tangent of a branch II.

According to Fig. 2 for a pavement with  $h = 20$  cm, the safe temperature increase to prevent buckling by lift-off is  $T_L = 50^\circ\text{C}$ . This means, that for a temperature increase of less than  $50^\circ\text{C}$  above "neutral", the pavement is safe against buckling by lift-off. For a temperature increase  $T_0 = 60^\circ\text{C}$  above "neutral", there exists three equilibrium configurations and when buckling does occur the pavement moves to the stable equilibrium configuration ③. Note the corresponding drop of the axial force  $N_t$  in the lift-off region.

Additional graphs [1,2] identify a number of important pavement parameters and show their effect on the safe temperature increase.

#### ACKNOWLEDGMENT

This research was supported by the National Science Foundation, Washington, DC, Grant CME8001928.

#### REFERENCES

- [1] Kerr, A. D. and Dallis, Jr., W. A. "Blowup of Concrete Pavements", University of Delaware, Department of Civil Engineering Report, CE-81-20, April 1981.
- [2] Kerr, A. D. and Shade, P. J. "Analysis of Concrete Pavement Blowups", University of Delaware, Department of Civil Engineering Report, CE-82-26, April, 1982.

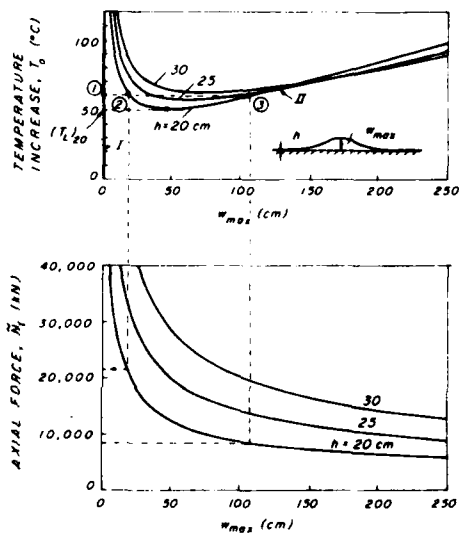


FIG. 2. POST-BUCKLING EQUILIBRIUM BRANCHES AND AXIAL FORCE,  $N_t$ .

Numerical Experiments with Two-Dimensional  
Elastic-Viscoplastic Bars

by

G. Q. Zhou\*, H. Ghoneim, Y. Chen  
Department of Mechanics and Materials Science  
Rutgers, The State University of New Jersey  
P.O. Box 909  
Piscataway, NJ 08854

Numerical solutions of two-dimensional elastic-viscoplastic wave propagation in bars of various shapes are discussed. Hondo code with the addition of a new sub-program for Bodner-Partom's constitutive equation [1] is used for the analysis. For a two-dimensional elastic bar and a one-dimensional elastic-linear-hardening plastic bar, Hondo [2] numerical results agree well with available analytical or numerical solutions [3,4,5]. For elastic-viscoplastic bar, numerical solutions show some interesting features of the dynamic responses. The responses for Bodner-Partom constitutive equation were found to lie between the results for elastic-plastic and purely elastic constitutive relation. The precursor wave always propagates at the speed of elastic wave. For a bar containing a discontinuity in cross-section, the numerical results show very realistic results in the region of the discontinuity. The stress concentration at the discontinuity is to be expected. The factor of stress concentration depends upon the ratio of diameters closely. For a bar with both discontinuities of cross-section and material properties, the computation showed the disappearance of stress localization, which usually exists for single-material bar with a geometric discontinuity.

- [1] S. R. Bodner and Y. Partom, "Large Deformation Elastic-Viscoplastic Analysis of a Thick-Walled Spherical Shell," Journal of Applied Mechanics, 9, 1972, pp. 751-757.
- [2] S. W. Key, Z. E. Beisinger, R. D. Krieg, Hondo II, SAND 78-0422.
- [3] L. D. Berthold, "Feasibility of Two-Dimensional Numerical Analysis of the Split-Hopkinson Pressure Bar System," Journal of Applied Mechanics, 3, 1974, pp. 137-144.
- [4] L. D. Berthold, "Numerical Solution for Two-Dimensional Elastic Wave Propagation in Finite Bars," J. Appl. Mech., Vol. 34, Trans. ASME, Vol. 39, Series E, 1967, pp. 725-734.
- [5] J. L. Habberstad, "A Two-Dimensional Numerical Solution for Elastic Wave in Various Configured Rods," J. Appl. Mech., Trans. ASME, March 1971, pp. 62-70.

\*Chinese University of Science & Technology, currently visiting Rutgers.

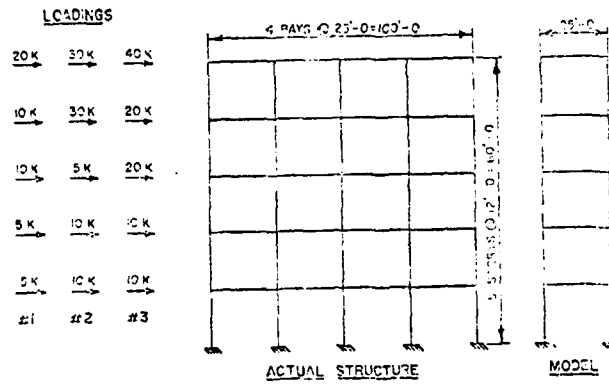
## Simplified Analysis of Structural Concrete Plane Frames

by

Cheng-Tzu Thomas Hsu  
Department of Civil & Environmental Engineering  
New Jersey Institute of Technology  
Newark, New Jersey

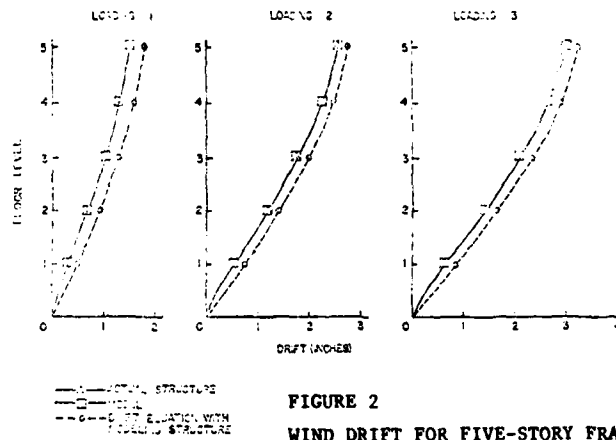
The control of wind drift is an essential part of the design procedures in multi-story building structures. Over the years, experience has proven that for mid-rise buildings, a design is prepared which satisfies both drift limitations and code provisions for stresses and generally, ignoring P-Delta consideration altogether. In very tall buildings, the lateral load design can become very sophisticated and usually requires wind tunnel tests. It is well known that even for low rise multi-bay reinforced concrete plane frames, the analysis and design process are both time consuming and could be expensive. For practical design purposes, it is feasible to develop a model to simulate the actual structure behavior for its response to wind loads. The techniques of modeling the multi-bay plane frame into a one bay plane frame is by means of correcting the stiffness in both beams and columns. Once the multi-bay plane frame has been modeled and simplified to a one bay plane frame, either conventional structural analysis or in-house computer can calculate the forces and displacements easily. For design purposes, however, there is a need for a simpler method which can fulfill the following requirements : (i) it must be capable of predicting, with sufficient accuracy, story stiffness; (ii) it must be capable of considering both first order and second order deflections (P-Delta effect included); and (iii) it must be capable of providing rapid means for modifying member sizes to meet pre-selected story deflection constraints. One such method was developed by Cheong-Siat-Moy (1) for unbraced steel frames. This very method will be used herein to demonstrate its reliability and accuracy as an analytical and design tool on practical multi-story reinforced concrete frame structures.

Figure 1 shows a five-story reinforced concrete plane frame with four bays. To fully prove the validity of the frame reduction method, the structure is selected to simulate drift and member end actions. Figure 2 shows the floor level and wind drift relations for actual and modeled frames. Both of them were analyzed by the first-order linear elastic computer program. The curves representing both the actual and model drifts appear to be superimposed upon one another. This condition confirms the usefulness of models to duplicate the wind drift in the actual structure. The drift values obtained from the empirical equations along with modeling structure yield somewhat conservative figures. As indicated by the graphs, the values are overestimated for the lower-most floors; however, they seem to cover with actual values for the upper-most stories. The results of this study conclude that the analysis for a multi-bay structure can be simplified through frame modeling. Using a model in place of the actual multi-bay structure reduces both member input and C. P. U. time required for analysis.



	MEMBER PROPERTIES		
	ACTUAL	MODEL	
		LEFT COLUMN	RIGHT COLUMN
1 (14')	3201.33	6003.5	6003.5
2 (14')	1000.0	4100.0	4100.0
3 (14')	7100.0	10150.0	10150.0
4 (14')	4100.0	4100.0	4100.0

FIGURE 1  
FIVE-STORY FRAME



**Reference:**

1. Cheong-Siat-Moy, F., "Stiffness Design of Unbraced Steel Frames," Engineering Journal, AISC, 1st Quarter, 1976, pp. 8-10.

Viscoelastic Deformations and Stresses of  
Floating Ice Plates

David Hui\* and P.C. Xirouchakis  
Department of Ocean Engineering  
Massachusetts Institute of Technology  
Cambridge, Mass. 02139, U.S.A.

The linear elastic as well as the viscoelastic response of simply supported rectangular floating ice plates with variable Young's modulus across the depth subjected to central (rectangular shaped) distributed loading are studied. The ice Young's modulus  $E$  across the beam thickness  $H$  is specified by [1-3],

$$E(Z)/E_0 = 1 - (1-\alpha) \left[ (Z/H) + (Z_0/H) \right]^\beta \quad (1)$$

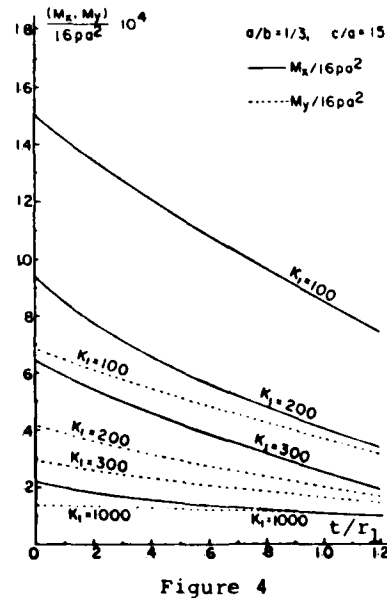
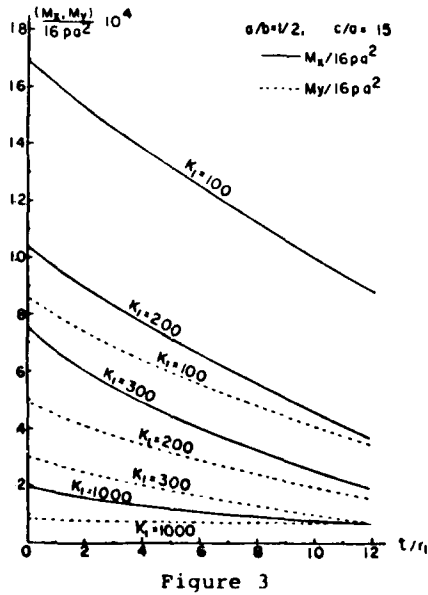
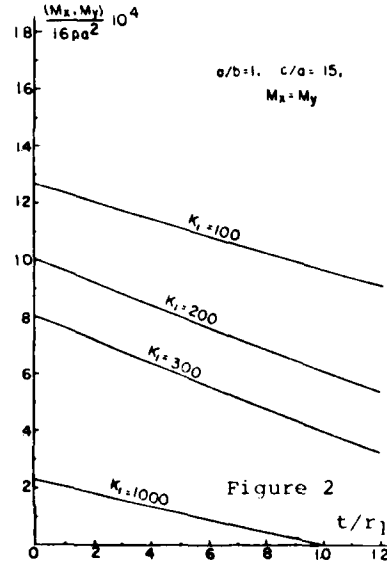
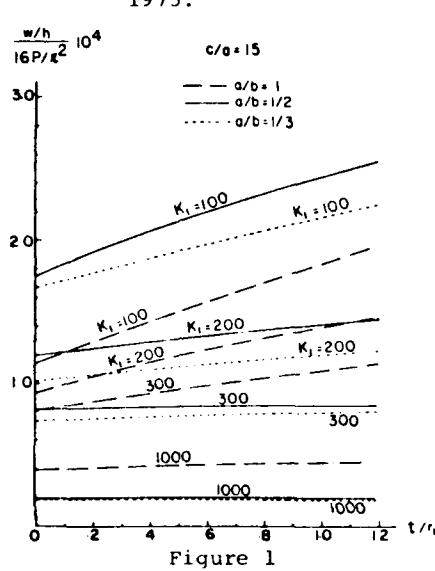
where  $E_0$  is the Young's modulus of the top fibres (located at  $Z=-Z_0$ ) and  $\alpha$  and  $\beta$  are non-dimensional positive material constants. The Rayleigh-Ritz procedure is used to obtain the elastic solution for the transverse deflections, the middle surface curvature changes and the bending moments. The assumption is made that ice is incompressible under hydrostatic stress and obeys Maxwell's model for deviatoric stress and strain [3,4]. The viscoelastic response can then be obtained from the corresponding principle [5].

Figure 1 shows the viscoelastic solution for the non-dimensional deflection at the plate centre versus the non-dimensional time for aspect ratio  $a/b$  being 1, 1/2 and 1/3, the extent of the loading region  $c/a$  being 0.15 and for various values of the non-dimensional linear foundation modulus  $K_1$ . Figure 2 shows the non-dimensional viscoelastic bending moments versus non-dimensional time for a simply supported square ice plate. It can be seen that the bending moments decrease monotonically to zero as time tends to infinity. Similar trends for  $a/b$  being 1/2 and 1/3 are found in Figure 3 and 4 respectively.

REFERENCES

1. Kerr, A.D. and Palmer, W.T., *Acta Mechanica*, Vol. 15, 1972, pp. 57-72.
  2. Hui, D. and Xirouchakis, P.C., "Viscoelastic Deformation and Stresses of Floating Ice Plates", M.I.T. Dept. of Ocean Engineering Report 81-3, March 1981.
  3. Hui, D. and Xirouchakis, P.C., "Non-Stationary Primary Creep Response of Floating Ice Beams", 9th Canadian Congress of Applied Mechanics, May 30th-June 3rd, 1983. (20th SES Annual Meeting, August 22-24, 1983)
- \* Graduate Student M.I.T.; now Assistant Professor, Dept. of Engineering Mechanics, The Ohio State University.

4. Xirouchakis, P.C., Chaplin, M. and St. Lawrence, W., "A Preliminary Investigation of the Acoustic Emission and Deformation Response of Finite Ice Plates", Cold Region Research and Engrg Lab. (CRREL) Report 180, Hanover, N.H., 1980, 40pp.
5. Flugge, W., "Viscoelasticity", 2nd Ed., Springer-Verlag, 1975.



INTEGRATED ANALYSIS AND DESIGN FOR  
MULTI-LEVEL PERFORMANCE CRITERIA

by

Mir M. Ali  
Sargent & Lundy  
55 East Monroe St.  
Chicago, Illinois 60603

This paper deals with the issue of interaction between analysis and design of structures when the designer is faced with the task of designing a structure for service and ultimate load conditions. As is well known, structural analysis is concerned with the equilibrium and compatibility of a structure with selected member sizes based on a preliminary design. The member forces and deformations are the end results of the analysis. The structural analyst has no control on the analysis process inasmuch as once the member sizes are preselected he cannot modify or manipulate the mathematical equations of equilibrium and compatibility. This is so because for a structure with given geometry, member properties and loading, there exists a unique solution that satisfies the equilibrium and compatibility requirements of the structure. Structural design on the other hand, is aimed at obtaining a structure that is safe, serviceable, reliable and economical. Since there may be theoretically an infinitely large number of feasible solutions to the design problem that may satisfy the adopted design criteria, the designer may exercise direct control on the choice of his design. Because of these conflicting philosophies, it becomes a difficult task for the designer to combine analysis and design into a single integrated scheme.

With the advent of high technology in the field of digital computer applications, interactive computer programs for analysis and design can achieve, to a large extent, an integrated scheme for linearly elastic structural behavior, even though a few manual operations may be necessary to realize an efficient design. However, once a governing design objective (e.g., cost, weight, energy, etc.) is adopted, an automated optimal design utilizing an iterative approach with interactive computer codes can be envisioned in not too distant a future. Although the human factor may not be totally eliminated, yet the task of the designer will then be largely to feed the computer with input data for a structure at a computer terminal. The computer program package will presumably contain the sub-programs of analysis, design, optimization and other related aspects of a complete design. The output will consist of material properties, member cross-section description, connection details and other parameters defining perhaps the constructibility of the structure and its member elements if such constraints are included in the design criteria.

The problem of integrating the analysis and design procedures becomes more pronounced when the design is to be conducted for a number of performance constraints at multiple levels of structural response. For reinforced concrete frames, for example, several methods have been developed whereby a limit-load analysis is performed on the structure against structural collapse and local deformational failure, and then member sizes and reinforcing are modified to meet deflection and cracking requirements under service loads (1, 2). Similar remarks also apply to steel framed structures (3, 4), when the ultimate and service conditions constitute the performance constraints to the design.

For reinforced concrete structures, usually two of the three basic conditions of design, i.e., limit equilibrium, limit compatibility and serviceability, are explicitly satisfied in the design while the third condition is checked subsequent to the design. This check for the third condition may often invalidate the design outcome in which case the entire design process is to be repeated. This process of iteration is to be continued until a design solution that satisfies all the three conditions is achieved. For monotonic structural response, this problem may be largely circumvented by explicitly considering certain design conditions (i.e., related to safety and serviceability) at one level of response (i.e. sectional or structural) and implicitly satisfying certain other conditions at another level of response and formulating the design problem as a whole amenable to numerical solution by using an appropriate algorithm. This may in turn be combined with interactive sub-programs for analysis and optimization in order to develop a completely integrated analysis/design package.

The present paper proposes such an approach to the design of reinforced concrete structures. The design problem treats the various service and ultimate performance constraints in a single formulation. Examples dealing with a continuous beam and a flexural frame are presented to illustrate the methodology and the concepts involved.

#### REFERENCES

1. Baker, A.L.L., "Ultimate Load Theory Applied to the Design of Reinforced and Prestressed Concrete Frames," Concrete Series, London, England, 1956.
2. Macchi, G., "A Proposal of Analysis Based on the Theory of Imposed Rotations," Bulletin d'Information, CEB, Paris, No. 21, January, 1960.
3. Emkin, L.Z. and Little, W.A., "Storywise Plastic Design for Multistory Steel Frames," ASCE J. of Str. Div., January, 1972.
4. Horne, M.R. and Morris, L.J., "Optimum Design of Multi-Story Rigid Frames," Int. Sym. on Computers in Optimization of Structural Design, University of Wales, Swansea, January, 1972.

**ANALYSIS OF CURVED BRIDGE DECKS  
SUPPORTED BY FLEXIBLE GIRDERS**

by

A.K.Azad, O.H.Al-Khadhra, M.H.Baluch, and A.J.Al-Tayyib  
University of Petroleum & Minerals  
UPM Box 1469, Dhahran, Saudi Arabia

The increasing popularity of curved bridges in highway construction due to their esthetically pleasing appearances have inspired researchers to seek reliable methods of analysis. This has resulted in numerous analyses based on different idealizations and mathematical approaches of which refs 1-4 can be cited only as a representative sample of works.

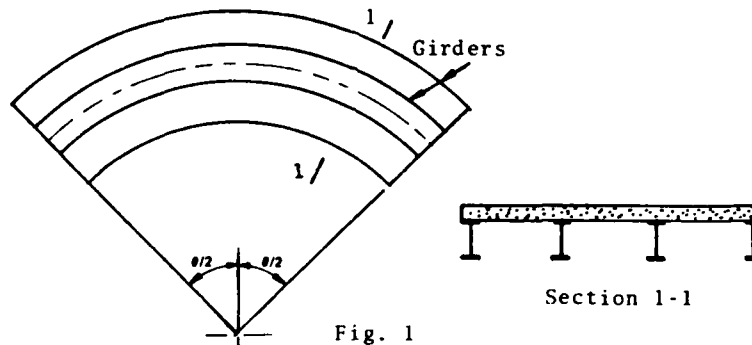


Fig. 1

In this paper, the finite difference method has been used to numerically analyse a horizontally curved orthotropic bridge deck which is simply supported at the two ends and continuous in the radial direction over flexible, curved longitudinal girders as shown in Fig. 1. By using a Levy-type solution, the governing partial differential equation of the curved orthotropic slab can be reduced to the following ordinary fourth order Euler-Cauchy differential equation :

$$\frac{d^4 w}{dr^4} + \frac{2}{r} \frac{d^3 w}{dr^3} - \frac{\alpha}{r^2} \frac{d^2 w}{dr^2} + \frac{\alpha}{r^3} \frac{dw}{dr} + \frac{\beta}{r^4} w = q/D_r \quad (1)$$

where  $r$  is the radius of curvature. Eq. 1 is then solved as a boundary value problem, taking into account the continuity of the deck over the flexible supporting girders. The effect of flexibility due to both flexure and torsion are taken into account in writing the difference equations at each girder location. The simplicity of this method of analysis lies in solving the equilibrium equations only at the nodal points along the central radial line of the deck

for each harmonic component of the Fourier load that would replace the actual load on the deck. The sinusoidal distribution of displacements and forces along the  $\theta$ -direction is used to find the displacement and forces elsewhere on the deck.

The reliability of the proposed computerized numerical method has been verified by comparing results with other known solutions. Numerous problems have been solved to examine the effect of the flexural rigidity and the deck slab thickness on the transverse load distribution among the supporting girders. The influence of the radius to the centre line of the deck on the maximum moment has also been observed.

#### References

1. Coull, A. and Das, P.C., "Analysis of Curved Bridge Deck", Proc. Instn. Civil Engrs. 37, 1967, pp.75-86.
2. Cheung, Y.K., "The Analysis of Cylindrical Orthotropic Curved Bridge Decks", Int. Assoc. of Bridge and Struc. Engrs. 29, 1969, pp.41-52.
3. Bell, L.C. and Heins, C.P., "Analysis of Curved Girder Bridges", Proc. Am. Soc. of Civil Engrs. 96, Aug., 1970, pp.1657-1673.
4. Dey, S.S. and Samuel, A.T., "Static Analysis of Orthotropic Curved Bridge Decks", Computers and Structures, 12, 1980, pp.161-166.

## Inelastic Behavior of Channel-Shaped Reinforced Concrete Columns

by

Cheng-tzu Thomas Hsu, D. Chidambarrao and M. C. Liu

Department of Civil & Environmental Engineering  
New Jersey Institute of Technology  
Newark, New Jersey

The inelastic behavior of irregular shaped reinforced concrete columns has been a constant concern for a structural engineer to design a safe and economic structure in modern buildings and bridge piers. The shape of the elements in a reinforced concrete structures may be used to optimize its structural strength, to make better use of the available space, to improve the esthetic appearance of the structure, or to facilitate construction. Due to the locations of the columns, the shapes of the buildings and the nature of the applied loads, many columns are subjected to combined biaxial bending and axial load.

Hsu et al (1) modified the extended Newton-Raphson method for the determination of strength, strain and curvature distributions in reinforced concrete members subject to biaxial bending moment and axial load. For analysis purpose, the channel-shaped column section is divided into several small elemental areas. Also a complete stress-strain curves for concrete in tension and in compression and for steel reinforcement have been used. Figure 1 shows the details of channel-shaped column section under studying. The resulting biaxial moment-curvature characteristics for the above column section are shown in Figure 2, where  $M_x$  and  $M_y$  represent the bending moments about x- and y- axis respectively. These theoretical moment-curvature and load-deformation results will be compared with the experimental work which is undergoing at the New Jersey Institute of Technology.

Five 1/4 - scale direct models of the short, tied columns with channel-shaped cross section were constructed for the present investigation. All the specimens were tested and studied for their complete strength and deformation behavior under combined biaxial bending moments and axial compression. Also, the specimens were used to examine some of the variables involved, such as the stirrup spacings and relative eccentricities. The end condition is designed to be pinned-ended. For  $e_x = 1.8$  in.,  $e_y = 1.0$  in.,  $f_y = 51.8$  ksi,  $f'_c = 3500$  psi, the experimental ultimate strength value of the column (see Figure 1) is 123.36 Kips., whereas the analytical value obtained from the above computer analysis is 115 Kips.. Thus, a satisfactory agreement was obtained at the ultimate load condition.

The above inelastic behavior of channel-shaped reinforced concrete column has formed the basis of the redistribution of the moments and forces in a statically indeterminate structure and these characteristics can also be found useful for the limit analysis and design of the reinforced concrete structures.

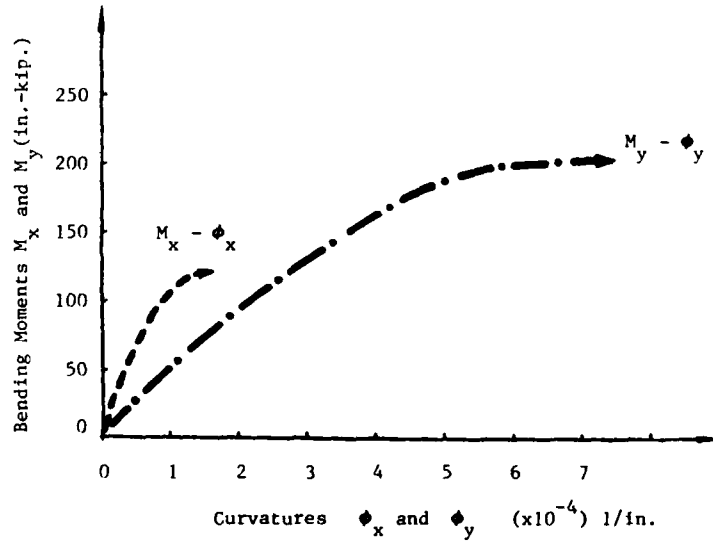
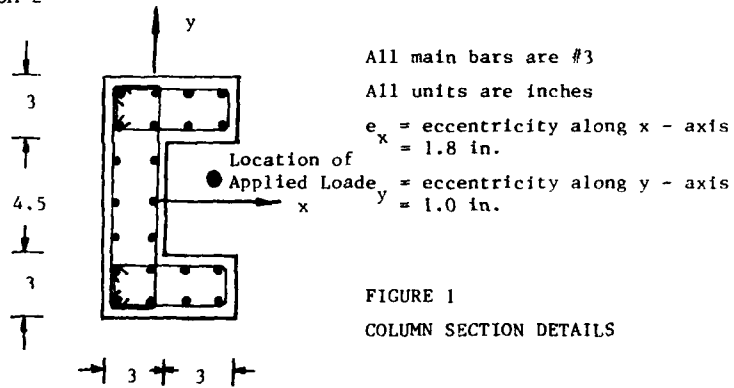


FIGURE 2 THEORETICAL MOMENT - CURVATURE CURVES

Reference:

1. Hsu, C. T. and Mirza, M. S., "Structural Concrete - Biaxial Bending and Compression," TN, Journal of the Structural Div., ASCE, Feb. 1973, pp. 285-290.

## STABILITY OF LOFTY AIR-SUPPORTED CYLINDRICAL MEMBRANES

by

S. Lukaszewicz and P.G. Glockner  
Department of Mechanical Engineering  
The University of Calgary  
Calgary, Alberta, Canada  
T2N 1N4

The use of air supported membranes is becoming increasingly common as enclosures for various structures such as greenhouses, sports complexes and temporary semi-permanent industrial and commercial buildings. Inflatables have been the subject of considerable research activity in recent years. However, there still are a number of problems related to the behaviour of these structures which have not been fully investigated, one of which is the lateral stability of lofty cylindrical air-supported membranes subjected to the action of loads applied near the apex of the structure.

In this study, two instability/collapse problems of inflated cylindrical membranes under the action of concentrated point and line loads are considered. Firstly, a cylindrical membrane with a vertical axis subjected to an asymmetrically applied concentrated load is treated (Fig. 1). Such membranes are sometimes used in military equipment as antennas or masts. It is shown that a certain 'critical value of the load, the configuration of the structure changes drastically, as a result of which the lower part of the membrane comes into contact with the support, corresponding to a change in rigidity of the structure. Using a Lagrangian variational principle  $\delta W = 0$ , in which  $W$  is the potential energy of the system and deformations are assumed to be isometric, simple expressions are derived which relate the applied load and the geometric parameters of the membrane. Although deformations are assumed to be isometric, membrane extensibility could be included. The dead weight of the structure is taken into account in this analysis.

The results obtained describe the behaviour of such structures in their pre- and post-buckling state.

Secondly, the cylindrical membrane with horizontal axis subjected to a concentrated line load is considered. The solution for this problem is obtained by solving the set of equilibrium and compatibility equations. It is shown that a certain 'critical load' the lateral rigidity of the structure becomes zero, provided the lateral displacements lie within certain limits. This behaviour was investigated for relatively high rise cylindrical membranes, i.e. for structures with a height to span ratio greater than 0.5

Lagrangian variational methods and equations of equilibrium were used throughout the paper in obtaining the solutions.

Lofty-air supported membranes become unstable at certain values of the vertical loads applied near the apex of the

structure. The membrane geometry changes dramatically and part of the membrane comes into contact with the surface of the support. Loss of stability is possible even before such contact occurs.

References

1. Malcolm, D.J. and Glockner, P.G., "Collapse by Ponding of Air-Supported Membranes", Proc. ASCE 104, No. St. 9, Proc. Paper 14002, Sept. 1978, pp. 1525-1532.
2. Lukasiewicz, S. and Glockner, P.G., "Ponding Instability of Cylindrical Air-Supported Membranes Under Non-Symmetrical Loadings", Report No. 205, Department of Mechanical Engineering, The University of Calgary, June 1981.
3. Lukasiewicz, S.A. and Glockner, P.G., "Collapse by Ponding of Shells", Report No. 211, Department of Mechanical Engineering, The University of Calgary, November 1981.
4. Lukasiewicz, S.A. and Glockner, P.G., "Ponding Instability of Air-Supported Spherical Membranes with Initial Imperfections", Report No. 212, Department of Mechanical Engineering, The University of Calgary, November 1981.

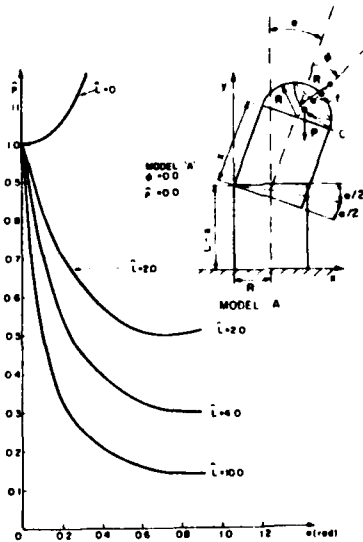


Figure 1 - Post-Buckling Load for Cylindrical Membranes with Vertical Axis vs.  $\alpha$ .

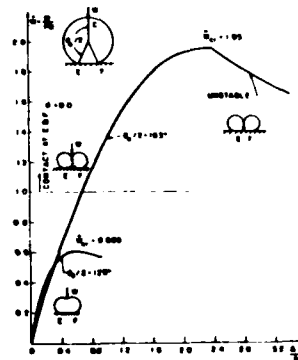


Figure 2 - Load Deflection Curve for Inextensible Cylindrical Membranes with Horizontal Axis.

## The Status of the Simple Fluid

by

R. S. Rivlin  
Lehigh University, Bethlehem, Pa., 18015

In 1957 Green and Rivlin [1] discussed the formulation of constitutive equations for materials with memory. They adopted the basic constitutive assumption that the Cauchy stress  $\underline{\sigma}(t)$  is a functional of the history of the deformation gradient matrix  $\underline{g}(\tau)$  for  $-\infty < \tau \leq t$ , thus:

$$\underline{\sigma}(t) = \underline{F}[\underline{g}(\tau)]. \quad (1)$$

They supposed that the superposition on the assumed deformation of a (time-dependent) rigid rotation merely rotates the stress by the amount of this rotation at time  $t$ . They showed that this leads to the conclusion that  $\underline{\sigma}(t)$  must be expressible in the form

$$\underline{\sigma}(t) = \underline{g}(t) \underline{G}[\underline{C}(\tau)] \underline{g}^{\dagger}(t), \quad (2)$$

where  $\underline{C}(\tau)$  is the Cauchy strain at time  $\tau$  defined by

$$\underline{C}(\tau) = \underline{g}^{\dagger}(\tau) \underline{g}(\tau). \quad (3)$$

This result was later obtained by Noll [2] using a different procedure which, while correct when there are no material constraints on the allowable deformations, can break down in certain cases in which such constraints exist [3].

In [1] the further restrictions which can be imposed on the form of the functional  $\underline{F}$  in (2) by material symmetry were discussed. If  $\{S\}$  is the group of transformations describing the material symmetry, then  $\underline{F}$  must satisfy the relation

$$\underline{F}[\underline{S} \underline{C}(\tau) \underline{S}^{\dagger}] = \underline{S} \underline{F}[\underline{C}(\tau)] \underline{S}^{\dagger}, \quad (4)$$

for all  $\underline{S}$  in the group  $\{S\}$ .

In [1] no distinction was made between solids and fluids. Such a distinction was proposed by Noll [2] in 1958. He called the materials to which (1) applies simple materials and defined a sub-class of such materials - simple fluids - for which  $\underline{F}$  in (1) satisfies the condition

$$\underline{F}[\underline{g}(\tau)] = \underline{F}[\underline{g}(\tau) \underline{U}], \quad (5)$$

for all unimodular  $\underline{U}$ . He purported to show that if this is the case then the stress  $\underline{\sigma}(t)$  must be expressible in the form

$$\underline{\sigma}(t) = \underline{G}[\underline{C}_t(\tau), \det \underline{g}(\tau)], \quad (6)$$

where

$$\underline{C}_t(\tau) = \underline{g}_t^{\dagger}(\tau) \underline{g}_t(\tau) \quad (7)$$

and  $g_t(\tau)$  is the deformation gradient matrix referred to the configuration at time  $t$ , and conversely if  $g(t)$  is given by (6) then the relation (5) is satisfied. In deriving this result, the so-called Principle of Material Indifference was also used.

It has been pointed out by Fahy and Smith [4,5] and, using a somewhat simpler argument, by Rivlin [6] that the latter statement is incorrect. In [6] it was pointed out that (5) states that  $\xi$  is a matrix-valued functional of the three row matrices formed by the rows  $g_A(\tau)$  ( $A=1,2,3$ ) of  $g(\tau)$ , each element of which is invariant under the unimodular group. It must therefore be expressible in the form

$$\xi(t) = G[\{g_A(\tau_1), g_B(\tau_2), g_C(\tau_3)\}], \quad (8)$$

where  $\{ \}$  denotes the scalar triple product. It is evident that not all functionals of the form (6) are expressible in this way. We conclude that the restriction on  $\xi(t)$  implied by (5) is far greater than that expressed by (6). The origin of Noll's fallacy which underlies the adoption of (5) may be guessed from the statement in §32 of [7] "a fluid should not alter its material response after an arbitrary deformation that leaves the density unchanged". This is not generally the case for non-Newtonian fluids. Furthermore, the statement in §32 of [7] which follows this and implies that it leads to (5) is in fact a *non sequitur*.

Nevertheless, the constitutive equation (6) may - perhaps with minor modification - describe an interesting class of fluid-like materials. If appropriately interpreted it embodies Oldroyd's characterization\* of an incompressible liquid [8]: "An incompressible liquid is not a material for which a special reference time  $t_0$  may be supposed to exist, such that the configuration at time  $t_0$  has a permanent significance in any subsequent motion. We deduce that the equations of state can be written in a form which does not involve a strain tensor  $e_{ik}$  explicitly".

If one accepts this point of view then the constitutive equation (6) follows immediately from (2) by choosing the reference configuration to be the configuration at time  $t$  and assuming that when it is so chosen no other reference configuration has any special status. We note that the assumption that we may choose the reference configuration in any way we please does not imply, as does (5), that the constitutive equation is form-invariant under changes of the reference configuration.

However, one can easily give examples of constitutive equations which evidently describe fluid-like behavior, but do involve the deformation gradients measured from a fixed reference configuration [10,11]. Also, it has been pointed out [12] that, strictly, the constitutive equation (6), modified to take account of incompressibility, does not include as a special case the incompressible Newtonian fluid.

This defect can be remedied in a number of ways [12]. For example, we can replace the constitutive assumption (1)

\* A similar motivation underlies the Rivlin-Ericksen constitutive equations for incompressible isotropic non-Newtonian fluids [9].

by the assumption

$$\underline{z}(t) = F[\underline{d}(\tau)] - p\underline{\delta} , \quad (9)$$

where  $\underline{d}(\tau)$  is the velocity gradient history measured with respect to the configuration at time  $t$ ,  $p$  is an arbitrary hydrostatic pressure and  $\underline{\delta}$  is the unit matrix. Then, in a manner similar to that by which the passage from (1) to (2) is achieved it can easily be shown that  $\underline{z}(t)$  must be expressible in the form

$$\underline{\sigma}(t) = G[\underline{g}_t^+(\tau)\underline{A}(\tau)\underline{g}_t(\tau)] - p\underline{\delta} , \quad (10)$$

where  $\underline{A}(\tau)$  is the strain-velocity matrix.

The comments in this paper are offered in the spirit of a statement attributed to Truesdell [13] "a scientist begs for intense, minute, critical study, however much he may dislike to be found wrong", in the hope that the authors whose theories are their subject will either signify their substantial agreement or present cogent reasons, devoid of bombast, for their disagreement. Anything less would render a position such as that attributed to Truesdell no more than empty posturing.

#### References

- [1] A. E. Green and R. S. Rivlin, Arch. Rational Mech. Anal. 1, 1 (1957).
- [2] W. Noll, Arch. Rational Mech. Anal. 2, 197 (1958).
- [3] G. F. Smith, private communication.
- [4] E. Fahy and G. F. Smith, Mech. Res. Comm. 5, 167 (1978).
- [5] E. Fahy and G. F. Smith, J. Non-Newtonian Fluid Mech. 7, 33 (1980).
- [6] R. S. Rivlin, J. Non-Newtonian Fluid Mech. 11, 209 (1982).
- [7] C. Truesdell and W. Noll, "The Non-Linear Field Theories of Mechanics" in Handbuch der Physik III, ed. S. Flugge, Springer, Berlin, 1966.
- [8] J. G. Oldroyd, Proc. Roy. Soc. A 200, 523 (1950).
- [9] R. S. Rivlin and J. L. Ericksen, J. Rational Mech. Anal. 4, 323 (1955).
- [10] A. E. Green, Proc. Roy. Soc. A 279, 437 (1964).
- [11] R. S. Rivlin, in "Materials with Memory", ed. D. Graffi, publ. Liguori, Naples, 183 (1979).
- [12] R. S. Rivlin, Continuum Mechanics of Geodynamics and Rock Fracture Mechanics 151-174, Reidel, Dordrecht (1974).
- [13] F. Kelly, Sun Magazine, Baltimore, 23 April, 1978.

"ON THE THERMODYNAMICS OF FLUIDS OF GRADE N  
AND CERTAIN FLUIDS OF COMPLEXITY 2"

by

J.E. Dunn  
Department of Engineering Science and Mechanics  
Virginia Polytechnic Institute and State University  
Blacksburg, VA 24061

K.R. Rajagopal  
Department of Mechanical Engineering  
University of Pittsburgh  
Pittsburgh, PA 15261

It is shown that thermodynamics forces many fluids of grade N to have certain special structural degeneracies. As a result of these degeneracies many grade N fluids can in fact be no more than very special Rivlin-Ericksen fluids of complexity 2.

## Experimental Studies and Second Order Fluids

E. A. Kearsley\*  
Rheology Research  
9409 Union Place  
Gaithersburg, Md. 20879

A second order fluid may be viewed as an approximation in a certain limit of a more general fluid with memory, or it may be viewed as a mathematical model. When viewed as an approximation, special restrictions especially on the boundary conditions may be appropriate in certain situations. Within these limitations, a number of experimental studies of materials will be discussed in terms of a second-order approximation to material with memory.

\*Research Associate, National Bureau of Standards

## INSTABILITY OF FLUIDS OF DIFFERENTIAL TYPE

by

D. D. Joseph  
Department of Aerospace Engineering  
and Mechanics  
University of Minnesota  
Minneapolis, MN 55455

It is shown that the rest state of all non degenerate fluids of complexity  $N$  or grade  $N$ , and  $N > 1$ , is unstable in the spectral sense of linearized theory.

References: Joseph, D.D., "Instability of the rest state of fluids of arbitrary grade greater than one," Arch. Rational Mech. Anal. 75, 1981, pp. 251-256.

Renardy, M., "On the domain space for constitutive laws in linear viscoelasticity," Arch. Rational Mech. Anal. (to appear).

Saut, J.C. & Joseph, D.D., "Fading Memory," Arch. Rational Mech. Anal. 81, 1983, pp. 53-95.

GRAVITATIONAL INSTABILITY OF AN INTERFACE BETWEEN  
TWO SECOND-ORDER FLUIDS\*

by

David F. McTigue  
Fluid Mechanics and Heat Transfer Division 1511  
Sandia National Laboratories  
Albuquerque, New Mexico 87185

Geophysics abounds with problems in which the stability of a perturbed interface between materials of contrasting properties is important. Two examples of creeping flow processes driven by gravity are: 1) the rebound of the earth's surface after unloading due to melting of continental ice sheets, and 2) the growth of salt domes due to buoyant rise through denser overlying strata. Previous analyses of these problems have considered linear or power-law fluid models, and thus neglect possible normal stress effects.

The stability of an interface between two halfspaces of contrasting second-order fluids ( $T = -pI + \mu_1 A_1 + \mu_2 A_2 + \mu_3 A_1^2$ ) has been examined through a perturbation scheme for small nonlinear stress terms and disturbances of small slope. The leading order problem is that for two linear fluids ( $\mu_2 = \mu_3 = 0$ ), and a well-known result is retrieved. In particular, it is found that the rate of growth or damping of periodic disturbances is independent of wavelength. This result can be anticipated simply by noting that the only parameters appearing in this problem with no imposed geometric length scale are the driving force  $\Delta\rho g$ , and the linear viscosity  $\mu_1$ , from which no length scale can be constructed.

The correction due to the nonlinear stress terms, however, leads to quite a different result. The term  $\mu_3 A_1^2$  contributes nothing in plane flows. The remaining parameters combine to form a unique length scale  $\lambda = \mu_1 / (|\mu_2| \Delta\rho g)$ . Indeed, it is shown that a critical wavelength of order  $\lambda$  exists, for which the instability is a maximum. The critical wavelength exists only if  $\mu_2 < 0$ . Because different Fourier components grow or decay at different rates, the configuration of the initial disturbance is not preserved. This is in direct contrast to the linear viscous case.

Finally, it is noted that the critical wavelength is such that the linear viscous problem must be carried out to second order in the interface slope.

\*This work performed at Sandia National Laboratories supported by the U.S. Department of Energy under Contract DE-AC04-76DP00789.

## A TENSOR CONSTITUTIVE EQUATION FOR TURBULENT FLOW

by

A. J. Baker  
Department of Engineering Science and Mechanics  
University of Tennessee  
Knoxville, TN 37996

The requirement exists to predict three-dimensional, steady, turbulent flowfield distributions in geometric configurations wherein the mean flow is essentially uni-directional, i.e., predominantly parallel to one (curvilinear) coordinate direction. Such flows predominate throughout aerodynamics, and are also exhibited in many ducted and otherwise semi-confined geometries that are devoid of abrupt changes in flow cross-sectional area. The numerical simulation of such flows introduces the requirement to establish a closure relationship for the Reynolds stress tensor  $R_{ij}$ ,

$$R_{ij}(\mathbf{x}, t) \equiv -\overline{u_i u_j} \quad (1)$$

which has been introduced by time-averaging the Navier-Stokes equations, [1]. Recall that, for the Reynolds decomposition of the velocity vector  $u_i(\mathbf{x}, t)$  as,

$$u_i(\mathbf{x}, t) \equiv \bar{u}_i(\mathbf{x}) + u_i'(\mathbf{x}, t) \quad (2)$$

the time-averaged form of the momentum equation for the incompressible mean steady flow is

$$L(\bar{u}_i) \equiv \frac{\partial}{\partial x_j} \left[ \bar{u}_i \bar{u}_j + \overline{u_i' u_j'} + \frac{1}{\rho} \bar{p} \delta_{ij} - \frac{\bar{\nu}}{Re} \left( \frac{\partial \bar{u}_i}{\partial x_j} + \frac{\partial \bar{u}_j}{\partial x_i} \right) \right] = 0 \quad (3)$$

In equation 3,  $\bar{p}$  and  $\bar{\nu}$  are the time-averaged pressure and kinematic viscosity respectively, and  $Re = \bar{\nu}U/L$  is the Reynolds number, where  $U$  is a reference velocity and  $L$  a reference length scale.

The present approach is to establish a tensor constitutive relationship for equation 1, involving components of mean flow strain rates. Lumley [2] has addressed this issue, and his analyses confirm existence at "sufficient distances from boundaries in space and time." Assuming existence of three vectors, one of which corresponds to a pure rotation, and two symmetric second order tensors, expressing invariants in the principle axes of the first tensor  $E_{ij}$ , and employing the quotient rule, Lumley [2, Appendix B] determines that the tensor constitutive relationship for equation (1) is of the form

$$R_{ij} = \alpha_1 \delta_{ij} + \alpha_2 E_{ij}^1 + \alpha_3 (E_{ij}^1)^2 + \alpha_4 E_{ij}^2 + \alpha_5 (E_{ij}^2)^2 + \alpha_6 \epsilon_{ijk} \Omega_k \quad (4)$$

The  $\alpha_l$  are functions of the invariants of  $E_{ij}^1$  and the rotation vector  $\Omega_k$ ,  $\delta_{ij}$  is the Kronecker delta and  $\epsilon_{ijk}$  is the alternating tensor. Since  $R_{ij}$  is a symmetric tensor,  $\alpha_6$  must vanish identically but the invariants of the formulation will depend upon the occurrence of  $\Omega_k$ .

A basic requirement is to establish the non-dimensionalizing length and time scales for equation 4. Based upon the cited analysis [2, Appendix A.3], for the present analysis the length and time scales are defined as

$$l \equiv \frac{k^{1/2}}{\epsilon}$$

(5)

$$\tau \equiv \frac{3\beta}{2} \frac{k}{\epsilon}$$

(6)

where  $0 \leq \beta \leq 1$  is a constant, and  $k$  and  $\epsilon$  are the turbulent kinetic energy and isotropic dissipation function respectively, defined as

$$k \equiv \frac{1}{2} \overline{u_i u_i}$$

(7)

$$\frac{2}{3} \epsilon \delta_{ij} \equiv 2\overline{\left[ \frac{\partial u_i}{\partial x_k} \frac{\partial u_j}{\partial x_k} \right]}$$

(8)

The results of the current analysis yield, for the unidirectional aerodynamic flows of interest, the determinations.

$$\alpha_1 = C_1 k$$

$$\alpha_2 = -C_4 \frac{k^2}{\epsilon}$$

$$\alpha_3 = -C_2 \tau$$

(9)

$$E_{ij}^1 \equiv \left[ \frac{\partial \bar{u}_i}{\partial x_j} + \frac{\partial \bar{u}_j}{\partial x_i} \right]$$

(10)

The correlation coefficients  $C_\gamma$ ,  $1 < \gamma < 4$ , are those of Launder, et. al. [3], with "standard values" equal to { 0.94, 0.067, 0.56, 0.068 }. No determination of  $E_{ij}^1$  results from this analysis. Numerical results for a variety of two- and three-dimensional flows have been generated to confirm appropriateness of the model.

#### References:

1. Cebeci, T. and Smith, A.M.O., Analysis of Turbulent Boundary Layers, Academic Press, New York, 1974.
2. Lumley, J.L., "Toward A Turbulent Constitutive Relation," J. Flu. Mech., V. 41, Pt. 2, 1970, pp. 413-434.
3. Launder, B.E., Reece, G.J. and Rodi, W., "Progress in the Development of a Reynolds-Stress Turbulence Closure," J. Flu. Mech., V. 68, Pt. 3, 1975, pp. 537-566.

TURBULENCE EFFECT ON LAMINAR SEPARATION  
ON A CIRCULAR CYLINDER

BY

Willy Z. Sadeh<sup>1</sup>, Daniel B. Saharon<sup>2</sup> and Peter P. Sullivan<sup>2</sup>  
Colorado State University  
Fort Collins, Colorado 80523

An investigation of the effect of freestream turbulence on laminar separation on a smooth circular cylinder in cross-flow at subcritical Reynolds numbers ranging from  $5.2 \times 10^4$  to  $2.09 \times 10^5$  was conducted. The results indicate that the interaction of incident turbulence with the initial laminar boundary layer modifies the characteristics of the mean surface pressure distribution, delays the separation and reduces the drag. These changes exhibited a distinct dependence upon the Reynolds number-background turbulence combination. Generally, the modifications of the characteristics of the mean surface pressure distribution consisted of: (1) a more favorable pressure gradient along the front of the cylinder; (2) a more negative minimum pressure and a rearward shift in its angular position; (3) a longer adverse pressure gradient region and a greater pressure rise across it; (4) a shorter base region; and, finally, (5) a less negative base pressure than in laminar incident flow. The aft shift in the separation point ranged from 5 to a maximum of  $50^\circ$  beyond the almost constant laminar separation angle of about  $80^\circ$ . At the same time, the mean turbulent drag coefficient reduced from around 1.0 to about 0.43 with increasing Reynolds number and, hence, it amounted from 97 to 46% of its nearly constant laminar counterpart.

These significant changes in the properties of the boundary layer result, according to the vorticity-amplification theory, from the energizing of the initial laminar boundary layer by penetrating turbulence concentrated at scales commensurate with its thickness. Turbulent energy accumulates within such eddies owing to the preferred amplification of freestream turbulence induced by the stretching of cross-vortex tubes in the diverging flow around the cylinder. These energy-containing eddies form a coherent substructure near the cylinder stagnation zone which ensures a continual supply of turbulent momentum and energy to the boundary layer.

<sup>1</sup>Professor of Engineering and Fluid Mechanics, Department of Civil Engineering, Member SES

<sup>2</sup>Research Assistant

The incident turbulence-boundary layer interaction mechanism is supported by correlations among characteristics of the mean surface pressure distribution and the position of the separation point with a turbulence intensity parameter and a turbulent separation parameter. These correlations attest to the transfer of turbulent momentum to the boundary layer and to the dependence of the interaction on the integral scale of background turbulence. In addition, these correlations supply a method that permits immediate estimation of the turbulent separation angle and associated characteristics of the adverse pressure gradient region for any given Reynolds number-background turbulence combination.

## FLOW BETWEEN ROTATING DISKS

## PART I, BASIC FLOW

by

S. J. Schneider, F. Labbe, H. N. Kaufman and A. Z. Szeri  
 Department of Mechanical Engineering  
 University of Pittsburgh  
 Pittsburgh, PA 15261

Multiplicity of basic flows, when the fluid is bounded by two infinite disks, has been reported by several investigators. Batchelor predicted that at high Reynolds numbers a thin boundary layer will develop on each disk, with the main body of the fluid rotating at a constant rate. This was challenged by Stewartson who reasoned that at large Reynolds numbers the flow outside the boundary layers is purely axial. Holodniok et al. identify as many as five solutions to the governing differential equations at a given (high) Reynolds number, two of which are of boundary layer type. Their low Reynolds number solution is unique and the flow is of the Batchelor type, with a substantial portion of the fluid rotating as a rigid body. Additional solutions make their appearance as the Reynolds number is increased. In their numerical treatment of disk flows Wilson and Schryer find the equilibrium flow approaching the Batchelor type flow at large Reynolds numbers, but exhibit a rotational start up scheme, which leads to an equilibrium solution in which the interior of the fluid rotates in the direction opposing disk rotation.

The question this research addresses is whether, and if so under what conditions, will infinite disk-flows approximate to laboratory flows between finite disks. The similarity solutions that have been demonstrated by various investigators, may be correct analytically, but are they physically acceptable? Should multiple solutions be accepted as truly such, for although they are shown to exist under ostensibly identical conditions, i.e., at the same Reynolds number, they lead to distinct flow behavior (boundary condition) at infinity.

Laser Doppler velocity measurements were obtained in water between finite rotating disks, with and without throughflow. When the film between the two finite disks is "thick", Adams and Szeri show that the flow is characterized by five dimensionless parameters: the rotational Reynolds number,  $Re = R_2^2 \omega / \nu$ , the throughflow Reynolds number,  $Re_0 = Q / 2\pi \nu s$ , the ratio of rotational speeds,  $\omega_2 / \omega_1$ , and two geometric ratios,  $\lambda = (R_2/s)^2$  and  $\Delta = R_2 / (R_2 - R_1)$ . The present study is limited to a single set of rotating disks with variable spacing. The parameter  $\Delta$  is fixed and the parameter  $\lambda$  is limited to two values corresponding to a "thin film" spacing,  $\lambda = 6,400$ , and corresponding to a "thick film" spacing,  $\lambda = 406.5$ . Three angular velocity ratios,  $\omega_2 / \omega_1$ , are studied. These, are:  $\omega_2 / \omega_1 = 0$ , one disk rotating and the other stationary,  $\omega_2 / \omega_1 = 1$ , co-rotating disks of equal angular velocity and  $\omega_2 / \omega_1 = -1$ , counter rotating disks of equal but opposite angular velocity. In addition we investigated the condition  $\omega_1 = \omega_2 = 0$ . Two different sets of boundary

conditions are examined for their effect on the flow.

Fig. 1 shows non-dimensional radial velocity, in an  $s = 1.26$  cm channel at  $Re = 20,319$ , when porous foam boundaries are used and one disk is rotating. On removing the foam the velocity profiles remain almost identical for  $0.3 < \bar{r} < 0.5$ , i.e., "far" away from the boundaries. This mid-radius limiting flow is identified as the Batchelor type flow that is calculated for infinite disks, Fig. 2. When conditions are such that infinite disk theory predicts multiple solutions, one of the solutions is always this type and is stable in some region  $0 < (r/s) < (r/s)_C$ . The others are unstable at all positions, i.e., at all values of the ratio  $(r/s)$  (Giron et al., 1983).

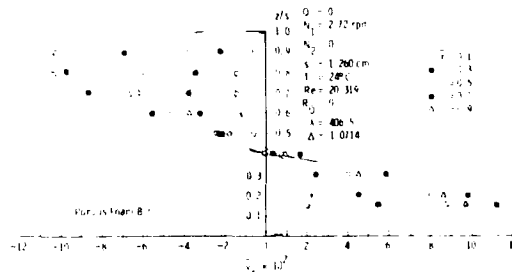


Fig. 1  
Radial velocity  
(LDV  
measurements)

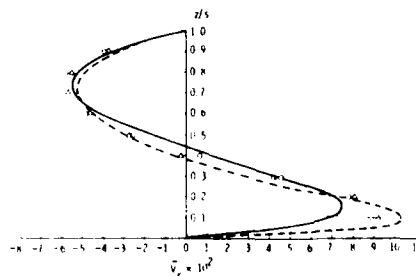


Fig. 2  
Limiting flow (o,  
foam;  $\Delta$ , natural  
boundaries;  $E^{-1}$   
=50) Infinite  
disk solution  
(...,  $E^{-1}$ =25; ...,  
 $E^{-1}$ =81;  $E$ =  
 $v/S^2\omega$ )

We have been unable to obtain radial velocity measurements between co-rotating disks. If there is a non-zero radial velocity field, it is too small for detection by our LDV system. Although numerical calculations of co-rotating disk flows reveal two radially spaced counter-rotating cells, the peak values of the non-dimensional radial velocity are of order  $10^{-9}$ .

Fig. 3 shows the radial velocity profile, at  $Re = 10,000$  with foam boundary conditions for counter-rotating disks. The earlier assertion, that the flow is a limiting flow at mid-radius, is not so obvious when comparing radial profiles of different boundary conditions. The tangential profiles, however, coincide for  $r < 0.7$ .

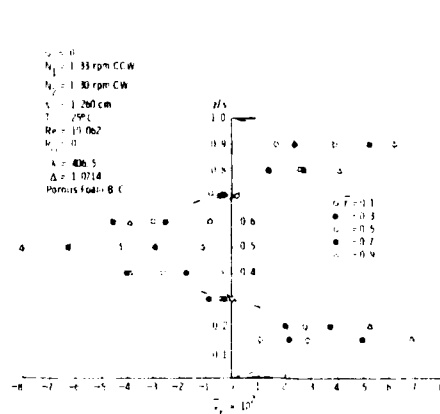


Fig. 3  
Radial velocity  
(LDV  
measurements)

Both the LDV measurements and the calculations are repeatable, irrespective of the starting conditions. We thus conclude that the limiting flows are unique and are independent of the flow history; they show a high degree of independence from boundary conditions in  $r$ . With one disk rotating and the other stationary, this mid-radius "limiting flow" is recognized as the Batchelor profile of infinite disk theory. Other profiles, predicted by this theory to coexist with the Batchelor profile, were neither observed experimentally nor were they calculated numerically by the finite disk solutions, obtained here via a Galerkin, B-spline formulation. Agreement on velocity between numerical results and experimental data is good at large values of the ratio  $R_0/Re$ . Infinite disk solutions satisfy the finite disk partial differential equations provided that the boundary conditions have been set correctly (Fig. 2).

#### REFERENCES

- Adams, M. L. and Szeri, A. Z. Incompressible flow between finite disks. *J. Appl. Mech.*, 49, 1-9, 1982.
- Batchelor, G. K. Note on a class of solutions of the Navier-Stokes equations representing rotationally symmetric flow. *Quart. J. Mech. Appl. Math.*, 4, 29, 1951.
- Giron, A., Schneider, S. J., Kaufman, H. N. and Szeri, A. Z. Flow between rotating disks. Part II, Stability. *J. Fluid Mech.*, (in print), 1983.
- Holodniok, M., Kubicek, M. and Hlavacek, V. Computation of the flow between two rotating coaxial disks. *J. Fluid Mech.*, 81, 680-699, 1977.
- Stewartson, K. On the flow between two rotating co-axial disks. *Proc. Camb. Phil. Soc.*, 3, 333-341, 1953.
- Wilson, L. O. and Schryer, N. L. Flow between a stationary and a rotating disk with suction. *J. Fluid Mech.*, 85, 479-496, 1978.

## FLOW BETWEEN ROTATING DISKS

## PART II, STABILITY

by

A. Giron, S. J. Schneider, H. N. Kaufman and A. Z. Szeri  
 Department of Mechanical Engineering  
 University of Pittsburgh  
 Pittsburgh, PA 15261

The purpose is to investigate which, if any, of the multiple solutions of infinite parallel disk flows might be realizable in the laboratory. We also analyze finite disk flows and show that the flow is least stable at the edge of the disk and near the center of rotation.

The flow field is bounded by two parallel disks of infinite radii, located at  $x^3 = 0$  and  $x^3 = s$ , respectively, in the cylindrical polar coordinate system  $\{x^1, x^2, x^3\}$ . We define another orthogonal curvilinear coordinate system, the origin of which is located on the lower disk at  $x^1 = r$ , some  $x^2$ , via the transformation

$$T: \begin{cases} x^1 = r \left[ \ln \left( \frac{x^1}{r} \right) \cos \epsilon - (x^2 + \Omega t) \sin \epsilon \right] \\ x^2 = r \left[ \ln \left( \frac{x^1}{r} \right) \sin \epsilon + (x^2 + \Omega t) \cos \epsilon \right] \\ x^3 = x^3 \end{cases}$$

In accordance with the linear theory of stability, we look for instability to perturbation which propagates in the  $x^1$  direction with speed  $\text{re}(\lambda/\alpha)$  relative to  $\{x^1\}$  and a wavelength of  $2\pi/\alpha$ . Let  $\{v; p\}$  represent the perturbation, then

$$\{\vec{v}(x); p(x)\} = \{\vec{v}(x^3); p(x^3)\} e^{i(\alpha x^1 - \lambda t)}$$

Holodniok et al. report unique basic motion at  $E^{-1} = 100$ ,  $E = v/s^2\omega$ . The velocity components of this flow, as obtained from Holodniok's paper, were projected onto directions inclined locally to the radius at the angle  $\epsilon$ . The various velocity profiles were then analyzed for stability to infinitesimal disturbances, assumed to propagate in the direction characterized by  $\epsilon$ . A plot of the Reynolds number,  $Re = r\omega s/v$ , obtained at the marginal state of stability for a given profile versus the corresponding vortex angle  $\epsilon$ , indicates that critical conditions occur at  $17^\circ < \epsilon < 20^\circ$ . The critical value of the Reynolds number is  $Re_c = 5000$ . With  $E^{-1} = 100$  this places the point of instability at  $(r/s) = 50$ . For  $(r/s) > 50$  the flow is unstable to infinitesimal disturbances.

At  $E^{-1} = 275$  Holodniok et al. display three distinct basic flows. One of these flows, designated profile (a), is of the Batchelor type. Profile (a), which shows strong resemblance to the experimental profiles of Schneider (1982), measured between finite disks, is projected onto the direction

$\epsilon$ . The curves of this figure show antisymmetry with respect to mid-channel, and indicate that the core of the fluid moves, with an almost uniform velocity, the average of the boundary velocities at the given location and in the given direction. The flow is due primarily to the motion of the boundaries and, at least superficially, it resembles Couette flow. The velocity distribution for  $\epsilon = 25^\circ$  appears to be the least stable. The critical Reynolds number is  $Re_c = 12,411.14$ . This places the point of instability at  $(r/s) \approx 41.13$ .

The other two solutions, profiles (b) and (c), obtained by Holodniok et al. at  $E^{-1} = 275$  are symmetric with respect to mid-channel. The core again moves with an almost uniform velocity. However, the core velocity may greatly exceed the velocity of either of the boundaries, and the flow resembles Poiseuille flow. Both of these profiles are found to be unstable at all values of the Reynolds number, i.e., at all positions  $(r/s)$ .

Experimental profiles of radial and tangential velocity components were obtained via laser Doppler velocimetry in water between finite disks, 50.8 cm in diameter (Schneider, et al.). The velocity components obtained in a gap  $s = 1.26$  cm with one disk rotating and the other stationary, are combined and projected onto various directions  $\epsilon$  at  $(r/s) = 14.4$  in Fig. 1. Velocity profiles measured at given position  $(r/s)$  are analyzed for stability, as in Fig. 2. At mid-radius where the basic motion approaches the infinite disk solution, the stability characteristics of the finite disk flow approach those for infinite disk flow. Figure 3 yields  $(r/s) = 15.0$  as the position of neutral stability. The critical value of the real Reynolds number is  $Re = 833.53$  and the critical vortex angle is  $\epsilon \approx 15^\circ$ .

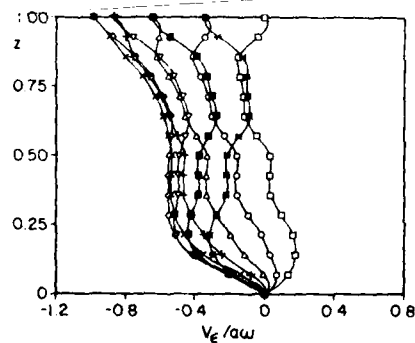


Fig. 1  
Velocity profiles for various  $\epsilon$  (Finite disks, one disk rotating).

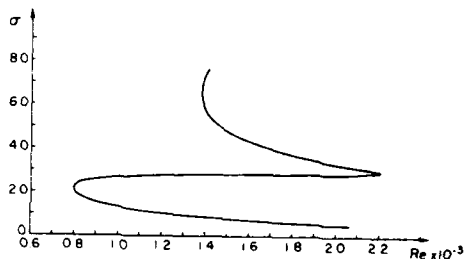


Fig. 2  
Stability dia-  
gram (Finite  
disks, one disk  
rotating).

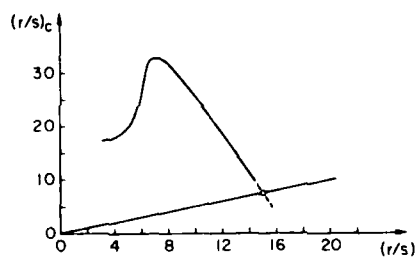


Fig. 3  
Critical radius  
(Finite disks,  
one disk rota-  
ting).

One of the observed instabilities has the appearance of equiangular spirals and seems to remain stationary relative to the rotating disk. With one disk rotating and the other stationary, the spiral angle varies between  $14^\circ$  and  $20^\circ$ . The number of vortices around the circumference is  $n \approx 51$ . Photographs yield  $r_c = 11.2$  cm for the critical radius at  $N_1 = 0$ ,  $N_2 = 11.02$  rpm and  $s = 1.26$  cm, giving  $Re = 1818.2$  for the local Reynolds number at transition. This structure is also observable between counter rotating disks, but here the vortex angle has the average value of  $\bar{\phi} = 14^\circ$  and the local Reynolds number at transition is  $Re_T(1) = 552.69$ . We estimate 30 spirals at  $N_1 = -N_2 = 2.7$  rpm and  $s = 1.26$  cm.

#### REFERENCES

- Holodniok, M., Kubicek, M. and Hlavacek, V. Computation of the flow between two rotating coaxial disks. J. Fluid Mech., 81, 680-699, 1977.
- Schneider, S. J., Labbe, F., Kaufman, H. N. and Szeri, A. Z., Flow between rotating disks. Part I, basic flow. J. Fluid Mech. (in press), 1982.

ON THE STRUCTURE OF ROTATIONAL INSTABILITIES  
IN NON-NEWTONIAN FLUIDS\*

by

Charles G. Speziale  
Mechanical Engineering Department  
Stevens Institute of Technology  
Hoboken, N.J. 07030

It has long been known that rigid body rotations can drastically alter the stability properties of a given fluid flow by having either a stabilizing or destabilizing effect. In this paper, the stability of an arbitrary base flow to large amplitude disturbances will be examined from a theoretical standpoint for incompressible non-Newtonian fluids which are subjected to superimposed rigid body rotations. This will be accomplished by a mathematical analysis of the non-inertial form of the full nonlinear disturbance equations that arise from Cauchy's equations of motion. For non-Newtonian fluids that satisfy the principle of material frame-indifference, it will be proven that instabilities which depend on the state of rotation of a fluid must arise exclusively from variations in the velocity disturbances along the axis of rotation of the fluid. Consequently, it follows that Squire's theorem cannot apply to any such rotationally dependent instabilities (i.e., the critical disturbance mode must be three-dimensional for a two-dimensional base flow).

It will be shown how these results are completely consistent with those obtained from the linear stability of rotating Newtonian fluids (see Speziale [1,2]). In this regard, instabilities of the Taylor type in Couette flow and rotating plane Poiseuille flow will be examined. The extensions of this analysis to the case of non-Newtonian fluids that violate material frame-indifference will also be discussed along with the prospects for future research.

## REFERENCES

- [1] Speziale, C.G., "On the Origin of Instabilities that Depend on the State of Rotation of a Fluid," Bull. Am. Phys. Soc., 27, 1982, p. 1202.
- [2] Speziale, C.G., "On the Nonlinear Stability of Rotating Newtonian and Non-Newtonian Fluids," Acta Mechanica, in press.

\* This work was supported by the Exxon Education Foundation.

FLOW AND FREE SURFACE OF A NON-NEWTONIAN  
 FLUID BETWEEN CONCENTRIC CYLINDERS MAINTAINED  
 AT UNEQUAL TEMPERATURES

Aydeniz Siginer  
 Department of Engineering Mechanics  
 The University of Alabama  
 University, Alabama 35486

This paper summarizes the results of an analytical investigation of the motion and the shape of the free surface of a non-Newtonian liquid which fills the open space between two concentric cylinders maintained at different temperatures. Under the effect of the temperature gradient the liquid circulates, driven by buoyant forces due to density variations and the free surface can not maintain its static shape. The analysis is set within the framework of Noll's concept of simple fluids. The motion is governed by the Oberbeck-Boussinesq equations. The non-linear problem is posed on a domain  $\mathcal{V}_{\Delta T}$  which must be determined as part of the solution. The Lagrangian theory of domain perturbations, which involves simultaneous perturbations of the field equations and the unknown flow domain  $\mathcal{V}_{\Delta T}$ , is used and the stress is assumed to be Fréchet differentiable and expanded in a series in terms of the perturbation parameter  $\Delta T$ , the temperature difference of the cylinder walls. The solution in the physical domain  $\mathcal{V}_{\Delta T}$  is represented as a power series in  $\Delta T$ , whose coefficients are the partial derivatives evaluated in  $\mathcal{V}_0$ , the rest state.

The total stress is a tensor valued functional mapping the history of the deformation  $F$  into present time  $t$ .

$$T = \mathcal{F}[F(\tau)]_{\tau=-\infty}^t$$

For steady, slow flow of an incompressible simple fluid the functional reduces to

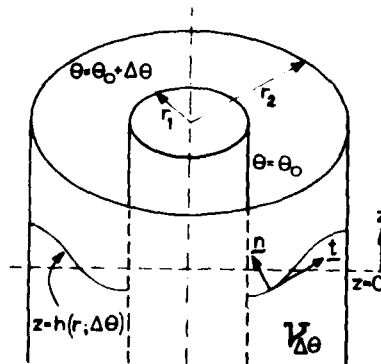
$$T = -pI + \sum_{i=1}^{\infty} S_i$$

The physical problem is described by

$$\frac{Du}{Dt} = -\nabla\phi + \rho g \alpha \theta + \nabla \cdot S, \quad \nabla \cdot u = 0, \quad u \cdot \nabla \theta = \kappa \nabla^2 \theta \quad \text{in } \mathcal{V}_{\Delta T}$$

$$\phi = p + \rho g z, \quad S = \sum_{i=1}^{\infty} S_i$$

$$\mathcal{V}_{\Delta T} = \{r, z \mid r_1 \leq r \leq r_2, -\infty < z \leq h(r; \Delta\theta)\}$$



$$u(r_i, z) = 0 \quad i=1, 2$$

$$\theta(r_1, z) = 0, \quad \theta(r_2, z) = \Delta\theta$$

$$\left. \nabla \theta \cdot \mathbf{n} \right|_{z=0} = h_r \frac{\partial \theta}{\partial r} - \theta_{,z} = 0$$

$$\left. \mathbf{u} \cdot \mathbf{n} \right|_{z=0} = u_z - h_r u_r = 0$$

$$S_{nt} = (S_{rr} - S_{zz})h_r + (h_r^2 - 1)S_{rz} = 0$$

$$u_z, u_r, S_{zz}, S_{zr} \rightarrow 0 \quad \text{as } z \rightarrow \infty$$

At the first order of the analysis there is no difference between a Newtonian and a rheologically complex fluid whose extra-stress is expandable in a Fréchet series. Although the flow and the temperature fields are coupled, at 1st order the latter can be obtained independently of the former. We find that the temperature has a logarithmic radial distribution. The flow field is obtained through the solution of an inhomogeneous, fourth order partial differential equation which involves the square of the Stokes-Beltrami operator, in the flat-top rest domain  $\mathcal{D}_0$ . A powerful set of biorthogonal, complex eigenfunctions is used for the solution of that equation. The shape of the free surface is determined through the solution of the equation which represents the balance of the jump in the normal stress by surface tension. Further details are given in [1].

- [1] Siginer, A., "Free Surface Flow of a Non-Newtonian Liquid Between Concentric Cylinders Under Constant Radial Temperature Gradient", forthcoming.

## Viscoelastic Crack in a Field of Pure Bending

by

J.M. Golden and G.A.C. Graham  
Department of Mathematics  
Simon Fraser University  
Burnaby, B.C.  
Canada V5A 1S6

The problem of a viscoelastic crack in a field of pure bending, recently considered (1), is re-examined using a different, in some ways more systematic, approach. Previous work is extended to allow demonstration of the fact that the crack may close smoothly. This is in contrast with the case of a purely elastic medium for which sudden closure always occurs. Also, a class of standard linear solids is defined which, under cyclic loading, close at only one end, at least in the early stages of loading history. This class is a function of loading frequency.

- (1) G.A.C. Graham, Mechanics Research Communications 9, 219 (1982).

The Interface Crack in a Tension Field

by

A. K. Gautesen  
Ames Laboratory  
and Department of Mathematics  
Iowa State University  
Ames, IA 50011

and

John Dundurs  
Department of Civil Engineering  
Northwestern University  
Evanston, IL 60201

The longstanding dilemmas associated with the interface crack were resolved a few years ago by Comninou, who showed that the interface crack always has contact zones at its tips. For the interface crack in a tension field, the contact zones are extremely small in comparison to the size of the crack. This leads to difficulties in the numerical solution of the governing integral equation derived by Comninou. We show that the Comninou integral equation can be solved analytically, and obtain exact results for the extent of the contact zones, the stress intensity factor, and the finite but large tension at the tips of the crack. It is also possible to derive sharp asymptotic results for these quantities when the mismatch in the elastic constants is mild. A comparison with the approximate results by Comninou and those by Adkinson is made.

THE DYNAMIC BEHAVIOR OF INTERFACIAL CRACKS  
BETWEEN DISSIMILAR ANISOTROPIC COMPOSITES

by

S. S. Wang and A. Y. Kuo\*  
Department of Theoretical and Applied Mechanics  
University of Illinois  
Urbana, IL 61801

The dynamic behavior of interfacial cracks between dissimilar anisotropic composites is studied in detail in this paper. The order of dynamic stress singularity of the interfacial crack is derived first. Both the cases of open and closed interfacial cracks are considered. Integral transform and Wiener-Hopf techniques have been used in deriving the orders of stress singularity of the interfacial cracks between dissimilar anisotropic media. An iterative scheme for determining the closure size and contact stresses of a partially closed crack is proposed. The orders of dynamic stress singularity of interfacial cracks are obtained for graphite-epoxy composites with different lamination variables and crack surface conditions. Complete asymptotic solutions and hybrid singular finite element solutions for an interfacial crack between two dissimilar anisotropic half spaces are presented for illustration and for comparison. Several unique characteristics of the transient behavior of interfacial cracks in composite materials are obtained and discussed.

---

\* Now with NEUTECH, San Jose, CA.

FINITE DEFORMATIONS OF A VISCOELASTIC ROLL COVER  
CONTACTING A RIGID PLANE SURFACE

by

C. Bapat and R.C. Batra  
Department of Engineering Mechanics  
University of Missouri-Rolla  
Rolla, MO 65401

The title problem, shown in the figure below, is studied by the finite element method. For the viscoelastic rubber-like layer we assume that

$$S_{ij} = -p(C^{-1})_{ij} + g_0 \delta_{ij} + \int_{-\infty}^t g_1(t - \tau) \frac{\partial E_{ij}}{\partial \tau}(\tau) d\tau$$

wherein  $S_{ij}$  is the 2nd Piola-Kirchoff stress tensor,  $g_0$  is the shear modulus,  $g_1$  is the relaxation modulus,  $p$  is the hydrostatic pressure not determined by the history of the deformation,  $2E_{ij} = C_{ij} - \delta_{ij}$ ,  $C_{ij}$  is the right Cauchy-Green tensor and  $\delta_{ij}$  is the Kronecker delta. Such a constitutive relation has been proposed by Christensen [1].

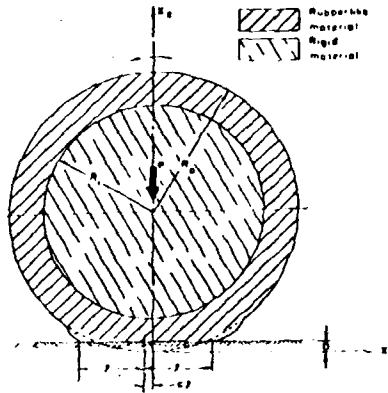
Earlier [2] we studied this problem for the case of infinitesimal deformations of the rubberlike layer and accounted for the incompressibility constraint by taking a very high value of the bulk modulus relative to the shear modulus of the material. We refer the reader to References 2, 3 and 4 for details regarding the formulation and the solution of the problem. We note that in References 3 and 4, finite deformations of rubberlike roll covers made of Mooney-Rivlin material are analyzed.

Results to be presented will include the pressure distribution at the contact surface, the stress distribution near the bond surface and the deformed shape of the roll cover. The effect of the thickness of the roll cover, the speed of rotation and the relaxation time for the rubberlike material on the pressure distribution at the contact surface has been studied.

#### References

1. Christensen, R. M., J. Appl. Mechs., 47, 762-768, 1980.
2. Bapat, C. and Batra, R. C., Mechs. Research Communication, 9, 265-272, 1982.

3. Batra, R. C., Proc. 2nd Int. Congress on Numerical Methods for Engineering, Paris, 745-754, 1980.
4. Batra, R. C., Int. J. Num. Meth. Engng., 18, 1823-1834, 1981.



## EXACT SOLUTION TO AN INVERSE PROBLEM IN THE CRACK THEORY

by

V.I. Fabrikant, T.S. Sankar and G.D. Xistris  
 Department of Mechanical Engineering  
 Concordia University  
 Montreal, Quebec, Canada H3G 1M8

Consider an isotropic elastic space weakened by an external crack  $r \geq a$ ,  $z = 0$ . The normal displacements on the crack faces are prescribed as:

$$w = w(r, \phi), \quad z = \pm 0, \quad r \geq a$$

$$\text{with } w(a, \phi) = 0 \quad \text{and} \quad \lim_{r \rightarrow \infty} w(r, \phi) = 0.$$

The tangential stresses are assumed to be zero all over the boundary. The normal stresses  $\sigma_r$ , which yield the prescribed displacements, are to be determined. This is an inverse problem because normally the stresses are given and the displacements are to be found.

According to [1], the problem reduces to the following integral equation in polar coordinates,

$$w(r, \phi) = \int_a^{\infty} \int_0^{2\pi} K(r, \phi, r_0, \phi_0) \sigma(r_0, \phi_0) r_0 dr_0 d\phi_0 \quad (1)$$

Here

$$K(r, \phi, r_0, \phi_0) = \frac{2(1-\nu^2)}{\pi^2 E} \frac{1}{r} \tan^{-1} \frac{\sqrt{r^2 - a^2} \sqrt{r_0^2 - a^2}}{ar} \quad (2)$$

and

$$r^2 = r_0^2 + r^2 - 2r_0r \cos(\phi - \phi_0)$$

A special integral representation of the kernel (2) was used to reduce the governing integral equation (1) to a sequence of two Abel-type integral operators and one L-operator as in [2]. The exact solution in a closed form was obtained using the technique developed in [2]. Several examples are also considered.

#### References

1. Galin, L.A., Contact Problems in the Theory of Elasticity, (Translation from the Russian, North Carolina State College, 1966).
2. Sankar, T.S. and Fabrikant, V.I., "Asymmetric Contact Problem including Wear for Nonhomogeneous Half-Space", Journal of Applied Mechanics, 49, 1982, pp. 43-46.

DEDUCING CONSERVATION LAWS  
VIA PHYSICAL ANALOGIES

by

Alan Hoenig  
Department of Mathematics  
City University of New York  
(John Jay College of Criminal Justice)  
445 West 59th Street  
New York, NY 10019

Certain similarities in the structure of the laws governing a class of electrostatic and elastostatic behavior can be exploited in order to generate a variety of path-independent integrals that hold true in the electrostatic domain. Specifically, consider time-independent elasticity in the absence of body forces and time-independent dielectric behavior. Upon making the substitutions

$$-\phi \rightarrow u_i, E_i \rightarrow \epsilon_{ij}, D_i \rightarrow \sigma_{ij}, \text{ and } D_i \rightarrow T_i = \sigma_{ij} n_j$$

in the equations governing elasticity one recovers the equations governing dielectrics. Here,  $\phi$ ,  $E_i$ , and  $D_i$  represent the electric potential, electric field, and dielectric field, while  $u_i$ ,  $\epsilon_{ij}$ , and  $\sigma_{ij}$  represent material displacement, elastic strain, and stress respectively. (The substitution also requires replacing the elastic constants by the dielectric permittivity.) The components of the unit normal tensor are  $n_i$ . (Subscript and tensor notation are employed throughout.)

Recently, some workers [1,2] have deduced a variety of path-independent integrals in elasticity theory, the most well-known of which is the so-called J-integral:

$$J = \oint (w dy - T_i \partial u_i / \partial x dl), \quad w = 1/2 \sigma_{ij} \epsilon_{ij}$$

The advantage of the above substitution is that it suggests the existence of an analogous integral, which we can denote by H:

$$H = \oint (w dy - D_i n_i \partial \phi / \partial x dl), \quad w = 1/2 D_i E_i$$

J has the physical property, when evaluated about the tip of a crack, that it is constant and equals the elastic energy release rate of the crack. H bears the identical interpretation with respect to the dielectric energy density release rate.

About six or so additional path-independent elastic integrals exist, and their physical interpretations relating to different energy release rates are discussed by Budiansky and Rice [2]. By means of the analogy suggested by the above substitutions, we may deduce the existence of the same number of path-independent dielectric integrals, each possessing the identical physical interpretation as their elastic analogs. (Their path independence can be independently verified via a straightforward use of the theorems of Green and Stokes.)

Note that there are a variety of physical phenomena analogous to electrostatics, and hence to elasticity. These include both electric and thermal conductivity. Again, the above analogies, coupled with judicious verification via Green's and Stokes' Theorems enable us to deduce whole families of path-independent integrals for these phenomena as well.

The H-integral can be used to solve the problem of determining the nature of the dielectric field in the vicinity of a sharp crack. Although this problem has a well-known solution which can be most easily obtained through conformal mapping techniques, this example is nevertheless presented to illustrate the potential use of such integrals.

#### References

1. J.K. Knowles and E. Sternberg, "On a class of conservation laws in linearized and finite elastostatics," Arch. Rational Mech., **44**, 3, 187-211 (1972).
2. B. Budiansky and J.R. Rice, "Conservation laws and energy release rates," J. Appl. Mech., 201-203 (March 1973).

PROBABILISTIC  
FRACTURE KINETICS

by

A.S. Krausz\* and K. Krausz  
\*Department of Mechanical Engineering  
University of Ottawa, Ottawa, Ontario  
K1N 6N5 Canada

Subcritical temperature dependent crack propagation processes are thermally activated. The fundamental elementary step of the physical mechanism is controlled by the flow of thermal energy within the solid and by the drive of the applied stress: the crack moves under the combined action of these two sources of energy. It will be shown that while the applied stress is a vector quantity the thermal energy is a scalar quantity. These basic physical considerations lead to the conclusion that fracture is essentially a stochastic process and that the macroscopically observable behavior is the net statistical result of the atomic bond breaking and healing processes.

The physical argument is expressed by a Markov chain description; it will be shown that the principles of the Markov chain mathematics are fully satisfied by the mechanism of crack propagation.

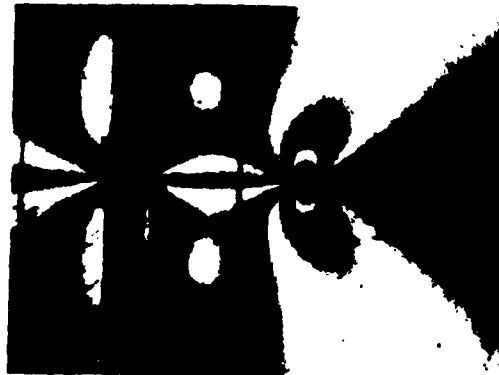
The analysis was applied to the classical Griffith theory and the corresponding modifications of the deterministic aspects are discussed. It will be also shown how the probabilistic approach can be applied in design and test engineering, and its significant advantage over the conventional fracture life time determination at the threshold will be discussed.

Dynamic Photoelastic Study of Crack Arrest  
with Attached Strip Arrestors

by

A. Shukla and K. Kumar  
University of Rhode Island  
Kingston, RI 02881

Dynamic photoelasticity is utilized to study the problem of arresting a crack after initiation so as to prevent catastrophic failure of a structure. The influence of integral strip and reinforcing strip arrestors on crack propagation and arrest in both single edge notched and modified compact tension specimens will be presented. Attention is focused on crack tip interaction with the arrestor. A typical photograph obtained during the dynamic experiment is shown in Fig. 1. The crack has passed in between the arrestor strips but the strips themselves are not broken. The strip applies a closing force behind the crack tip as shown by the isochromatic fringes. From the photographs obtained, stress intensity factor and crack tip velocity during the interaction period are calculated. Influence of the position, size and material properties of the strip arrestors is also studied.



FRAME 10,  $t = 100 \mu s$

Fig. 1: Dynamic Isochromatic Fringes Showing Running Crack Interaction with a Strip Arrestor.

Acknowledgement

This study was supported by NSF under grant No. MEA-8203277.

Sliding Contact with Friction  
and Displacement Coupling Effects

by

L. M. Brock  
Department of Engineering Mechanics  
University of Kentucky  
Lexington, Kentucky 40506

Mechanism action often involves sliding contact between elastic bodies resisted by dry or viscous friction. The friction may be accentuated by mutual indentation of the contact zone surfaces. If this indentation level and the contact zone size vary rapidly with time, then the sliding contact process is dynamic in nature, so that wave propagation effects must be considered.

The surface displacements in the contact zone must be compatible with the rigid body motions the two surfaces would undergo if no contact occurred [1]. For example, consider an elastic half-plane  $y < 0$  with a rigid die resting on but not deforming the surface, so that the die profile can be described by the equation  $y = f(x) \geq 0$ , where the  $x$ -axis lies along the half-plane surface. If, beginning at time  $t = 0$ , the die travels a distance  $D(t) \geq 0$  into the half-plane, then the displacement  $v(x, t)$  for  $t \geq 0$  of a surface point  $x$  in contact with the die is given by

$$v(x, t) = D(t) - f[x + u(x, t)]$$

where  $u(x, t)$  is the  $x$ -displacement of the point  $x$  and  $x + u(x, t)$  is clearly the new  $x$ -coordinate after displacement. If strains are small, so that a linear elastic analysis can be employed, it is sometimes argued that only the displacements perpendicular to the contact planes need be considered in satisfying the compatibility requirement. Thus,  $u(x, t)$  is dropped from the previous equation, so that the displacement components are uncoupled. However, this simplification should actually follow from the assumed negligibility of the tangential contact zone surface displacements and the undeformed surface profile gradients [1]. Thus, the above equation becomes, in the Taylor series sense,

$$v(x, t) = D(t) - f(x) - \frac{df(x)}{dx} u(x, t) - \dots - D(t) - f(x)$$

where only the first expansion term is kept because products of  $u(x, t)$  and derivatives of  $f(x)$  are assumed to be negligible when compared to  $f(x)$  itself.

This presentation considers all these factors in an idealized problem of half-plane indentation by a sliding rigid surface. Among the results obtained, it is found that dry friction accentuates the stress singularity order under the apex of wedge-shaped indentors while the coupling of both displacement components in satisfying compatibility in the absence of friction removes the singularity [2]. Since such physically unrealistic singularities do occur in typical [3] non-linear analyses without displacement coupling, this result sheds light on the arguments of [1].

[1] Muskhelishvili, N. I., Some Basic Problems of the Mathematical Theory of Elasticity, Noordhoff, Leyden 1975.

FR-2

- [2] Brock, L. M., International Journal of Engineering Science, 19, 1981, pp. 33-40. <sup>134</sup>
- [3] Beatty, M. F. and Usmani, S. A., Quarterly Journal of Mechanics and Applied Mathematics, 28, 1975, pp. 47-62.

## Tangential Loading of Elastic Bodies in Contact

by

L. M. Keer, N. Ahmadi, and T. Mura  
Department of Civil Engineering  
Northwestern University  
Evanston, Ill. 60201

This paper concerns the elastic contact between two bodies which are pressed together by normal loads and are given a tangential relative displacement. The tangential load may not be sufficient to cause sliding over the entire contact region so that a portion of the contact sticks while the remainder slips. The two bodies can have different geometrical and elastic properties. Using rectangular subdivisions for the normal and tangential stresses, a numerical scheme for the complete sliding and stick-slip cases is developed. The contact region for complete sliding is first found and assumed to be approximately correct for the stick-slip case. The method is iterative and convergence to the unknown shape of the contact region (complete slip) and the shape of the stick region (stick-slip) is rapid.

Slip Between A Layer And A Substrate Caused By  
A Normal Force Moving Steadily Over The Surface

by

F.-K. Chang, Maria Comninou and J.R. Barber  
Dept. of Mechanical Engineering and Applied Mechanics  
University of Michigan  
Ann Arbor, Michigan 48109

A normal force moves slowly over the surface of a layer which is pressed against a substrate. Two asymmetric slip zones are generated if the load exceeds a friction dependent critical value. The slip is opposite in direction in the two zones, but due to the lack of symmetry, a net tangential shift of the layer is left behind by the passage of the load. This net shift is generally influenced by the coefficient of friction: for high coefficient, the layer shifts in the direction of motion, while for low coefficient, the shift is opposite. The latter result has been observed experimentally.

Close Encounters with Friction

by

John Dundurs  
Department of Civil Engineering  
Northwestern University  
Evanston, IL 60201

and

A. K. Gautesen  
Ames Laboratory  
and Department of Mathematics  
Iowa State University  
Ames, IA 50011

An elasticity problem is invented for the purpose of illustrating some of the basic features of solutions for frictional contact, such as a loose versus strict dependence on the load path. The problem is also suitable for studying separation and slip zones caused by moving loads, and it shows explicitly the difference in the conditions at the leading and trailing edges of a slip zone under the conditions of steady state motion. Moreover, the problem can be used to assess how quickly a steady state is reached.

## NON-HERTZIAN ROLLING CONTACT WITH LONGITUDINAL CREEPAGE

by

B. Paul<sup>1</sup> and S. Singh<sup>2</sup>  
Department of Mechanical Engineering and  
Applied Mechanics  
University of Pennsylvania  
Philadelphia, PA 19104

It is known that ideal rolling is not possible for deformable rolling bodies subjected to normal and tangential forces. In such bodies, relative slip will occur over an initially unknown subregion of the contact patch. This departure from ideal rolling is called creepage. When, as in the current paper, the applied tangential force is in the direction of rolling, the creepage is called longitudinal. When the contact patch is determined a-priori by Hertz's analysis, the creepage problem may be solved by Carter's solution for rolling parallel cylinders, or by Kalker's methods for rolling ellipsoids.

The present paper introduces a method to solve the problem of longitudinal creepage for contact of rolling bodies of arbitrary (not necessarily ellipsoidal) surface geometry. Such situations arise in practice with rails and wheels which are manufactured to have discontinuities in profile curvatures, or for closely fitting conformable contact, as in well-worn convex-concave contact. Previous attempts by others to directly solve the discretized integral equation system which governs this problem have led to numerical instabilities. In the present paper, we have overcome such numerical difficulties by a number of devices, including the use of an analytical partial quadrature, prior to discretization. The procedure is efficient and has been tested against the known analytical solutions for the (Hertzian) contact patches investigated by Carter and Kalker, and against experimental results of Haines and Ollerton. We have also applied the method to problems with conformable (nonHertzian) wheel rail profiles for which the normal contact pressures and the shape of the contact patch have been determined by methods developed earlier by the authors.

The numerical procedures developed to solve the title problem work well for longitudinal creepage, and seem to have the potential to be further extended to the more general case of lateral and spin creepage. They seem to provide an attractive alternative to variational and related procedures that have recently been introduced for this class of problems.

---

<sup>1</sup>Asa Whitney Professor of Dynamical Engineering.

<sup>2</sup>Research Associate.

## NORMAL AND TANGENTIAL CONTACT STRESS FIELDS

by

L. E. Goodman  
Record Professor of Civil Engineering  
University of Minnesota  
Minneapolis, Minn. 55455 U.S.A.

G. M. Hamilton  
Department of Engineering  
The University of Reading  
Whiteknights, Reading RG6 2AY, England

When two rounded deformable bodies are pressed together a small common contact area is created and a normal contact stress field is generated in the bodies. If, subsequently, a tangential traction is applied frictional effects produce a second, tangential, contact stress field. Historically, these two solutions of the classical field equations of linear elasticity, one due to Hertz and the other to Mindlin, have been derived by quite distinct approaches. In the present presentation it is shown that the two problems, closely related physically, are also closely related mathematically. The entire three-dimensional stress fields in both cases can, moreover, for bodies having axial symmetry, be expressed in closed form in terms of elementary functions. So also can the two displacement fields. After this is done it is a relatively straightforward matter to produce the displacement fields associated with normal and torsional tractions. The path is thereby opened to a treatment of the Hertz theory of impact that will include the effects of spin as well as normal velocity.

A Finite Element Method for Two Elastoimpact Contact  
Bodies with Translational Motions

by

Naoki Asano\*  
Visiting Associate Professor  
Department of Mechanical and Aerospace Engineering  
University of Delaware  
Newark, Delaware 19711  
U.S.A.

A finite element method applicable to an analysis of elastoimpact contact structures with translational motions is formulated using the virtual work principles for elasto-impact bodies in contact and separate states, which the author has already presented [1].

The method is applied to a two-dimensional behavior for the longitudinal impact of two uniform rods with an equal cross section. Although the contact stress by the method fluctuates periodically due to the lateral effect of inertia, their mean value agrees well with that by the theory of propagation of a one-dimensional elastic stress wave. Moreover, we investigate the stick, slip and separate states on the impact surface between the two rods. Hence, the use of the method makes it possible to calculate contact and separate states of various elastoimpact contact structures.

- [1] Asano, N., "Virtual Work Principles for Two Elastoimpact Contact Bodies", Transaction of Japan Soc. Mech. Engrs. (in Japanese), Vol. 49, No. 438, Series A, (1983-2) to appear; *ibid*, Bulletin of the JSME, Vol. 26, No. 220, (1983-10) to appear.

\*On leave from Department of Mechanical Engineering, Tamagawa University, Machida, Tokyo 194, Japan.

## ELASTOHYDRODYNAMIC LUBRICATION OF SMOOTH SURFACES

by

Bernard J. Hamrock  
Tribology Branch  
NASA Lewis Research Center  
Cleveland, Ohio 44135

The emphasis in the first part is on fully flooded, elastohydrodynamically lubricated contacts. A fully flooded conjunction is one in which the film thickness is not significantly changed when the amount of lubricant is increased. Elastohydrodynamic lubrication (EHL) analysis requires the simultaneous solution of the elasticity, viscosity, density, and Reynolds equations. The most important practical aspect of elastohydrodynamic lubrication theory is the determination of the minimum film thickness within the conjunction. The maintenance of a fluid film of adequate magnitude is an essential feature of the correct operation of lubricated machine elements. The results show the influence of contact geometry on minimum film thickness as expressed by the ellipticity parameter ( $k$ ) and the dimensionless speed ( $U$ ), load ( $W$ ), and materials ( $G$ ) parameters. Film thickness equations are developed for materials of high elastic modulus, such as metal, and for materials of low elastic modulus, such as rubber. The solutions for materials of high elastic modulus are sometimes referred to as "hard EHL" and the solutions for materials of low elastic modulus as "soft EHL." In "hard EHL" not only is elastic deformation of the surfaces important, but the pressure-viscosity effects are equally as important. In "soft EHL" the elastic effects predominate. The corresponding minimum film thickness formulas are

Hard EHL

$$H_{\min} = 3.63U^{0.68}G^{0.49}W^{-0.073}(1 - e^{-0.68k}) \quad (1)$$

Soft EHL

$$H_{\min} = 7.43U^{0.65}W^{-0.21}(1 - 0.85 e^{-0.31k}) \quad (2)$$

The major difference between equations (1) and (2) is the absence of a materials parameter ( $G$ ) in the expression for low-elastic-modulus materials (eq. (2)). The main reason for this is the negligible effect of pressure on the viscosity of the lubricating fluid for the soft EHL situation. More details about the results given in the first part can be obtained from Hamrock and Dowson (1981).

In part 1 it was assumed that the lubricant is Newtonian or that the shear stress ( $\tau$ ) is linearly related to the shear rate ( $\dot{\gamma}$ ). In hard EHL the film thickness is typically about 1  $\mu\text{m}$ ; the pressure, 1 GPa; and the time that the fluid is subjected to this pressure,  $10^{-1}$  s. That the lubricant is subjected to very severe shear stresses and rates of shear has called into question the Newtonian

behavior of the fluid. Part 2 attempts to incorporate non-Newtonian fluid rheological effects into the elastohydrodynamic lubrication analysis and makes use of recent results from Jacobson and Hamrock (1983). The approach uses a Newtonian model as long as the shear stress is less than the limiting shear stress of the fluid. If the shear stress exceeds the limiting shear stress, the shear stress is set equal to the limiting shear stress. The limiting shear stress is expressed as a semiempirical linear function of pressure. From the non-Newtonian fluid model results the minimum film thickness was found to be a function of the dimensionless sliding velocity ( $U^*$ ) and the limiting-shear-strength proportionality constant ( $\alpha$ ) in addition to the conventional EHL parameters ( $U$ ,  $G$ , and  $W$ ). The resulting minimum film thickness is

Non-Newtonian - Hard EHL

$$H_{\min}^* = H_{\min} \left\{ \exp \left[ -4.07 \times 10^{-9} (U^*)^{0.60} U^{0.23} (WG^2)^{3.85} \right. \right. \\ \left. \left. + 2.06(\alpha - 0.07) \right] + U^* \right\}^{0.71} (1 - U^*)^{0.71} \quad (3)$$

where  $H_{\min}$  is obtained from equation (1). Equations (1) to (3) are an attempt to define some of the more recent formulas in existence for hard and soft EHL while considering Newtonian and non-Newtonian fluid rheology effects for smooth lubricating surfaces.

References

- Hamrock, B. J. and Dowson, D. (1981) Ball Bearing Lubrication - The Elastohydrodynamics of Elliptical Contacts, Wiley, New York.
- Jacobson, B. O. and Hamrock, B. J. (1983) "Non-Newtonian Fluid Model Incorporated into Elastohydrodynamic Lubrication of Rectangular Contacts," submitted to J. Lubr. Technol., Trans. of ASME, for publication.

## Elastohydrodynamic Lubrication of Rough Surfaces

by

H. S. Cheng  
Northwestern University  
Evanston, Illinois 60201

The effect of surface roughness on elastohydrodynamic lubrication (EHL) is dependent on the ratio of the mean film thickness to the roughness height. When this ratio approaches or falls below three, the roughness effect becomes increasingly important.

The mean film thickness in elastohydrodynamic contacts is shown to be strongly affected not only by the roughness height but also by the orientation of the asperity lays with respect to the flow. Lays in the direction of the flow, or longitudinally oriented roughness, tend to reduce the mean film thickness. For transversely oriented roughness with lays normal to the flow, the mean film thickness is improved.

In addition to the mean film thickness, the mean lubricant pressure is also affected by the roughness height and asperity lay orientation. The mean lubricant pressure has a direct influence on the mean lubricant viscosity which is shown to be strongly related to scuffing failures in EHL contacts. If the surface is too rough, lubricant viscosity in the valleys of the asperities fails to reach a high pressure, and the contact will scuff.

Surface roughness also produces local fluctuations of film thickness, pressure, and temperature at asperity contacts. Such phenomenon is known as micro-elastohydrodynamic lubrication. Micro-EHL can generate a minute film thickness which may be only in the order of 100 Å but can be sufficient to give an adequate protection against sliding failure. This micro-EHL film can be generated by a normal approach action of asperities at the inlet region of the Hertzian conjunction, by a simple sliding of one asperity, or by the collision between two asperities. An assessment is given to the level of the micro-EHL film expected by each of the three mechanisms.

An evidence is also shown that the initiation of sliding damage is related not only to the average surface temperature but also to the distribution of the local asperity temperature within the conjunction. A procedure is described for determining these micro-temperatures at the asperity contacts.

## Friction in Elastohydrodynamic Contacts

by

W. O. Winer  
School of Mechanical Engineering  
Georgia Institute of Technology  
Atlanta, Georgia 30332

Friction and traction in elastohydrodynamically lubricated contacts are complicated by the lubricant exhibiting different shear rheological responses depending on the imposed conditions and by the possible presence of mixed film behavior when the asperities of the two surfaces collide. The resistance to motion in a highly loaded non-conformal lubricated contact (elastohydrodynamic or EHD contact) is referred to as friction if it is the result of solid friction between the asperities or as traction if it is the result of shearing a lubricant film. The contact is referred to as a mixed film contact if both forms of resistance are present.

Whether or not the resistance is mixed is determined by the mean lubricant film thickness developed and the relationship of that film thickness to the composite surface roughness of the two surfaces in the run-in state. The mean film thickness is dependent upon the contacting surfaces macro-geometry and elasticity, the load on the contact, the surface velocities, the lubricant viscosity and its dependence on pressure at the temperature in the inlet wedge region. The mean film thickness is also dependent upon the surface micro-geometry but to a less well understood extent. If the mean film thickness is less than the composite surface roughness, the resistance to relative motion will result from both shearing the lubricant film and shearing the contact interface between colliding asperities. Because this solid-solid friction force is greater than the force required to shear the lubricant film, the energy dissipation in the mixed film is greater than that in fully separated contacts. The greater energy dissipation leads to higher local temperatures. Mixed film contacts are unsteady and may lead to catastrophic failure of the contact by local seizure or may wear slowly to a condition when the temperature fluctuations are small and tolerable.

The shear stress resulting from shearing the lubricant film in an elastohydrodynamic contact is often large enough to introduce non-Newtonian behavior in the lubricant. The local pressures often exceed 1 GPa and shear rates well in excess of  $10^6 \text{ sec}^{-1}$  are common. In addition the typical transit time for a particle of lubricant to be in the contact is much less than a millisecond. Average shear stresses of 50 to 100 MPa and more are not uncommon. There may be no other application in which liquids are subjected to such severe transient stress conditions. It is generally accepted that the Newtonian shear rheological model, even when the pressure and temperature dependence of viscosity are accounted

for, will not explain experimental observations except in a few cases.

A modified Maxwell model with a nonlinear viscous component has been introduced which incorporates three basic properties each a function of temperature and pressure. The three properties can be measured in primary laboratory experiments independent of the elastohydrodynamic experiment and then employed in a constitutive equation in an analysis of the elastohydrodynamic contact to predict traction. The three primary properties are the low shear rate viscosity, the elastic shear modulus and a maximum or limiting yield shear stress. It is shown that the traction predicted employing these properties in the nonlinear Maxwell model agrees well with measured traction in an elastohydrodynamic contact.

Surface Topography-Connections Between  
Lubrication and Failure Initiation

by

L.D. Wedeven  
NASA Lewis Research Center  
Cleveland, Ohio 44135

The characteristics of the initial surface topography is intimately connected to the machining process by which it is produced. It changes with time, particularly during the process of "run-in". Both processes create a near surface region of residual stresses, microstructure and hardness that is different from the bulk. The material properties in this rather undefined region can significantly influence the mode of failure, such as wear, scuffing or fatigue, as well as the degree of failure resistance for a given material.

The durability of a lubricated contact, found for example in bearings and gears, is not only associated with the properties in the near surface region, but also the various lubricating films which determine the normal and tangential stresses in the near surface region. These stresses are present on both a global and local scale with the latter associated with the topographical features of the surface. The lubricated contact problem is a systems problem with the surface topography playing a key role in the operation of the system.

It is possible to characterize surfaces with statistical parameters such as height distribution ( $\sigma$ ) and autocorrelation function, but it is difficult to establish their functional relationship to lubrication or failure processes. While the ratio of film thickness to average surface roughness ( $h/\sigma$ ) is useful to describe the degree of asperity interaction or penetration, it is well recognized that the height distribution ( $\sigma$ ) alone is not sufficient to characterize the surface. In addition, there is the problem of singular defects which frequently dominate the failure process.

Under full film elastohydrodynamic (EHD) conditions, where shear is accommodated within a relatively thick lubricant film, the normal and shear stresses are distributed uniformly over the near surface region, and the surface topography has little influence on the lubrication or failure process. Under more typical conditions where surface roughness and lubricant film thickness are of the same order of magnitude, the surface topography not only emerges as an important parameter in failure initiation, but it also becomes intimately involved in the lubrication process itself.

Experimental measurements using interferometry show how the local topographical features of a surface can influence the EHD process. The local surface geometry can change the shape of the inlet region where the EHD pressure is generated to establish a lubricant film. In addition, when the mating surfaces experience differential surface velocities, micro-EHD pressures are generated at local asperity sites giving rise to substantial asperity deformations. These deformations along with the observed increase in friction (traction) imply very high local pressures, temperatures and stresses at asperity sites even without local "asperity contact". These micro events influence the degree of asperity contact as well as the location where chemical reaction films are formed. This is shown in Fig. 1 where the formation of a reaction film is associated with the inability to form a micro-EHD film. For shallow surface depressions this occurs at the leading edge and for deeper depressions it occurs at the trailing edge.

When one considers the functionality of the surface topography it is concluded that its connection with EHD lubrication must be considered with respect to the size and shape of the inlet region. The role of surface topography is therefore connected to both the geometry of the machine elements and the parameters characterizing the operating dynamics of the lubricating mechanism. These include rolling and sliding velocities, viscosity, properties of the lubricant and load. The formation and preservation of a favorable surface topography is central to the whole issue of lubrication and failure resistance.



-Fig. 1 Formation of chemical reaction film at specific surface topography sites.

## Pitting Caused by Near-Surface Inclusions

by

L. M. Keer, G. R. Miller and H. S. Cheng  
The Technological Institute  
Northwestern University  
Evanston, Illinois 60201

An attempt is made to characterize the formation of macroscopic pits that develop under rolling conditions with light friction ( $f \sim 0.1$ ). In this circumstance it appears that at first microcracks will develop due to asperity interaction. However, their behavior can be arrested as they grow into the material due to the presence of a quiescent zone in the maximum shear stress. A possible mechanism for continued crack growth leading to a macroscopic pit may be the presence of relatively hard, near-surface inclusions. It is shown by analysis that the formation of such a pit can indeed be caused by a subsurface inclusion located within a critical depth band below the surface. Analytical and experimental results are presented that illustrate this phenomenon.

Changes in the Earth's Gravity Field  
Resulting From Deformation

by

J. B. Walsh  
Department of Earth and Planetary Sciences  
Massachusetts Institute of Technology  
Cambridge, Massachusetts 02139

The earth's gravity field changes continually by measureable amounts as mass is redistributed by natural processes affecting relatively large areas. Here, I consider gravity changes due to deformation of the earth caused by processes such as earthquakes, volcanic eruptions, and other tectonic events. The earth is assumed to be an homogeneous, elastic half-space which is deformed by introducing displacement discontinuities at depth or by applying shear and normal tractions. Applying Betti's reciprocal theorem reduces the problem to evaluating a surface integral over the source area. The necessary Green's functions are derived and found to be simple algebraic expressions. The simple form of the results allows the response of a homogeneous viscoelastic half-space to be found by inspection.

## FRICTIONAL CONSTITUTIVE LAWS AND SLIP INSTABILITIES

by

Andy Ruina  
Theoretical and Applied Mechanics  
Cornell University  
Ithaca, NY 14853

Slip instabilities are the result of interaction between a mechanical system and a slip surface. Typically the mechanical system has some elastic element which can be relaxed by slip. Slip instability can thus be discussed in terms of the interaction between stress changes on the surface as governed by the surface constitutive law, and stress changes on the surface as governed by the surrounding elastic material. An important application is the slip on geological faults interacting with the surrounding elastic rock and remote tectonic loading.

Based on the above ideas, a friction law that is described by a static coefficient of friction (strength) that is higher than a sliding coefficient of friction predicts instabilities when interacting with any elastic system. This earthquake model is, however, deficient in that it contradicts observed features of instabilities such as: a dependence on stiffness, normal force, or slip rate; non-dynamic instabilities; or slow oscillatory instability. Further, detailed study of surface constitutive laws reveals a much richer surface description.

Recent work with polished rock has suggested the surface constitutive law (at constant normal force):

$$\text{Friction force} = F(\text{state, slip rate}) \quad (1)$$

where the state is described by one or more state variables. The state variables are defined by evolution equations relating their rates of change to their current values and the slip rate. The evolution equations are restricted by the assumption (not universally valid) of a steady state.

This friction law fits some experiments well. Additionally, when used in stability analysis with elastic systems it can predict: all of the effects named above; propagating slip waves; and erratic slip. The description, depending on details and the simulated experiment, can appear similar to a variety of other constitutive laws.

## NEAR-SURFACE FLOW IN GLACIERS OBEYING GLEN'S LAW

by

Robert E. Johnson and Robert M. McMeeking  
Department of Theoretical and Applied Mechanics  
University of Illinois at Urbana-Champaign  
Urbana, IL 61801

The gravity driven motion of glaciers and ice sheets has been an active area of theoretical research since 1959 when Nye (1) first presented a steady state solution for a bounded ice sheet on a horizontal plane. Since that time there have been numerous studies of glacial motion, with the recent efforts examining the phenomena in considerable detail. For a comprehensive review of the subject, the reader is referred to the article by Hutter (2).

In determining the flow of a glacier or ice sheet which obeys Glen's flow law, previous methods have predicted infinite longitudinal stress at the glacier's surface. This physically unacceptable occurrence is due to a break-down in the mathematical methods used to obtain the solution. Here we present a method which properly determines glacial flow in the neighborhood of the free-surface for a glacier obeying Glen's law. Our interest in this subject was first aroused by Hutter (3), but the difficulty associated with determining the flow near the surface of a glacier is also discussed by Morland & Johnson (4,5) and Hutter (2).

For a material obeying Glen's law, the effective viscosity of the material is proportional to the inverse of a power of the second stress invariant. The inverse of the viscosity is often called the creep response function. The difficulty with the previous solutions has been that the second stress invariant is found to be approximately equal to the square of the shear stress. As a result it becomes small in the neighborhood of the surface because the shear stress vanishes at the free-surface. Consequently the effective viscosity becomes infinitely large near the surface and the conventional solution schemes predict infinitely large stresses at the surface when there is a non-zero stretching or compression of the material. The singular behavior in the stress field indicates that the existing solution schemes are not valid near the free surface for materials obeying Glen's law. The same would be true for any material having a creep response function which depends only on the second stress invariant and vanishes at zero stress. As pointed out by Hutter (3) the difficulty is not due to Glen's law failing to describe ice flow near the surface, but rather a failure in the method used to obtain the solution.

One attempt at avoiding the singular behavior of the stresses at the surface has been to modify Glen's law. One such modification, referred to as the finite-viscosity law (Hutter, 2,3), assumes that the effective viscosity is the inverse of a power of the second stress invariant plus a constant. Therefore when the second stress invariant

vanishes, the viscosity is finite and stress singularities are avoided. Hutter (2) speculates that the difficulty with Glen's law may be corrected by using an asymptotic method which considers the limit as the additive constant in the finite-viscosity law tends to zero. Hutter further states that, "Matched asymptotic expansions with a boundary layer at the surface are (most likely) inappropriate.... ." We show here that the method of matched asymptotic expansion is able to correct the solution in the near surface region. Hutter apparently incorrectly believed that the method relied heavily on the nature of the boundary conditions at the surface.

We begin by considering the outer solution which is valid over the majority of the glacier thickness except for a small neighborhood of the free-surface. The outer solution is well known to glaciologists and is discussed by Hutter (2,3) and Morland and Johnson (4,5). We reproduce it so that we may examine why the solution fails and thereby develop the proper scheme for the near-surface or inner region. After examining the outer solution we obtain the governing equations for the near surface region, and ultimately find a solution valid for field points in close proximity to the free-surface. The size of the near-surface region or boundary layer is found to be of order  $\delta^{1/n}$ , where  $\delta = h/L$  is the assumed small ratio of the characteristic thickness and length of the ice sheet and  $n$  is the exponent in Glen's power law. An important point to make here is that the present boundary layer analysis is essential to establishing the validity of the outer solution currently in the literature. We find that the boundary layer is relatively passive and does not significantly effect the flow field in the glacier's core. On the other hand, the present near-surface flow description has intrinsic value since many experimental observations are made at the glacier's surface.

This work was supported, in part, by grants from the National Science Foundation (MEA 81-07564, REJ; MEA 82-11018, RMM).

#### References

1. Nye, J.F. 1959 The motion of ice sheets and glaciers. *J. Glaciology* 3, 493-507.
2. Hutter, K. 1982 Dynamics of glaciers and large ice masses. *Ann. Rev. Fluid Mech.* 14, 87-130.
3. Hutter, K. 1981 The effect of longitudinal strain on the shear stress of an ice sheet: in defense of using stretched coordinates. *J. Glaciology* 27, 39-56.
4. Morland, L.W. and Johnson, I.R. 1980 Steady motion of ice sheets. *J. Glaciology* 25, 229-246.
5. Morland, L.W. and Johnson, I.R. 1982 Effects of bed inclination and topography on steady isothermal ice sheets. *J. Glaciology* 28, 71-90.

## MECHANICS OF SEISMIC GAP ZONE RUPTURE

by

Victor C. Li  
Department of Civil Engineering  
Massachusetts Institute of Technology  
Cambridge, Mass. 02139

A seismic gap zone approaching instability is modelled as a plate boundary segment bounded by one or more strength asperities. Slippage is assumed to be initiated at depth in a shear zone and progresses upwards toward the ground surface due to relative tectonic plate movements. Stress transmission in the coupled lithosphere/asthenosphere is treated by an Elsasser/Rice model. Slip zone progression at a transform plate boundary is modelled by advance of an anti-plane edge crack in an elastic strip.

Our numerical results show that the presence of strength asperities strongly influence the advancement of the zone of slip. Stress concentrations cause slip penetration at the asperities, and eventually lead to a large scale instability. The coupling between the elastic lithosphere and the Maxwellian viscoelastic asthenosphere is shown to stabilize the coupled-system, resulting in a delay in the final failure of the plate segment.[1] The influence of asperity size, strength, distribution and geometry on the behavior of the seismic gap is discussed in the context of spatial and temporal patterns of precursory seismicity. The general formalism is useful in incorporating more exact description of plate boundary constitutive laws as well as more complex fault zone geometry. The model may establish plausible physical basis for precursory phenomenon prior to large earthquakes. The near surface deformation field[2] associated with pre-seismic rupture progression may be used for interpretation of geodetic data.

- [1] V.C. Li and J.R. Rice, "Preseismic Rupture Progression and Great Earthquake Instabilities at Plate Boundaries," Accepted for Publication in Journal of Geophysical Research, Jan., 1983.
- [2] V.C. Li and J.R. Rice, "Precursory Surface Deformation in Great Plate Boundary Earthquake Sequences," Submitted to BSSA, Jan., 1983.

EFFECT OF DOUBLE ELASTIC CONSTANTS ON THE BENDING  
OF THICK ROCK SLABS

by

J.G. Singh and P.C. Upadhyay  
Institute of Technology - Banaras Hindu University  
Varanasi - 221005, INDIA

When the resultant stress field (pre-mining plus induced due to mining) around a wide opening in a stratified ground (e.g., coal measure rocks) overcomes the cohesion between the rock layers in the neighbourhood, phenomenon of bed separation takes place overhead, as shown in Figure 1. With the progress of the longwall face (coal face) more and more of overhead rock layer gets unstuck and forms a slab like structure, which undergoes progressively increasing deflection under its own increasing weight and span until it finally collapses around a span of 30-45 m. This phenomenon, called the first weighing on the face, has been a serious impediment for the general adoption of longwall caving technology. Since deflection and, hence, the stressing of such unstuck rock slab governs the stability of the hanging wall (roof) in the mine openings, it is important to have an accurate estimate of the bending stresses and deflections of such rock slabs. This can be achieved by developing more rigorous theoretical analysis and correct idealization of rock behaviour so that minimum assumptions and approximations are used.

Most of the rocks exhibit the property of double elasticity in the sense that they have unequal values of Young's modulus and Poisson's ratio in tension and compression ( $E_c \neq E_t$ ,  $\nu_c \neq \nu_t$ ). For the elastic bending of rock beams it has been shown by Jaeger [1] that the inclusion of this double elastic property affects the bending results significantly. Same conclusion has been derived in some recent works [2,3] concerned with the rock beam bending. Therefore, it was felt to be of interest to recast the bending theory for rock slabs incorporating the double elastic property of rocks.

In this paper, therefore, bending analysis of thick (including shear) rock slab has been performed including both, the effect of double Young's modulus and Poisson's ratio through the parameters  $\beta (= E_c/E_t)$  and  $\psi (= \nu_c/\nu_t)$ , respectively. Results have been presented in a form compatible to the one available for mono-elastic materials, so that all the existing results of slab bending may readily be used for rocks just by altering the results by some known factors. For example, it is found that the bending part of maximum deflection (without shear) changes by a factor,  $\xi$  given by

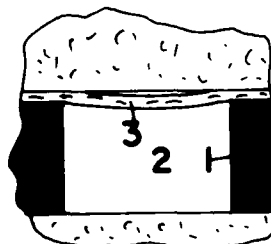


Fig. 1

1. COAL SEAM
2. HEADING (TUNNEL)
3. ROCK SLAB

$$\xi = \frac{(1 + \beta^{\frac{1}{2}}) [\psi^2(1 + \beta^{\frac{1}{2}}) - \nu^2(\psi^2 + \beta^{\frac{1}{2}})]}{4 \psi^2(1 - \nu^2)} \quad (1)$$

where,  $\nu$  refers to  $\nu_c$ .

Figure 2, which shows  $\xi$  versus  $\beta$  plots for different values of  $\psi$ , suggests that  $\beta$  has a very significant influence on the maximum deflection of the slab. It may be seen that for  $\beta$  more than 3, which is a common value for hard sandstone rocks found on top of coal seams, the maximum deflection prediction can be off by even more than 100% if the double modulus property is not duly incorporated in the analysis. The difference in the Poisson's ratio in tension and compression, however, is not found to affect the bending results, and may be assumed to be equal. This conclusion is quite useful as it will help not only in simplifying the bending analysis of rock structures but the bi-modular structures in general.

Effect of  $\beta$  and  $\psi$  are found to be similar on other quantities like the maximum shear deflection, etc., of the slab, and are discussed in the paper in detail.

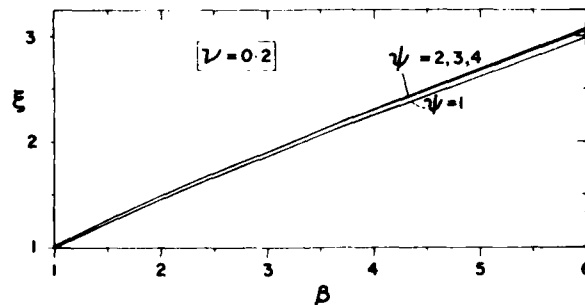


FIG. 2. EFFECT OF  $\beta$  ON  $\xi$  FOR A ROCK SLAB.

- [1] Jaeger, J.C. and Cook, N.G.W., Fundamentals of Rock Mechanics, Chapman and Hall Ltd., London, 1971
- [2] Singh, J.G. and Upadhyay, P.C., "Effect of Double Elastic Constants on the Bending of Thick Rock Beams", to be published in the Proceedings of 24th U.S. National Symposium on Rock Mechanics, June 1983.
- [3] Singh, J.G. and Upadhyay, P.C., "Creep Bending of Rocks", presented at the 19th Annual Meeting of Society of Engineering Science, October 1982.

H. Y. Fang, Lehigh Univ., R. C. Chaney, Humboldt State Univ., R. A. Failmezger, Lehigh Univ. and J. C. Evans, Woodward-Clyde Consultants.

Soil cracks are frequently observed in compacted embankments and natural slopes and are due largely to moisture variations, wet-dry and freeze-thaw cycles. Early investigations emphasized the moisture-volume changes and used the shrinkage limit as the standard index for evaluation of the cracking characteristics of soils. Recent study indicates that soil cracking is not caused only by shrinkage but thermal, tensile and fracture stresses as well. It is believed that soil cracking is the major cause of the progressive failure of earth slopes, erosion, and premature failure of highway and airfield pavements. In this paper emphasis is placed on four mechanisms of soil cracking.

Shrinkage cracking is the most commonly observed cracking in earth structures. As water is lost from the soil surface, tensile forces are established in the drying surface layer. Because of the water loss, soil loses its ability to relieve these tensile forces by plastic flow. These stresses are finally relieved by the formation of cracks that break up the surface layer into pieces of more or less distinct geometric shapes. These cracks depend on the clay mineral composition, temperature processes and pore fluid. If the soil is homogeneous, the formed pattern will be hexagonal. If the soil system is nonhomogeneous, as in the case of presence of organic matter of different water affinity and greater mobility than the mineral components, the hexagons will tend to become rounded and organic matter becomes concentrated at the surface of the fissures. Additional insight into the mechanism of shrinkage cracking is provided by the concepts of the diffuse double layer theory (1). Thermal cracks are caused by the change of the thermal stress of material. The stresses are developed when material is heated and then suddenly cooled, such as in freezing-thawing or wet-dry processes in soil. The thermal cracks for soil are somewhat different than other construction materials because the temperature and moisture in the soil mass are interrelated and the state of stress in soil is very sensitive to the moisture condition. Therefore, the thermal cracks in soil will be influenced by both temperature and moisture simultaneously. Tensile cracks due to external load application result from pressures including structural loading, rainfall, ice and snow loads, tree, vegetation and seasonal creep loads. Tensile cracks can also be associated with changes in moisture or thermal stress as previously discussed. In a soil mass, either in reworked or natural-state, there always exists some cracks. Seasonal groundwater table fluctuation, rainfall or melting snow which can fill the cracks and, consequently, result in positive or negative porewater pressures. These porewater pressures vary with changes in the environmental stimuli as will the capillarity tension produced from porewater between the soil particles. When a saturated soil dries, menisci developed in each void of the soil structure produces tension in the soil-water system and a corresponding compression force in the soil skeleton. This compressive stress acts as an effective stress in producing soil compression just as an external load. Pressure of 200 to 300 kPa can be produced in fine-grained soils. This internal cyclically applied load caused by the combination of shrinkage and/or thermal stresses and the fluctuation of the porewater pressure between soil particles is identified as a fracture load. The cracks produced from this load are referred to as fracture cracks in soil.

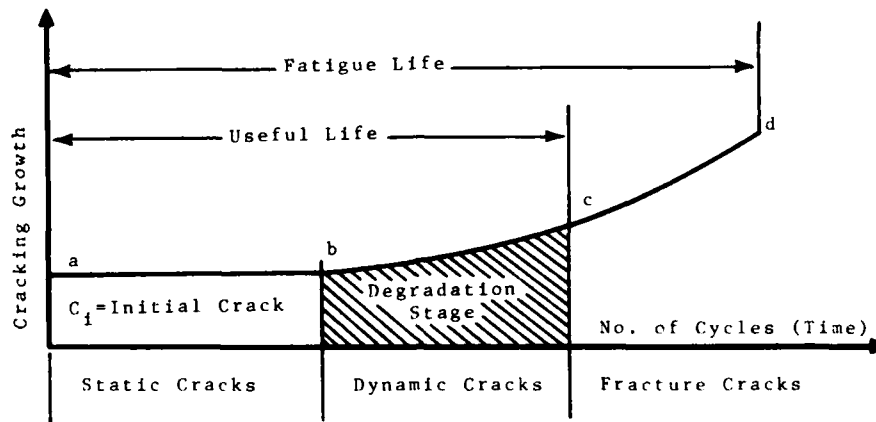


Figure 1 Diagram Illustrating the Soil Cracking-Time Relationship at Various Cracking Stages

For quantitative measurement of the cracking behavior of a soil, determining the tensile strength (2) or fracture load by use of compliance test (3) are simple approaches. A diagram illustrating the cracking-time relationship at various cracking stages is shown in Fig. 1. In examining Fig. 1 it is seen that an initial crack of size,  $C_i$  (point a) can remain constant for a large number of load cycles before an increase is noted. From points b to c is designated the ground degradation stage. In that period, ground improvement or repair work must be made in order to extend the useful life of the material. Shortly thereafter the useful life of the structure is met (point c) and if no remedial work is done, the fatigue life (point d) will rapidly occur.

Shrinkage, thermal, tensile and fracture stresses are the main factors contributing to the soil cracks. They are interrelated with the useful life of any geostucture, especially in progressive failure of slopes, erosion and premature failure of highway and airfield pavements.

#### REFERENCES

1. Evans, J.C., Fang, H.Y. and Kugelman, I.J. "Influence of Hazardous and Toxic Wastes on Fine-grained Soils," Proc. 3rd Ohio Environ. Eng. Conf. March, 1983, 46 p.
2. Fang, H.Y. and Fernandez, J. "Determination of Tensile Strength of Soils by Unconfined-Penetration Test," ASTM STP 740, 1981, pp.130-144.
3. Fang, H.Y. and Owen, T.D., Jr. "Fracture-Swelling-Shrinkage Behavior of Soft Marine Clays," Proc. Intern. Symposium on Soft Clay, Bangkok, July, 1977, pp. 15-25.

## APPLICATION OF TURBULENT MIXTURE THEORY TO THE PROBLEM OF BLOWING SNOW

By

R. L. Brown  
Civil Engineering/Engineering Mechanics Department  
Cobleigh Hall  
Montana State University  
Bozeman, MT 59717

Blowing snow involves the turbulent transport and deposition of negatively bouyant particles from the atmosphere onto the ground. Normally the particles are of complicated geometry which precludes the usual analysis techniques used for spherical particles. Experimental analysis, while scarce, indicate that settlement velocities are radically affected by turbulence, particle size, and shape. In addition, once a threshold free stream velocity is reached, particles no longer impact the surface and adhere to it; rather some of the particles rebound and enter the flow again. At sufficiently large free stream velocities, saltation and scouring occurs, and mass is actually added to the flow from the lower boundary.

A mixture theory similar to that of Bowen (1) is used to evaluate the problem of blowing snow. The momentum supply, which reflects inter-constituent forces due to their interaction, is assumed to be due primarily to Stokesian drag and bouyancy effects resulting from density gradients. First a laminar flow solution for flow over a flat surface is considered. This solution is found to be inconsistent with experimental results. Then a turbulent formulation is used to study the problem. The mixing length theory is used in the analysis. In one case the mixing length parameters were assumed to scale as the coordinate distance from the surface. This formulation was also found to be unsatisfactory when compared to the data. Next the mixing length parameters were assumed to scale with the airstream velocity. This approach gave results which compared well with the data.

The effect of particle rebound and reentrainment in the airflow was then studied. This problem was modelled by altering the sediment flow boundary conditions at the snow surface. The results of this study show increased particle density profiles near the snow surface. These results are also compared with available experimental data for these conditions. While quantitative differences were found to exist, the proper trends were observed. More experimental results are needed for a more thorough study.

Finally particle shape and size is altered to determine the effect of these variables on snow velocity and density profiles. The results show that as the particle shape becomes more complicated, as in the case of stellar crystals, free stream turbulence has an increasingly significant effect on settlement velocities and density profiles.

#### Reference

- (1) Bowen, R. M. "Theory of Mixtures, Continuum Physics Vol. III, A. C. Eringen, editor, Academic Press, New York 1976, p.p. 1-75.

## Modeling Avalanches

by

James T. Jenkins  
Department of Theoretical and Applied Mechanics  
Cornell University, Ithaca, New York

and

Hayley H. Shen  
Department of Civil and Environmental Engineering  
Clarkson College, Potsdam, New York

We operate in the context of a continuum theory for rapid deformations of granular materials recently proposed by Jenkins and Savage [1]. The balance laws and the constitutive relations of the continuum theory were obtained using arguments similar to those employed in the kinetic theory for dense gases. The constitutive relations apply to an idealized material consisting of identical smooth, nearly elastic, spherical particles.

Depth averages of the balance laws and constitutive relations in a "lubrication approximation" yield equations of evolution for the thickness profile of a mass of flowing rock or granular snow and for the depth averaged energy associated with the velocity fluctuations. We discuss the relevance of these equations to flows of granular materials down slopes and across horizontal planes.

Reference

1. Jenkins, J.T. and Savage, S.B., "A Theory for the Rapid flow of Identical, Smooth, Nearly Elastic, Spherical Particles," J. Fluid Mechanics, (in press).

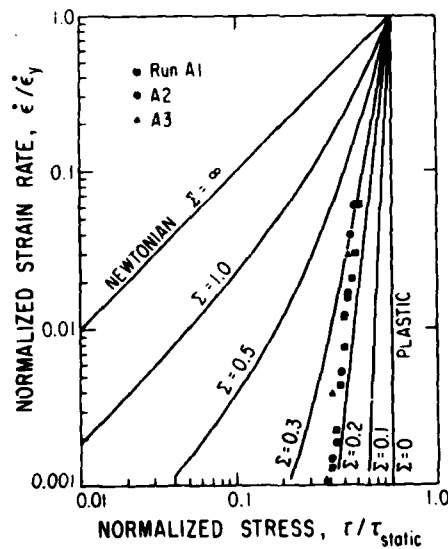
## Acoustic Fluidization

by

H. J. Melosh  
Lunar and Planetary Laboratory  
University of Arizona  
Tucson, AZ 85721

Large volumes of dry rock debris are capable of flowing as nearly frictionless fluids under the appropriate geologic circumstances. Landslides of the "long runout" variety show that rock debris can flow at high velocity (100's of km/hr) down slopes as low as  $5^\circ$ . Such landslides have been observed on the earth, Mars and the Moon, indicating that neither liquid nor gas can be the lubricant. The collapse of impact craters shortly after their formation also requires that the surrounding rock debris behave as a low friction fluid for some time after crater excavation.

I have proposed that a strong, high-frequency acoustic field might permit rock debris to flow as a fluid by locally relieving the overburden pressure and allowing the rocks in a small portion of the debris to slide at low stress. Repetition of this process throughout the debris mass causes wholesale flow under low applied stresses. This concept has been tested experimentally. A mass of quartz sand was excited by ultrasonic sound at frequencies ranging from 25 to 50 kHz, and the relation between stress and strain measured by a rotational viscometer. The sand is observed to flow under applied stresses an order of magnitude smaller than the static yield strength. The flow law



is highly non-Newtonian; strain rate is proportional to stress raised to approximately the 8th power. The stress exponent is predicted to depend upon acoustic field strength: the flow law is Newtonian for the strongest fields. Further work is proceeding on the energies of acoustic energy generation and decay. Results to date support the idea that dry rock debris (or any other granular material) can be fluidized by high-frequency sound.

Figure: The relation between the theoretical (solid lines) and experimental (points) flow laws in sand fluidized by 37 kHz ultrasonic sound.  $\Sigma$  is the ratio between the mean and the overburden pressure.

Relations Between Mixture Theory  
and Classical Soil Mechanics\*

Stephen L. Passman  
Division 1533

and

David F. McTigue  
Division 1511

Sandia National Laboratories  
Albuquerque, New Mexico 87185

The local equations for conservation of mass and balance of momentum for two-constituent mixtures are well known. We assume a saturated mixture of this type, in which the constituents cannot interpenetrate. We let one constituent be a solid and the other a fluid. The proportion of space occupied by the fluid is called the porosity, with the solid occupying the rest of space. Three constitutive equations are of interest: that for the stress in the fluid, that for the stress in the solid, and that for the force of interaction. The force of interaction is of particular interest. We generalize a classical argument showing that if the constituents cannot interpenetrate, that force must have a term proportional to the porosity gradient. To simplify the subsequent arguments, we assume the fluid has no viscosity. Then the equations of balance of momentum may be rewritten in a form commonly accepted by specialists in soil mechanics and flow through porous media. A particular combination of the stress in the solid, the stress in the fluid, and the porosity occurs in such a fashion that it is natural to call this quantity the "effective stress". We show that our equations easily and logically yield the classical theories of Biot. Moreover, since we have not made any assumption about speed or acceleration of the motion, it is possible to provide clear formulations of constitutive equations for dynamic situations, thus overcoming a difficulty discussed extensively in the literature on applications. The theory may be extended without difficulty to more than one component, to unsaturated mixtures, and to situations where thermodynamic effects are significant.

\*This work performed at Sandia National Laboratories supported by the U.S. Department of Energy under Contract DE-AC04-76DP00789.

THE EFFECT OF PARTICLE SIZE DISTRIBUTION ON  
STRESSES IN RAPID GRANULAR FLOWS

by

Hayley H. Shen  
Dept. of Civil and Environmental Engineering  
Clarkson College of Technology  
Potsdam, New York 13676

Existing theories which predict the stress-strain rate relationship in a rapidly sheared granular flow can only treat materials that are made of single sized particles [3, 4,5,7]. However, granular flows generally involve materials of mixed sized particles. Although it has been observed in many laboratory studies that size distribution has significant effect on the stress generated in granular flows [1,2,6], no existing theory can explain this effect. The present study quantifies stresses in a rapidly sheared granular mixture consisting of particles of different sizes. Collisional interactions between adjacent particles are considered as the dominating stress generating mechanism. The stresses are computed as the rate of momentum transfer across a unit surface area due to binary collisions. The effect of size ratio and the relative concentration on the resulting stresses are determined for a mixture of two sized spherical particles. The quantitative results of a typical case is shown in the figure. Comparisons of the present theory with existing experimental data are presented. Generalization to incorporate a complete spectrum of size distribution is also discussed.

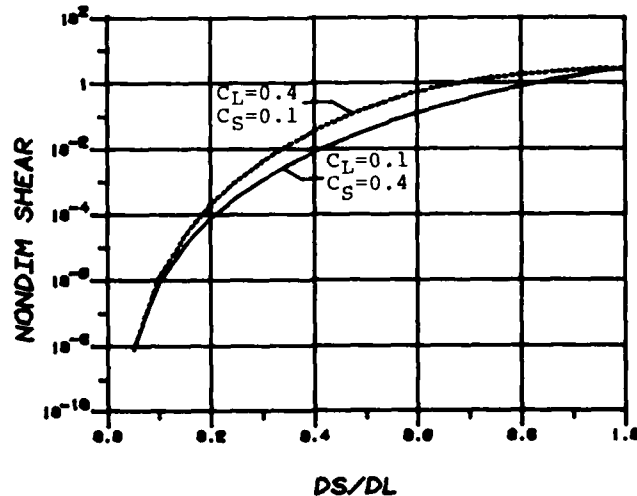


Fig. Nondimensional Shear Stress vs. Ratio of Particle Diameters.  $C_L$ ,  $C_S$  = concentration of large and small particles;  $D_L$ ,  $D_S$  = diameter of large and small particles.

## REFERENCES

1. Durand, R., Proc. Minnesota Int. Hyd. Convention, 1953, pp. 89-103.
2. Gilbert, G.K., Professional Paper No. 86, USGS, 1914.
3. Jenkins, J.T. and Savage, S.B., pending publication.
4. Kanatani, K.I., Int. J. of Engg. Sci., V. 17, 1979, pp. 419-432.
5. Ogawa, S., Umemura, A. and Oshima, N., ZAMP, Vol. 31, 1980, pp. 483-493.
6. Sayed, M., Ph.D. Dissert., McGill Univ., Montreal, 1981.
7. Shen, H. and Ackermann, N.L., ASCE/EMD, V. 108, No. EM5, 1982, pp. 748-763.

Oscillatory Densification of Fully Fluidized Granular  
Materials Undergoing Cyclic Shear Loadings

by

M. Shahinpoor

Department of Mechanical and Industrial Engineering  
Clarkson College of Technology  
Potsdam, NY 13676

Under fully fluidized conditions granular materials have been shown [1], [2] to behave similar to a non-Newtonian fluid. In this fully fluidized state the stresses depend on the square of the velocity gradients. The relevant material coefficients depend on interparticle friction, coefficient of restitution and a number of internal statistical parameters [1], [2]. We assume in the present analysis that a state of vibrofluidization of a two-dimensional granular assembly undergoing cyclic shear loadings in a simple shear box (Fig. 1) can be represented by a system of stresses suggested in [1] and [2].

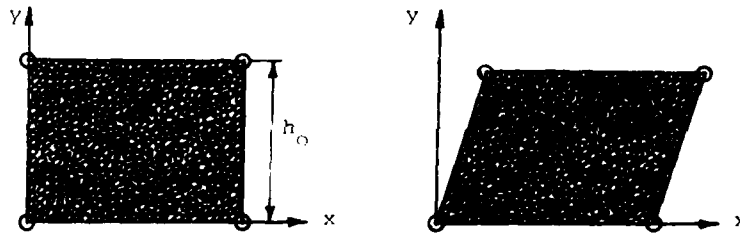


Fig. 1. Cyclic Shear Loading Process in a Simple Shear Box

Thus we assume that

$$\tau_{xx} = K\tau_{yy}, \quad \tau_{xy} = \tau_{yx} = \alpha_1 \left(\frac{\partial u}{\partial y}\right)^2, \quad (1), (2)$$

$$\tau_{yy} = -p_0 + \alpha_2 \left(\frac{\partial u}{\partial y}\right)^2, \quad (3),$$

where  $K$  is a pressure ratio,  $\alpha_1$ ,  $\alpha_2$  are material parameters,  $p_0$  is a confining pressure, and  $(u, v)$  are the components of the velocity vector in the  $x$  and  $y$  directions such that  $(x, y)$  form a rectangular Cartesian system of coordinates. The governing equations of motion in the absence of gravitational effects reduce to

$$\rho \left( \frac{\partial u}{\partial t} + v \frac{\partial u}{\partial y} \right) = 2\alpha_1 \left( \frac{\partial^2 u}{\partial y^2} \right) \left( \frac{\partial u}{\partial y} \right), \quad (4)$$

$$\rho \left( \frac{\partial v}{\partial t} + v \frac{\partial v}{\partial y} \right) = 2\alpha_2 \left( \frac{\partial^2 u}{\partial y^2} \right) \left( \frac{\partial u}{\partial y} \right), \quad (5)$$

where  $\rho$  is the bulk density. In deriving equations (4) and (5) we have assumed  $\rho$ ,  $\alpha_1$  and  $\alpha_2$  to be only functions

$t$  and the coordinate dependence is only on  $y$ . The continuity equation reduces to

$$\frac{\partial \rho}{\partial t} + \rho \frac{\partial v}{\partial y} = 0, \quad (6)$$

such that it can be immediately integrated to yield

$$[\rho(t)/\rho(t_0)] = \exp\left[-\int_{t_0}^t \left(\frac{\partial v}{\partial y}\right) d\xi\right], \quad (7)$$

where  $t_0$  is the initial time before each loading cycle.

One special solution to the above set can be shown to be given by

$$u(y,t) = \left\{ \frac{y}{h_0(t+a^*)} \right\}, \quad (8)$$

$$v(y,t) = \left\{ \frac{y}{(t+a^*)} \right\}, \quad (9)$$

where  $a^*$  is an integration constant and  $h_0$  is the height of the sample measured from  $y=0$  at the beginning of each cyclic loading. Thus, equation (7) reduces to

$$[\rho(t)/\rho(t_0)] = \left[ \frac{t_0+a^*}{t+a^*} \right], \quad t \geq t_0, \quad (10)$$

which indicates the initial densification of the granular assembly in each cycle of loading. As  $t_0 \rightarrow \infty$  the amount of densification per cycle diminishes and finally approaches zero. These observations are in harmony with the experimental results of Leslie Youd [3], [4].

Of course the above solutions are rather restricted. However, they indicate that more sophisticated solutions may be obtained pertaining to a detailed description of vibratory compaction of granular materials.

#### References

1. Shahinpoor, M. and Siah, J.S.S., "New Constitutive Equations for the Rapid Flow of Granular Materials," 9 (1981), pp. 147-156.
2. Shahinpoor, M., "New Constitutive Equations for the Rapid Flow of Granular Materials - II," 12 (1983), pp. 31-38.
3. Leslie Youd, M., "The Engineering Properties of Cohesionless Materials During Vibration," Ph.D. Thesis, Iowa State Univ., Ames, Iowa (1967).
4. Leslie Youd, M., "Compaction of Sands by Repeated Shear Straining," ASCE Soil Mech. Found. Engng., 98, SM7 (1972), pp. 709-725.

Upper Bound Limit Analysis of the Stability  
of a Seismic-Informed Earthslope

by

W. F. Chen  
Sch. of Civil Engineering  
Purdue University  
W. Lafayette, IN 47907

S. L. Koh  
Department of Mechanical and  
Aerospace Engineering  
West Virginia University  
Morgantown, W.V. 26506

S. W. Chan  
Formerly Research Assistant  
School of Mechanical Engineering  
Purdue University  
W. Lafayette, IN 47907

Earthquakes continue to be a subject of intensive studies. The damage to properties and the widespread deaths that may be traced back to earthquakes as the main cause are well-recorded. In many instances, the severest destructions and greatest number of casualties result from earthquake-induced landslides. Records show that landslides occur most frequently on sloping earthmasses. They are observed on the slopes of dams, embankments and other man-made cuts; on the banks of rivers, lakes, reservoirs, and along coasts as well as on mountain slopes. For simplicity, such sloping earthmasses will be referred to as 'earth-slopes' throughout this paper.

Because of the potential threats associated with these landslides, there is an urgent need to advance the state of the art to develop more effective methods for the assessment of such dangers. Common practice in such analyses involves the neglecting of the more complex soil behaviors and properties, as well as the simplification of the seismic forces as being constant. While at the present, attempts are underway by other investigators [Ref. 1 & 2] to more precisely formulate the critical soil behaviors, this study will be limited to the improvement of the analysis through the incorporation of non-constant seismic forces throughout the slope height. This study will not only allow for the refinement of results, but would also shed light on the possibility of incorporating the nonhomogeneity of some soil properties. To this end, more realistic estimation on the earthslope stability can be made with relative ease.

Historically, the study of an earthslope's potential for collapse under its own weight has been the main concern of the earth-structure engineers. Because of its geometrical configuration, density, and strength properties, a slope with a height above certain critical value may become too weak to support the weight of its own mass. This soil mass is then assumed to move downslope by the gravitational pull along a well-defined failure surface. Practices have been to approach the problem in a phenomenological way, where the variety of postelastic soil behavior is replaced by a model of perfect plasticity [Ref. 3]. The idealized homogeneous and isotropic soil is further

assumed to yield under the well-known Coulomb criterion and its associated flow rule. Then methods were derived to predict the existence of a slip surface, which would yield without restrictions, carrying the soil mass above it down-slope. Among the more famous methods are the slip-line method, the limit-equilibrium methods, and the limit analysis approach. Of these, the limit analysis approach is relatively easier and have applications to a larger range of slope geometries.

The extension of the limit analysis method for the static case to the case of seismic loadings is a logical step forward. The existing approach involves essentially adding to the deadweight of the potential collapse mass a pseudo-static force simulating the seismic load. This force acting through the center of gravity of the soil mass is expressed as the product of the soil mass and a "seismic coefficient". The choice of such a coefficient is to reflect the maximum force exerted on the slope for the time history of an earthquake.

The criticism on this rather crude approach are: (i) The seismic coefficient of a slope is not a constant value during any instant of an earthquake. Owing to the non-rigidity of the soil layers, the reactive forces developed throughout the height of the slope as a result of the movement of the ground always vary. (ii) Because of the granular nature of the soil, it is reasonable to expect the density and strength properties to vary along the height as the consequence of different degrees of water saturation inside the inter-granular voids of the soil.

To get around the first problem, a more recent effort [Ref. 2] was made to incorporate zones of different seismic coefficients along the height to approximate the actual variation. While such approach is a definite improvement over the earlier ones, there are also restrictions to its applications. A conceivable difficulty is the case where the variation of the seismic coefficient is so sharp that a large number of thin zones have to be used.

The next logical step towards a better analysis of the earthslope is to develop formulations to account for a more accurate seismic profile. The seismic coefficient as a function of the elevation above the ground level must be recognized. The vertical component of the seismic force, neglected in earlier works, must be included. Through appropriate interpretation, the vertical seismic profile can also be used to represent the variation of density along the height as well. With more rigorous and general formulations, further implications of the possibility of incorporating the profiles of strength parameters into the model can be made. All these are undertaken in this study.

#### References

1. Chen, W.F., and Koh, S.L., "Earthquake-Induce Landslide Problems," Proc. Cen. Am. Conf. on Earthquake Eng., San Salvador, El Salvador (1978).
2. Chen, W.F., "Plasticity in Soil Mechanics & Landslides," J. Eng. Mech. Div., Proc. Am. Soc. Civ. Eng., June 1980.
3. Chen, W.F., Giger, M., and Fang, H.Y., "On the Limit Analysis of Stability of Slopes," Soils & Found. Japan. Soc. Soil Mech. & Found. Eng., v. 9, #4 (1969).

## Porosity, Permeability and Plastic Flow in Rocks

by

Brian Evans

Department of Geological and Geophysical Sciences  
Princeton University  
Princeton, NJ 08544

The natural diagenesis and lithification of sediments to form indurated rocks may involve biological, chemical and physical mechanisms. If one considers only non-brittle mechanical deformation (e.g. dislocation motion; diffusional creep; solution, transfer, and precipitation of the matrix in a pore fluid) parallels may be drawn with such engineering processes as hot isostatic pressing (HIP), sintering and crack annealing.

The permeability of both indurated and nonindurated material can be reduced by plastic flow processes. Recent HIP experiments on calcite powders show that permeability decreases dramatically as the aggregate density reaches approximately .95 theoretical density in general agreement with various published theories of the HIP process. Similar drops in permeability have been observed or inferred from the final microstructure during experiments involving the deformation of gouge by workers in several laboratories.

Reductions in permeability of cracked crystalline rock can occur by crack healing. In quartz such processes significantly alter microcrack connectivity in laboratory times at temperatures as low as 300°C. Preliminary modelling of crack annealing using a theory due to A. G. Evans and R. Charles shows that intragranular microcrack porosity in the earth will have geologically short lifetimes. Joint porosity is inferred to remain open for much longer times allowing the circulation of fluids at some depth. The actual rate of change of porosity of rocks at depth is determined by the competition of porosity producing processes (e.g. brittle failure by static fatigue or hydrofracture, or the circulation of large volumes of undersaturated fluids) and porosity reducing processes. However, many questions remain before accurate modelling may be done.

## MICROCRACK INTERACTION AND ROCK FAILURE\*

by

S. Nemat-Nasser and H. Horii  
Department of Civil Engineering  
The Technological Institute  
Northwestern University  
Evanston, Illinois 60201

Rocks generally contain microcracks, fissures, and other inhomogeneities, which profoundly affect their overall mechanical response. For example, growth of microcracks under farfield compression may lead to the phenomena of axial splitting, rockburst, surface spalling, and exfoliation; see Holzhausen [1], Holzhausen and Johnson [2], and Nemat-Nasser and Horii [3]. Another interesting feature of rocks with microcracks is their overall stress-induced anisotropy. Under applied loads, some microcracks may close, some may undergo frictional sliding, and some may extend in a preferred direction, resulting in a highly anisotropic response as well as failure modes.

The lecture summarizes some recent studies by the authors on the overall response and on the local failure mechanisms of solids containing microcracks (Nemat-Nasser and Horii [3], Horii and Nemat-Nasser [4,5], and Nemat-Nasser [6]), emphasizing the role of crack interaction in producing the final failure modes. Some new experimental results will also be discussed.

References

1. Holzhausen, G. R., "Sheet Structure in Rock and Some Related Problems in Rock Mechanics," Ph.D. Thesis, Stanford University, Stanford, CA, 1978.
2. Holzhausen, G. R. and Johnson, A. M., "Analyses of Longitudinal Splitting of Uniaxially Compressed Rock Cylinders," Int. J. Rock Mech. Min. Sci. Geomech. Abstr., 16, 1979, pp. 163-177.
3. Nemat-Nasser, S. and Horii, H., "Compression-Induced Nonplanar Crack Extension with Application to Splitting, Exfoliation, and Rockburst," J. Geophys. Res., 87, 1982, pp. 6805-6821.
4. Horii, H. and Nemat-Nasser, S., "Curved Crack Growth in Brittle Solids Under Far-Field Compression," 1982 Advances in Aerospace Structures and Materials, Laurenson, R. M. and Yuceoglu, U., Eds., ASME Publ. No. AD-03, ASME, New York, 1982, pp. 75-82.

---

\*This work has been supported by the United States Air Force Office of Scientific Research under Grant No. AFOSR-80-0017 to Northwestern University.

5. Horii, H. and Nemat-Nasser, S., "Overall Moduli of Solids with Microcracks: Load-Induced Anisotropy," Earthquake Research and Engineering Laboratory, Tech. Rept. No. 82-6-46, Dept. of Civil Engineering, Northwestern University, Evanston, IL, June 1982; J. Mech. Phys. Solids, to appear.
6. Nemat-Nasser, S., "Non-Coplanar Crack Growth," Earthquake Research and Engineering Laboratory, Tech. Rept. No. 83-1-49, Dept. of Civil Engineering, Northwestern University, Evanston, IL, January 1983; Proc. ICF Int. Symp. on Fracture Mechanics, Beijing, China, Nov. 22-25, 1983, to appear.

## NONLINEAR TRANSIENT PHENOMENA IN SATURATED SOIL MEDIA

by

Jean H. Prevost  
Department of Civil Engineering  
Princeton University  
Princeton, New Jersey, 08544

In this paper the transient response of saturated soils is analyzed. The saturated soil is modelled as a two-phase system consisting of a solid and a fluid phase. The coupled field equations based on mixture's theories are presented, and solved numerically by the use of the finite element method. Time integration of the resulting coupled nonlinear semidiscrete finite element equations is achieved by using an implicit/explicit predictor/multicorrector scheme developed by Hughes and co-workers. The procedure allows for a convenient selection of implicit and explicit elements, and/or for an implicit/explicit splitting of the various operators appearing in the differential equations. Numerical results which demonstrate the accuracy and versatility of the proposed procedure are presented.

Frequency Distribution of Contact Angles in Random  
Monogranular Layers

M. Shahinpoor  
Department of Mechanical and Industrial Engineering  
Clarkson College of Technology  
Potsdam, NY 13676

For certain special configurations in random packing of monogranular layers it is possible to determine the frequency distribution of contact angles among neighboring grains. The frequency distribution of contact angles can be computed by solving an integral equation of first kind of the Fredholm type. These distributions will be shown to be generally Maxwellian, with tails biased towards the population of denser "Voronoi Cells" that are statistically more stable.

Let us consider a typical arrangement of disks in a randomly packed monogranular layer as shown below:

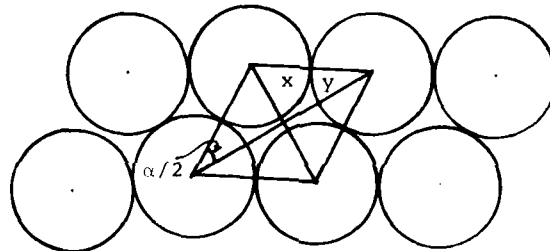


Fig. 1. A typical arrangement in monogranular layers

Here  $\alpha$  is defined as a relative contact angle among the neighboring grain. Note that the local void ratio  $e$  is given by

$$e(\alpha) = (4/\pi) \sin \alpha - 1 \quad (1)$$

such that  $\frac{\pi}{3} \leq \alpha \leq \frac{\pi}{2}$  is a randomly distributed internal statistical parameter. Our aim is to find a frequency distribution  $p(\alpha)$  for  $\alpha$  for any given average void ratio  $\bar{e}$  such that

$$\int_{\pi/3}^{\pi/2} p(\alpha) d\alpha = 1, \quad (2)$$

$$\bar{e} = \int_{\pi/3}^{\pi/2} p(\alpha) e(\alpha) d\alpha = \int_{\pi/3}^{\pi/2} p(\alpha) [(4/\pi) \sin \alpha - 1] d\alpha, \quad (3)$$

If we assume that the  $x$ 's are uniformly distributed throughout the assembly, then  $p(\alpha) = (6/\pi)$  and from equation (3) we obtain

$$\bar{e}_u = \int_{\pi/3}^{\pi/2} \frac{6}{\pi} [(4/\pi) \sin \tau - 1] d\tau = (12/\pi^2) - 1 = 0.2158542, \quad (4)$$

This average void ratio corresponding to the most random distribution of  $\tau$  is larger than the critical void ratios  $\bar{e}_{cr.} = 0.182$  of 2-D random packings [1].

In order to find the pertinent critical distribution  $p(\alpha)$  corresponding to  $\bar{e}_{cr.} = 0.182$  one should solve the integral equation (3) which is a Fredholm of first kind. An exact solution for this integral equation is found to be

$$p(\alpha) = \left\{ \frac{\lambda \exp(-\lambda\alpha)}{\exp(-\lambda\pi/3) - \exp(-\lambda\pi/2)} \right\}, \quad (5)$$

where  $\lambda$  is a root of the following transcendental equation

$$\pi(\bar{e}+1)(1+\lambda^2)[\exp(-\lambda\pi/3) - \exp(-\lambda\pi/2)] + 2\lambda[2\lambda \exp(-\lambda\pi/2) - \exp(-\lambda\pi/3) - \sqrt{3}\lambda \exp(-\lambda\pi/3)] = 0. \quad (6)$$

So that for any given  $\bar{e}$  a value for  $\lambda$  can be found. In particular for  $\bar{e}_{cr.} = 0.182$  one finds from equation (6) that  $\lambda_{cr.} = 4.685$  so that

$$p_{cr.}(\alpha) = 7330.62 \exp(-4.685\alpha). \quad (7)$$

As can be seen the frequency distributions are generally Maxwellian with tails biased towards the population of denser "Voronoi Cells." These distributions are important in studying the stresses developed in granular media [2] and specially in computing the average fabric tensors [3].

#### References

1. Shahinpoor, M., "A Model for Crystallization of Monomolecular Layers on Contracting Surfaces," *J. Colloid Interface Sci.*, **85** (1982), pp. 227-234.
2. Matsuoka, H., "A Microscopic Study on Shear Mechanism of Granular Materials," *Soils and Foundat.*, **5** (1974), pp. 29-43.
3. Oda, M., Nemat-Nasser, S. and Mehrabadi, M.M., "A Statistical Study of Fabric in a Random Assembly of Spherical Granules," *Int. J. Num. Anal. Meth. Geomech.*, **6** (1982), pp. 77-94.

Stochastic Simulation of  
Creep Behavior

By

Dr. Chandra S. Brahma, P.E.  
Professor of Civil Engineering  
California State University, Fresno  
Fresno, California 93740

And

Consultant, Sverdrup & Parcel and  
Associates, Inc.  
St. Louis, Missouri 63101

The deformation of granular media is studied from the point of view of the particulate structure. A granular soil is a random assembly of particles and a probability function is used to describe the number of contacts and their direction. Under a given stress increment, particle movements occur because of slips at the contacts. These considerations lead to the conclusion that the displacements at the contacts during deformational process can be treated by the methods of stochastic processes. Under the action of intergranular forces in the granular mass, the particles move back and forth in a series of steps. Accordingly, a random walk model has been postulated to describe the displacement behavior of particles. The differential equations, characterizing the transient phenomenon in the process, have been solved for appropriate boundary conditions and a strain-time relationship is derived for externally applied loading conditions.

A model test box, capable of applying principal stress, is designed to investigate the qualitative behavior of assembly of steel rods under hydrostatic as well as deviatoric loading conditions. A high speed camera is used to further provide a pictorial medium of study for the motion of individual rods. The agreement between the experimental results and those computed theoretically reveals that the stochastic model adequately simulates the behavior of the steel rod assemblies under various external loadings. Furthermore, the behavior of the two-dimensional experimental model not only agrees with the observed deformational properties of granular soils but also satisfies

specified requirements of the stochastic model.

The forms of volumetric strain ( $\epsilon_v$ ) and time or distortion strain ( $\epsilon_d$ ) and time curves for various stress ratios ( $\sigma_1/\sigma_2$ ) in figures 1 and 2 suggest the similarity in behavior of the assembly of rods with those of soils. The volumetric creep rate  $d\epsilon_v/d \log t$  decreases and the distortion creep rate  $d\epsilon_d/d \log t$  increases with the increase in stress ratio  $\sigma_1/\sigma_2$ . This is expected due to the significant decrease in shear modulus with the increase in stress ratio and due to increase in bulk modulus with the increase in mean pressure. It is also observed that the behavior of the assembly during volumetric and shear deformation processes is dependent on the stress-history.

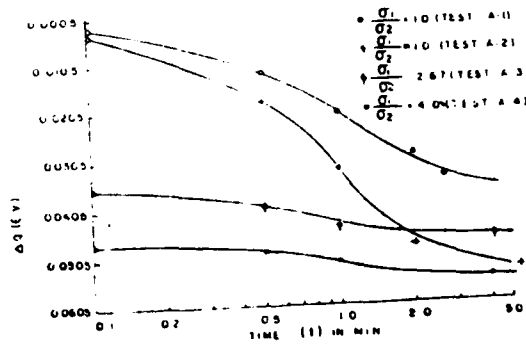


FIGURE 1  
VOLUMETRIC CREEP

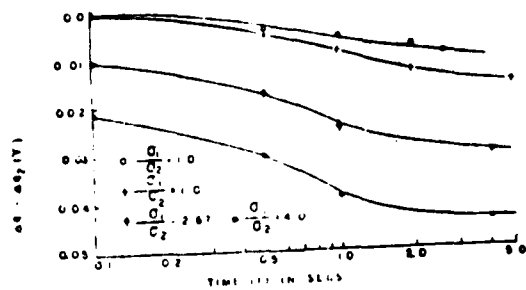


FIGURE 2  
DISTORTION CREEP

STUDIES OF ELASTIC-PLASTIC RESPONSE UNDER  
HIGH PRESSURE SHOCK LOADING

by

J. R. Asay\*  
Thermomechanical and Physical Division, 1534  
Sandia National Laboratories  
Albuquerque, New Mexico 87185

Recent developments in shock wave instrumentation techniques have allowed studies of the mechanical and physical properties of materials to pressures near 1 Mbar. In particular, it is possible to evaluate elastic moduli in the shocked state, as well as elastic-plastic effects, under well-controlled conditions of strain, strain rate and stress. These studies allow investigation of materials in unique states of compression, which are not achievable by conventional methods. Measurements of material properties in the shocked state can then be correlated with metallurgical studies on shock-recovered specimens to develop physically-based models of dynamic material response.

A brief introduction to shock wave techniques will be given in this presentation. This will be followed by a discussion of recent shock wave studies conducted at Sandia National Laboratories on aluminum and other metals to shock pressures approaching 1 Mbar. This work has identified changes in the shear strength of shock-compressed metals which are not easily explained by conventional theories of elastic-plastic response. To develop an understanding of physical effects responsible for these observed changes in material properties, a wide variety of metallurgical studies were conducted on shock recovered specimens, including residual hardness, optical microscopy and TEM, x-ray diffraction and line broadening and positron annihilation measurements. These studies have identified correlations between the mechanical measurements of strength in the shocked state, and the defect state of recovered specimens. Combined studies of the mechanical response under high-rate loading and metallurgical investigations on recovered specimens are beginning to illuminate physical effects which are important to shock deformation processes.

\*This work performed at Sandia National Laboratories supported by the U. S. Department of Energy under Contract DE-AC04-76DP00789.

"Temperature Measurements During The Formation  
of Adiabatic Shear Bands in Steel"

J. Duffy  
Division of Engineering  
Brown University, Providence, RI

A torsional Kolsky bar is employed to deform thin-walled tubular steel specimens at strain rates up to  $10^3 \text{ s}^{-1}$ . Depending on the particular steel and the strain rate, a shear band may be produced within the gage length after sufficient strain has accumulated. An infra-red radiation detection system employing a linear array of tin indium-antimonide detectors senses the surface temperature along the 0.1 inch gage length and provides the temperature profile along the specimen as the shear band forms. An average rise on the order of  $300^\circ\text{C}$  has been observed within shear bands forming in 1020 hot rolled steel specimens deforming at a strain rate of  $10^3 \text{ s}^{-1}$ .

## Tensile Impact Testing of Fibre-Reinforced Composites

by

J. Harding  
Department of Engineering Science  
University of Oxford  
Oxford OX1 3PJ UK

Techniques which have been used to determine the mechanical properties of fibre-reinforced composite materials under tensile impact loading are briefly reviewed. The difficulties encountered in the design of a satisfactory tensile impact testing machine for composite materials are discussed and a new method, using a modified version of the standard tensile split Hopkinson's pressure bar (SHPB), is described. Dynamic stress-strain curves for unidirectionally-reinforced CFRP, in which failure occurs in times of less than 30  $\mu$ s at a mean strain rate of about 400/s, are obtained, see fig.1. By the use of an instrumented input bar it is possible to confirm both that the stress is uniform within the specimen from an early stage in the test and also to measure the velocity difference across the specimen with sufficient accuracy for the dynamic modulus of the composite to be determined.

The physical dimensions of the test equipment, however, prevent the application of this technique to specimens which fail at times much greater than 30  $\mu$ s. In such cases a modified approach has to be followed, whereby CFRP specimens are used to calibrate for the input conditions in subsequent tests on GFRP specimens, for which the fracture strains may be much higher and thus the times to failure may considerably exceed 30  $\mu$ s. This method is successfully applied to woven-reinforced GFRP specimens, see fig.2, where, in tests at a mean strain rate of about 1000/s, the time to failure approaches about 100  $\mu$ s.

To allow an investigation of the effect of strain rate on the mechanical response of fibre-reinforced composites, tests were also performed at a low and at an intermediate rate. For the unidirectionally-reinforced CFRP the modulus, fracture strength and failure mode were found to be independent of strain rate over some seven orders of magnitude, ie from about 0.0001/s to approaching 1000/s. In contrast the woven-reinforced GFRP specimens showed a dramatic increase in failure strength at impact rates of strain, a significant increase in failure strain and a marked increase in initial modulus. The change in mechanical response with increasing strain rate for the GFRP specimens was associated with a change in the fracture appearance. Limited matrix cracking close to the fracture surface at low rates was found, at impact rates, to extend over the entire gauge section and to be accompanied by extensive debonding between the fibres and the matrix.

FIG. 1 TENSILE STRESS-STRAIN CURVES FOR CFRP SPECIMENS

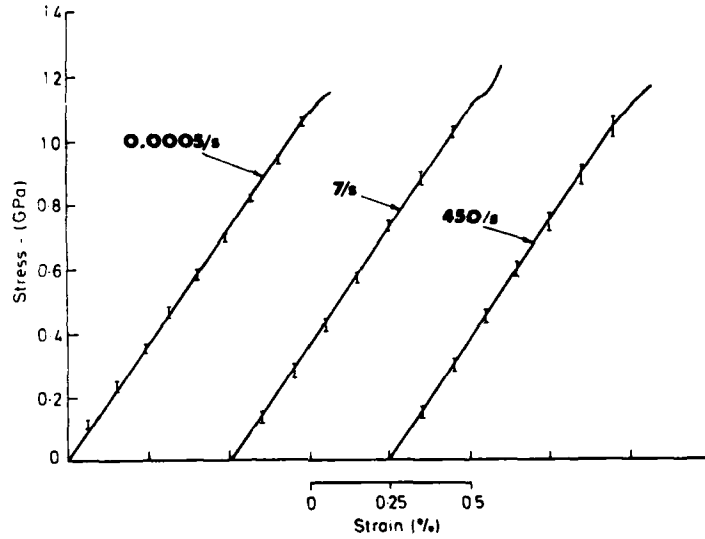
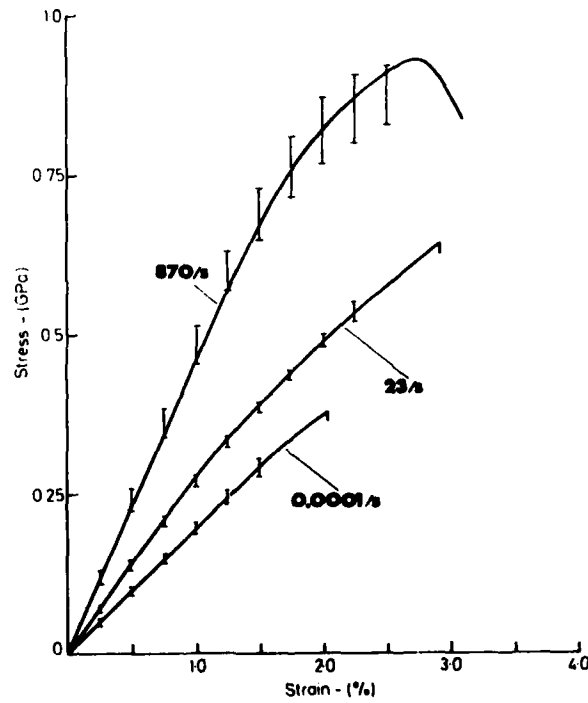


FIG. 2 TENSILE STRESS-STRAIN CURVES FOR GFRP SPECIMENS



**Material Characterization by High Velocity Tension**

by

Kozo Kawata

Department of Mechanical Engineering  
Faculty of Science and Technology  
Science University of Tokyo  
2641 Higashi-Kameyama, Yamazaki,  
Noda, 278 Japan

Firstly, the concepts of high velocity brittleness and ductility are introduced, and the crystal lattice systems effect on them is shown.

Principle of "one bar method" developed by the author's laboratory is introduced. This method is devised for the characterization of materials in high velocity tension up to breaking.

Next, dynamic tensile mechanical properties at about  $10^3 \text{ s}^{-1}$  are stated, comparing with the data of quasi-static tension at about  $10^{-3} \text{ s}^{-1}$ .

The solid materials cover metallic materials for aerospace use and other uses, including dual phase steel and pure irons, composite materials such as GFRP and CFRP, and CF/GF hybrids, and Pyrex glass. Some of them show high velocity brittleness and on the other hand another materials show high velocity ductility.

These mechanisms are not yet fully clarified but they are discussed basing upon the present knowledge obtained.

On the Formulation of Constitutive Equations  
for Dynamic Plasticity

by

R. J. Clifton  
Division of Engineering  
Brown University  
Providence, Rhode Island 02912

Recent experimental results on the dynamic plastic response of single crystals and of polycrystalline metals are reviewed briefly. Dislocation mobility in metallic and ionic crystals is observed to undergo a transition from an essentially exponential dependence of dislocation velocity on resolved shear stress at low stress levels to a linear dependence at high stress levels [1]. Evidence of a similar transition is observed in high strain rate experiments on polycrystalline metals. In particular, plate impact pressure-shear experiments on polycrystalline aluminum specimens show that the flow stress at strain rates of  $10^3 \text{s}^{-1}$  increases approximately linearly with the strain rate whereas at strain rates of  $10^3 \text{s}^{-1}$  or less the flow stress increases approximately linearly with the logarithm of strain rate [2].

Modelling of dynamic plastic deformations requires constitutive equations that are applicable over strain rate ranges where such transitions in plastic response occur. Because these transitions are expected to correspond to changes in the rate controlling mechanisms of dislocation motion and generation one can expect that there will be transitions not only in the dependence of flow stress on strain rate but also in its dependence on strain, temperature, and pressure. Furthermore, the transition strain rate presumably depends on the temperature, the deformation history, and possibly the pressure. The complexity of such phenomena appears to auger against the use of wholly empirical constitutive models and for the use of physically based models.

Physically based models are considered for plastic deformation due to the glide of dislocations. The second law of thermodynamics provides only the relatively weak restriction  $(\tau b)v > 0$  where  $(\tau b)$  is the local force on a dislocation segment that has a velocity  $v$ . Measurements of ultrasonic attenuation and average velocities of dislocations subjected to pulse loading suggest that  $v$  is essentially proportional to the local resolved shear stress  $\tau$  over wide ranges of dislocation velocity [3]. This relatively simple relationship at the dislocation level is difficult to apply at the level of macroscopic constitutive equations because of the difficulty of relating the macroscopic stress field to the local resolved shear stress, which is strongly affected by stress fields due to impurities, grain boundaries and other dislocations. However, this may be less of a difficulty at very high strain rates for which the applied stresses are sufficiently high to dominate the residual stress fields.

The relationship between the dynamic plastic response of a polycrystalline aggregate and that of a single slip system

is examined by applying Taylor theory approximations to a rate dependent material. Transitions in the rate controlling mechanisms of plastic flow at the level of single slip are related to changes in the plastic response of polycrystals. The influence of hydrostatic pressure on the plastic response at different strain rates is investigated by comparing the pressure sensitivity of plastic flow for two different rate-controlling mechanisms: the viscous glide of dislocations through the clear lattice and the thermally activated motion of dislocations past obstacles. Dislocation dynamics effects are indicated by comparing the elastic precursor decay relations obtained from macroscopic visco-plasticity theory with those obtained from models of the elastic waves emanating from nonuniformly moving dislocations [4].

This work has been supported by ARO and NSF, including support through the NSF/Brown MRL.

#### References

1. Kim, K. S., and Clifton, R. J., "Dislocation Motion in MgO Crystals Under Plate Impact," to appear in J. Matls. Sci., 1983.
2. Clifton, R. J., Gilat, A., and Li, C. H., "Dynamic Plastic Response of Metals Under Pressure-Shear Impact," Proceedings of the 29th Sagamore Army Materials Research Conference on Material Behavior Under High Stress and Ultrahigh Loading Rates, held at Lake Placid, New York, July, 1982.
3. Kumar, P., and Clifton, R. J., "Dislocation Motion and Generation in LiF Single Crystals Subjected to Plate Impact," J. Appl. Phys., 50, 1979, pp. 4747-4762.
4. Clifton, R. J., and Markenscoff, X., "Elastic Precursor Decay and Radiation from Nonuniformly Moving Dislocations," J. Mech. Phys. Solids, 29, 1981, pp. 227-251.

THE DEVELOPMENT OF COUPLED THERMO-VISCO PLASTIC  
CONSTITUTIVE EQUATIONS

U. S. Lindholm  
Director  
Department of Materials Sciences  
Southwest Research Institute  
P.O. Drawer 28510  
San Antonio, Texas 78284

and

S. R. Bodner  
Faculty of Mechanical Engineering  
Technion-Israel Institute of Technology  
Haifa, Israel

Abstract

In the development of viscoplastic theory, most attention has been paid to thermal effects in the low strain rate or creep range. However, the need for accurate thermo-viscoplastic constitutive equations also exists for critical problems involving high deformation rates. Such problems may include, for example, wave propagation through structures containing temperature gradients and modeling of dynamic thermo-plastic instability such as adiabatic shear band formation and propagation. Additionally, temperature and rate dependence of plastic deformation are generally coupled in such a way that correspondence can be made between high strain rate and low temperature behavior. This correspondence can be useful in evaluating constitutive models and experimentally determining constants therein. In this paper, the authors will attempt to summarize recent developments in formulating unified thermo-viscoplastic constitutive models and the experimental evidence supporting or relevant to such model development. Particular attention will be paid to the functional form of the constitutive equations, the manner in which temperature dependence is introduced, and to the asymptotic behavior at high strain rates and low temperature.

## CONSTITUTIVE MODELS FOR HIGH-RATE DEFORMATION

by

L. E. Malvern, Professor  
Department of Engineering Sciences  
University of Florida  
Gainesville, Florida 32611

Some of the rate-dependent constitutive equations that have been applied to analyze moderately high-rate deformation of metals are reviewed. Most applications have used some variation of the one-dimensional overstress equations proposed independently by Sokolovskii and Malvern 35 years ago or similar multiaxial stress equations developed by Perzyna. The uniaxial stress and strain versions have been applied extensively with considerable success. Campbell (1973) has reviewed representations of the dependence of the plastic strain rate on the overstress, some empirical and some based on micromechanical concepts.

Over the strain-rate range from quasistatic values to about 10,000/sec exponential or power laws have been popular, based on observations that constant strain-rate tests can be represented over this range by either semilog or log-log plots of stress versus strain rate for various values of plastic strain. These representations show a decreased rate sensitivity at the higher rates, so that transient plastic wave propagation has sometimes been treated by a single dynamic curve. At still higher rates, however, the rate sensitivity increases again, with an approximately linear dependence of stress on strain rate above a rate of about 10,000/sec, where no thermal activation is required.

Experimental rate-jump studies have shown that there is often a rate-history effect not accounted for by the simple overstress models. A rate-history effect can be represented by an internal state variable theory. Some success was achieved, for example, by Merzer and Bodner (1979) in modeling jump tests with a one-dimensional constitutive law containing a single internal state variable. Several other internal state variable models have been proposed, including some with the internal state variables interpreted in terms of the micromechanical state, but these have not been much applied to high-rate deformation.

Combined-stress plastic waves have been analyzed with the Perzyna equations in simple geometries, and these equations have been incorporated recently into finite-element codes that can be used in more complex geometries. Most applications of viscoplastic equations

AD A138 155

ABSTRACTS OF THE ANNUAL MEETING OF THE SOCIETY OF  
ENGINEERING SCIENCE INC. (U) DELAWARE UNIV NEWARK  
M TAYA SEP 83 ARO-20222.1-EG-CF DAAG29-83-M-025R

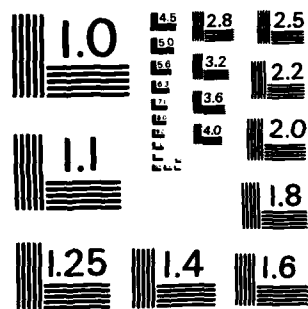
3/4

UNCLASSIFIED

F/G 5/1

NI

The table consists of 10 columns and 15 rows. The top row contains the text 'UNCLASSIFIED', 'F/G 5/1', and 'NI'. The remaining 14 rows and all 10 columns are filled with black redaction, obscuring the underlying data.



MICROCOPY RESOLUTION TEST CHART  
NATIONAL BUREAU OF STANDARDS - 1963 - A

to multiaxial loading have, however, been limited to slow creep or stress relaxation.

Codes for analysis of projectile impact and penetration have used an equation of state to model the hydrostatic stress-strain relationship, and a rate-independent formulation for the deviatoric relationship, usually a classical Prandtl-Reuss perfectly plastic model or an isotropic linear-hardening model. Rate effects on the deviatoric stress have been taken into account only in an average way by using a dynamic yield stress value in the codes; see Zukas et al. (1982). This may be adequate when the hydrostatic effects are dominant.

Since about 1974 a number of studies have incorporated properly invariant finite-deformation kinematics and plasticity laws into finite-element analysis. Some have applied properly invariant versions of the Perzyna equations to dynamic problems. These formulations share with the rate-independent formulations an inadequate representation of the response to nonproportional loading. Most of them assume isotropic hardening or a combination of isotropic and kinematic hardening. The additional errors caused by using a rate-independent model with a dynamic yield stress value instead of the Perzyna equations may be dwarfed by the errors inherent in the inadequate representation of hardening for nonproportional loading.

In order to focus attention on the concepts involved in modeling the rate effects, without the complications of the finite-deformation kinematics and the nonproportional loading, only one-dimensional equations will be presented in any detail in the paper. The multiaxial laws and finite deformation formulations will be discussed only in an expository descriptive review.

#### References

- Campbell, J.D., "Dynamic Plasticity: Macroscopic and Microscopic Aspects," Materials Science and Engineering, 12, 1973, pp. 3-21.
- Merzer, A. and Bodner, S., "Analytical and Computational Representation of High Rate of Straining Behaviour," Mechanical Properties at High Rates of Strain 1979, Harding, J., Ed., Conf. Ser. No. 47, Institute of Physics, London, 1980.
- Zukas, J.A., Nicholas, T., Swift, H.F., Greszczuk, L.B., and Curran, D.R., Impact Dynamics, John Wiley & Sons, New York, 1982.

## TESTING MATERIALS AT HIGH RATES OF STRAIN

Dr. T. Nicholas  
AFWAL Materials Laboratory  
Wright-Patterson AFB, OH 45433  
(513) 255-2689/255-2498

## ABSTRACT

Testing techniques for the determination of material properties at high rates of strain are reviewed. Two types of techniques are considered. In the first, inertia and wave propagation effects are ignored. The split Hopkinson pressure bar and some of its variations fall into this category. In the second type, wave propagation is considered in the analysis. This method requires an indirect approach in that the material behavior must be known a priori before an analysis of the experiment can be conducted. Yet it is the material properties which are being sought in the first place. This approach will lead to results whose uniqueness cannot be assured. Examples will be shown covering stress states from uniaxial stress to uniaxial strain and conditions from isothermal to adiabatic. Assumptions and limitations of the various approaches will be discussed. An introduction to some less widely used techniques will be presented. Included among these are the expanding ring, the notched tensile test, and the skew plate impact experiment of Clifton and co-workers at Brown University.

Reference: T. Nicholas, "Material Behavior at High Strain Rates" in Zukas, J.A., et al., Impact Dynamics, Wiley, New York, 1982.

U.S. Lindholm, "High Strain Rate Tests" in Bunshah, R.F., ed., Techniques in Metals Research, Vol 5, part 1, Interscience, New York, 1971.

T. Nicholas, "Measurement of Material Properties for High Rate Deformation Processes", Technical Report AFWAL-TR-81-4176, Wright-Patterson AFB, February 1982.

## DYNAMIC FRACTURE OF RATE SENSITIVE MATERIALS

by

A. S. Douglas  
Department of Mechanics  
The Johns Hopkins University  
Baltimore, Maryland 21218

The simulation of the dynamic crack propagation process in ductile materials is complex requiring an understanding of the role of material inertia [1,2], the nature of the stress-strain-strain-rate behavior of the material and the effect on the material response due to the local rise in temperature [3]. Although the in-plane modes of deformation (modes I and II) are of greater importance in fracture mechanics, the anti-plane mode of deformation (mode III) presents fewer difficulties in the mathematical treatment and several features of in-plane deformation modes have been anticipated by analysis of the anti-plane shear mode [4].

Here, dynamic steady-state crack growth in the anti-plane shear mode through an elastic-viscoplastic material is studied. The motion is restricted to steady-state propagation (in which the deformation is time independent as viewed by an observer moving at constant velocity,  $v$ , with the crack tip) but includes inertial effects of the material explicitly. The full deformation field is determined in the local neighborhood of the crack (viz. conditions of small yielding are assumed [5]) using an iterative procedure which employs the finite element method. According to the small scale yielding hypothesis, the local elastic-plastic field is dominated by the surrounding elastic field which is conveniently characterized by the elastic stress intensity factor  $k$ .

Results.

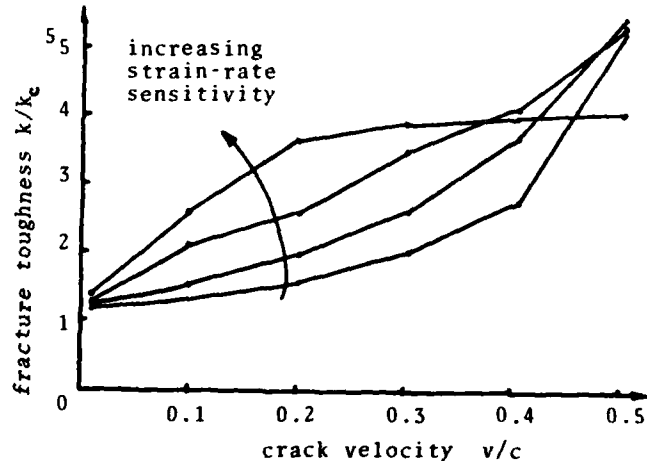
To determine the level of remotely applied stress intensity factor,  $k$ , required to sustain crack growth at the predetermined speed  $v$ , a ductile fracture criterion adopted here is that proposed in [6], namely, that a crack will grow when a critical level of plastic strain,  $\gamma_c$ , occurs at a characteristic distance,  $d$ , ahead of the crack tip. For levels of plastic strain below the critical level at distance  $d$  no growth occurs, levels of strain above  $\gamma_c$  at distance  $d$  are inaccessible. It is, however, useful to eliminate the characteristic distance  $d$  in favor of the critical stress intensity factor  $k_c$ . The value of  $k_c$  is defined as that stress intensity factor required (assuming small scale yielding) to satisfy the fracture criterion for a stationary crack in an elastic-ideally plastic material under slow loading conditions.

Using the above models, theoretical fracture toughness versus crack speed relationships can be generated.

A typical fracture toughness ( $k/k_c$ ) versus crack tip speed, nondimensionalized by the elastic shear wave velocity,  $c$ , response is shown in figure 1., for a material

which has a rate-sensitivity response and a fracture criterion typical of ductile mild steels. Experimentally observed toughness versus speed responses have been summarized in [7]. Other pertinent information gained includes the changes in the plastic zone size and shape for different crack velocities in a range of material types.

Figure 1.



References:

1. Douglas, A. S. et. al. "Dynamic Steady Antiplane Crack Growth in an Elastic-Plastic Material", Advances in Fracture Research-ICF5, Pergamon Press, Oxford, 1981, pp. 2233-2241.
2. Freund, L. B. and Douglas, A. S., "The Influence of Inertia on Elastic-Plastic Antiplane-Shear Crack Growth", J. Mech. Phys. Solids, 30, 1982, pp. 59-74.
3. Weichert, R. and Shonert, K., "Heat Generation at the Tip of a Moving Crack", J. Mech. Phys. Solids, 26, 1978, pp. 151-161.
4. McClintock, F. A. and Sukhatme, S. P., "Travelling Cracks in Elastic Materials Under Longitudinal Shear", J. Mech. Phys. Solids, 8, 1960, pp. 187-193.
5. Rice, J. R., "Mathematical Analysis in the Mechanics of Fracture", Fracture, Liebowitz, H., Ed., Vol. II, Academic Press, New York, 1968, pp. 191-311.
6. McClintock, F. A. and Irwin, G. R. "Plasticity Aspects of Fracture Mechanics", Fracture Toughness Testing and its Applications, ASTM STP 381, Am. Soc. Test. Materials, Philadelphia, 1964, pp. 85-133.
7. Freund, L. B., "Dynamic Crack Propagation", The Mechanics of Fracture AMD Vol. 19, Erdogan, F., Ed., Am. Soc. Mech. Eng., New York, 1976, pp. 105-134.

RATE PROCESSES AND MATERIAL PROPERTIES  
RELATED TO THE SPALLATION OF ROLLED STEEL

by

Gerald L. Moss  
Ballistic Research Laboratory  
Aberdeen Proving Ground, Maryland 21005

A description is given of the dynamic fracture of steel broken with stress waves. Failure occurs by the development of crack arrays. The cracks are found to nucleate at heterogeneities in the steel -- primarily at MnS inclusions. The cracks grow and coalesce, and each of these failure processes continues as long as sufficiently intense tensile stresses are applied. The progression of failure can be modeled in terms of functions that describe the rates of nucleation, growth, and coalescence. The governing rate equations and relevant material parameters have been determined through a treatment of experimental observations with a stress-wave computer code used in conjunction with the BFRAC2 2 computer subroutine.

With an accurate determination of stress histories and an extrapolation of curves of crack density versus stress to the stress level of no damage, crack threshold stresses were determined for material preconditioned by only those stresses required to reach the incipient failure condition. It is shown how crack threshold stresses vary with yield strength. A range of yield strengths was discovered in which the threshold stress decreases with increasing yield strength. An interpretation as to why this happens will be described.

It was found that the crack nucleation rate increases gradually with stress from a value of zero at the threshold stress. Rates of void growth determined from information about crack arrays created with stress waves were found to be apparent crack velocities because there is microcrack coalescence as well as crack growth. A comparison of predicted and observed crack densities in the direction of wave propagation indicates that crack shielding plays a major role in determining crack density gradients.

A MIXTURE THEORY APPLIED TO SHOCK-INDUCED DETONATION OF  
HETEROGENEOUS EXPLOSIVES\*

by

M. E. Kipp, J. W. Nunziato, and D. B. Hayes  
Sandia National Laboratories  
P.O. Box 5800  
Albuquerque, NM 87185

## ABSTRACT

A thermomechanical theory of chemically-reacting mixtures has been developed and applied to the shock initiation of chemical reaction in a granular explosive. Each pure phase in the mixture is characterized by an independent temperature, density, pressure, equation of state, and volume fraction. The explosive is treated as two solid phases and a gaseous product phase. The concept of energy partitioning into the phases during shock loading is of particular importance here, since initiation of chemical decomposition is believed to result from shock-induced heterogeneous heating. To achieve a description of this heating, all of the irreversible work that occurs in the shock front is assumed to be dissipated in a fraction of the solidus material. This fraction, called the hot solid, is treated as a separate phase. The balance of the solid (the cold phase) is assumed to be reversibly compressed so that its temperature remains on its compression isentrope. The hot solid rapidly decomposes via thermal explosion. Subsequent decomposition of the cold solid is described by grain burning.

The chemical energy of the unreacted explosive is sufficiently large that, upon decomposition, large pressure and temperature rises occur. Thus, initial shocks transmitted into the explosive grow to detonation waves that may be an order of magnitude larger in amplitude than the initial shock. The model is employed in a finite difference shock wave code to permit solution of the complex coupling that exists between the mechanical response of the material and the evolution of the chemical reactions.

---

\*This work performed at Sandia National Laboratories supported by the U.S. Department of Energy under contract number DE-AC04-76DP00789.

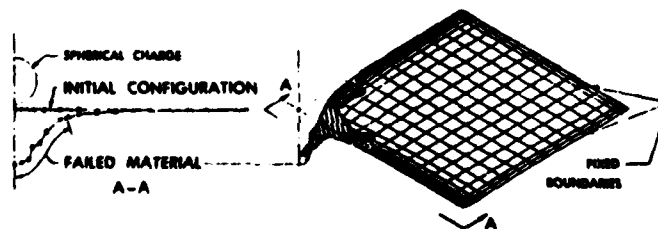
## RESPONSE OF STRUCTURAL PANELS TO AIR BLAST

by

Norris J. Huffington, Jr.  
Henry L. Wisniewski  
US Army Ballistic Research Laboratory  
US Army Armament Research and Development Command  
Aberdeen Proving Ground, MD 21005

A methodology suitable for predicting the damage inflicted upon structural panels by blast from nearby high explosive detonations has been developed by extensive modifications of an existing finite-difference structural response code. A new constitutive formulation involving prescribed through-thickness stresses was introduced to account for the effects of intense surface pressures. A recycling option based on a strain equivalence criterion was introduced to inhibit the unrestricted growth of a breathing mode. A triaxial stress criterion for material failure has been incorporated into the analysis to permit prediction of panel rupture and of post-failure response. This stress failure criterion was supplemented by a limitation on the maximum principal strain (not to exceed the uniaxial tensile rupture strain).

This methodology was then applied to prediction of the response of a square panel of armor plate which was loaded by the blast from a spherical charge of high explosive detonated at a small distance from the midpoint of the panel. A typical result is shown in the figure below which displays one-quarter of the deformed reference surface of the panel at a time when the blast loading has decayed to insignificant magnitude. The cross-hatched region in the isometric plot represents material which has failed clear through the panel; i.e., rupture has occurred. This result is in good qualitative agreement with available experimental evidence.



DEFORMATION BEHAVIOUR OF A HIGH CARBON - HIGH CHROMIUM STEEL  
AT HIGH STRAIN RATES: OCCURRENCE OF ADIABATIC SHEAR BANDS

by

S.M. Doraivelu  
Visiting Scientist  
Air Force Materials Laboratory  
Dayton, Ohio 45433

V. Gopinathan  
Deputy General Manager  
CMFI, H.M.T.Ltd.  
Hyderabad 500854, India

and

K.P. Rao  
Metal Forming Laboratory  
Department of Metallurgical Engineering  
Indian Institute of Technology  
Madras 600036, India

Various forming techniques like high velocity forging, rolling, high energy rate forming, etc. stress the need to understand the plastic behaviour of metals and alloys under the influence of temperature at different strain rates prevailing in these processes. The knowledge of flow curves is necessary at different strain rates for the calculation of working loads for a metal forming process. Also, during deformation, the temperature of a material increases due to conversion of mechanical energy into heat energy. When this temperature rise is instantaneous and large, normally at high strain rates, thermal instability occurs and deformation takes place inhomogeneously (1) in the form of small bands called adiabatic shear bands. Severe adiabatic shearing leads to failure or fracture of the material.

In the present investigation, in-situ compression tests in the temperature range 300-1175 K were conducted on High Carbon (1.51%) - High Chromium (11.2%) steel specimens with a height to diameter ratio of 1.5. A high velocity gravity drop hammer, a friction screw press, a hydraulic press and a compression testing machine were employed to compress the specimens at mean strain rates of 470, 11, 0.6 and 0.02 s<sup>-1</sup> respectively. Force, stroke/punch travel and temperature rise during deformation were recorded using proper instrumentation.

From the results it was found that with increase in strain the temperature of the specimen increased at all strain rates and is found to vary almost linearly with true strain. The actual specimen temperature referred to as adiabatic temperature has been computed for each of the tests at various strain levels. The flow stress vs. adiabatic temperature curves have been plotted for different strain rates at various strain levels and a typical plot is shown in Fig.1. It can be seen that excepting the two regions where humps are observed, the flow stress as a function of temperature can be represented by the equation

$$\sigma = \sigma_z e^{-ST} \quad \dots [1]$$

where  $\sigma$  is flow stress,  $\sigma_z$  is flow stress at absolute zero,

S is thermal coefficient and T is adiabatic temperature.

The hump observed in the low temperature region (400-600K) is more prominent at high strain rates ( $11 \text{ s}^{-1}$ ) and starts diminishing as the strain rate is lowered. A typical micrograph of the specimen compressed in this hump region is shown in Fig.2, which shows the presence of thin bands, that are normally associated with shear deformation. A comparison of this micrograph with those observed by Manin Backman and Fennegan (1) for SAE 4130 steel subjected to high strain rate compressive load, reveals that these bands are nothing but shear bands which are formed due to adiabatic heating effect. The other hump observed at 1150 K is due to the transformation of BCC to FCC structure which involves a change in volume.

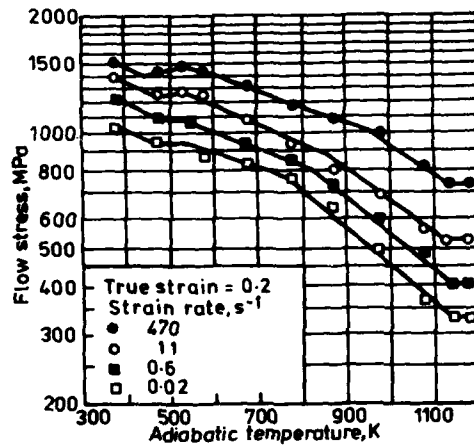


Fig. 1  
Variation of flow stress with adiabatic temperature at different strain rates for a true strain of 0.2



Fig. 2  
Micrograph showing adiabatic shearing in the specimen deformed at 525K (strain rate =  $470 \text{ s}^{-1}$ )

REFERENCE

1. Manin, E., Backman, E., and Fennegan, S.A., "Metallurgical Effects at High Strain Rates", Plenum Press, New York, 1976, p. 531.

IN-TARGET STRESS AND STRAIN MEASUREMENTS WITH AN  
APPLICATION TO A COMPUTER SIMULATION

D. S. Pritchard  
USA ARRADCOM, Ballistic Research Laboratory  
Aberdeen Proving Ground, Maryland 21005

The primary objective of the investigation presented here was to use experimental measurements of stress generated in targets impacted by penetrators to provide input data for a simple penetration model. First, experiments were performed to measure the stress developed in 50.8 mm thick rolled homogeneous armor (RHA) targets by long rod S-7 tool steel penetrators (RC40). The penetrators were 254 mm long with a length to diameter ratio of 30. The gauge locations in a particular target where the stress was monitored were varied for each experiment. A stress vs. time profile for each gauge location normal to and in the path of penetration was obtained. Four experimental tests incorporating the same initial projectile velocities (1000 m/s) fixed a stress history profile for these similar tests. Several characteristic reactions of the target were apparent upon examination of the stress profile. A non-linear increase in stress and strain levels at a particular gauge site occurred as penetration progressed. No net decrease in these levels arose due to shock rarefactions from the back surface of the target. There was a marked increase in stress for a corresponding penetration time (common reference fixed at initial projectile impact) as a gauge site was located closer to the front target surface. Longer signal durations were evident as gauges were placed farther from the initial impact point.

The profile data was incorporated into a simple computer simulation program that is based on hydrodynamic theory. Material properties of the target and penetrator materials, including the target resistance to penetration ( $R_t$ ) and the projectile yield strength ( $Y_p$ ), also served as input to the program. The model, which closely follows one proposed by Tate (1), predicts penetration distance, penetration velocity, residual penetrator length and velocity, all as a function of time starting at impact. Output data from this program were compared to other experimental results obtained by Lawrence (2). Specifically, the penetration distance vs. time profile for the arbitrarily standardized projectile and target combination used by both Lawrence and myself were compared to the simulated results. Good agreement was obtained within experimental and computational error. Future plans include continuation of the experimental measurements mentioned and simulation of results for other experimental target-penetrator matches.

1. Tate, A., A Theory for the Deceleration of Long Rods After Impact, J. Mech. Phys. Solids, Vol. 15, 1967, pp. 387-99.
2. Lawrence, W., Measurements of Penetration Using Instrumented Targets, to appear in a BRL report, Ballistic Research Laboratory, APG, MD.

FRACTURE MODE OF SINGLE CRYSTAL Cu-SiO<sub>2</sub> SUBJECTED  
TO UNIDIRECTIONAL HIGH STRAIN-RATE IMPACT

by

M. Taya  
I. Hall  
H. S. Yoon  
D. S. Pritchard

Department of Mechanical and Aerospace Engineering  
University of Delaware  
Newark, Delaware 19711

A dynamic ductile fracture of a two-phase material is simulated by use of a single crystal Cu-SiO<sub>2</sub> where SiO<sub>2</sub> plays a role of a strong secondary particle in a ductile matrix (Cu). The behavior of a single crystal CuSiO<sub>2</sub> under a quasi-static loading has been well studied, for example, [1-2]. However, there has been no attempt to investigate the behavior of a single crystal Cu-SiO<sub>2</sub> under a high strain-rate condition.

In our experiment, a disc-shaped single crystal Cu-SiO<sub>2</sub> is subjected to a flyer impact which generates one-dimensional strain through the specimen. Thus the state of stress in the single crystal CuSiO<sub>2</sub> specimen becomes triaxial, leading to the formation and development of voids in the specimen. The mode of void growth in this specimen where SiO<sub>2</sub> particle is strong was studied theoretically by Taya and Patterson [3] by neglecting the inertia effect. The threshold impact velocity  $V_{th}$  to nucleate voids around SiO<sub>2</sub> particles is studied experimentally. Also is the distribution of voids across the specimen depth investigated.

References

1. Palmer, I. G. and Smith, G. C., in "Oxide Dispersion Strengthening," Metall. Soc. Conf. of AIME, Bolton Landing (1966), p. 253.
2. Tanaka, K., Mori, T., and Nakamura, T., *Phil. Mag.* 21 (1970), p. 267.
3. Taya, M. and Patterson, W. G., *J. Mater. Sci.*, 17 (1982), p. 115.

## BOILING IN A GRANULAR BED

by

E. R. G. Eckert  
University of Minnesota  
Department of Mechanical Engineering  
Minneapolis, Minnesota 55455

Combined heat and mass transfer processes in porous media are strongly influenced by capillary forces when the voids contain liquid and gas or liquid and its vapor and when local temperature differences exist in the medium. Such situations occur in many engineering applications and have been studied in the past with pioneering contributions by Otto Krischer (1), Alexi Vasilievich Luikov (2), and D. E. De Vries (3).

The present lecture is concerned with processes in which a liquid [water] is contained in granular material and is boiling under the influence of heat sources so that liquid and vapor coexist in the voids. A geometry, which is considered as a model for the study of vapor formation in the earth or as simulating oil extraction through injection of vapor, is a horizontal layer (4) of constrained porous material with heat addition through the lower boundary and heat removal by cooling through the upper boundary. A layer adjoining the lower boundary in which the voids are filled with superheated vapor is formed when a sufficiently large heat flux is applied. Another layer in which liquid and vapor coexist in the voids is formed above it and in a third layer on top of the others the voids are saturated with liquid.

Our study is concerned with a column of unconstrained granular material containing water which is evaporated by heat addition through its vertical boundaries. It was instigated by difficulties occurring in the boilers of nuclear reactors by sludge deposits.

Flow visualization and temperature measurements were used to study the behavior of the granular bed when water filling the voids is boiling. The bed with 65% porosity consisted of nickel particles of irregular shape and with an equivalent mean diameter of 28.3  $\mu\text{m}$  filling the annular shape between two concentric glass tubes which were closed at the bottom.

Water was added up to a height well above the granular bed. The glass tubes were placed into a vessel with windows filled with Therminol 55 which has a boiling point at atmospheric pressure above 200°C. This fluid could be brought to a prescribed temperature by a thermostat connected with the vessel. A heat flux through the wall of the outer glass tube into the bed was in this way generated so that boiling was initiated.

Observation revealed the formation of several layers in the bed with different characteristics during the start-up process and the layers also persisted when steady state was attained. A region adjacent to the bottom of the bed did not contain any liquid. The vapor filling the voids was superheated as demonstrated by the temperature measurements and heat transport occurred mainly by conduction. The rest of the bed above this "dryout region" contained liquid as well as vapor with both phases moving in counter current.

In the lower part of this "wetted region", the particles remained at rest, whereas above a certain height, the bed was in continuous slow heaving motion. Horizontal cracks appeared and disappeared and the vapor contained in the cracks created vertical channels in the bed through which it escaped. This is concluded from the appearance of a number of discreet openings in the upper surface of the bed which could be observed after termination of a test run. Some particles were carried upwards through the top surface of the bed and moved in an irregular motion in the water as in a fluidized bed.

It is concluded from the observation and the measurements and corroborated by a parametric analytic study (5) that counter flow between the vapor generated by the boiling and the liquid can exist over a certain height of the granular bed only and that the creation of the channels increases this height in a way similar to the action of arteries in the porous layer of heat pipes to facilitate the circulation of the fluid. Dryout occurs at the lower part of the bed when the total bed height exceeds the height which can accommodate counterflow.

Support for the study by the Electric Power Research Institute is gratefully acknowledged. R. J. Goldstein, A. I. Behbahani and R. Hain participated in it.

References:

- 1) Krischer, O., Wärme, Flüssigkeits - und Dampfbewegung bei der Trocknung poriger Stoffe, Z. VDI-Beiheft Verfahrenstechnik, 1, 1940, pp. 17-25.
- 2) Luikov, A. V., Drying Theory, Gosenergoizdat, Moscow, 1950.
- 3) Philip, J. R. and De Vries, D. A., "Simultaneous Transfer of Heat and Moisture in Porous Media," Trans. Amer. Geophys. Union, 39, No. 5, 1958, pp. 909-916.
- 4) Bau, H. H. and Torrance, K. E., "Boiling in Low-Permeability Porous Materials," Int. J. Heat Mass Transfer, 25, 1982, pp. 45-55.
- 5) Abe, T., Eckert, E. R. G., and Goldstein, R. J., "A Parametric Study of Boiling in a Porous Bed," Wärme-und Stoffübertragung, 16, 1982, pp. 119-126.

A NEW METHOD OF FLUID VELOCITY MEASUREMENT  
IN POROUS MEDIA\*

by

J. C. Dunn  
Geophysics Research Division  
Sandia National Laboratories  
Albuquerque, NM 87185

Many situations exist where heat transfer in porous media is controlled by pore fluid convection. In these cases, heat transfer measurements are usually difficult due to the nature of pore fluid movement and the small magnitude of average velocities. A new method for measuring these average velocities is being developed that has the promise of excellent resolution. The method is based on a thermal perturbation technique where the porous medium is disturbed by a constant heat flux source. In a convecting environment, surface temperatures on the source are skewed from their values in a purely conductive environment. These temperature differences can then be used to determine the average velocity vector in the vicinity of the source.

A full three-dimensional thermal perturbation analysis has been completed for spherical and cylindrical sources. The analysis is restricted to Peclet and Rayleigh numbers less than one, but includes heat transfer in a porous medium by conduction, forced fluid convection and natural convection induced by the source. The analysis shows that surface temperature differences can fully define the local fluid velocity vector in the absence of the source. It also predicts that very low fluid velocities will create significant temperature differences. Numerical values have been verified using a finite element computer program written for incompressible porous flow problems.

A prototype instrument based on this thermal perturbation technique was recently built to measure groundwater velocity. The instrument was designed for use in an uncased drillhole. Silicone heating pads containing sixteen thermistors are used to resolve the local groundwater velocity vector. The perturbation analysis predicts that the resolution of this probe is approximately  $10^{-8}$  m/s. During October 1982, the instrument was tested in the Long Valley Caldera in central California. The probe was operated in two separate drillholes. A vertical upflow

\* This work performed at Sandia National Laboratories supported by the U. S. Department of Energy under contract number DE-AC04-76DP00789 for the Office of Basic Energy Sciences.

of  $3.4 \times 10^{-5}$  m/s was measured in a region of thermal discharge and a horizontal flow of  $6.8 \times 10^{-7}$  m/s was measured in a known aquifer. This thermal perturbation technique should also have other applications, such as the laboratory measurement of fluid velocity in a porous medium.

EXPERIMENTAL INVESTIGATION OF BUOYANCY DRIVEN  
HEAT TRANSFER IN VERTICAL POROUS ANNULI

by

V. Prasad and F. A. Kulacki  
Department of Mechanical and Aerospace Engineering  
University of Delaware  
Newark, Delaware 19711

Buoyancy driven heat transfer in a vertical annuli filled with saturated porous media has been experimentally investigated for a case when the inner wall is heated at a constant temperature and the outer wall is isothermally cooled. The heat transfer rates and the temperature distributions in the medium has been obtained for a radius ratio,  $\kappa$ , of 5.338 and the aspect (height-to-gap width) ratio,  $\Lambda$ , of 1 and 0.545 for Rayleigh numbers,  $Ra^*$ , up to 9000. Various combinations of solid balls and liquids have been used to study the effects of the solid and fluid properties. These include glass and chrome steel balls of various sizes, and water, heptane and ethylene glycol.

In general, the experimental values of average Nusselt number,  $Nu$ , for glass-water media agree well with our numerical results [1]. When the difference between the conductivity of the fluid,  $k_f$ , and the stagnant conductivity of the porous medium,  $k_s$ , increases, the experimental results start deviating. The Nusselt number for a medium of lower fluid conductivity is observed to be smaller than that for the higher fluid conductivity for a given solid. For example, at moderately high Rayleigh numbers,  $Nu$  for glass-heptane is lower than that for the glass-water. Again, for a given liquid the Nusselt number is smaller for higher thermal conductivity of the solid;  $Nu$  for glass-water is higher than that for steel-water. For any two given porous media, the difference between the Nusselt numbers increases as the Rayleigh number increases.

It is expected that as the flow rate increases (with increase in Rayleigh number) more and more energy is transported by the fluid. This implies that the fraction of total energy transferred through the stationary balls reduces and that by the convection in the fluid increases as the Rayleigh number is increased. As such the influence of the fluid is much more on the total heat transfer as compared to the solid at higher  $Ra^*$ . And, hence,  $k_s$ , the stagnant thermal conductivity of the porous media is not the correct value of the effective thermal conductivity to be used to calculate the Rayleigh and Nusselt numbers in asymptotic and boundary layer flow regimes. This is, further, substantiated by the temperature measurements. A similar behavior is demonstrated by Schneider's experimental results [2].

All these suggest that the effective thermal conductivity of the porous medium is a strong function of the flow and, in a way, the Rayleigh number. Also the results obtained for two different aspect ratios show that for the same  $Ra^*$  and the medium, the deviation is different in two different cases. This indicates that a proper effective thermal conductivity is

$$k_e = k_e(k_f, k_s, Ra^*, A, \kappa)$$

where  $A$  is the aspect ratio and  $\kappa$  is the radius ratio. Once the above functional relationship is known, the difference between the Nusselt number values would not be appreciable for different porous media, for a fixed Rayleigh number, for both  $Ra^*$  and  $Nu$  based on  $k_e$  (not  $k_s$ ).

It is important to note that this is the value of Nusselt number (based on  $k_e$ ), which is predicted by the analytical or numerical results in terms of the Rayleigh number based on  $k_e$ . Hence, all the analytical results based on Wooding's formulation [3]<sup>†</sup> would predict inappropriate heat transfer rates if  $Ra^*$  and  $Nu$  based on  $k_s$ , instead of  $k_e$ , are used.

Furthermore, the agreement between the glass-water and glass-ethylene glycol results clearly show that there is no appreciable effect of the Prandtl number of the porous media, on the heat transfer rates, which is contrary to the observation of Seki, Fukusako and Inaba [4]. It may be noted that no other analytical or experimental investigation has concluded a Prandtl number effect.

#### REFERENCES

1. Prasad, V. and Kulacki, F. A., "Natural Convection in a Vertical Porous Annulus", to be published in International Journal of Heat and Mass Transfer (in press).
2. Schneider, K.-J., "Investigation of the Influence of Free Thermal Convection on Heat Transfer through Granular Material", Progress in Refrigeration Science and Technology, Proceedings, 11th International Congress on Refrigeration, Paper No. II-4, 1963.
3. Wooding, R. A., "Steady Free Thermal Convection of Liquid in a Saturated Porous Medium", Journal of Fluid Mechanics, Vol. 27, 1957, pp. 609-623.
4. Seki, N., Fukusako, S., and Inaba, H., "Heat Transfer in a Confined Rectangular Cavity Packed with Porous Media", International Journal of Heat Mass Transfer, Vol. 21, pp. 985-989, 1978.

<sup>†</sup>Note that most of the published analytical work for natural convection in porous media, are based on this information.

A NEW INTERPRETATION OF INTERNAL HEAT TRANSFER  
COEFFICIENTS OF POROUS MEDIA

by

A. Dybbs and R. V. Edwards  
Departments of Mechanical and Aerospace and Chemical Engineering  
Case Western Reserve University, Cleveland, Ohio 44106

ABSTRACT

The purpose of this paper is to present a new interpretation of the internal heat transfer coefficients for flows through porous media. This interpretation is based on a fluid mechanic study of the flow regimes in porous media from Darcy to turbulent. The fluid mechanic results are based on laser anemometry and flow visualization studies and the internal heat transfer coefficients are determined experimentally by measurements of the porous media and fluid temperatures.

For the flow studies, three dimensional velocity profiles and movies of dye streaklines will be shown. The porous media consisted of plexiglas spheres in a hexagonal packing and glass and plexiglas rods arranged in a complex, fixed three dimensional geometry. The liquids used were water, silicone oils, Sohio MDI-57 oil and mineral seal oil. The Reynolds number based on average pore size and average pore velocity ranged from 0.16 to 700. The results indicate the existence of four flow regimes in a porous medium: 1. The Darcy or creeping flow regime where the flow is dominated by viscous forces and the exact nature of the velocity distribution is determined by local geometry. This type of flow occurs at  $Re < 1$ . At the  $Re = 1$ , boundary layers begin to develop near the solid boundaries of the pores. 2. The inertial flow regime. This initiates at  $Re$  between 1 and 10 where the boundary layers become more pronounced and an "inertial core" appears. The developing of these "core" flows outside the boundary layers is the reason for the non-linear relationship between pressure drop and flow rate. As the  $Re$  increases, the "core" flows enlarge in size and their influence becomes more and more significant on the overall flow picture. This steady non-linear laminar flow regime persists to a  $Re \sim 150$ . 3. An unsteady laminar flow regime in the Reynolds number range of 150 to 300. At a  $Re \sim 150$ , the first evidence of unsteady flow is observed in the form of laminar wake oscillations in the pores. These oscillations take the form of traveling waves characterized by distinct periods, amplitudes and growth rates. In this flow regime, these oscillations exhibit preferred frequencies that seem to correspond to specific growth rates. Vortices form at  $Re \sim 250$  and persist to  $Re \sim 300$ . 4. A highly unsteady and chaotic flow regime for  $Re > 300$ . Indicating turbulent flow.

These results indicate that new parameters are important for the understanding of transport phenomena in porous media. In particular a new characteristic length, the passage length, is important in the Darcy and inertial flow regimes and the Stokes number is important in the unsteady laminar regime. These parameters are used to develop correlations in each flow regime.

The heat transfer correlations were determined by an experimental study of the internal heat transfer coefficients of porous metals. Porous metal specimens were subjected to counter current heat and mass transfer

boundary conditions. For this purpose the high irradiance source was a Xenon gas jet pinched 50 KW arc image furnace coupled with a light pipe condenser to produce uniform heat intensity on the test specimen surface. The solid and gas phase temperatures were measured. With the resulting temperature profiles, the average internal heat transfer coefficient was evaluated and using the parameters determined from the fluid mechanic studies correlations were developed between appropriately defined Nusselt (Nu) and Reynolds (Re) numbers.

The actual porous metal specimens tested consisted of twelve different sintered powder and fiber metals ranging in porosity from 26% to 80% and made of stainless steel 316, Nickel 200 and copper. Nitrogen gas was used as the transpirant. Using the passage length,  $L$ , as a characteristic length, the Darcy and Inertial flow regimes are clearly distinguished and the correlations are:

$$\text{Darcy: } Nu \left[ \frac{L}{d} \right] / \left[ Pr^{1/3} \right] = 0.0027 Re^{0.91} \quad 0.1 < Re < 3;$$

$$\text{Inertial: } Nu \left[ \frac{L}{d} \right] / \left[ Pr^{1/3} \right] = 0.0037 Re^{1.4} \quad 3 \leq Re < 50; \text{ where } d \text{ is the pore size.}$$

## Natural Convection Heat Transfer in Porous Media

by

Craig Somerton	Ivan Catton
Mechanical Engineering Dept	Nuclear Energy Lab
Louisiana State University	UCLA
2508 CEBA Building	2567 Boelter Hall
Baton Rouge, LA 70803	Los Angeles, CA 90024

Four distinct but interrelated investigations have been performed. Natural convection experiments involving a porous layer or superposed layer system were conducted. Results were obtained in terms of Nusselt number versus Rayleigh number (either external or internal for the three physical parameters: Darcy number, layer height ratio, a thermal conductivity ratio. The experiments were seen to be self-consistent and the porous layer results were in fair agreement with previous work.

An analytical solution, using a power integral method, was developed for the superposed layer problem (a fluid layer over a saturated porous layer). A computer program was developed which yields Nusselt number as a function of a combined Rayleigh number for given values of  $Da$ ,  $\gamma$ , and  $n$  (Darcy number, thermal conductivity ratio and layer height ratio.) Comparison with experiment showed the same trends in Nusselt number, though the power integral solution provided results at small Rayleigh numbers while experiments provided results at large Rayleigh numbers. By interpolating between the analytical and experimental results a complete curve of Nusselt number versus Rayleigh number was obtained. When internal heating was included, no modifications proved necessary due to the use of a combined Rayleigh number. This use was confirmed by experiment.

The problem of natural convection in a horizontal porous layer with or without volume heating was solved numerically using a mixed finite difference-Galerkin method in conjunction with a wavenumber prediction scheme based on nonequilibrium thermohydrodynamic theory. Results were found to be in excellent agreement with experiments. The possibility of Prandtl number dependence was explored.

The following conclusions may be drawn from the experimental and power integral investigations of convection in a superposed layer system. 1) It is inappropriate to uncouple the fluid layer from the system as far as Nusselt number is concerned over the range of parameters considered. 2) An increase in the Darcy number is seen to cause an increase in convective transport due to the reduction in flow resistance. 3) An increase in the thermal conductivity ratio leads to a decrease in the Nusselt number. 4) The convective contribution for  $n > 2$  is primarily in the fluid layer and for  $n < 1$  in the porous layer, with the layers being strongly coupled and a Nusselt number maximum occurring in this range. 5) The power integral solution appears to breakdown, as indicated by comparison with experiment, at a Rayleigh number 50 to 100 times critical. At this point there is sudden increase in the Nusselt number apparently due to a sudden increase of fluid motion in the porous layer. 6) Internal heating may be included by using a combined Rayleigh number which is a linear

combination of  $Ra_E$  and  $Ra_I$  where

$$Ra_E = \frac{g\beta\Delta TL^3}{\nu_f\alpha_f}, \quad Ra_I = \frac{g\beta Q_v L^5}{2km\nu_f\alpha_f},$$

and the combined Rayleigh number

$$Ra^* = Ra_E(1 + n)^2 + Ra_I.$$

The following conclusions are made from the numerical solution to the porous layer problem. 1) The nonequilibrium thermohydrodynamic theory of Glansdorff and Prigogine [1971], as applied by McDonough [1981] to the Bénard problem, is applicable for wavenumber prediction in the porous layer problem. 2) Theoretical heat transfer predictions are in good agreement with experiment when preferred wavenumbers are used. 3) Brinkman's extension to Darcy's law becomes significant for  $Da > 5 \times 10^{-4}$ . For smaller values of  $Da$ , Darcy's law is adequate for heat transfer predictions. 4) Wavenumber predictions show that the wavenumber decreases with increasing Rayleigh number. 5) For the case with internal heating, the internal Rayleigh number serves as the parameter of interest. 6) When there is both internal heating and an applied temperature gradient the ratio

$$\frac{Ra_E}{Ra_I}$$

has a significant effect on the Nusselt number. 7) A Prandtl number dependence is proposed as the reason for the differences in heat transfer for different porous systems.

.....  
 Glansdorff, P. and Prigogine, I. Thermodynamic Theory of Structure, Stability and Fluctuations, Wiley Interscience, New York, 1971.

McDonough, J. M. "The Rayleigh-Benard Problem on a Horizontally Unbounded Domain: Determination of the Wavenumber of Convection," Ph.D. Dissertation, UCLA, School of Engineering, Los Angeles, 1981.

MECHANICS OF SOIL-HEAT INTERACTION IN  
A DESERT ENVIRONMENT

by

R. C. Chaney  
Associate Professor  
Dept. of Environmental Resources Engineering  
Humboldt State University, Arcata, CA 95521

G. Ramanjaneya  
Senior Engineer  
Ertec Western Inc., 3777 Long Beach Blvd.,  
Long Beach, CA 90807

H. Y. Fang  
Professor  
Dept. of Civil Engr.,  
Lehigh University, Bethlehem, PA 18015

In nature, soil temperature varies continuously in response to the everchanging meteorological regime acting upon the soil-atmosphere interface. That regime is characterized by a regular periodic succession of days and nights, and of summers and winters. These regular diurnal and annual cycles are perturbed by irregular phenomena such as cloudiness, cold waves, warm waves, rainstorms or snowstorms, and periods of drought. In addition to these external influences the soils own changing properties will alter the soil temperature profile. These soil properties are temporal changes in reflectivity, heat capacity, and thermal conductivity as the soil alternately wets and dries, and the variation of all these properties with depth.

Evaluation of heat flow characteristics of desert soils was performed using a combination of field monitoring, laboratory determination of thermal soil properties, and analytical modeling. The field program consisted of installing three thermal sensor arrays (T type thermocouples) in 38.1m (125 ft) deep boreholes located in two valleys in Nevada. The thermal sensors were located at soil depths of 0.6m (2ft), 1.2m (4ft), 2.4m (8ft), 15.2m (50ft) and 38.1m (125ft). These thermal sensors were monitored over a period of eight months to evaluate insitu subsurface soil temperatures as a function of time and depth. Soil temperature versus time plots are presented for a continuous 24 hr. period as well as over a period of 8 months for one selected borehole in Fig. 1 and 2 respectfully. Results from the 24 hr. monitoring period indicate that soil temperatures below 2 ft. were not affected by variations in ambient air temperatures. Minimum soil temperatures were achieved at a depth of 15.2m (50ft) and then found to increase again at a depth of 38.1m (125ft). Soil temperatures monitored over an extended time period (April to Nov.) showed that a minimum constant temperature of 10°C was maintained at a depth of 15.2m (50ft) while the ambient air temperature varied from a minimum of 10°C to 32°C. The laboratory program consisted of performing thermal conductivity and specific heat determinations using a thermal needle and calorimeter respectively on 41 samples from the 3 boreholes. A graph of thermal resistivity ( $\rho$ ) versus saturation is presented for sands and silt material. Values of  $\rho$  range from 150°C-cm/watt at a

saturation of 20% to 70°C-cm/watt at 90% saturation. Values of specific heat ranged from 0.154 to 0.197 cal/g-°C.

References

"Thermal Properties of Soils MX Siting Investigation",  
 Reprot to U.S. Department of the Air Force Ballistic Missile  
 Office, Fugro National, Inc., Long Beach, CA. 90807, 23 Nov.  
 1979.

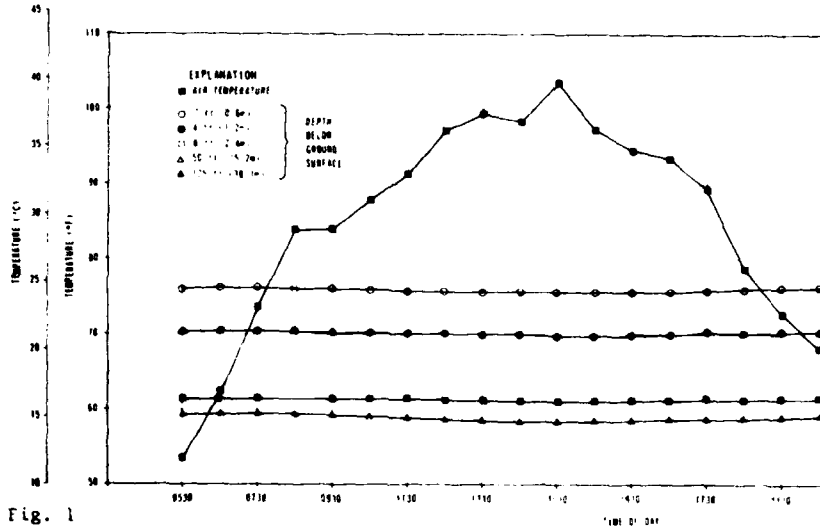


Fig. 1

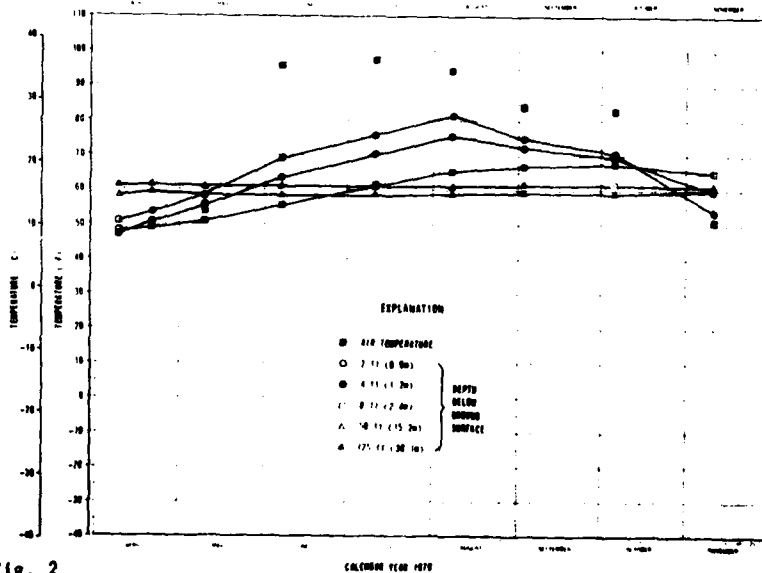


Fig. 2

Transient Cooling/Heating  
of Air Saturated Spherical Porous Media

by

W.E. Stewart, Jr.

Department of Mechanical and Aerospace Engineering  
University of Missouri-Kansas City  
Independence, Missouri 64050

An experimental investigation was made of the cool down/heat up time of a vertical cylindrical column of spherical lead porous media, saturated with air. The porous media was cooled and heated between different uniform steady-state temperatures.

The boundaries of the stainless steel cylinder were kept at a constant uniform temperature, except the base, which was insulated. The lead spherical porous media and air then reached this boundary temperature at steady-state conditions. Temperature measurements of the porous media and air were made with several thermocouples throughout the cylinder.

The lead spheres were approximately 2mm in diameter and represented a "shaken" spherical bed, the porosity,  $\epsilon$ , being approximately 0.37. Nineteen thermocouples were used to measure the lead sphere center temperatures and nineteen thermocouples used to measure the air temperature throughout the cylinder. A modified Nusselt was defined as

$$Nu^* = k_f^*(T_{f,avg} - T_b) + k_s^*(T_{s,avg} - T_b) / k^*(\Delta T), \quad (1)$$

Where  $T_{f, avg}$  = average air temperature, at time  $t$ .

$T_{s, avg}$  = average porous media temperature, at time  $t$ .

$T_b, avg$  = constant boundary temperature

$k_f^*$  = effective air thermal conductivity,  $(1-\epsilon) k_f$ .

$k_s^*$  = effective porous media thermal conductivity,  $\epsilon k_s$ .

$k^*$  =  $k_f^* + k_s^*$

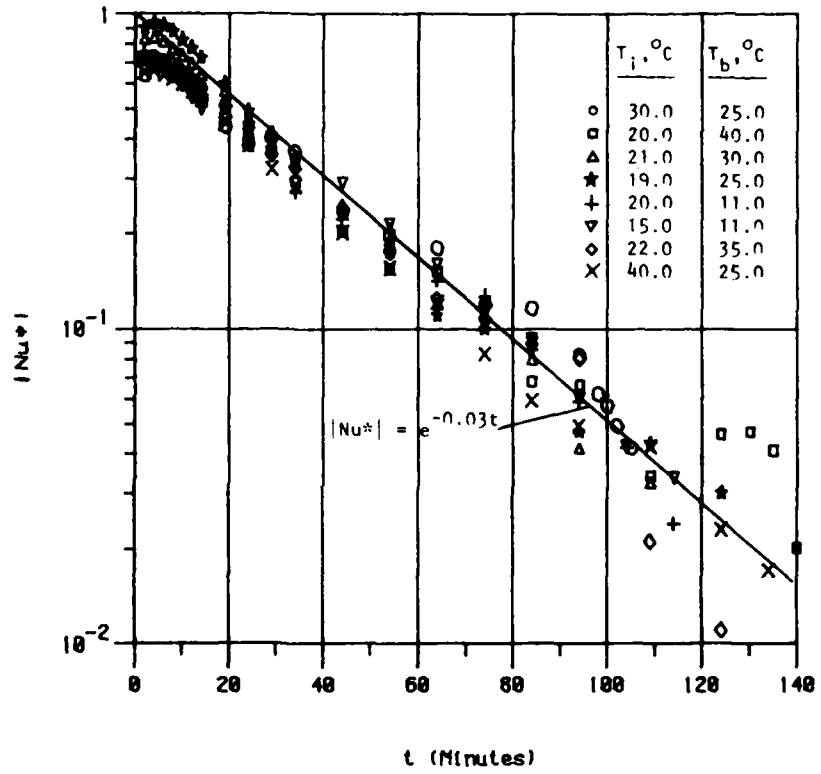
Cool down and heat up times were found to be primarily a function of conduction through the porous material to the constant temperature boundary and not the convective heat transfer by the surrounding air in the cylinder. A correlation of modified Nusselt and time was determined. The modified Nusselt number was determined to be a simple exponential function of time.

The reduced data for the experiments are shown in the figure below, which shows the correlation,

$$[Nu^*] = e^{-0.03 t}, \tag{2}$$

a least squares fit of the data adjusted to

$$[Nu^*] = 1 \text{ at } t = 0.$$



## CONVECTIVE HEAT TRANSFER IN POROUS MEDIA

by

Ping Cheng  
Mechanical Engineering Department  
University of Hawaii, Honolulu, Hawaii 96822

Introduction

Recent emerging technologies on the extraction of geothermal energy, the design of insulation systems for energy conservation, the use of aquifers for hot-water storage, the disposal of nuclear wastes in sub-seabeds, the enhanced recovery of oils by thermal methods, and the design of catalyst-bed reactors have demanded an improved understanding of heat transfer mechanisms in fluid-filled porous media.

Darcy's and Brinkman's Models

Most of the theoretical studies of heat transfer in porous media have used the Darcy law as the momentum equation. Because the order of the Darcy law is lower than that of the Navier-Stokes equation, the formulation of heat transfer problems based on Darcy's law must abandon the no-slip boundary conditions. For this reason, some authors prefer to use the Brinkman's equation with no-slip conditions for the formulation of convective heat transfer problems in porous media. The Brinkman's equation is essentially the Darcy law with the addition of a classical viscous frictional term.

Free and Mixed Convection

Early work on free convection in porous media focused its attention on the onset of convection as well as on the cellular convection in an enclosed porous medium heated from below. Critical Rayleigh numbers for the onset of free convection in parallel-plate geometries heated from below with different hydrodynamic and thermal boundary conditions have been obtained based on linear stability analyses. The effects of horizontal temperature gradients of the heated surface, the inclination angle of the parallel plates, the temperature dependence of the fluid properties, as well as the horizontal and vertical flow on the critical Rayleigh number have been examined.

Finite difference and finite amplitude analyses have been performed for transient and steady, three or two-dimensional free convection in rectangular geometries with heating from below or from the sides. The effects of layered structure of the porous medium have been studied numerically. A two-temperature model was used to explain the phenomena of hot springs. Finite difference solutions have been carried out to study free convection in porous media between concentric cylinders and spheres. On the other hand, finite element solutions have been used for the simulation of free convection for a number of real geothermal systems. The effects of the withdrawal of hot water and the reinjection of cold water in geothermal systems have been studied based on numerical models.

Exact analytical solutions have been obtained for plume rises from a point source, with application to nuclear wastes disposal. Perturbation solutions for small Rayleigh numbers have been obtained for free convection in triangular enclosures with application to attic shape porous insulation.

Boundary layer approximations have been introduced to obtain similarity solutions for steady free and mixed convection from heated plates, cylinders and spheres to the surrounding fluid-filled porous media. The critical Rayleigh or Peclet number for the onset of longitudinal vortices in horizontal and inclined porous layers heated from below have been obtained based on linear stability analyses.

Most recently, increased attention has been given to the studies of various effects that have been neglected in the similarity solutions. These include the effects of inertia, thermal dispersion, no-slip boundary conditions, non-uniform wall porosity, entrainments from the edge of the boundary layer, the axial heat conduction, and the normal pressure gradient. It is found that the combined effects of inertia and no-slip boundary conditions tend to retard the surface heat flux. The effects of entrainments, the axial heat conduction, and the normal pressure gradients are found to be small for free convection in porous media adjacent to heated surfaces.

Experiments have been conducted to investigate the onset of free convection in rectangular and cylindrical enclosures filled with porous media and heated from below. The Nusselt numbers determined from these experiments during steady conditions are correlated in terms of the Rayleigh number. The data for free convection in rectangular geometries show considerable scattering among investigators using different porous media and fluids. Recently, some data has been obtained for free convection in water-filled glass beads adjacent to a heated vertical flat plate, a horizontal cylinder and between vertical concentric cylinders. The data obtained at low Rayleigh numbers is found to be in good agreement with theoretical predictions based on Darcy's law.

#### Forced Convection

Forced convection of gases in porous media has important applications to pack-bed reactors. At high speeds, the thermal dispersion and the non-local thermal equilibrium effects are found to be important. Early theoretical work on forced convection in porous media assumes plug flow. Recently, some numerical studies have been performed for two-dimension forced convection of gases in a tube with thermal dispersion, non-uniform wall porosity and no-slip boundary conditions taking into consideration. Experiments have been conducted to determine heat transfer coefficients from the inner wall to forced flow of air inside a tube that is filled with porous media. Other experiments were conducted for the purposes of determining the longitudinal and transverse thermal dispersion coefficients, as well as interphase heat transfer coefficients.

TWO PHASE FLOW AND HEAT TRANSFER  
IN POROUS MEDIA

by

Vijay K. Dhir  
School of Engineering and Applied Science  
University of California, Los Angeles  
Los Angeles, California 90024

This Study deals with hydrodynamic and thermal characteristics of two phase flow through porous layers. Basic experimental and analytical investigations of two phase flow through porous layers composed of nonheated and heated particles have been made. For both co and counter current flows of gas and liquid, two phase pressure drop and void fraction have been measured in porous layers composed of nonheated particles. In the experiments, the particle size, particle shape, the particle size distribution, bed porosity and superficial velocities of gas and liquid are varied parametrically. A model based on drift flux approach has been developed for the void fraction. Using the two phase friction pressure drop data, bounding values of the relative permeability multipliers for the gas and liquid phases in homogeneous beds have been determined. The void fraction and two phase friction pressure gradient in beds composed of mixtures of spherical particles as well as sharps of different nominal sizes have also been examined. It is found that the models for single size particles are also applicable to mixtures of particles if a mean particle diameter for the mixture is defined. The conditions for the onset of fluidization of porous layers composed of single size and mixtures of several size particles have been obtained by using the expressions for relative permeability multipliers and void fraction.

Several processes involving two phase heat transfer during steady state or transient cooling of bottom or volume heated particulate beds have been studied. These processes include forced flow cooling of a layer of volumetrically heated particles with feeding of subcooled liquid at the bottom and quenching of a hot particulate bed by bottom flooding. In the experiments the particles are heated inductively and Freon-113 and water are used as coolants. The above models for two phase drop and the energy equations for the fluid and the particles are used to determine the state of the fluid and the temperature of the particles in different regions of the porous layer. Observations of the particle temperature and quench front velocity are found to compare well with the predictions.

Under certain flooding conditions, self fluidization of the particulate beds has been observed. The particle fluid heat transfer coefficients in the fluidized state are found to be considerably high. Conditions leading to self fluidization of the hot particulate bed are delineated.

ONSET OF THERMAL CONVECTION IN A SATURATED  
POROUS MEDIUM HEATED FROM BELOW

by

M. Kaviany  
University of Wisconsin--Milwaukee  
Department of Mechanical Engineering  
Milwaukee, Wisconsin 53201

Dynamic linear stability theory is applied to the governing equations developed by Vafai and Tien who, by combining the results of local volume averaging and empirical results, have been able to include the inertia and boundary effects.<sup>1</sup> The problem considered is a horizontal saturated porous medium which is confined between an impermeable rigid boundary at the bottom and a shear free boundary at the top. Initially the fluid is quiescent and the media is at a uniform temperature. Then, the temperature of the lower surface is raised at a constant temporal rate, resulting in a potentially unstable, nonlinear and time-dependent stratification. The temperature field and the boundary conditions are chosen to be similar to those that will be involved in the experimental study which will follow. The method of solution is similar to that reported previously.<sup>2</sup>

As the result of the analysis, the time of the onset of convection is predicted. The effects of the non-dimensionalized parameters, i.e., a) the Rayleigh number based on the heating rate and the depth of the media, b) the Prandtl number, c) the ratio of the porosity to the permeability, and d) the ratio of the products of the density and specific heat for the fluid phase and the fluid and solid phases combined, on the time of the onset of convection are demonstrated and discussed.

<sup>1</sup>Vafai, K. and Tien, C.L., "Boundary and Inertia Effects on Flow and Heat Transfer in Porous Media," Int. J. Heat and Mass Transfer, 24, 1981, pp. 195-203.

<sup>2</sup>Kaviany, M., "Thermal Instabilities in Porous Medium," Heat Transfer in Porous Media, ASME, HTD, 22, 1982, pp. 1-8.

## Cavity flows in porous media: the merged layer regime

by

P. A. Blythe  
Center for the Application of Mathematics  
Lehigh University, Bethlehem, PA 18015

and

P. G. Simpkins  
Bell Laboratories, Murray Hill, NJ 07974

This paper is concerned with steady two-dimensional flows in a rectangular cavity filled with a fluid-saturated porous medium. The motion is generated by differentially heating the vertical end walls of the cavity such that the Rayleigh number  $R$ , based on the cavity height, is large. In addition, the solution also depends on the cavity aspect ratio  $L$  (length/height), and for the flows considered here  $L > 1$ . New analyses<sup>1,2</sup> of this problem have demonstrated the existence of a broad spectrum of solution regimes that depend critically on the relative magnitudes of  $R$  and  $L$ . Although the vertical boundary layer structure is well known, the compatible structure for the flow near the horizontal surfaces has only recently been developed.<sup>1</sup> It has been shown<sup>2</sup> that, when the horizontal surfaces are adiabatic, distinct horizontal layers exist only if  $R \gg 10^4 L^2$ . Since this restriction is severe, the concept of thin horizontal boundary layers is often not valid. Many practical configurations appear to give rise to flows in which the horizontal layers merge.

Merged layer regimes occur in the formal limit  $R \rightarrow \infty$  with the group  $r = R/L^2$  fixed. It can be argued that the structure of the core flow, away from the vertical end walls, is governed by the expansion

$$\bar{\psi} = R^{1/2} \bar{\psi}_m(s, z; r) + \dots, \quad \bar{T} = T_m(s, z; r) + \dots \quad (1)$$

where the stream function  $\bar{\psi}$  is made dimensionless with respect to the thermal diffusivity, the temperature  $\bar{T}$  with respect to the temperature difference across the cavity, the horizontal distance scale  $s$  with respect to the cavity length, and the vertical distance scale  $z$  with respect to the cavity height. In this limit the vorticity and energy equations reduce, respectively, to

$$\partial^2 \bar{\psi}_m / \partial z^2 = -r^{1/2} \partial T_m / \partial s, \quad \frac{\partial (T_m, \bar{\psi}_m)}{\partial (s, z)} = r^{-1/2} \frac{\partial^2 T_m}{\partial z^2}, \quad (2)$$

and thermal diffusion is important everywhere in the core. Even though  $L \gg 1$ , the core solution does not correspond to a shear flow that is parallel with the horizontal boundaries. This behavior is in qualitative agreement with existing numerical solutions that are appropriate to the merged layer domain, but it is not of the classical Hadley cell form.

It must be stressed that equations (2) are valid only in the limit  $R \rightarrow \infty$  at fixed  $r$ . These relations fail near the ends of the cavity where the major part of the flow is governed by the usual vertical boundary layer equations<sup>3</sup> which provide matching conditions for the core solution.

Over the merged layer regime, it can be argued that the Nusselt number  $Nu(R,L)$  must satisfy the scaling law

$$Nu = L^2 N(r), \quad (3)$$

where, as  $R \rightarrow \infty$ ,

$$N \sim c r^{1/2} \quad (c \approx 0.515) \quad (4)$$

consistent with the standard boundary layer result ( $R \rightarrow \infty$  at fixed  $L$ ). Existing data, relevant to merged layers, are found to be in good agreement with the scaling law (3).

#### References

- 1 P. G. Daniels, P. A. Blythe & P. G. Simpkins, Thermally driven cavity flows in porous media. II The horizontal boundary layer structure. Proc. Roy. Soc., A382, 135-154 (1982).
- 2 P. A. Blythe, P. G. Simpkins & P. G. Daniels, Thermal convection in a cavity filled with a porous medium: a classification of limiting behaviors, Int. J. Heat Mass Trans. In press.
- 3 J. C. Weber, The boundary layer regime for convection in a vertical porous layer. Int. J. Heat Mass Trans., 18, 569 (1975).

Low Rayleigh Number Convection in an Eccentric Porous  
Annulus and Around a Pipe Buried in Permeable Medium

by

Haim H. Bau  
Department of Mechanical Engineering and  
Applied Mechanics  
University of Pennsylvania  
Philadelphia PA 19104

This study considers low Rayleigh number convection in a saturated porous medium confined between two eccentric cylinders. Both cylinders are impermeable to fluid motion and are maintained at two different, uniform temperatures. As a result of the temperature difference between the cylinders, natural convection is induced in the medium. The complicated boundary conditions are handled through the use of bi-cylindrical coordinates. Three geometrical configurations are considered: an eccentric annulus; a pipe buried in a semi-infinite medium; and two cylinders, one outside, the other, imbedded in an infinite medium.

The Darcy-Oberbeck-Boussinesq's equations are solved using regular perturbation expansion in terms of the Darcy-Rayleigh number ( $R$ ). The results include a description of the flow and temperature fields as well as Nusselt ( $Nu$ ) versus Darcy-Rayleigh number correlations in the form:

$$Nu = 1 + C_1 R^2 + C_2 R^3 \cos \theta + O(R^4)$$

where  $\theta$  is the angle between the axis connecting both cylinders' centers and the gravity vector.

The results are applicable only for the cases of the eccentric annulus and the buried pipe. For the case of one cylinder outside the other, in general, meaningful regular perturbation series cannot be constructed. The series obtained for the two first cases have a limited radius of convergence which decreases with increasing eccentricity. For the case of the buried pipe, the range of utility of the perturbation series is increased via the use of nonlinear transformations.

Both the case of the eccentric annulus and that of the buried pipe are germane to various industrial problems. The case of the eccentric annulus has bearing on thermal insulations. It is shown that eccentric insulators are more efficient than concentric ones. The case of the buried pipe is of relevance, for example, to the oil/gas industry in estimating heat losses from heated/chilled fuel flowing in buried pipes. It is shown that there exists an optimal burial depth for which heat losses from the pipe are minimized. Both the optimal eccentricity in the case of the eccentric insulation and the optimal burial depth are functions of the Darcy-Rayleigh number

## Porous Media Models With Mass Exchanges

by

Ray M. Bowen

Division Director  
Division of Mechanical Engineering  
and Applied MechanicsNational Science Foundation  
Washington, D.C. 20550

This work concerns the formulation, by use of the Theory of Mixtures, of a porous media model which allows mass exchanges among the constituents. The motivation for allowing mass exchanges results from the interest in studying pore-fluid to fracture-fluid transformations in fractured reservoirs. The classical model of a rigid fractured reservoir is due to Barenblatt, Zheltov and Kochina. Aifantis and his co-workers generalized the rigid model so as to allow the solid matrix to undergo infinitesimal deformations.

In addition to mass exchanges among the constituents, the thermo-mechanical formulation given in this work allows each constituent to have its own temperature. The resulting model has sufficient generality to characterize heat and mass transfer in the pores, in the fractures and from the pores to the fractures. The classical Barenblatt model and certain of its generalizations will be discussed as special cases of the results given here.

## References

1. Bowen, R. M., *Compressible Porous Media Models by use of the Theory of Mixtures*, Intl. J. Engr. Sci., 20, 697-735, 1981.
2. Barenblatt, G. I., Iu. P. Zheltov, and I. N. Kochina, *Basic Concepts in the Theory of Seepage of Homogeneous Liquids in Fissured Rocks (Strata)*, PMM, 24, 852-864, 1960.
3. Barenblatt, G. I., *On Certain Boundary Value Problems for the Equations of a Liquid in Fissured Rocks*, PMM, 27, p. 348-350, 1963.
4. Aifantis, E. C., *On the Response of Fissured Rocks*, *Developments of Mechanics*, 10, 249-253, 1979.

## MIXED CONVECTION IN EXTERNAL FLOWS

by

T. S. Chen

Department of Mechanical and Aerospace Engineering  
University of Missouri-Rolla, Rolla, Missouri 65401

In recent years the phenomenon of mixed convection has gained considerable importance in the study of heat and/or mass transfer characteristics in many industrial and environmental processes. In forced convection flows, the buoyancy forces that are generated as a result of the density variation due to the diffusion of thermal energy and/or chemical species may have a significant effect on the velocity, temperature, and/or concentration fields and hence on the flow, heat, and/or mass transfer characteristics. Similarly, buoyancy-induced natural convection flows are affected by the presence of an external forced flow. Mixed convection refers to the flow situations in which the forced and natural convection mechanisms are of comparable magnitude and as such both the forced and natural convection effects must be considered in the analysis of the transport process. Mixed convection processes may be divided into external boundary layer flows over bodies (such as flat surfaces, cylinders and wires, spheres, and moving surfaces), free boundary flows (such as buoyant plumes, jets, and wakes), and internal flows (such as flows inside pipes, channels, ducts, and enclosures). Examples of mixed convection processes can be found in connection with heat exchangers, nuclear reactors, hot-wire anemometers, flow of droplets, high-voltage transformers, solar collectors, electronic devices, heat rejection and energy storage systems, etc. The domain of mixed convection regime depends on the fluid and on the flow configuration as well as on the surface heating condition. It is defined by the value of the buoyancy force parameter  $Gr/Re^n$ , in which  $Gr$  and  $Re$  are, respectively, the Grashof and Reynolds numbers, and  $n$  is a constant determined by the flow geometry and thermal boundary condition. For the case of combined heat and mass transfer in mixed convection, the transport process becomes more complex and, in the absence of diffusion-thermo and thermo-diffusion effects, the ratio of the concentration Grashof number to the thermal Grashof number,  $N$ , appears as an additional parameter.

This paper is concerned primarily with mixed convection heat transfer processes in which the buoyancy force arises from thermal diffusion. It discusses the present state of knowledge, some of the important critical issues, and future research needs in the area of mixed convection in external boundary layer flows. The flow and heat transfer characteristics are examined in detail for laminar, transition, and turbulent flow regimes, with reference to flow over surfaces in general and a flat plate geometry in particular to gain insight into the mixed convection mechanism. Most of the materials are derived from the recent work of the author and his co-workers.

One of the main objectives in the study of mixed convection heat transfer, both analytical and experimental, is to determine the bounds of the mixed convection regime,  $a \leq Gr/Re^n \leq b$ , over which neither the forced convection nor the natural convection mechanism is dominant. The values of the lower and upper bounds  $a$  and  $b$  for various fluids have been presented for simple geometries (such as flat surfaces, cylinders, and spheres), for both assisting and opposing flow conditions.

Instability of the flow is another important aspect of the problem in mixed convection. Buoyancy forces have been found to have a pronounced effect on the stability of the flow and its subsequent transition to the turbulent flow regime. Linear stability analysis has been conducted for the wave mode as well as the vortex mode of instability for flat plate geometry, and critical Reynolds and Grashof numbers have been presented. However, analysis of mixed convection in transition and turbulent regimes is very lacking. Very recently, a modified version of the mixing-length model has been used by the author to analyze turbulent mixed convection flows over vertical and horizontal surfaces, from which some interesting features have been obtained. In particular, it was found that under the assisting flow condition the surface heat transfer rate drops below that for pure turbulent natural convection when the parameter  $Gr/Re^n$  reaches a certain critical value, decreases further and then gradually increases to approach the natural convection limit from below as the value of  $Gr/Re^n$  is further increased. This is in sharp contrast to the findings for the laminar case in which mixed convection provides higher heat transfer rates than natural convection for all values of the parameter  $Gr/Re^n$ . Experimental studies pertaining to mixed convection heat transfer in transition and turbulent flow regimes are also very lacking. Experimental data for transition Reynolds and Grashof numbers are needed to verify the critical values predicted by the linear theory. A complete analysis of turbulent mixed convection heat transfer should start with a laminar flow regime and go through a subsequent transition to the turbulent flow regime. This would require a knowledge of the transition Reynolds and Grashof numbers, which are not known with any degree of certainty at the present time, even for a simple flat plate geometry.

In conclusion, considerable knowledge has been gained in recent years in laminar mixed convection heat transfer over simple geometries. However, much analytical and experimental work on the instability of the flow, transition, and turbulent flow remains to be done. There is a pressing need of experimental data for laminar, transition, and turbulent regimes in mixed convection. Modeling of turbulent heat transfer in mixed convection needs to be developed, and experimental data for formulation of such a model or models are lacking. Studies of three-dimensional and unsteady mixed convection are needed, so are the studies of heat transfer characteristics in the region of flow separation in the opposing flow condition. Further study is also needed in the instability of mixed convection flow, particularly from the standpoint of nonparallel-flow and nonlinear analysis.

## SOME SCALES FOR MIXED CONVECTION

by

L. S. Yao  
Dept. of Mechanical and Aerospace Engineering  
Arizona State University  
Tempe, Arizona 85287

The importance of mixed convection is being slowly recognized by researchers in the heat transfer community and related industries. In fact, many situations which are, by tradition, viewed as being forced convection dominated are instead influenced by the presence of free, or more generally, mixed convection. The scatter in experimental data plotted in a forced-convection correlation, which is frequently attributed to experimental error, is often due to the presence of mixed-convection phenomena. The selection of appropriate scales is one of the important parts of the study of mixed convection, and is not an easy task. Problems involving a horizontal pipe and a vertical pipe are selected to demonstrate the subtleties of scaling mixed convection.

In general, the importance of natural convection grows along streamlines for a forced flow. For a horizontal pipe, the flow development can be divided into three different regions according to the magnitude of natural convection. Near the inlet of the pipe, natural convection is relatively unimportant compared to forced convection. The size of this region is usually very small and depends on a combination of the associated Reynolds number and the Grashof number. The mixed-convection boundary layer determines the heat transfer mechanism in the second region where the inviscid core flow has only been slightly disturbed. Eventually, a strong secondary flow is developed in the third region, which completely alters the heat transfer mechanism and changes the transition Reynolds number.

The flow development in a vertical pipe is similar to that in a horizontal pipe; however, the flow is further complicated by the occurrence of a slowly evolving thermal instability in the third region. For external flows, the third region does not exist; instead, the flows asymptotically approach a natural-convection dominant state.

Appropriate parameters for correlating data will be discussed for these examples under two idealized heating conditions: constant heat flux and constant wall temperature. Some recent experimental data as well as numerical results will be used to elucidate the physics.

## PROPERTIES OF ISOLATED CONVECTION IN A ROTATING MEDIUM

by

Michael R. Muller and Jeffery Neil Burch  
Department of Mechanical and Aerospace Engineering  
Rutgers University  
New Brunswick, New Jersey 08903

The properties of isolated convection in a rotating medium were studied experimentally by the transient ohmic heating of a small wire placed on the floor of a rotating annulus containing air. The air within the annulus rotated as a solid body yielding a flow with constant non-zero vorticity and a radial pressure gradient necessary to balance the centrifugal force. The radial position of the heat source was offset from the axis of rotation by 30.5 cm. In this way, impulsively heated parcels of air would experience a body force due to an imbalance between the centrifugal and pressure forces in the radial direction. In addition to this force (and that of gravity making the parcel rise), when horizontal motion is generated a Coriolis force develops further complicating the flow.

We are concerned with the interaction of these three competing forces and the resulting motions of laminar buoyant thermals. The laboratory generated thermals were observed by making temperature measurements for a number of thermal events at several different horizontal locations on a radial line intersecting the heating wire. In order to make each thermal event as similar as possible to the others, the heating of the wire as well as table rotation, data acquisition and probe positioning were controlled by a dedicated LSI 11-23 micro-computer. The form of the thermals was deduced by piecing together data taken at different locations and creating contour maps of the temperature time histories. Some of the phenomena associated with increased rotation can be seen in the two figures shown here. Fig. 1a shows the temperature field for a radial traverse obtained in a fluid with relatively small vorticity (the rotation rate was 3 rpm). The radial position plotted is such that zero represents the heater location and positive values correspond to inward radial positions. In both figures, constant temperature lines are plotted every 0.5 degrees C. and the ohmic heater was charged for exactly 0.9 seconds. Figure 1a shows the temperature history for a thermal with an initial rise angle of only 0.17 degrees away from the vertical due to rotational effects and falls into the range where rotation can be ignored. The thermal appears to be symmetric and centered around the location of the heater. Figure 1b shows the case for higher rotation (20 rpm) which had an initial rise angle almost 8 degrees away from the vertical. One can observe an inward shift of the thermal of as much as 2.5 cm, which is the expected result of the local decrease in the fluid's angular momentum due to heating. There are however, more details in these figures which show effects of rotation which are not as easily explained. Firstly, the temperature within the plume in the high rotation case is significantly hotter than the lower rotation case. In addition, the isotherms indicate that the air

under the thermal cools more rapidly in the presence of significant rotation. Secondly, the inward shift is not largest where the temperature is highest. If the displacements being seen were due only to angular momentum changes within the plume, the hottest point would be displaced radially the greatest distance. The observation that this is not the case shows that secondary effects, such as the wake left by the

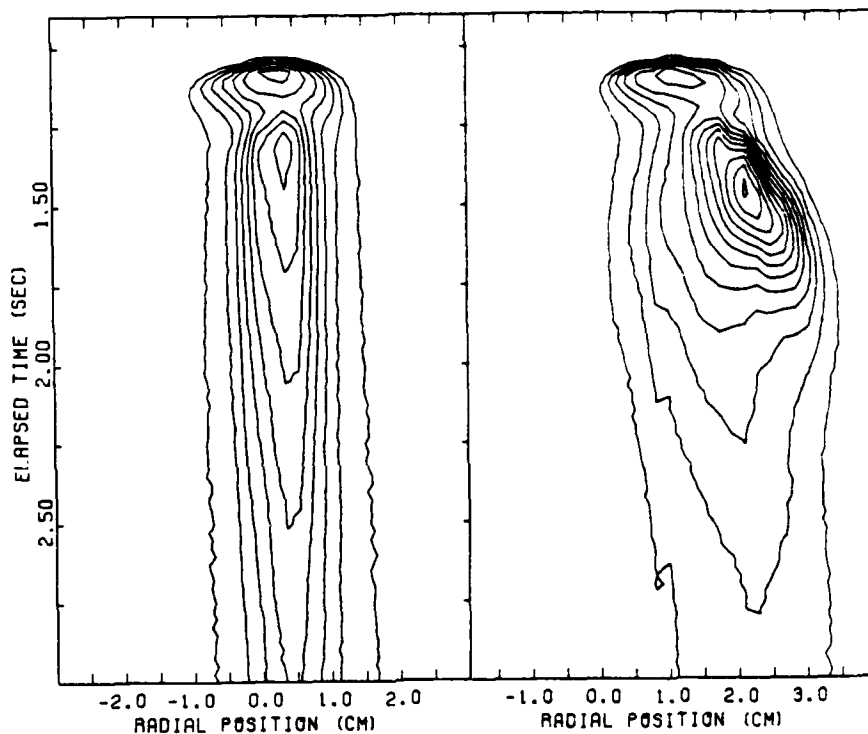


Figure 1a.

Figure 1b.

thermal and the circulations caused by its radially inward drift, must be important in predicting the overall appearance of buoyant thermals in rotating flows. Of further interest is the observation that the thermal caps of both cases arrive at the probe (here located 8.4 cm above the heater) at very nearly the same time and place. Additional experiments with thermals of different buoyancies showed similar radial drifts and increasing observed temperature with rotation, but indicated that the magnitude was clearly a function of density deficit.

Developing Laminar Mixed Convection Flow Between  
Vertical Parallel Plates

by

G. Worku  
International Energy Associates, Ltd.  
Washington, D.C.

and

Win Aung  
Graduate Professor  
Howard University  
and  
Director, Heat Transfer Program  
National Science Foundation  
Washington, D. C.

A numerical investigation of the effects of buoyancy on the hydrodynamic and heat transfer parameters of a developing forced convective flow between vertical parallel plates has been conducted. Buoyancy effects have been examined for symmetric as well as asymmetric cases of uniform wall temperature (UWT) and uniform heat flux (UHF) thermal boundary conditions. Utilizing a boundary layer-type equation set coupled with an implicit finite difference technique, solutions have been obtained for velocity, temperature, pressure, and Nusselt number in a developing flow for  $0 \leq Gr/Re \leq 750$ , and at values of the wall temperature ratio  $r_T = 1, 0.8, 0.5$  and  $0.3$  for UWT, and of the wall heat flux ratio  $r_H = 1$  and  $0.5$  for UHF. Limiting fully developed flow solutions are also derived in closed forms. The methods utilized in the numerical solutions are validated by comparing the results, for pure forced convection with symmetric heating, with existing solutions in the literature. Excellent agreement is obtained.

It is found that in UWT buoyancy dramatically increases the hydrodynamic entry length but diminishes the thermal development distance. At a fixed  $r_T$ , buoyancy enhances the heat transfer on the hot wall but has little impact on the cool wall heat transfer. When  $Gr/Re$  is fixed, a change in  $r_T$  produces a significant variation in the cool wall Nusselt number but has little impact on the hot wall.

In the case of UWT, flow reversal is observed at  $Gr/Re = 250$  for  $r_T = 0.5$  and  $0.3$ . The actual axial position of flow reversal is found to be a function of  $r_T$ . For the symmetric case, the asymptotic bulk temperature at large axial distances remains at 1.0 for all values of  $Gr/Re$  while for the asymmetric case, the asymptotic value varies with  $Gr/Re$  and  $r_T$ . It is found that the numerical method can yield solutions smoothly across the point of separation. Downstream of the point of flow reversal, the numerically derived velocity profiles are in close agreement with those obtained from the analytical results for fully developed flow. The reason for the possibility of calculating across

the point of separation is ascribed to relatively small values of the convective terms and the small extent of the region of separation. Using the fully developed flow solutions, the criteria for the occurrence of flow reversal are derived.

In the case of UHF, the phenomenon of flow reversal is absent. The bulk temperature is found to vary with  $r_w$ , but remains invariant with  $Gr/Re$  for both symmetric and asymmetric conditions.

Details of the present study are contained in Ref. [1].

#### REFERENCE

1. G. Worku, "Developing Laminar Combined Natural and Forced Convection Flow Between Vertical Parallel Plates", M. S. Thesis, Department of Mechanical Engineering, Howard University, Washington, D. C., May, 1982.

COMBINED CONVECTION ABOUT LOCAL  
SOURCES IN A HORIZONTAL CHANNEL

by

K. J. Kennedy and W. J. Shakespeare  
American Bell, Holmdel, N.J., 07733

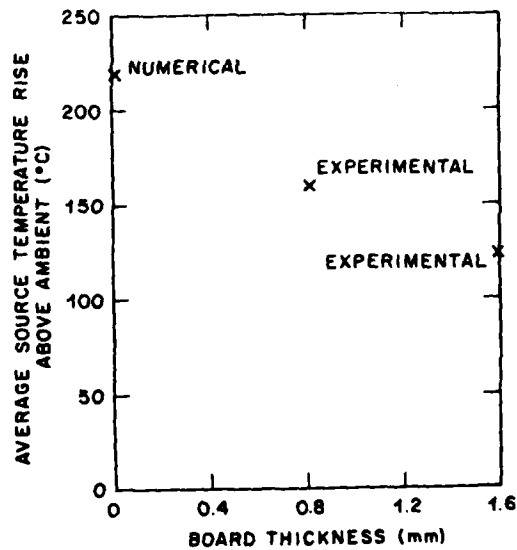
A summary of recent investigations of combined free and forced convection about local heat sources between parallel planes is presented. Experimental results are discussed for a 6mm wide heat source on a 1.5mm thick epoxy glass printed wiring board (PWB) and 13mm plane separation. Three dimensional longitudinal vortex rolls are found for  $Re \sim 100$  or more and  $Gr \leq 10^7$ . For lower Reynolds numbers a two dimensional recirculation region is observed above the heat source. The flow adjacent to the top wall dramatically dips toward the lower wall, upstream of the source. Beyond the heater strip, a region of sharply rising streamlines, a reverse cascade, is observed. For a Grashof number of 544,800 (dissipation of 3.66 watts and  $Re=37$ ), the wall temperature rise above ambient on the source was found to be 125°C.

Numerical results for the same configuration (neglecting axial wall conduction) were obtained using elliptic two dimensional finite difference approximations and the method of false transient. The numerically predicted flow pattern agrees with the experimental observations. The numerically predicted source temperature rise above ambient, however, was found to be 220°C. This discrepancy between the numerical and experimental results was attributed to axial wall conduction. Recent experiments with 0.75mm thick PWBs result in a source temperature rise above ambient of 160°C, 73% of the numerically predicted (zero wall thickness) value. These results confirm the suspected strong effect of axial conduction. (See Figure 1).

Numerical results predict local heat transfer coefficients for the above mentioned combined convection case approximately twice those found in the developing thermal entry length for forced flow between parallel planes. For a similar 6mm source located on the upper wall, numerical results predict the source temperature rise to be twice that of the single source on the lower wall. Heat transfer coefficients are roughly half those found on the lower wall. A relative temperature maximum occurs for the source on the upper wall due to the presence of a stagnation region.

The heat transfer and flow regimes resulting from two local heat sources on the bottom wall of a horizontal duct have also been investigated. It has been found that four recirculation regions occur; one upstream and one downstream of each heat source at the lowest Reynolds numbers, and Grashof numbers of order  $10^7$ . As Reynolds number is increased, the two central recirculation zones disappear and, for a narrow range of Reynolds numbers, the flow exhibits a periodic oscillation with vortices carried downstream by the bulk flow. At Reynolds numbers of order 30 to 40, the two central vortices disappear and, above  $Re \sim 40$ , helical motion is observed downstream of the second source. The transitions from one regime to another do not seem to have a great effect on the heat transfer although the convective motion has been shown to more than double the heat transfer compared to the predictions without natural convection. Currently, only the 1.5mm board thickness has been investigated, with heat source widths of one duct height.

FIGURE 1 EFFECT OF BOARD THICKNESS ON 6 MM SOURCE TEMPERATURE



Measurements of Combined Forced and Free Convection  
Heat Transfer to Low Temperature Helium  
in a Horizontal Channel

R.C. Hendricks  
NASA Lewis Research Center  
Cleveland, OH 44135

An experimental study of heat transfer has been carried out for helium near its thermodynamic critical point flowing in a horizontal tube, ref. 1. The tube, fig. 1, was 2.85 m long with an internal diameter of 19 mm. A 6-mm diameter rotatable coaxial probe was used to obtain fluid temperature profiles at two locations and to simulate a coaxial power transmission cable. The experimental parameters ranged from 6.5 to 15 K for bulk temperature, pressure from 1.2 to 3.0 bars, heat fluxes to 1 kW/m<sup>2</sup>, and Reynolds number from 9.E3 to 2.E5. Under these conditions, the heat transfer coefficient varied considerably over the periphery of the tube. The temperature difference within the fluid from the top to the bottom of the tube varied by as much as 6 K, with the maximum at the top, while the surface temperatures only varied 3 K. The bulk temperature isotherm patterns showed evidence of six vortex flow cells of thermogravitational origin, fig. 2. Such variations result in a flow thermal stabilization length on the upper surface of nearly 1.5 times that for the lower surface.

Local and average heat transfer data are correlated using the density fluctuation model. With the average heat transfer coefficient defined as,

$$\bar{a}_\phi = \frac{1}{\pi} \int_0^\pi a(\phi) d\phi = \frac{q}{\sqrt{\Delta T_{\phi=0} \cdot \Delta T_{\phi=\pi}}} = \sqrt{a_{\phi=0} \cdot a_{\phi=\pi}}$$

then  $\bar{Nu}_\phi = \sqrt{(Nu_{\phi=0} Nu_{\phi=\pi})}$ . The model, ref. 1, -0.55

$$f = Nu_r = \frac{Nu}{Nu_b} = \psi^{-0.55} = (1 + \theta \Delta T)^{-0.55} = \left[ 1 - \left( \frac{\partial \ln \rho}{\partial T} \right)_p (T_w - T_b) \right]$$

where  $Nu_b$  is the McAdams equation, correlates 73-percent of the lower surface data to  $\pm 20$  percent, fig. 3a. Heat transfer at the lower surface is weakly dependent on thermogravitation.

For the upper surface, the relation  $Nu_r = f \cdot f_3$  was used where  $Gr_L$  is the limiting Grashof number

$$f_3 = (1 + 0.035 (Gr/Gr_L)^{0.43}) / (1 + (Gr/Gr_L)^3)^{0.048} ; Gr = \frac{99\theta^2 \rho D^4}{\lambda \eta^2}$$

$$Gr_L = 3 \times 10^{-5} Re^{2.75} [1 + 2.4 Re^{-0.125} (Pr^{2/3} - 1)] Pr^{1/2}$$

The data are correlated to  $\pm 30$  percent, fig. 3b, and the deterioration of heat transport seems to be related to the trend to suppress turbulent flow in the upper portion of the channel.

1. V.M. Yeroshenko, et al., "Measurements of Mixed Convective Heat Transfer to Low Temperature Helium in a Horizontal Channel", XV Int. Cong. of Refrigeration, Venice, 23-29 Sept. 1979., Paper B 1/120.

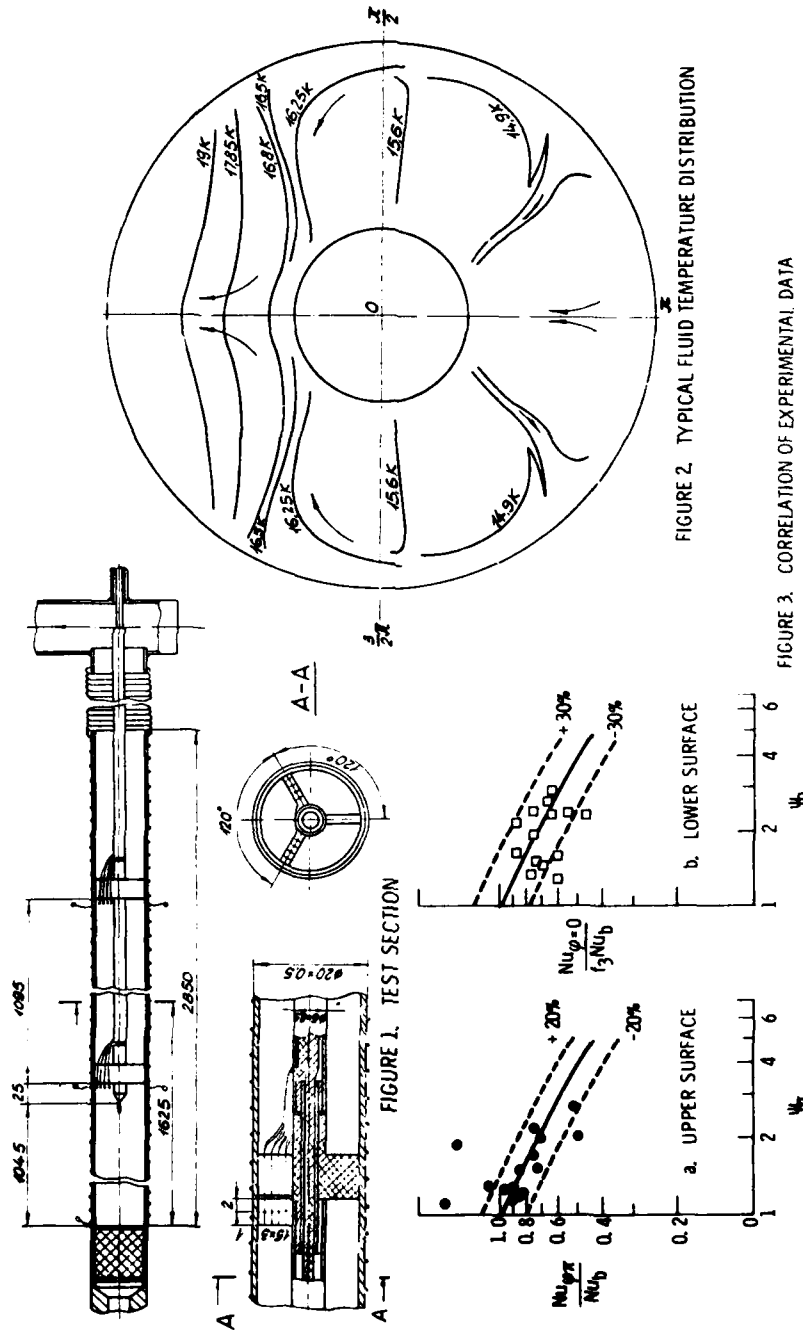


FIGURE 1. TEST SECTION

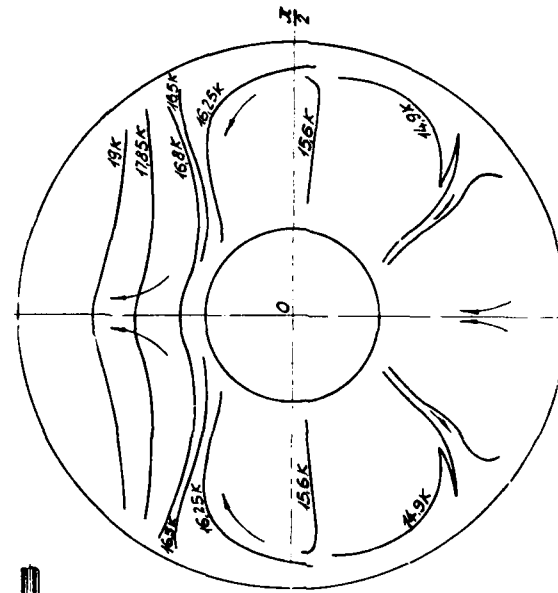


FIGURE 2. TYPICAL FLUID TEMPERATURE DISTRIBUTION

FIGURE 3. CORRELATION OF EXPERIMENTAL DATA

Convection Heat Transfer from a  
Rotating Isothermal Sphere

by  
Bakhtier Farouk and David N. Koert  
Mechanical Engineering and Mechanics  
Drexel University, Philadelphia, PA. 19104

ABSTRACT

Free convection heat transfer from stationary spheres has been the subject of several investigations [1-2]. In this paper, the flow generated by and the convection heat transfer from a rotating isothermal sphere have been investigated theoretically. The interaction of the buoyancy and centrifugal forces provides many interesting flow situations ranging from natural to forced convection. The distribution of the boundary-layer thickness, the extent of the inflow and outflow regions and the flow interaction at the equator are influenced also by the buoyancy and the centrifugal forces. The solutions are obtained considering the Boussinesq approximations and the full Navier-Stokes and energy equations. The governing equations are expressed in the  $(R, \theta, \phi)$  coordinates and due to the symmetry of the problem considered,  $\partial\gamma/\partial\phi = 0$ , where  $\gamma$  is any dependent variable considered. The  $R$  and  $\theta$  momentum equations are expressed in the stream function-vorticity formulation.

The stream function and vorticity are defined as:

$$V_R = \frac{1}{\rho} \frac{1}{R^2 \sin\theta} \frac{\partial\psi}{\partial\theta} \quad \omega = \frac{1}{R} \left[ \frac{\partial(RV_\theta)}{\partial R} - \frac{\partial V_R}{\partial\theta} \right]$$

$$V_\theta = -\frac{1}{\rho} \frac{1}{R \sin\theta} \frac{\partial\psi}{\partial R}$$

The governing equations for  $\psi$ ,  $\frac{\omega}{R \sin\theta}$ ,  $R \sin\theta V_\phi$  and  $T$  are expressed as follows:

$$-\frac{\partial}{\partial R} \left[ \frac{1}{\rho \sin\theta} \frac{\partial\psi}{\partial R} \right] - \frac{\partial}{\partial\theta} \left[ \frac{1}{\rho R^2 \sin\theta} \frac{\partial\psi}{\partial\theta} \right] = \frac{\omega R}{R \sin\theta} \cdot R \sin\theta \quad (1)$$

$$R^2 \sin^2\theta \left( \frac{\partial}{\partial R} \left( \frac{\omega}{R \sin\theta} \frac{\partial\psi}{\partial\theta} \right) - \frac{\partial}{\partial\theta} \left( \frac{\omega}{R \sin\theta} \frac{\partial\psi}{\partial R} \right) \right) - \frac{\partial}{\partial R} \left[ R^4 \sin^3\theta \frac{\partial \left( \frac{\omega}{R \sin\theta} \right)}{\partial R} \right]$$

$$- \frac{\partial}{\partial\theta} \left[ R^2 \sin^3\theta \frac{\partial \left( \frac{\omega}{R \sin\theta} \right)}{\partial\theta} \right] = \left( \cos\theta \frac{\partial}{\partial R} (\rho V_\phi) - \frac{\sin\theta}{R} \frac{\partial}{\partial\theta} (\rho V_\phi) \right)$$

$$R^2 \sin\theta + g\beta R^3 \sin\theta \left[ \frac{\cos\theta}{R} \frac{\partial T}{\partial\theta} + \sin\theta \frac{\partial T}{\partial R} \right] \quad (2)$$

$$\left( \frac{\partial}{\partial R} (R \sin \theta v_{\phi}) - \frac{\partial}{\partial \theta} (R \sin \theta v_{\theta}) - \frac{\partial}{\partial R} [R^2 \sin^3 \theta \frac{\partial}{\partial R} \left( \frac{v_{\phi}}{R \sin \theta} \right)] \right. \\ \left. - \frac{\partial}{\partial \theta} [R^2 \sin^3 \theta \frac{\partial}{\partial \theta} \left( \frac{v_{\theta}}{R \sin \theta} \right)] \right) = 0 \quad (3)$$

and the energy equation is given by

$$\left( \frac{\partial}{\partial R} (T \frac{\partial \psi}{\partial \theta}) - \frac{\partial}{\partial \theta} (T \frac{\partial \psi}{\partial R}) - \frac{\partial}{\partial R} \left[ \frac{\lambda}{C_p} R^2 \sin \theta \frac{\partial T}{\partial R} \right] - \frac{\partial}{\partial \theta} \left[ \frac{\lambda}{C_p} \sin \theta \frac{\partial T}{\partial \theta} \right] \right) = 0 \quad (4)$$

The resulting four coupled elliptic equations (for stream function, vorticity,  $v_{\phi}$  and temperature) are solved numerically. A spherical pseudo outer boundary is considered at a finite distance from the sphere center. Results have been obtained over a large range of Grashof number and Reynolds number based on the angular velocity of the sphere surface. The gravitationally induced free convection effects become negligible when the Grashof number is ten per cent or less than the square of the rotational Reynolds number. The results were compared with previously published experimental observations and theoretical predictions based on the boundary layer equations.

#### References

1. Farouk, B., "Natural Convection Heat Transfer from an Isothermal Sphere," Proceedings (In press), Sixteenth Southeastern Seminar on Thermal Sciences, Miami, Florida, April, 1982
2. Geola, F. and Cornish, A. R. H., "Numerical Solution of Steady State Free Convective Heat Transfer from a Solid Sphere," Int. J. Heat Mass Transfer, Vol. 24, 1369 - 1378 (1981).

MIXED CONVECTION IN NON-NEWTONIAN FLUIDS  
OVER BODIES OF REVOLUTION

By

James L.S. Chen

Department of Mechanical Engineering  
University of Pittsburgh  
Pittsburgh, PA 15261

During the past decades much work has been done on the study of combined free and forced convection heat transfer in Newtonian fluid flow over two-dimensional bodies such as a wedge or a cylinder. Attention is directed here to the problem of mixed convection in non-Newtonian fluids over vertical axisymmetric bodies. In analyzing such a problem, the natural first step is to seek its similarity solution, which constitutes the objective of this investigation.

At the outset of the study, it is recognized that the existence of similarity solutions for such a problem may be limited to certain cases. Nevertheless, the restricted solutions obtained herein may serve two important goals: (i) to provide valuable insight in understanding the physics of such heat transfer process in non-Newtonian fluids, and (ii) to provide a standard for comparison of non-similarity results obtained by approximate methods.

Consider a steady-state, incompressible, power-law non-Newtonian fluid flow past a vertical axisymmetric body of revolution. The free stream velocity and surface heat flux are assumed to vary according to the power laws of  $x^m$  and  $x^p$ , respectively, where  $x$  is the axial coordinate with the origin at the vertex of the body. It is found that similarity solution exists only when (i) the fluid is Newtonian:  $m$  is arbitrary but  $p=(5m-3)/2$ , or (ii) the fluid is non-Newtonian: the restriction being  $m=1/3$  and  $p=2/3$ .

Similarity velocity and temperature profiles as well as local skin-friction coefficient and Nusselt number are obtained for non-Newtonian and Newtonian flow past bodies of revolution with various sizes and shapes. The controlling parameter for the mixed mode of forced and free convection is found to be  $Gr/Re^2(=\gamma)$ , where  $Gr$  and  $Re$  are the generalized Grashof number and Reynolds number, respectively. Figure 1 shows the dimensionless temperature distribution of laminar Newtonian flow over a vertical needle-shaped body having a uniform surface heat flux distribution. At a given value of needle size  $a$  and of  $Pr$ , the surface temperature decreases with increasing free-convection effect or  $\gamma$ . The case of  $\gamma=0$  corresponds to that of pure forced-convection. The effects of  $Pr$  and needle size are also shown therein. As is expected, the thermal boundary-layer is thinner with higher  $Pr$  or reduced needle size. The dimensionless temperature profiles of non-Newtonian fluids over needles of two different sizes having a prescribed non-uniform wall heat-flux

are illustrated in Figure 2. For a given value of  $\gamma$  and of  $a$ , the pseudoplastic fluid ( $n=0.5$ ) yields lower surface temperature, and hence higher local Nusselt number as shown in Figure 3, than Newtonian ( $n=1.0$ ) and dilatant ( $n=1.5$ ) fluids. Figure 3 shows the effect of  $\gamma$  on local Nusselt number. For low values of  $\gamma$ , the forced-convection dominates. Due to limited space available herein, additional results and discussions will be presented at the Conference.

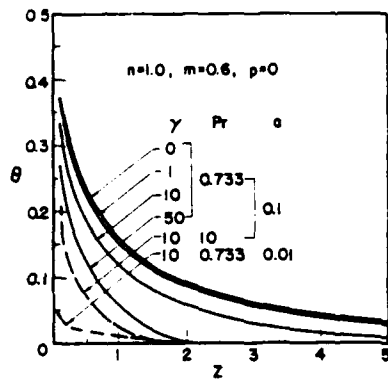


Fig. 1 Dimensionless temperature profiles in Newtonian Fluid

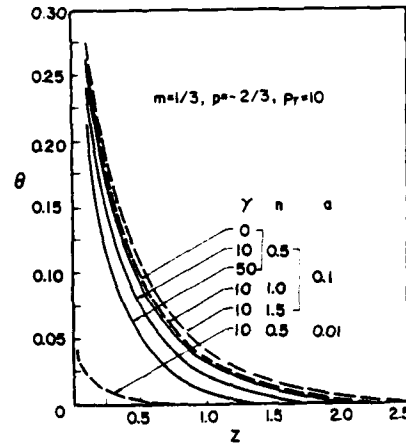


Fig. 2 Dimensionless temperature profiles in non-Newtonian Fluids

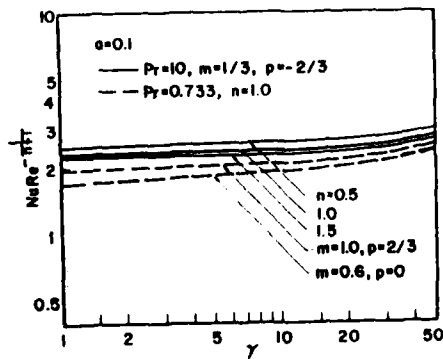


Fig. 3 Local Nusselt number for  $a=0.1$

HYDROMAGNETICS OF THE ELLIPTICAL  
POROUS SLIDER

by

P.D. Ariel and B.D. Aggarwala

Department of Mathematics and Statistics  
University of Calgary, Alberta, Canada

ABSTRACT

Recently considerable attention is being paid to porous thrust bearings because of their attractive performance. In these bearings the fluid is forced between the two surfaces moving relative to each other. If the injection velocity is large, Navier-Stokes equations govern the motion. Wang and his collaborators have considered the porous sliders of various shapes such as long rectangular, circular, elliptical. In the present paper investigation has been carried out to include the effects of magnetic field. Through the similarity transformation, Navier-Stokes' equations are reduced to the following system of ODE.

$$\begin{aligned}h''' - M^2 h' + A &= R[h'^2 - (h+k)h''] \\k''' - M^2 k' + \beta A &= R[k'^2 - (h+k)k''] \\f'' - M^2 f &= R[fh' - f'(h+k)] \\g'' - M^2 g &= R[gh' - g'(h+k)]\end{aligned}$$

with the boundary conditions

$$\begin{aligned}h(0) &= 0, h'(0) = 0, k(0) = 0, k'(0) = 0; \\h'(1) &= 0, k'(1) = 0, h(1) + k(1) = 1 \\f(0) &= 1, g(0) = 1, f(1) = 0, g(1) = 0.\end{aligned}$$

Here the functions  $h$  and  $k$  characterize the velocity normal to the slider and  $f$  and  $g$  determine the lateral components of the velocity.  $M$  denotes the Hartmann number,  $\beta$  is the measure of eccentricity and  $R$  is the cross-flow Reynolds' number.

The system of equations is solved for two cases: (i) for low Reynolds' number a perturbation solution is obtained; (ii) for arbitrary values of Reynolds' number numerical results are obtained using the technique of quasilinearization. The perturbation solution has an error of  $O(R^2)$ . A novel idea is presented to reduce the order of the system when quasilinearization technique is applied to obtain numerical solution.

The physical quantities of interest, namely, the lift and drag have been computed. The results are presented in the form of graphs. It is found that both lift and drag increase with  $R$  but with  $M$ , lift increases and the drag decreases. Thus the presence of magnetic field greatly enhances the performance of a slider.

On Some Extensions of a Nonlinear Stability Method  
as Applied in Reactor Dynamics

by

M. Podowski  
Department of Nuclear Engineering  
Rensselaer Polytechnic Institute  
Troy, New York 12181

It has been shown (1,2) that the nonlinear stability analysis for a class of integral-differential equations describing the dynamics of nuclear reactors can be successfully accomplished by using a method based on the concept of Liapunov functional.

The method uses the fact that physical reactor parameters, such as neutron flux or thermal power, are non-negative, and, in general, are related to the systems described by state variables bounded from below (e.g.,  $x(t) \geq -1$ , where  $x$  is the dimensionless incremental reactor power). Consequently, the allowable regions of initial functions, established in this way, are asymmetric. This, in turn, enables for considerable extensions of the method beyond the stability itself.

As discussed in this paper, some interesting characteristics of the system responses can be established and numerically evaluated. In particular, an estimate can be made for the magnitude of reactor responses as a function of that of the initial perturbations around a steady-state operating level. The upper bounds for the perturbed trajectories are usually different from the lower bounds.

Another extension of the method deals with its applications to nonautonomous reactor models subjected to external actions which do not terminate at any specific time. It has been shown, for instance, that the reactor peak power can be evaluated, following such effects as a sudden increase in coolant flow conditions, control rod withdrawal, etc.

Finally, it has been shown that the concept of Liapunov functional, applied in the stability analysis, can also be used to evaluate the "memory" of nonlinear reactor models, i.e., to find such a period of time,  $T$ , that the reactor responses are practically insensitive to the properties of initial functions for  $t < -T$ .

#### References

1. Podowski, M., "A Stability Criterion for Nonlinear Reactor Models with Linear Reactivity Feedback," Trans. Am. Nucl. Soc. 41, 1982, p 313.
2. Podowski, M., "Stability of Reactors with Nonlinear Reactivity Feedback," Trans. Am. Nucl. Soc. 43, 1982, p. 372.

SHAPE OPTIMAL DESIGN OF STRUCTURAL ELEMENTS  
WITH HEAT FLUX CONSTRAINTS

by

Y. W. Chun  
Department of Mechanical Engineering  
Villanova University  
Villanova, PA 19085

The problem of shape optimization of structural components with constraints on heat flux under steady-state temperature distribution is formulated and analyzed. Constraints are placed on heat flux due to thermal loading conditions encountered by the structural element. Minimum weight is taken as the design objective. Finite element method is used to obtain the temperature distribution at each stage of optimization process. The material derivative concept of continuum mechanics and the adjoint variable method are used to obtain design sensitivity of cost and constraints with respect to boundary movement. The boundary is parametrized and sensitivity results are used to obtain derivatives of constraints with respect to parameters defining the boundary. A nonlinear programming technique is then used to numerically construct optimal designs. Optimal design of a thermal diffuser is presented as a numerical example.

## MATHEMATICAL SIMULATION OF TEMPERATURES IN COLD REGIONS

by  
Sivajogi D. Koppula  
16403 - 102 Street  
Edmonton, Alberta, T5X 2G9, Canada

One of the prerequisites for understanding the geothermal process(es) in permafrost regions of the north American continent is the prior knowledge of thermal boundary condition(s) at the ground surface. The present study examines the time series of surface temperatures to estimate their future occurrences; and employs the exponentially weighted moving average (EWMA) method and the harmonic analysis. The success of these methods is well documented (Koppula, 1981).

The data consists of 444 monthly average minimum air temperatures measured at the Norman Wells airport in Northwest Territories (Environment Canada, 1981) for the period, January 1944 - December 1980. The first 384 observations are used in model(s) building; the predictive ability is tested by comparing the ex-post forecasts with the remaining 60 observations.

The EWMA method (Winters, 1960) attaches most weight to the most recent observation(s) and less weightage to preceding observation(s) by assigning exponentially declining weights. In period  $t$ , let  $M(t)$ =current mean of the temperature time series,  $L(t)$ ;  $S(t)$ =seasonal factor; and  $T(t)$ =trend. The starting values of  $M(t)$ ,  $S(t)$ , and  $T(t)$  are derived from the initial observations. The method makes a forecast; compares the forecasts with actual observations; absorbs the recorded data into the model; makes forecasts for the next period; and the cycle is repeated. A grid of values of smoothing constants  $\alpha$ ,  $\beta$ , and  $\gamma$  corresponding to  $M(t)$ ,  $S(t)$ , and  $T(t)$  is used to calculate the mean squared error (MSE),  $\sum (\text{actual-forecast})^2/60$ . The optimal set of constants yielding the minimum MSE for the data is:  $\alpha=0.$ ,  $\beta=0.54$ , and  $\gamma=1$ . The smoothing constant  $\gamma$  is very large revealing that the trend in the series changes abruptly;  $\beta$  is substantially large indicating frequent revision of the seasonal variation; and  $\alpha$  is zero suggesting that the original estimate of the current mean needs no revision. This set of  $(\alpha, \beta, \gamma)$  is used to estimate future temperature occurrences.

A time series, when trend is removed, exhibits a cyclical appearance, for which a sine-cosine curve may be fitted. This method is called harmonic analysis (Abel, 1962). Eq (1), fitted for the initial 384 observations, includes an intercept, a trend variable, and a seasonal cycle with a period of 12 months. Of the total variation in temperature fluctuations, 96% is explained by eq (1); this suggests that the

$$L(t) = -10.65 - 0.003t - 12.91 \sin(2\pi t/12) - 18.33 \cos(2\pi t/12) \quad (1)$$

F-stat            (4.1)    (3011)            (6073)             $R^2 = 96\%$

existence of other cycles, if any, of longer/shorter periods may be neglected for all practical purposes. Further the residuals, obtained by subtracting the harmonic fit from the actual observations, have been found to be 'white noise'. Consequently eq (1) is considered to be the

appropriate model for estimating future occurrences of temperature.

The forecasts made by the mathematical models together with the corresponding actual observations are shown in Fig 1; the forecasts agree very well with the recorded data. An objective evaluation of forecast performance is measured by the mean of forecast errors,  $\sum e/60$ , the mean of absolute errors  $\sum |e|/60$ , and the mean squared error  $\sum e^2/60$ ; in which  $e$ , error=(observed -forecast) temperature. Table 1 provides a comparison, and the EWMA estimates are clearly superior to those given by the harmonic analysis.

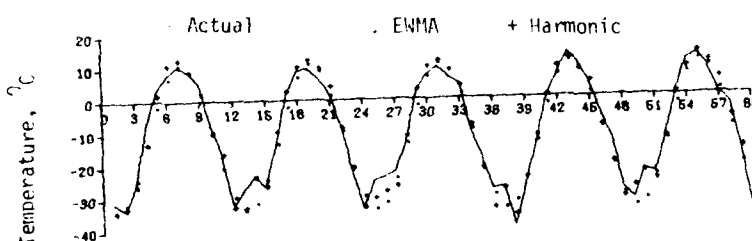


Fig 1. Temperature Forecasts - A Comparison

Table 1. Forecast(s) Evaluation

Method	$\sum e/60$	$\sum  e /60$	$\sum e^2/60$
EWMA	1.02	2.42	9.63
Harmonic	2.07	2.86	16.11

The study shows that both the mathematical models yield reasonably accurate ex-post estimates of the average monthly minimum temperatures. The EWMA method makes better forecasts; is relatively simple and has been found to be inexpensive.

Abel, M.E., "Harmonic Analysis of Seasonal Variation with an Application," J. American Statistical Association, 57, 1962, pp. 655-667.

Environment Canada., "Monthly Record of Meteorological Observations in Northern Canada," Atmospheric Environment Service, 1981.

Koppula, S.D., "Predicting Lake Levels by Exponential Smoothing," J. Hydraulics Division, Am. Soc. Civ. Engrs., 107, 1981, pp. 867-878.

Koppula, S.D., "Forecasting Engineering Costs: Two Case Studies," J. Construction Division, Am. Soc. Civ. Engrs., 107, 1981, pp. 733-743.

## THERMOPHYSICAL PROPERTIES OF ZEOTROPIC MIXED-REFRIGERANTS

by

Professor C. Wu  
Mechanical Engineering Department  
U.S. Naval Academy  
Annapolis, Maryland 21402

ABSTRACT

The mixture of two zeotropic (or non-azeotropic) refrigerants that might produce a better binary refrigerant has been investigated by both European and American chemists and engineers only recently since the energy crisis. It has been claimed that the coefficient of performance of such a mixed-refrigerants energy conversion cycle may be higher than that of a conventional single or azeotropic mixed-refrigerant cycle if the heat source and heat sink of the energy conversion system are not at constant temperatures. A key step for an engineer to understand the zeotropic mixed-refrigerants and to apply the working fluids to heat pumps, refrigerators and air conditionings is to know the thermophysical properties of the fluid. Unfortunately, thermodynamic tables, charts and figures for a zeotropic mixed-refrigerants have not been commercially available. The purpose of this paper is to obtain relationships among pressure, temperature, enthalpy, entropy, specific heat, specific volume, mass concentration and liquid quality for a zeotropic mixture in saturated liquid, saturated vapor, and superheated phases. The equations of state which describe the expressions among thermophysical properties are derived from fundamental physics, chemistry and thermodynamics knowledge. These equations are chosen for easy understanding, simplicity and permitting fast generation of the thermophysical data needed for a zeotropic mixed-refrigerants cycle analysis without sacrifice much of the accuracy.

SOME HEAT TRANSFER AND TEMPERATURE STRESS STUDIES ON A DIESEL ENGINE PISTON

V.P. Singh, N.K. Samaria and P.C. Upadhyay\*  
 Institute of Technology - Banaras Hindu University  
 Varanasi - 221005, INDIA

Heat transfer studies in the piston-cylinder group of an I.C. engine has gained importance because of its close effect on the engine performance. Heat-balance sheet of diesel engines show that the heat loss to the cylinder wall is quite significant as it varies as much as from 15 to 35 percent. Simultaneously, it is also realized that the temperature distribution in the various parts of an I.C. engine has to be controlled by proper cooling so that the temperature stresses do not become high and chances of excessive thermal deformations due to creep etc. are avoided. An engine designer is thus confronted with the problem of deciding upon the optimum conditions such that the engine does not loose an excessive heat to the cooling media as well as the engine parts are not subjected to high temperature stresses and deformations. This can best be done by obtaining maximum possible experimental and theoretical results of heat transfer studies on different kinds of I.C. engines (different shapes of piston geometry and different combinations of boundary conditions).

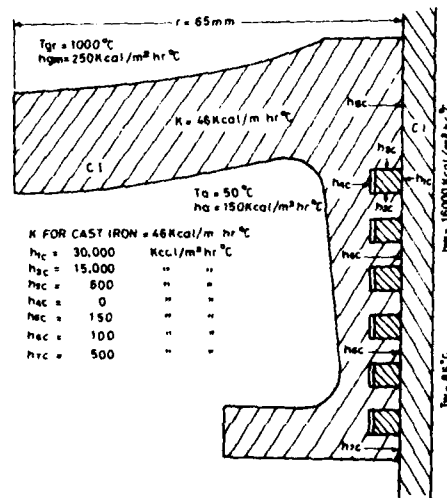


FIG 1 - BOUNDARY CONDITION OF A CAST IRON IC ENGINE PISTON

\*Visiting Asst. Professor, Dept. of Engr. Mech., Univ. of Missouri-Rolla, Rolla, MO 65401.

With this objective, different kinds of heat transfer studies on I.C. engine pistons have been going on, each stressing on some particular aspects of the problem. As a contribution towards the same goal, this paper is concerned with the heat transfer studies on a cast-iron diesel engine piston of 130mm diameter as shown in Fig. 1. Electrical analogy method (network shown in Fig.2) has been used for establishing the steady state temperature field in the piston body. Percentage heat transfer to different cooling sources (crank case, cooling media and piston rings) has been calculated for different load conditions of, both, water-cooled and the air-cooled engines. Load variation on the engine is accounted by changing the hot gas temperature above the piston top from 400°C to 1000°C. Radial thermal stress variation has also been estimated and presented as a function of hot gas temperature inside the engine. Apart from discussing the effect of temperature of cooling water and gas etc., some interesting results concerning the heat loss through the piston rings have been reported and discussed in the paper.

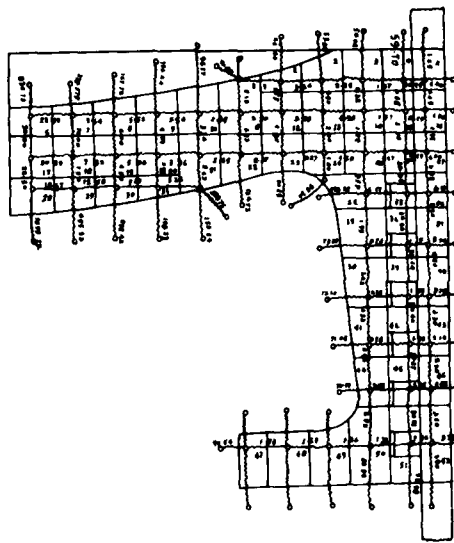


FIG. 2

EQUIVALENT RESISTANCES FOR ELECTRICAL ANALOG

A PERTURBATION METHOD FOR SELF-COUPLED  
COMBUSTION-INSTABILITY PROBLEMS

by

Asghar Googerdy and John Peddieson Jr.  
Department of Mechanical Engineering  
Tennessee Technological University  
Cookeville, Tennessee 38505

The model partial-differential equation

$$\partial_t^2 \phi - \nabla^2 \phi + \epsilon (\bar{\sigma} ((1-n) \partial_t \phi + n \partial_{t\tau} \phi) + 2z \partial_z \partial_t \phi) + 2 \bar{\nabla} \phi \cdot \bar{\nabla} \partial_t \phi = 0 \quad (1)$$

arises in a simplified analysis of pressure-sensitive combustion instability in liquid-fuel rocket motors. In (1) all quantities are dimensionless with  $z$  denoting the mean-flow direction,  $t$  time,  $\phi$  a velocity potential,  $\bar{\sigma}$  a measure of the mean burning rate,  $n$  a measure of the unsteady burning rate,  $\epsilon$  a measure of the initial disturbance,  $\tau$  a measure of the importance of the history of unsteady combustion and  $\bar{\nabla}$  the gradient operator. A subscript  $\tau$  indicates that  $t$  is replaced by  $t-\tau$  in the argument of the corresponding quantity. Several investigators have obtained approximate solutions to equations similar to (1) by performing an approximate modal analysis using the Galerkin method and then solving the resulting system of ordinary differential equations by the two-variable perturbation method (method of multiple scales) or, equivalently, by the method of averaging.

A single-mode Galerkin analysis of symmetric transverse instability in a rectangular chamber (the simplest model problem exhibiting so-called self coupling) leads to the ordinary differential equation

$$f'' + f + \epsilon (\bar{\sigma} ((1-n)f' + nf'_\tau) + 8ff'/(3\pi)) = 0 \quad (2)$$

where  $f=f(t)$  and a prime denotes differentiation. A straightforward application of the two-variable perturbation method with  $\epsilon$  as perturbation parameter does not predict the full range of behavior exhibited by numerical solutions of (2). The present work presents a method based on rewriting (2) as

$$f'' + f + \delta ff' + \epsilon \bar{\sigma} ((1-n)f' + nf'_\tau) = 0; \quad \delta = 8\epsilon/(3\pi) \quad (3)$$

and carrying out a two-parameter perturbation analysis in  $\epsilon$  and  $\delta$  (or equivalently  $\epsilon$  and  $\epsilon\bar{\sigma}$ ) using the two-variable method for the  $\epsilon$  perturbation and the strained-coordinate method for the  $\delta$  perturbation. It is shown that this method is capable of predicting all the features of previous numerical solutions and is useful in explaining them. The neutral-stability condition can be found in closed form as

$$n = 1/(1 - \cos((1 - 8\epsilon^2/(27\pi^2))\tau)) \quad (4)$$

## Numerical Solution of Compressible Network Flow Problems

by

T.A. Porsching  
Department of Mathematics and Statistics  
University of Pittsburgh  
Pittsburgh, PA 15261

Compressible network flow problems occur in the safety analysis of nuclear power plants. The underlying physical system is idealized as a collection of  $N$  nodes and  $L$  interconnecting links. Laws governing the conservation of mass and momentum of the flowing medium apply respectively on the nodes and links of the network. For compressible flows an equation of state is also required.

In the case of transient problems, this process leads to a system of  $L+N$  ordinary differential equations. Since some of the time constants in this system are of the order of the acoustic transport times between nodes, economical numerical integration of the system necessitates the use of implicit methods. These in turn produce non-trivial systems of algebraic equations to be solved at each time level.

In this talk we describe a consistent system of implicit network difference equations. We then derive an equivalent system involving  $N$  fewer unknowns than the original, and discuss some algorithmic considerations concerning the reduced system's solution.

Finite Element Algorithms for Incompressible  
Viscous Flows in Exterior Domains

by

M.D. Gunzburger  
Department of Mathematics  
Carnegie-Mellon University  
Pittsburgh, PA 15213

The numerical approximation of the flow of a viscous fluid around a bounded obstacle must deal with the infinite extent of the flow region. We discuss two classes of algorithms for such problems, both of which use a finite element discretization of the governing equations in a truncated, finite region. The two algorithms differ in their treatment of numerical boundary conditions which are imposed on the boundary of the truncated domain.

The first method couples the finite element solution in the truncated domain with an integral equation solution in the exterior of the truncated domain, i.e., a coupled finite element-boundary integral technique. In this case we are essentially imposing an exact boundary condition at the edge of the truncated domain. However, this boundary treatment is non-local and requires the introduction of additional variables defined on the boundary.

The second method replaces the exact non-local boundary condition on the artificial computational boundary by approximate local boundary conditions. We discuss three choices for the approximate boundary conditions. The accuracy and computational complexity associated with each choice is discussed. The three boundary treatments are essentially a Dirichlet, Neumann, and a mixed boundary condition. Their accuracy may be determined through the knowledge of the asymptotic behavior of the flow field.

The above algorithms have been analyzed for the case of the linear Stokes equations. A particular feature of the analysis is the use of weighted Sobolev spaces. Optimal error estimates are derived. Algorithmic issues for the non-linear Navier-Stokes equations are also addressed.

Mathematical Modeling of Chemically Reacting  
Flows in Automotive Converters

by

James C. Cavendish  
Mathematics Department  
General Motors Research Laboratories  
Warren, Michigan 48090-9055

Packed-bed chemical reactors are used in automobiles for the catalytic oxidation of engine exhaust emissions. Called catalytic converters, these reactors are located underneath the car and contain from 250,000 to 500,000 small porous pellets, each impregnated with a thin noble metal shell. Shown in Figure 1 is a cross section of a typical packed-bed automotive converter.

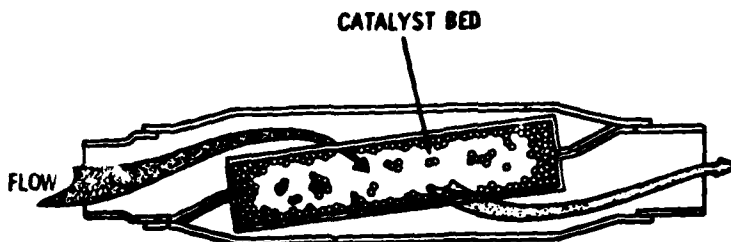


FIG. 1 SCHEMATIC OF CATALYTIC CONVERTER

The transient conversion performance of catalytic converters is highly sensitive to the flow and temperature fields existing within the bed at any given time. Flow nonuniformities (so-called flow maldistribution) existing within the converter can be caused by, for example, non-uniform flow distribution to the inlet of the bed or by the presence of a nonuniform spatial flow resistance caused by nonuniform pellet size or void fraction within the bed. Strong local variations in velocity fields in the bed can lead to the formation of "hot spots" and temperature excursions which in turn have a marked effect on the performance of the system.

In this presentation, we discuss how fluid dynamics, heat and mass transport, chemical kinetics and numerical analysis are blended together in the formulation and solution of a mathematical model of chemically reacting flows in catalytic converters. Some of the numerical complexities associated with the solution of the model equations will be addressed. Computed solutions to the model equations indicate that nonuniform flow fields produce considerable distortion in the velocity, temperature and concentration contours throughout the entire packed-bed.

- [1] G. F. Robertson and J. C. Cavendish, "The Effect of Flow Maldistribution on the Thermal Response of Packed-Bed Converters and Thermal-Energy Storage Units," Proceedings of the 20th Joint ASME/AIChE National Heat Transfer Conference, Milwaukee, Wisconsin, ASME publication 81-HT-59, (April, 1981).

A Semi-Implicit Numerical Method for the Solution of  
Single-Phase and Two-Phase Flow Equations

by

Andrei L. Schor and Neil E. Todreas  
Department of Nuclear Engineering  
Massachusetts Institute of Technology  
Cambridge, Massachusetts 02139

A recent numerical method for the solution of fluid dynamics equations will be presented. The method is being increasingly used in nuclear systems analysis, proving itself robust and computationally efficient.

The basic approach is a semi-implicit scheme which has been found to be near-optimum for a wide range of applications with respect to the total computing effort, when considering the entire spectrum of possible schemes, from the fully explicit to the fully implicit ones. While the cheapest per time step, a fully explicit scheme would require very short time steps in most transients of interest and thus lead to an impractically large total computing effort. At the opposite end of the spectrum, a fully implicit scheme would in principle offer unconditional stability, its only time step restriction being dictated by accuracy requirements. For the partial differential equations associated with single-phase and especially two-phase flows, a fully implicit scheme, especially in three dimensions, would generate a very large and complicated system of highly nonlinear equations, whose solution would generally be quite difficult and expensive. It is worth mentioning a somewhat subtler point related to the nonlinear character of the equations. To start a nonlinear iteration, a guess must be provided. In a time-dependent problem, a natural choice for such a guess for the new time solution is obviously the old time solution. Now for a nonlinear iterative process, the better the initial guess, the faster the convergence to the solution will be. In fact, in some circumstances, convergence can be guaranteed only if the guess is "close enough" to the solution. Obviously, the shorter the time step, the closer the guess is to the solution, assuming a continuous dependence on time. Thus a large time step may lead to slow convergence or even divergence.

Clearly an optimum scheme would allow acceptable time steps (on the scale of the transients under consideration) and would not lead to a prohibitively complex (and possibly unreliable) and expensive algorithm. Thus it is important to realize that the phenomena described by the governing partial differential equations are associated with different time scales. In the method being described, pressure pulse propagation and local effects (such as interphase exchanges, wall-fluid interaction) are treated implicitly, given the short time constants associated with these phenomena. In contrast, the convection and diffusion are characterized by longer time constants and are treated explicitly. This choice of implicit/explicit treatments leads to a method which remains tractable and efficient in multidimensional

applications.

The temporal and spatial discretization process generates a set of nonlinear equations, solved by Newton's method, in its regular form or in one of its modified versions, the secant and the parallel-chord methods, which sometimes become computationally advantageous. When only one Newton iteration is performed, the scheme becomes equivalent to a linearization about the old time, a procedure which has been and still is widely used in numerical fluid dynamics. In this implementation, the mass and energy residuals are monitored and kept adequately small through an automatic time step adjustment.

The particular discretization and linearization scheme chosen provides local reducibility, allowing the elimination of all new time quantities in favor of new time pressures. It can be shown [1] that the matrix of the system of equations for pressures possesses favorable properties with regard to iterative or direct solutions.

The application of this method to an equal temperature/unequal velocity two-phase flow model will be presented and our results and experience will be discussed.

#### Reference

1. A. L. Schor and N. F. Todreas, "A Four-Equation Two-Phase Flow Model for Sodium Boiling Simulation of LMFBR Fuel Assemblies", MIT Energy Laboratory Report No. MIT-EL-82-039, December 1982.

## NUMERICAL MODELING OF SOME COMPLEX TURBULENT FLOWFIELDS

L. Krishnamurthy  
Senior Research Engineer  
Fluid Mechanics Group  
University of Dayton Research Institute  
Dayton, Ohio 45469

This presentation deals with numerical prediction of certain turbulent flows that may be termed complex. No doubt such a characterization is subjective and is necessarily governed by continuing advances in computer capability on the one hand and improvements in physical and numerical models on the other. Nevertheless, it is instructive to define, after Bradshaw, that a complex turbulent flowfield is one which cannot be predicted with acceptable accuracy by methods that have been successfully developed in classical thin shear layers. Examples of the latter include both the free-shear flows occurring in jets and wakes and the wall-shear flows occurring in boundary layers and ducted flows. A large class of turbulent flows of engineering and environmental importance, however, does not come under this category of simple shear flows. Instead, the more realistic flowfields are often characterized by a number of features that invalidate the assumptions inherent in the thin-shear-layer approximation. Some of these features, as noted by Bradshaw, involve interacting shear layers or extra rates of strain. In view of their practical importance, complex turbulent flowfields have been the subject of a number of experimental and numerical investigations. The purpose of this presentation, however, is not to embark upon a comprehensive review of the recent literature in this area. Instead, it is a more limited one of presenting the results of the ongoing numerical modeling research at the University of Dayton on an extremely complex flowfield investigated by the author and his associates.

Numerical calculations have been in progress to predict the recirculating turbulent flowfields under isothermal conditions in an axisymmetric combustor, hereafter referred to as the centerbody combustor configuration (CBCC). The CBCC represents confined dual coaxial jet mixing in the near-wake region downstream of a cylindrical bluff body. A full-scale CBCC has been in operation at the Aero Propulsion Laboratory (APL) and a 1/5-scale model of the APL CBCC is in operation at the Combustion Laboratory of the

---

\*Sponsored by Air Force Wright Aeronautical Laboratories, Aero Propulsion Laboratory, Wright-Patterson Air Force Base, Ohio under Contracts No. F33615-78-C-2005 and No. F33615-82-K-2252. Dr. W. M. Roquemore is the Technical Monitor.

University of California, Irvine (UCI). The APL CBCC consists of a 25.4 cm diameter outer duct, 14 cm diameter centerbody and 0.48 cm diameter central jet. The ratio of the centerbody diameter to the central jet diameter is 29. Thus, the present interjet separation is much larger than that encountered in typical coaxial jet mixing studies of both confined and unconfined flowfields in the literature. This wide a separation between the jets and the concomitant presence of the toroidal recirculating bluff-body wake in the mixing region have given rise to some interesting flowfield ramifications addressed only recently in numerical modeling. For example, the CBCC flowfield exhibits wake-like and jet-like characteristics, depending upon the strength of the two jets. The juxtaposition of the annular and central jets with the near-wake region in a confined configuration renders the CBCC flowfield an extremely complex one. In addition to the interacting shear layers, large streamline curvature is also present. Furthermore, the bluff-body vortex shedding imparts a dynamic character to the turbulent mixing in CBCC. Consequently, our numerical modeling research has been examining several of these aspects.

The numerical modeling involves finite-difference computational procedures and addresses both the time-averaged and time-dependent flowfields. The time-averaged CBCC flowfield behavior is investigated by the solution of the Reynolds-averaged Navier-Stokes equations. The formulation entails an elliptic system of equations for properly describing the recirculating flowfields. The numerical calculations employ the standard features of TEACH-type numerics as well as additional refinements in both the numerical and physical aspects. The dynamic features of the CBCC flowfield are investigated by the solution of the time-dependent, compressible Navier-Stokes equations. These calculations involve MacCormack's explicit scheme and present numerical experiments have considered the CBCC flowfield due to the annular jet only. The incorporation of a mixing-length type turbulence model and the introduction of the central jet (with air as well as CO<sub>2</sub> as the central-jet fluid) will be investigated subsequently.

Numerical investigations have demonstrated the complex character of the CBCC flowfields. Nevertheless, the mean axial velocity field appears to exhibit certain similarity behavior observed in simple shear flows. The turbulence structure, however, is significantly influenced by a number of factors such as shear-layer interaction and streamline curvature. The predicted time-averaged results are found to be sensitive to several physical and numerical model parameters. Preliminary results of the time-dependent flowfields emphasize that the dynamic features relating to the vortex shedding could be significant in the CBCC flowfields.

NM-1

HIGH REYNOLDS NUMBER SOLUTIONS FOR INCOMPRESSIBLE VISCOUS  
FLOW USING THE REDUCED BASIS TECHNIQUE

by

Janet S. Peterson  
Department of Mathematics and Statistics  
University of Pittsburgh  
Pittsburgh, PA 15261

The reduced basis technique is a reduction method which is based in the setting of a standard continuation method for nonlinear problems. The essence of the reduced basis technique is the selection of an approximating subspace which has properties which are intrinsic to the solution segment under consideration. Its effectiveness for solving nonlinear structural mechanics problems has been pioneered by A. Noor.<sup>1</sup> Recent work by Fink and Rheinboldt<sup>2</sup> has provided a theoretical foundation for the method for a general class of nonlinear problems. In this talk, standard finite element techniques are combined with the reduced basis method to obtain high Reynolds number solutions for incompressible viscous flows. In particular, the method is applied to the incompressible Navier-Stokes equations written in streamfunction formulation. Numerical results for the model problem of a driven flow in a square cavity are presented and compared with results from other numerical treatments of the driven cavity problem.

---

<sup>1</sup> Noor, A. K. and J. M. Peters, "Recent Advances in Reduction Methods for Instability Analysis of Structures", Computers and Structures, 16, 1983, 1.

<sup>2</sup> Fink, J. and W. C. Rheinboldt, "On the Error Behavior of the Reduced Basis Technique for Nonlinear Finite Element Approximation", Tech. Report ICMA-82-37, University of Pittsburgh, 1982.

FINITE ELEMENT METHODS FOR BOUNDARY INTEGRAL  
EQUATIONS ARISING IN ELASTICITY AND FLUID MECHANICS

by

George C. Hsiao  
Department of Mathematical Sciences  
University of Delaware  
Newark, Delaware 19711, U.S.A.

The boundary integral equation method for numerical solutions to elliptic boundary value problems has received much attention and gained wide acceptance in recent years. As is well known, the method is particularly suitable for obtaining numerical solutions of exterior boundary value problems and implies an approximate technique by which the problem dimensions are reduced by one. The latter leads to an appreciable reduction in the number of algebraic equations generated for solutions, as well as much simplified data preparation. It is a method which is better than most and worthy of study.

Irrespective of the particular numerical implementation chosen, central to the method is the reduction of boundary value problems to equivalent boundary integral equations over the boundary of the domain for the problems under consideration. This reduction is by no means unique. In the conventional approach, Fredholm integral equations of the second kind are generally obtained either by using the "direct method" or by using the "method of potentials" in which case solutions are expressed in terms of double layer potentials. However, as indicated by Fichera, and Hsiao and MacCamy [1], a large class of two-dimensional elliptic boundary value problems in elasticity and fluid mechanics can also be expressed in terms of simple layer potentials. This leads to systems of boundary integral equations of the first kind with logarithmic kernels as principal part.

This lecture gives a survey of some recent results [2] in the use of finite element methods for such a class of integral equations. Error estimates, stability analysis as well as numerical implementations of the method are discussed. Some numerical experience for the problem of slow viscous flow past an obstacle are included to indicate how the method operated in specific situations.

- 
- [1] Hsiao, G. C. and MacCamy, R. C., "Solution of Boundary Value Problems by Integral Equations of the First Kind", *SIAM Rev.*, 15, 1973, pp. 678-705.
  - [2] Hsiao, G. C., Kopp, P. and Wendland, W. L., "Some Applications of a Galerkin-Collocation Method for Integral Equations of the First Kind (to appear).

A Boundary Integral Technique For Some Laminar  
Forced Convection Problems

by

A. M. Sadegh  
Department of Mechanical Engineering  
The City College of The City University of New York  
New York, N.Y. 10031

and

K. R. Rajagopal  
Department of Mechanical Engineering  
University of Pittsburgh  
Pittsburgh, PA 15261

The equations governing the velocity and the temperature field in the case of steady laminar forced convection problems for the fully developed flow in a cylinder of arbitrary cross-section can be reduced to a biharmonic equation (cf. Tao [1])

$$\begin{aligned}\Delta^4 f &= 0 && \text{in } \Omega \\ f &= \frac{C}{64}(x^2 + y^2)^2 && \text{on } \partial\Omega \\ \Delta^2 f &= \frac{-C}{64}(x^2 + y^2)\end{aligned}$$

In the above equation  $f$  is a function defined in terms of the velocity and temperature. While exact solutions can be obtained for the above problem for specific simple cross-sections one has to resort to a numerical solution in the case of arbitrary cross-sections. A boundary integral method, which is ideally suited for the problem on hand, is devised for cylinders of arbitrary cross-sections. A comparison is made with available exact solutions.

- [1] L.N. Tao, On some laminar forced-convection problems, Paper No. 60-Wa-188, Winter Annual meeting of the ASME Nov. - Dec., (1960).

AN ALGORITHM FOR THE SOLUTION OF A THREE DIMENSIONAL  
STOKES FLOW IN BIPOLAR COORDINATES

Aydeniz Siginer  
Department of Engineering Mechanics  
The University of Alabama  
Post Office Box 2908  
University, Alabama 35486 U.S.A.

This paper presents a numerical algorithm for a three dimensional, top driven Stokes flow which arises when solving the problem of the free surface flow of a Newtonian or a non-Newtonian fluid between eccentric cylinders undergoing steady differential rotation. Eccentricity gives rise to secondary motions which are mathematically modeled by the top driven Stokes flow. Recently Siginer [1] used the theory of domain perturbations which involves simultaneous perturbation of the non-linear field equations and the physical flow domain  $\mathcal{V}_\Omega$  to solve the problem of the flow between eccentric cylinders. At second order the linearized equations yield two subproblems [1], one of which is a top driven, three dimensional Stokes flow in the transformed domain  $\mathcal{V}_0$  with a flat top. The boundary conditions on top and on the side walls are respectively of mixed and Dirichlet type. The problem is solved using a three dimensional lattice of finite differences with unequal spacings in bipolar coordinates. The algorithm results from the implementation of a traverse method with a relaxation factor.

When the flow and the domain are perturbed simultaneously one of the linearized problems at second order becomes:

$$\Delta U^{<2>} = \nabla \phi^{<2>}, \quad \nabla \cdot U^{<2>} = 0 \quad \text{in } \mathcal{V}_0, \quad (1a)$$

$$\mathcal{V}_0 = \{(\xi, \eta, z) \mid \xi_1 \leq \xi \leq \xi_2, 0 < \eta < 2\pi, -\infty < z \leq 0\}$$

$$U^{<2>}(\xi_i, \eta, z) = 0 \quad i = 1, 2; \quad U^{<2>}(\cdot, \cdot, 0) = (u^{<2>}, v^{<2>}, w^{<2>}), \quad (1b)$$

$$u, z^{<2>} \Big|_{z=0} = r_1(\xi, \eta), \quad v, z^{<2>} \Big|_{z=0} = r_2(\xi, \eta), \quad w, z^{<2>} \Big|_{z=0} = r_3(\xi, \eta). \quad (1c)$$

Using conservation of mass the field equations (1a) may be rewritten

$$\Delta U^{<2>} = \nabla \phi^{<2>}, \quad \Delta \phi^{<2>} = 0 \quad \text{in } \mathcal{V}_0. \quad (2)$$

With second order truncation error throughout and the inclusion of a relaxation parameter  $\alpha$  every discretized equation corresponding to (2) may be expressed as

$$\left[1 + \frac{(1-\alpha)}{\alpha}\right] a_p T_p = a_{nb} T_{nb} + \frac{(1-\alpha)}{\alpha} a_p T_p^* + t, \quad (3)$$

where  $P = (i, j, k), T = (u^{<2>}, v^{<2>}, w^{<2>}, \phi^{<2>})$  and  $(nb)$  denotes a neighbor point.  $T_p^*$  is the previously calculated value of  $T$  at  $P = (i, j, k)$ . The optimum value of  $\alpha$  has to be found through numerical experimentation. Upon noting that all the dependent variables in (2) and (1c) are even in

$\eta$  except  $v^{<2>}$ , we take as the domain of the finite difference solution

$$P = \{ \xi, \eta, z \mid \xi_1 \leq \xi \leq \xi_2, 0 \leq \eta \leq \pi, Z \leq z \leq 0 \}$$

where  $Z$  is determined through exploratory computations such that the pressure or the velocity field at or near  $z=0$  is not affected further by a change in the depth of flow field. A line by line iteration method is used. The traverse direction is taken as the direction in which the coefficients of the discretized equations are much larger than the other directions. First we take the  $\xi$  direction as the traverse and the increasing  $\eta$  as the sweep direction on horizontal planes  $z = \text{constant}$ . On the same plane  $z = \text{constant}$  we solve successively for  $u^{<2>}, v^{<2>}, w^{<2>}$  using the improved values at each step. Then we sweep through all the planes  $z = \text{constant}$ . Next we take the  $z$  direction as the traverse and  $\xi$  as the sweep directions on vertical planes  $\eta = \text{constant}$  and solve again successively for  $u^{<2>}, v^{<2>}, w^{<2>}$ . Then we sweep through all the planes  $\eta = \text{constant}$  before we solve for  $\phi^{<2>}$  which corresponds to the updated velocity field.  $\phi^{<2>}$  is solved for on planes  $z = \text{constant}$  first and then on planes  $\eta = \text{constant}$ . The iteration terminates when the relative error of  $\phi^{<2>}|_{z=0}$  is smaller than a preset value. The boundary values for the solution of  $\phi^{<2>}$  at each step are obtained from the first of (2). We note that when iterations converge  $T_p = T_p^*$ . We use this fact to check the rate of convergence after each iteration during the process. The absolute sum of the residues computed by substituting  $T_p^*$  into (2) should tend to zero for a converging process. We found that the optimum convergence speed is reached if the same  $\alpha$  is used in all the discretized equations. We also found that the optimum value of  $\alpha$  has to be determined with the full grid size in mind. The boundary conditions for  $\phi^{<2>}$  depend on  $w_{,ZZ}^{<2>}(\xi, \eta, 0)$  which increases without bounds in the discretized form of the equations as the grid spacing in the  $z$  direction is made finer. Thus the pressure field will not be unique if the discontinuity is not removed. We use the second field equation in (1a) together with (1c) to remove the discontinuity.

Once the optimum  $\alpha$  has been determined for a given geometry and grid size, convergence is quite rapid. It is shown that secondary flows due to eccentricity are generated by this top driven flow. Further details are reported in [1] and [2].

#### References

- [1] Siginer, A., Free surface on a Simple Fluid Between Rotating Eccentric Cylinders, Part I: Analytical Solution, to appear, JNNFM.
- [2] Siginer, A., A Numerical Solution for Secondary Flows in the Free Surface Flow Between Eccentric Cylinders, to appear, International Journal for Numerical Methods in Fluids.

Some Studies in Stress-Based Methods  
in Nonlinear Mechanics

by

C-T. Yang\*, K. W. Reed\*\*, and S. N. Atluri\*\*\*  
Center for the Advancement of Computational Mechanics  
School of Civil Engineering  
Georgia Institute of Technology, Atlanta, GA 30332

In this talk, computational methods based on assumed stress fields, and considerations of complementary energy, are discussed in the following two areas: (i) unsteady, incompressible fluid flow at high Reynolds numbers and (ii) large quasi-static deformations of inelastic solids. In both cases, the computational methods are of the mixed/hybrid finite element type. Comments are made concerning the relative advantages of these methods over the currently popular methods, such as assumed velocity-penalty-function approaches, etc.

\* Doctoral Candidate

\*\* Presently a Fellow, Alexander von Humboldt Foundation

\*\*\* Regents' Professor of Mechanics

## ON A UNIFIED THEORETICAL VIEWPOINT IN COMPUTATIONAL FLUID MECHANICS

A. J. Baker  
Department of Engineering Science and Mechanics  
University of Tennessee, Knoxville, TN 37996

The past two decades have witnessed a rapidly expanded interest in characterization of multi-dimensional flows. This has fostered formulation and use of numerical algorithm constructions for the governing non-linear partial differential equation system. The theoretical basis for construction of algorithms is quite varied, and examples include approximate factorization (AF) finite difference [ 1,2 ] consistently-split, linearized block implicit (LBI) finite difference [ 3 ], finite element (FE) tensor product [ 4 ], and an implicit MacCormack - type algorithm [ 5 ]. In every instance, a non-physical, "artificial viscosity" term is required appended, either "implicitly or explicitly" to the matrix algebra solution statement, to promote convergence. The order of the "artificial viscosity" in this term is nominally  $O(10^{-3})$ , while the level of physical viscosity is  $O(R_e^{-1})$ . The requirement for an artificial dissipation mechanism for non-linear hyperbolic conservation law systems, eg., the inviscid (Euler) form of the Navier-Stokes equations, is well verified [ 6 ], so the problem is really one of degree.

The focus of this paper is to identify the basic theoretical aspects of algorithm construction, and in the process to firmly state the decisions that are required made by the designer. The Table summarizes the five essential categories of construction. Denoting the representative partial differential equation of the Navier-Stokes set as  $L(q(x,t))$ , the first and most obvious requirement is that an approximation must be specified. The options available include (at least) finite element, finite difference, and/or finite volume concepts. Since the approximation cannot be the exact solution, a formal statement is required specified as to what constraints (if any) are placed on the resulting semi-discrete approximation error.

TABLE

Basic Requirements For CFD Algorithm Constructions

Algorithm Category	Options (Among Others)
1. Approximation	Finite Element (FE) Finite Difference (FD) Finite Volume (FV)
2. Semi-Discrete Approximation Error	Orthogonality (FE) Taylor Series (FD, FV)
3. Dispersion Error	Modified Orthogonality (FE) Artificial Diffusion (FD, FV)
4. Truncation Error	Implicit/Explicit (ALL)
5. Matrix Solution Jacobian	Tensor Matrix Products (FE) Approximate Factorization (FD)

The FD and FV constructions differ from FE concepts, in these two specific regards, in that categories 1 and 2 are grouped together in replacing  $L(q(x,t))$  with difference quotients yielding  $L(Q(\Delta x_j, \Delta t)) \equiv 0$ . In the FE construction of category 1, the approximation is made to the solution  $q(x,t)$  rather than  $L(q(x,t))$ . A vast reservoir exists from which one can select particular members that endow the solution approximation  $q^h(x,t)$  with specific properties, eg., completeness.

Then,  $L(q^h(x,t)) \neq 0$  is the semi-discrete approximation error embedded into the governing differential equation. The category 2 specification simply requires this error to be orthogonal to the function space used to construct  $q^h$ . Calculus and vector field operations permit an exact evaluation of this constraint statement yielding a matrix statement.

For a viscous-dominated (small Reynolds number) flow, the category 3 issue of dispersion error need not be addressed. However, for flows characterized by a large Reynolds number, the equation set is dominantly hyperbolic and non-linear. The resultant principal error mechanism is dispersion error, the tendency of the Fourier components constituting information packets to possess distinct phase velocities differing from the group velocity. The Navier-Stokes non-linearity aggravates this character, and the algorithm requirement is to control (diffuse) this error, and the standard FD(FV) practice is to explicitly add a diffusion term, multiplied by a coefficient of "artificial viscosity," to the governing equation  $L(q(x,t))$ . Alternatively one FE choice recognizes that the semi-discrete approximation error  $L(q^h(x,t))$  will be highly non-smooth in regions where dispersion error is excessive. Interpreting  $L(q^h(x,t))$  as a hyper-surface, regions of large error are characterized by large changes in amplitude, hence direction of the normal. Noting that  $\nabla L(q^h(x,t))$  exhibits measures of both these phenomenon, the FE concept requires the associated error also be orthogonal to the approximation subspace, subject to a constraint set  $\mathcal{B}$ . This of course yields an "artificial viscosity" term, as well as some additional terms.

The completion of categories 1-3 yields a matrix ordinary differential equation system, that is converted into an algebraic equation system  $\{F\}$  by identification of an integration algorithm with its associated truncation error, category 4. The equation system  $\{F\}$  is non-linear unless explicit time-integration is specified. In all other instances, the Jacobian of an iteration algorithm for solution of  $\{F\}$  is a large sparse matrix. A direct matrix solution using this Jacobian is usually ill-advised, based strictly on the operations count, core storage and CPU requirements. One FD approach is to construct an approximate factorization. Conversely, one FE approach is to construct the tensor matrix product approximation. There exists a wide range of alternative procedures including SOR, SLOR, and ADI to name a few. A specific selection can be the prime determining factor of the cost of the solution. Solution cost is typically much less affected by, but solution accuracy is critically dependent upon, choices made in categories 1-3. The paper discusses details on this subject.

#### References:

1. R.M. Beam and R.F. Warming, "An Implicit Factored Scheme for the Compressible Navier-Stokes Equations," AIAA J., V. 16, 1978, pp. 393-402.
2. T.H. Pulliam and J.L. Steger, "On Implicit Finite Difference Simulations of Three-Dimensional Flow," AIAA J., V. 18, 1980, pp. 159-167.
3. W.R. Briley and H. McDonald, "Solutions of the Three-Dimensional Compressible Navier-Stokes Equations by an Implicit Technique," Lecture Notes in Physics, Springer-Verlag, V. 35, pp. 105-110.
4. A.J. Baker, "Research on a Finite Element Numerical Algorithm For The Three-Dimensional Navier-Stokes Equations," U.S. A.F. Report AFWAL-TR-82-3012, 1982.
5. R.W. MacCormack, "A Numerical Method for Solving the Equations of Compressible Viscous Flow," AIAA Paper 81-0110, 1981.
6. R.D. Richtmeyer and K.W. Morton, Difference Methods for Initial-Value Problems, 2nd ed., Interscience Publishers, New York, 1967.

## HYBRID METHODS OF ANALYSIS

by

Ahmed K. Noor

George Washington University Center  
NASA Langley Research Center  
Hampton, Virginia 23665

Hybridization has long been recognized as an innovative and effective way of developing new materials and products. Examples are provided by advanced fibrous composites which are obtained by embedding high strength, high modulus fibers in a matrix; and more recently, by hybrid composites which consist of different fibrous composites. In the computational mechanics area hybrid methods and algorithms have been developed to overcome some of the drawbacks of parent methods. Examples are provided by mixed explicit/implicit temporal integration techniques; combination of boundary integral formulation and finite element concepts to form the boundary integral method; and the combined use of direct and iterative techniques for the solution of algebraic equations associated with hierarchical finite elements (or multigrid finite differences). However, the potential of the hybrid numerical, analytical methods has not been fully exploited, and focused research is needed to realize this potential.

The present paper reports the progress on the development of effective hybrid classical and/or numerical discretization techniques for the solution of practical engineering problems. Specifically, two hybrid methods for solution of highly nonlinear problems are discussed. The two methods are: 1) hybrid perturbation/Bubnov-Galerkin technique; and 2) reduction method.

The *first method* is based on the successive application of the regular perturbation expansion and the classical Bubnov-Galerkin approximation. The technique exploits the best elements of the two parent techniques as follows (Ref. 1):

- a) The regular perturbation method is used as a systematic and general approach for generating coordinate functions; and
- b) The Bubnov-Galerkin technique is used as an efficient procedure for minimizing and distributing the error of the approximation to the solution throughout the domain. Moreover, this hybrid technique alleviates the following major drawbacks of the two classical techniques:

- a) The requirement of using a small parameter in the regular perturbation expansion; and
- b) The arbitrariness in the choice of the coordinate functions (or modes) in the Bubnov-Galerkin technique.

Therefore, the hybrid technique extends the range of applicability of the perturbation method and enhances the effectiveness of the Bubnov-Galerkin technique.

The *second hybrid method* is a reduction method which is a combination of the finite element method, the classical Bubnov-Galerkin technique and the regular perturbation method. In the reduction method, the initial discretization is done via finite elements, then the vector of fundamental unknowns is expressed as a linear combination of a *small number of global modes* or basis vectors and the Bubnov-Galerkin technique is used to compute the coefficients in the linear combination. The basis vectors are chosen to be those commonly used in the regular perturbation technique, namely, the derivatives of the solution vector with respect to preselected control (or path parameters) in the solution space. The basis vectors are

generated by using the finite element model of the initial discretization.

The reduction method combines the advantages of the parent methods, namely, the modeling versatility of the finite element method, the reduction in the total number of degrees of freedom provided by the Bubnov-Galerkin technique and the simplicity of assessing the sensitivity of the response to variations in the control (or path) parameters. Moreover, the method greatly alleviates the following major drawbacks of the three parent techniques:

- a) Excessive amounts of computer time required for the nonlinear finite element analysis of large, complex systems.
- b) Difficulty of selecting global approximation functions for the classical Bubnov-Galerkin technique.
- c) Small radius of convergence of the Taylor series expansions used in the classical perturbation techniques.

Several applications of reduction methods to nonlinear thermal as well as structural and solid mechanics problems have demonstrated their effectiveness (Refs. 2, 3 and 4).

Other hybrid numerical and analytical techniques which appear to have high potential for practical engineering problems will be outlined in the paper.

#### References

1. Noor, A. K. and Balch, C. D., A Hybrid Perturbation/Bubnov-Galerkin Technique for Nonlinear Thermal Analysis, NASA TP-2145, 1983. To be published in AIAA Journal.
2. Noor, A. K., "Recent Advances in Reduction Methods for Nonlinear Problems," Computers and Structures, 13, 1981, pp. 31-44.
3. Noor, A. K., Balch, C. D. and Shibus, M. A., Reduction Methods for Nonlinear Steady-State Thermal Analysis, NASA TP-2098, 1983. To be published in International Journal for Numerical Methods in Engineering.
4. Noor, A. K. and Peters, J. M., "Recent Advances in Reduction Methods for Instability Analysis of Structures," Computers and Structures, 16, 1983, pp. 67-80.

COMPUTATIONAL METHODS FOR PROBLEMS OF FRICTIONAL  
CONTACT AND IMPACT

by

J.T. Oden  
Department of Aerospace Engineering  
and Engineering Mechanics  
The University of Texas  
Austin, Texas 78712

This paper is concerned with various phenomenological theories of friction, and discusses mathematical models of various aspects of friction between dry metallic surfaces. Included in the models are the effects of velocity and temperature on the coefficients of friction, nonlocal effects for the deformations of asperities, nonlinear effects due to the elasto-plasticity and viscoplasticity of metallic junctions, etc. A general class of nonlinear variational inequalities of evolution are derived which characterize a model class of boundary-value problems to which these nonlinear friction laws hold. Existence theorems are presented, approximate methods are presented, and error estimates and algorithms are derived. Applications to representative two-dimensional boundary value problems in solid mechanics are discussed.

## COMPUTATIONAL METHODS IN METEOROLOGY

by

Y.K. Sasaki and L.P. Chang  
Cooperative Institute for Mesoscale Meteorological Studies  
University of Oklahoma  
Norman, Oklahoma 73019

The major goal of meteorological studies is to provide accurate weather prediction. The once empirical and subjective skill of weather prediction has become a rather objective numerical procedure since the advent of electronic computers. During the course of developing various weather-prediction models, four types of numerical methods have found notable application; they are the finite-difference method (FDM), the finite-element method (FEM), the spectral method (SPM) and the normal-mode method (NMM). The fundamental principles and the meteorological application of these methods will be briefly introduced.

The FDM is a grid-point method derived from the truncated Taylor series approximation. It has the longest history of meteorological application of all four methods. In fact, the method is still the most frequently used numerical approach for its conceptual simplicity and ease of application. In spite of all this, there exist situations where the other methods may be more suitable to apply. This will become clear in passing.

Unlike the FDM, the FEM, the SPM and the NMM are the series-expansion methods. In these methods, the dependent variables of the differential equations are expanded in a finite set of analytically defined spatial basis functions. Different choices of the basis functions lead to the three different methods.

In the FEM, locally defined basis functions are employed. These functions take on nonzero values only in a small span of the entire domain, hence the final coefficient matrix of the resultant algebraic system is sparse and computationally desirable. Since the shape and size of individual elements are very flexible, local refinement of model resolution in areas of expected strong gradient can be easily achieved, and curved elements can be readily used to represent irregular orographical boundaries. Moreover, different types of elements can be optionally employed to cover different portions of the domain to obtain optimal accuracy and efficiency. These flexibilities enable the FEM to become very powerful for modeling mesoscale meteorological flows of which variable model resolution, mesh nesting and complex terrains are typical difficulties. Literature of the meteorological application of the FEM can be found, for example, in Cullen, Staniforth and Daley.

The SPM is usually applied to the global- or hemispherical-scale meteorological flow problem. Because of the macroscopically spherical shape of the earth, spherical harmonics can be conveniently chosen as the expansion basis functions in the SPM. However, when nonlinear terms are computed, a large number of interaction coefficients needs to be stored. This number increases extremely fast with increasing model resolution. Thus the SPM was not considered a realistic alternative to the FDM in the first decade it was introduced. In 1970, Eliassen et al. and Orszag independently introduced the much more efficient transform method into the SPM to skip the necessity of storage of the vast amount of interaction coefficient. It was only after then that the SPM gradually became a favored method for the global- and hemispherical-scale modeling of atmospheric flows. The major advantages of the method include (1) the exact representation of the linear phase velocity to

avoid wave dispersion; (2) the elimination of the aliasing problem using the transform method approach; and (3) the computational efficiency over the FDM and FEM for global and hemispherical modeling. However, the difficult incorporation of the complex terrains and the local model refinement turns the method inefficient for simulating flows of smaller scales. Platzman and Baer are two examples of the SPM application to meteorological problems.

In the NMM, eigensolutions of the linearized governing equations are used as the basis functions. This method has been mainly applied to the initialization problem of the primitive-equation models. We know that a primitive-equation model is much more susceptible to errors in the initial data. Any slight imbalance between the wind and mass fields will immediately generate unrealistic high-frequency gravity waves in the model. Without suppressing them, these gravity waves can soon mask the meteorologically important Rossby-type waves in the model integration. Therefore, a suitable adjustment of the initial data is essential before starting the time integration. In the NMM initialization, all dependent variables are expanded in the linear eigensolutions (normal modes) each of which is characterized by specific eigenfrequency. The tendencies of the unwanted gravity waves are then made small to keep the gravity modes from growing in subsequent time integration steps. Note that a mere removal of all the gravity modes from the initial data is not able to suppress these modes for all time because the nonlinearity tends to re-excite the gravity modes. Problems that are still open in the NMM initialization include (1) the convergence of the iterative procedure when many vertical modes need to be adjusted; (2) the undiscernible difference between the Rossby and the gravity modes in the tropics; and (3) the boundary effect on the initialization procedure for limited-area models. The following may be used as a source of references of the NMM: Daley and Baer and Tribbia.

It is seen that one numerical method may become superior to another under certain circumstances. Therefore, a judicious decision on what method to use is of great importance. We also expect that some new and more powerful methods may be invented to solve certain types of problems to help us better understand the meteorological processes in the future.

- Cullen, M.J.P., "Integration of the Primitive Equations on a Sphere Using the Finite Element Method", Quart. J. Roy. Meteor. Soc., 100, 1974, pp. 555-562.
- Staniforth, A.N. and R.W. Daley, "A Baroclinic Finite Element Model for Regional Forecasting with the Primitive Equations", Mon. Wea. Rev., 107, 1979, pp. 107-121.
- Eliassen, E. et al., "On a Numerical Method for Integration of the Hydrodynamical Equations with a Spectral Representation of the Horizontal Fields", Report No. 2, Institut for Teoretisk meteorologi, University of Copenhagen, 1970, pp. 890-895.
- Orszag, S.A., "Transform Method for Calculation of Vector-Coupled Sums: Application of the Spectral Form of the Vorticity Equation", J. Atmos. Sci., 27, 1970, pp. 890-895.
- Platzman, G.W., "The Spectral Form of the Vorticity Equation", J. Meteor., 17, 1960, pp. 635-644.
- Baer, F., "Integration with the Spectral Vorticity Equation", J. Atmos. Sci., 21, 1964, pp. 260-276.
- Daley, R.W., "Normal Mode Initialization", Rev. Geophys. Space Phys., 19, 1981, pp. 450,468.
- Baer, F. and J. Tribbia, "On Complete Filtering of Gravity Modes through Nonlinear Initialization", Mon. Wea. Rev., 105, 1977, pp. 1536-1539.

AUTOMATIC PROCEDURES IN EVOLUTIONARY FINITE  
ELEMENT CALCULATIONS\*

by

Patrick F. Chavez  
Computational Physics and Mechanics I, 1531  
Sandia National Laboratories  
Albuquerque, NM 87185

We have considered the problem of automatically restoring reasonable shapes to elements and introducing refinements in finite element meshes associated with the solution of a system of partial differential equations. Although the theory developed is applicable to any number of spatial dimensions, we have primarily considered equations with two space variables and whose solution evolves in time. The solution of the system of equations are interpreted as components of velocity in the directions of the spatial coordinates. The geometry of the mesh is updated based on the solution yielding an "updated" Lagrangian mesh. This can lead to non-uniform flow of the mesh in which the resulting mesh at some time needs upgrading in either the form of mesh regularization and/or mesh refinement.

A computer program has been developed that is capable of restoring reasonable shapes to elements in meshes that flow with the solution, without generating totally new meshes each time the mesh is found to be in need of improvement. Our procedure is based on the computer program QMESH whose original development was for the initial construction of meshes. The routines developed will restore reasonable shapes to elements by repositioning interior nodes, deleting elements, and rearranging the element topology locally. The repositioning of the nodes is based on a convex functional that attempts to equilibrate the distance between neighboring nodes and the areas of neighboring elements. Element deletion is based on an attempt to improve the mesh locally by eliminating elements that are severely rhomboid. Rearrangement of the mesh topology, known as restructuring, attempts to improve the aspect ratios and angle conditions of the elements comprising the mesh.

The redefinition of the mesh necessitates the redefinition of the variables associated with the new node locations. The method of transferring data from the old mesh to the new mesh is based on the  $L_2$ -projection of the old mesh data onto the finite dimensional approximating space defined by the new mesh. The transferal of the mesh data will be the best in the  $L_2$ -sense which leads us to conclude that for constant mass density systems the

\*This work performed at Sandia National Laboratories supported by the U.S. Department of Energy under contract number DE-AC04-76DP00789.

$L_2$ -projection conserves momentum as well as any other approximation in the subspace. Comparison of the  $L_2$ -projection method for transferring mesh data to the more typical method of interpolation motivates a simple proof that for constant mass density systems the  $L_2$ -projection also conserves energy as well as any other approximation in the subspace. Finally, although the  $L_2$ -projection is globally defined, any rough spots in the old mesh data does not pollute the new mesh function data far from these rough spots.

The program also has a new method of error indication that will activate the automatic refinement of the mesh locally. The error indicator is based on easily computable pointwise maximum norm estimates. This error indicator will be conservative for evolution problems with smooth solutions and is, perhaps, better suited to account for problems with singularities. The error indicator is maximized over the quadrature points of the elements. Refinement of the elements is based on equilibrating the indicator over all the elements of the mesh. The routine will increase the local degree of approximability of the solution by adding interior degrees of freedom to elements. The routine can remove previously added interior degrees of freedom if they are not necessary as the solutions of the equations evolve. This produces an optimal mesh for the number of nodes employed in regards to the error indicator.

A Finite Element Method for Viscous Flows Based on  
a Hybrid Type of Virtual Work Principle

by

Naoki Asano\*  
Visiting Associate Professor  
Department of Mechanical and Aerospace Engineering  
University of Delaware  
Newark, Delaware 19711  
U.S.A.

Hiroshi Kamegaya  
Associate Professor  
Department of Mechanical Engineering  
Tamagawa University  
Tokyo 194  
JAPAN

Both the finite difference method (FDM) and the finite element method (FEM) treating the Navier-Stokes equation (NS) and the equation of continuity (EC) are generally used for the numerical analysis of viscous flows.

In this paper, we propose a new FEM without the NS and the EC for viscous flows. The formulation of this FEM is based on a hybrid type of the virtual work principle used in solid mechanics.

In order to investigate the validity of this FEM, we calculate a two-dimensional cavity flow. The results calculated by the FEM agree well with those by the FDM.

The merit of this FEM makes it easy to treat boundary conditions which the quantities on the boundary are hydrodynamic ones such as velocity and pressure.

\*On leave from Department of Mechanical Engineering, Tamagawa University, Machida, Tokyo 194, Japan.

Hydrodynamic Simulation Using Finite Elements:  
A Solution Method for Microcomputers

by

Roy A. Walters  
U.S. Geological Survey  
Menlo Park, California 94025

A common problem with many microcomputer systems is that the core memory capacity is exceeded before any realistically sized numerical simulations can be run. For a wide class of problems using finite element discretization, the matrix required for assembly and solution poses the most serious memory constraint. Furthermore, many methods which attempt to mitigate this constraint have severe impacts upon computational speed. The philosophy used here is to utilize core memory fully and use mass storage devices only as necessary because of their relatively slow speed. An area of interest, then, is how to use the mass storage efficiently in conjunction with the matrix solution procedure.

The microcomputer application presented here focuses upon the numerical solution of the shallow water equations using the finite element method. These equations are derived from the vertically-integrated Navier-Stokes equations with a free surface (Heaps, 1978) and are applicable to the propagation of gravity waves. In this application, these equations are used to simulate the tidal and residual currents in various portions of the San Francisco Bay estuary. The equations are approximated using the Galerkin method in space and time-centered finite differences in time. A linearized algebraic system is derived using a Newton-Raphson iterative method and is solved using a frontal solution method.

A variety of modifications of the frontal solver are examined with respect to memory size and computational speed, and include a consideration of pivoting strategies, dynamic management of equation size, and mass versus vector storage (Walters, 1980). In general, diagonal pivoting and vector storage (in core) of the coefficients of the eliminated equations leads to higher efficiencies than standard methods. By using semi-implicit time integration rather than the time-centered approach, one can reduce the run time by about a factor of 4 because only the right hand vector needs to be recomputed. Furthermore, a harmonic approach in time can be used with the tidal simulations with a reduction in run time of about 2 orders of magnitude (Walters, 1983).

#### References

Heaps, N.S., "Linearized vertically-integrated equations for residual circulation in coastal seas," Deutsche Hydrographische Zeitschrift, 30, 1978, pp 147-169.

Walters, R.A., "The frontal method in hydrodynamics simulations," Computers in Fluids, 8, 1980, pp265-272.

Walters, R.A., "Numerically induced oscillations in finite element approximations to the shallow water equations," International Journal for Numerical Methods in Fluids, 1983, in press.

Adapting Iterative Algorithms  
For Solving Large Sparse Linear Systems  
For Efficient Use on Supercomputers

by

David R. Kincaid  
Center for Numerical Analysis  
The University of Texas at Austin  
Austin, Texas 78712

The ITPACK project involves the development of research-oriented mathematical software, based on iterative algorithms, for solving large systems of linear algebraic equations with sparse coefficient matrices. The emphasis is on linear systems arising in the solution of partial differential equations by discretizations such as finite difference or finite element methods. Among other things this project has resulted in the development of a package of subroutines known as ITPACK which is available to the scientific community [1]. Important features of the ITPACK routines include the adaptive determination of the iteration parameters and realistic procedures for terminating the iterative processes. An important application of ITPACK is for use as solution modules in the ELLPACK package of computer routines for solving a class of partial differential equations [2].

We review the objectives of the ITPACK project, summarize the progress made to date and outline plans for future work. A summary is given of work on both software and research that has contributed to the present mathematical software package. The 2C version of ITPACK for scalar computers and a version for use on high performance vector computers are discussed. Adapting and designing mathematical software to achieve optimum performance on supercomputers will be discussed. Comments and observations are made in light of recent work done on modifying the ITPACK software package for the CDC CYBER 205. An overview is given of the developmental work on other software involving more general preconditioners and additional nonsymmetric procedures.

1. Kincaid, D., Respass, J., Young, D., and Grimes, R., "Algorithm 586 ITPACK 2C: A FORTRAN Package for Solving Large Sparse Linear Systems by Adaptive Accelerated Iterative Methods," ACM Transactions on Mathematical Software, Vol. 8, No. 3, September 1982, pp. 302-322.
2. Rice, J., "ELLPACK User's Guide," CSD-TR 372, Computer Science Department, Purdue Univ., West Lafayette, Indiana, 47907, July 1981.

Some Experience with Micro-Computers  
for Finite Element Computations

by

Noboru Kikuchi and Kazuhiro Yamazaki  
Department of Mechanical Engineering  
and Applied Mechanics  
University of Michigan  
Ann Arbor, Michigan 48109

The study is concerned with a development of finite element softwares for microcomputers such as TRS-80, Apple II, IBM P.C., and others in order to facilitate education of finite element methods and their use in small size research. This project is developed during teaching a course "Introduction to Finite Element Methods" in the University of Michigan to senior and 1-st year graduate students. All programs are written in BASIC and are primarily for "Apple II-plus" with 64K memory. Some of the programs are available for TRS-80 and IBM P.C.

The package of finite element softwares developed so far consists of three groups. The first solves heat conduction, potential flow, elastic torsion, and elastic membrane problems using 3-node and 6-node triangular elements. These are mainly for stationary problems although separate programs are developed for heat conduction with convection terms and time dependent heat conduction. All programs are divided into three subprograms: pre, finite element, and post processings. Finite element models are created by a semi-automatic mesh generator and are displayed on the TV screen by the post processing. To save storage space, a skyline method is used in the finite element processing to solve systems of linear equations. Results are again displayed by the post processing. For example, isothermal lines and heat flux vector are written in the TV screen.

The second group is developed to study structural mechanics, especially for frame structures. Trusses, Simple Beams, Plane frames for bending and axial forces, Plane frames for bending and torsion, and 3-dimensional frames are solved by finite element methods. Stationary, Eigenvalue, and Dynamic problems can be solved using softwares in the second group. For eigen-solvers, we prepare Jacobi's, Generalized Jacobi', and inverse iteration methods. For dynamics of plane frames, only the Newmark  $\beta$ -method is applied. In order to relate to the area of computer aided design, one program is developed to find the optimal cross section of a beam with respect to buckling and free vibration.

The third group is for stress analysis of plane elastic structures. We developed programs using 3-node, 6-node, and 4-node elements for plane problems. In this case, speed of computation and accuracy of approximation are the main issues. Three node elements provide faster computation but quality of approximations is not so fine, especially, for bending dominated problems. Implementation of isoparametric

4-node elements are too expensive while quality is almost the same to 3-node elements. Thus we need a modification to use 4-node elements to improve their quality. To do this, we applied the selective reduced integration method to evaluate stiffness matrix. Indeed, the constitutive equation is divided into two parts:

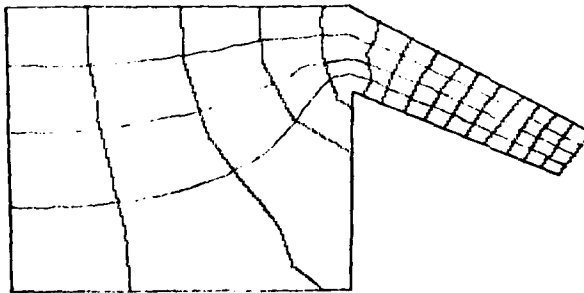
$$\begin{Bmatrix} \sigma_x \\ \sigma_y \\ \tau_{xy} \end{Bmatrix} = \begin{bmatrix} \lambda & \lambda & 0 \\ \lambda & \lambda & 0 \\ 0 & 0 & \mu \end{bmatrix} \begin{Bmatrix} \epsilon_x \\ \epsilon_y \\ \gamma_{xy} \end{Bmatrix} + \begin{bmatrix} 2\mu & 0 & 0 \\ 0 & 2\mu & 0 \\ 0 & 0 & 0 \end{bmatrix} \begin{Bmatrix} \epsilon_x \\ \epsilon_y \\ \gamma_{xy} \end{Bmatrix}$$

where  $\lambda$  and  $\mu$  are Lamè elastic constants. We applied reduced integration to the first term and full integration to the second. This scheme provides far better solutions to bending dominated problems for both compressible and incompressible materials. To compute each element stiffness matrix using this selective reduced integration method, we need about 23 seconds. Six-node elements are introduced to solve singular problems including cracks by adjusting location of nodes.

Details of the softwares described in the above can be found in the report (1) prepared by the authors.

#### Reference

1. N. Kikuchi and K. Yamazaki, "MICHIGAN MICROFEM," Department of Mechanical Engineering and Applied Mechanics, University of Michigan, Ann Arbor, 1983.



Equi-Potential and Stream Function  
Lines by "Apple II-plus"

Differential Renormalization-Group  
and Multicritical Phenomena

by

Tom Chang  
Center for Space Research  
Massachusetts Institute of Technology  
Cambridge, Massachusetts 02139

Recent advances in the theory of the "renormalization-group" [1] have led to the analytical determination of critical point exponents and description of crossover phenomena among competing critical effects in real materials.

At an ordinary critical point, two separate coexisting phases become indistinguishable. Critical points more complex than ordinary (multicritical points) have been found in many experimental systems. Examples include the He<sup>3</sup>-He<sup>4</sup> mixture, order-disorder transition in ammonium halides, antiferromagnets exhibiting metamagnetic or spin-flop transitions, displacive structural phase transitions, fluid mixtures, compressible magnets, and systems exhibiting helicoidal ground states. In metamagnets, for example, tricritical points are observed. At such an extraordinary critical point, three separate coexisting phases become identical simultaneously. For systems involving coupled order-parameters with reversal symmetry, critical points at which four phases become identical can occur at localities where several lines of tricritical points intersect. The Lifshitz point in MnP [2] to be discussed by Dr. Y. Shapira in the following lecture has exactly this property. Other examples include the fourth-order point discussed by Chang et al. [3] and the bicritical point in spin-flop transitions [4].

The use of differential generators for the renormalization-group has several advantages over the recursive formulation. (1) In a recursive renormalization-group, the recursion relations contain the renormalization factor explicitly. The eventually calculated critical point exponents, etc., are, of course, independent of this factor; it therefore represents an unnecessary complication that is avoided with a differential generator. (2) The differential equations obtained from a differential generator are, in general, far simpler than the corresponding recursion relations. This is the case because the recursion relations must exhibit all the feedback that results from the finite amount of renormalization. (3) Differential equations are amenable to more analytic solution techniques than recursion relations. This has been demonstrated by some of our analyses of the global features of the renormalization-group involving the competition of several critical behaviors [5] and in the explicit calculations of nonlinear crossover equations of state for these systems [6].

The outline of this lecture is as follows. Firstly, the basic concepts of Wilson's renormalization-group is discussed. Secondly, the exact "One-Particle-Irreducible Differential Generator" [7,8] is introduced and the technique of the " $\epsilon$ -expansion" proposed by Wilson and Fisher [9] is explained. Thirdly, sample calculations are presented to demonstrate the utility of the differential generators to real materials exhibiting multi- and ordinary critical behavior. Finally, based on a path-integral formalism, these ideas are extended to the dynamic critical phenomena of phase transitions [8,10].

#### References

- [1] Wilson, K.G. and J. Kogut, Physics Reports, 12, 85 (1974).
- [2] Shapira, Y., C.C. Becerra, N.F. Oliveira, Jr., and T.S. Chang, Phys. Rev. Lett., 44, 1692 (1980); Phys. Rev., B24, 2780 (1981).
- [3] Chang, T.S., A. Hankey, and H.E. Stanley, Phys. Rev., B8, 346 (1973).
- [4] Kosterlitz, J.M., D.R. Nelson, and M.E. Fisher, Phys. Rev., B13, 412 (1976).
- [5] Nicoll, J.F., T.S. Chang, and H.E. Stanley, Phys. Rev. Lett., 32, 1446 (1974); Phys. Rev., B12, 458 (1975).
- [6] Nicoll, J.F., T.S. Chang, and H.E. Stanley, Phys. Rev. Lett., 36, 113 (1976); Phys. Rev., A13, 1251 (1976).
- [7] Nicoll, J.F. and T.S. Chang, Phys. Lett., 62A, 287 (1977).
- [8] Vvedensky, D., T.S. Chang, and J.F. Nicoll, Phys. Rev. A (to be published in 1983).
- [9] Wilson, K.G. and M.E. Fisher, Phys. Rev. Lett., 28, 240 (1972).
- [10] Chang, T.S., J.F. Nicoll, and J. Young, Phys. Lett., 67A, 287 (1978); Vvedensky, D. and T.S. Chang, Phys. Lett., 90A, 459 (1982).

## The Experimental Evidence for a Lifshitz Point in MnP

by

Y. Shapira

Francis Bitter National Magnet Laboratory  
Massachusetts Institute of Technology  
Cambridge, MA 02139

In 1975 Hornreich, Luban and Shtrikman introduced a new multicritical point, which they called a Lifshitz point (LP).<sup>1,2</sup> Some of the essential properties of the LP are: (1) The LP is a point where paramagnetic, ferromagnetic, and helicoidal phases meet. (2) The para-ferro and para-helicoidal transitions are of second order. (3) The wave vector  $q$  in the helicoidal phase should approach zero continuously as the LP is approached. (4) There exists at least one direction,  $i$ , for which the term  $c_i(\partial M/\partial x_i)^2$  in the free-energy expansion vanishes. In this talk experimental studies which strongly suggest the existence of a LP in MnP will be reviewed. This review is largely based on works done in collaboration with C.C. Becerra and N.F. Oliveira, Jr. (University of São Paulo), R.M. Moon and J.W. Cable (Oak Ridge National Laboratory), and T.S. Chang (MIT).<sup>3-8</sup>

MnP is a magnetic material with orthorhombic structure ( $a > b > c$ ). Early works<sup>9</sup> revealed that the phase diagram in the presence of a magnetic field along the  $b$  axis exhibits a triple point at which paramagnetic, ferromagnetic and fan phases meet. (A fan is an example of an helicoidal structure.) The para-ferro and para-fan transitions are of second order. More recent detailed measurements of the phase diagram near the para-ferro-fan triple point<sup>3,4</sup> show the features expected near a LP. Thus, all phase boundaries are tangent to each other at the triple point, and the  $\lambda$  line has an inflection point at the triple point. The cross-over exponent  $\phi = 0.63 \pm 0.04$  agrees with a calculation to first order in  $\epsilon$ . Neutron-diffraction data for the variation of  $q$  in the fan phase strongly suggest that  $q$  goes continuously to zero as the triple point is approached.<sup>5</sup> The variation of the  $q$  vector on the para-fan segment of the  $\lambda$  line is consistent with theory. Other neutron data for the spin-wave dispersion curves (measured thus far only at  $H = 0$ ) indicate a competition between ferromagnetic and antiferromagnetic exchange interactions.<sup>10</sup> The ratio between the competing effective exchange constants is favorable for the occurrence of a LP.<sup>7,8</sup> Susceptibility data are also consistent with a LP.<sup>3,4</sup>

Recently the phase diagram when  $\vec{H}$  is parallel to the  $a$  crystallographic direction was measured for the first time.<sup>6</sup> The results suggest that a LP exists for this field direction also.

## References

1. Hornreich, R.M., Luban, M., and Shtrikman, S., "Critical Behavior at the Onset of k-Space Instability on the  $\lambda$  Line", Phys. Rev. Lett. **35**, 1978, pp. 1678-1681.
2. Hornreich, R.M., "The Lifshitz Point: Phase Diagrams and Critical Behavior", J. Magn. Magn. Mater. **15-18**, 1980,

- pp. 387-392.
3. Becerra, C.C., Shapira, Y., Oliveira, N.F.Jr., and Chang, T.S., "Lifshitz Point in MnP", Phys. Rev. Lett. 44, 1980, pp. 1692-1695.
  4. Shapira, Y., Becerra, C.C., Oliveira, N.F.Jr., and Chang, T.S., "Phase Diagram, Susceptibility, and Magnetostriction of MnP: Evidence for a Lifshitz Point", Phys. Rev. 24, 1981, pp. 2780-2806.
  5. Moon, R.M., Cable, J.W., and Shapira, Y., "Neutron Scattering Evidence on Lifshitz Behavior in MnP", J. Appl. Phys. 52, 1981, pp. 2025-2027.
  6. Shapira, Y. and Oliviera, N.F.Jr., "Magnetic Phase Diagram of MnP: Field Parallel to the Hard Direction", Phys. Lett. A 89, 1982, pp. 205-207.
  7. Shapira, Y., "The Evidence for a Lifshitz Point in MnP", J. Appl. Phys. 53, 1982, pp. 1914-1919.
  8. Shapira, Y., "The Experimental Evidence for a Lifshitz Point in MnP", Proc. of a NATO School on Multicritical Phenomena, Geilo, Norway, 1983 (to be published).
  9. Komatsubara, T., Suzuki, T., and Hirahara, E., "Magnetization Process and Spin Structure Diagram in Manganese Phosphide Single Crystal", J. Phys. Soc. Jpn. 28, 1970, pp. 317-320.
  10. Tajima, K., Ishikawa, Y., and Obara, H., "Neutron Scattering Studies of the Ferro to Spiral Transition in MnP", J. Magn. Magn. Mater. 15-18, 1980, pp. 373-374.

## Diffusional Nucleation and Growth

by

H. I. Aaronson

Department of Metallurgical Engineering and Materials Science  
Carnegie-Mellon University  
Pittsburgh Pennsylvania 15213

An overview is presented of the theory and key experimental observations on solid-solid phase transformations proceeding by diffusional nucleation and growth. As instructed, attempts are made to isolate important mathematical problems in these areas which are urgently in need of solution.

Brief summaries of both classical and non-classical nucleation theory are presented, emphasizing homogeneous nucleation. Experimental evidence just obtained by F. K. LeGoues provides the first sound support for the essential correctness of the theories. Realistic and rigorous extension to the technically more important problem of heterogeneous nucleation requires that the strain energy associated with a faceted nucleus first be quantitatively described in the context of anisotropic elasticity. Interaction of the resulting strain field with that of isolated straight edge and screw dislocations should next be addressed.

Mechanisms and kinetics of diffusional growth are logical consequences of the low energy orientation relationships between nucleus and matrix phases imposed by the nucleation process. Two types of interphase boundary are important during growth: the disordered and the partially (or fully) coherent. The energy of the structural component of partially coherent interphase boundaries is presently best described by van der Merwe theory. Re-examination of the theory to incorporate more realistic force laws and the chemical component of the interfacial energy would be desirable. A general treatment of the structure and energy of disordered interphase boundaries is even more urgently needed. Many measurements of the growth kinetics of precipitates considered to have interphase boundaries with a relatively large proportion of disordered areas are conducted on grain boundary allotriomorphs. To calculate the growth kinetics of allotriomorphs assuming volume diffusion-control, the assumption is presently made that this morphology is an oblate ellipsoid. However, a more realistic approximation to its shape is that of a double spherical cap; solutions are needed for the parabolic rate constants for growth of the spherical cap and for the diffusion field in the matrix phase round the cap.

Partially and fully coherent interphase boundaries between crystals with significantly different structures are now known to migrate solely by the ledge mechanism.

Atkinson, and earlier Jones and Trivedi, have published conflicting solutions to this important problem for the case of diffusionally isolated ledges. Critical re-examination of the problem is now much in order. Problems also exist in the often more realistic situation wherein the diffusion fields of adjacent ledges overlap. In particular, experimental measurements of the thickening and lengthening kinetics of plates can sometimes be rationalized by assuming that the plates are oblate ellipsoids growing with uniform atomic attachment, as if they were bounded by disordered rather than by partially coherent boundaries. Under what circumstances should overlap of the diffusion fields of adjacent ledges lead to such a result?

Returning to the growth of grain boundary allotriomorphs, a more accurate view of this problem is that the interphase boundaries of this morphology are composed of alternate disordered and partially coherent boundaries, with the former growing by essentially uniform atomic attachment and the latter by the ledge mechanism. A treatment of the growth of such complex boundaries in which the proportion of the two types of interfacial structure and the average spacing between ledges on the facets are variables would be very valuable. Finally, a brief introduction is given to the optimization problem in solid state growth: what determines the radius of the edges of precipitate plates and the interlamellar spacing of pearlite (which is composed of alternate plates of two phases growing into matrix of a third phase)? Solution of this problem will involve substantial physical as well as mathematical insight.

Appreciation is expressed to NSF, ARO and AFOSR for support of research programs from which some of the foregoing material has been drawn.

SOME CHARACTERISTIC FEATURES OF  
MARTENSITIC TRANSFORMATIONS IN METALLIC ALLOYS

by

Walter S. Owen  
Department of Materials Science and Engineering  
Massachusetts Institute of Technology  
Cambridge, Massachusetts 02139

The fact that the evolution of a precise definition of a "martensitic" transformation has involved an almost continuous international debate running over several decades illustrates that identifying the essential, and fundamental, features of this class of transformation is difficult. In recent years, it has become accepted practice to define a martensitic transformation as a first-order transformation in which the shear strains involved in the total shape change are sufficiently large to dominate the transformation kinetics. The importance of these shear strains in the nucleation and growth of a plate of martensite will be discussed.

Many alloys exhibit pre-martensitic effects resulting in significant softening of the elastic constants and in an increase in the elastic anisotropy with decreasing temperature of the parent phase. There are other, often complex, effects which have been reported in a variety of alloys. It should be emphasized, however, that in many of the alloy systems which have been studied most thoroughly no significant pre-martensitic effects have been detected. Thus, it seems that lattice softening and other effects which can occur at temperatures above the temperature of nucleation of the martensite are not essential precursors. It is necessary to discover the influence, if any, of pre-martensitic phenomena on the nucleation and growth of martensite in those alloy systems in which such phenomena occur. Recent work concerned with two distinctly different classes of alloys,  $\beta$ -phase copper-based alloys and iron-based Invar alloys, which exhibit unique forms of pre-martensitic lattice softening, will be discussed.

PHASE TRANSITIONS IN  
EQUILIBRIUM STATISTICAL MECHANICS

by

Joel L. Lebowitz  
Department of Mathematics and Physics  
Rutgers University  
New Brunswick, New Jersey 08903

Phase transitions are certainly interesting phenomena - if we were not so used to them, they would also be very surprising: a very small change in the temperature or pressure can produce drastic changes in density. The understanding of such transitions from first principles is the central theme of (equilibrium) statistical mechanics - a subject whose aim is the derivation of laws governing the (equilibrium) behaviour of macroscopic objects from the laws governing their microscopic constituents.

The information about the thermodynamic phases of a system is summarized in the phase diagram. The simplest such phase diagram is that of a one component fluid where the thermodynamic space has only two dimensions labeled by temperature and pressure. For most values of  $p$  and  $T$  the system is in some definite phase uniquely determined by the parameters. There are, however, some values of  $p$  and  $T$ , lying on smooth curves, at which the state of the system is not unique - it can exist in either of two pure states, e.g. a gas or a liquid, the two states having different densities. At the triple point the system can exist in three different pure states - gas, liquid and solid - which have different densities and one of them, the solid, even has a different symmetry.

I am stressing this point to emphasize that from the point of view of statistical mechanics the essential feature of a first order phase transition is that the equilibrium system can exist in more than one state: these states may differ by their density, energy, crystal structure or by something much more subtle such as their pair or triple correlation function. It might be hard to observe a co-existence of phases in which the difference appeared only in the higher order correlation - it would need good probes - but the general theory would treat it on the same footing as the more familiar transitions.

The key to all these cases is to consider the appropriate free energy of the macroscopic system as a function of all the systems parameters: temperature and chemical potentials are particularly important parameters. This function is convex and appropriate partial derivatives of it determine the density and the correlation functions. First order phase transitions, which are equivalent to non-uniqueness of equilibrium states, then correspond to discontinuities in these derivatives. This will be

illustrated by means of explicit models which can be treated rigorously from first principles.

We shall also discuss some recent results about the surface tension and the structure of the interface between coexisting pure phases.

#### References

1. Lebowitz, J. L., Coexistence of Phases in Ising Ferromagnets, *Journal of Statistical Physics*, 16, 6, 463 (1977).
2. Lebowitz, J. L. (with C. E. Pfister), Surface Tension and Phase Coexistence, *Phys. Rev. Letters*, 46, 1031 (1981).

Acknowledgment: Research supported in part by NSF Grant.

Pseudoelasticity in Memory Alloys  
as a Thermally Activated Process.

by

Ingo Müller  
FB 9 - Hermann-Föttinger-Institut  
TU Berlin  
1000 Berlin 12

Memory alloys show a strong dependence of the stress-strain relations on temperature. This behaviour can be understood as the consequence of an austenitic-martensitic phase transition, where the martensitic phase may exist in different twin formations.

A model is presented and exploited by statistical mechanics that permits insight into the competitive tendencies of the body to maximize entropy and minimize energy. There result static stress-strain curves that conform qualitatively to those that are observed.

The most important feature of the model is an internal potential energy with three minima - corresponding to austenitic and martensitic twins - and barriers in-between. As the temperature rises, the barriers may be overcome so that a phase transition is possible. The application of a load changes barriers so that we may see load-induced transitions. A set of ordinary differential equations governs this behaviour and their numerical solution is again in good qualitative agreement with measured stress-strain curves.

The Effect of Texture and Microstructure on the Large Strain Behavior  
of Metals

by

M. G. Stout  
Materials Science and Technology Division  
Los Alamos National Laboratory  
Los Alamos, NM 87545

Strain hardening and flow behavior is very important in structural analysis and metal forming processes. A complete knowledge of material response at finite strains is particularly necessary for the prediction of local plastic instabilities and for the development of accurate constitutive relations. In this paper we describe a number of finite strain experiments on a variety of materials in an attempt to catalogue general trends of material behavior. We place particular emphasis on the roles played by material texture and texture development as well as material microstructure in determining hardening behavior. Finally, an attempt is made to quantify the effects of stress-state and stress-path and to relate these effects to texture and microstructure.

Hecker and Stout<sup>1</sup> have examined a number of researchers data and compared the stress-strain behavior in torsion to axisymmetric deformation for a variety of metals. In all cases the torsion data had a flow stress ~15% lower than the axisymmetric data, when compared on the basis of the von Mises effective stress-strain criterion. Qualitatively it appears that this difference can be explained, at least partially, by the different textures which develop in torsion and axisymmetric deformation. Supplementing this data we have prestrained both 1100 aluminum and 70-30 brass to large strains, in torsion, and subsequently tested the samples in an axisymmetric deformation mode. The ultimate tensile strength, in axisymmetric deformation was ~15% higher than the flow stress of the torsional prestrain. Again, these stress levels are qualitatively in agreement with measured textures.

We have also tested 1100 aluminum sheet, in a recrystallized, hot rolled but not recrystallized and cold rolled condition; in tension, through thickness compression, and plain strain compression. A quantitative "Taylor type" calculation has been done to predict the flow behavior of each of the three material conditions based on initial texture. Discrepancies between the "Taylor" predictions and measured stress-strain behavior are attributed to material dislocation substructure.

- 1) S. S. Hecker and M. G. Stout, ASM Materials Science Seminar "Deformation, Processing and Structure" October, 1982, St. Louis, MO.

AD A138 155

ABSTRACTS OF THE ANNUAL MEETING OF THE SOCIETY OF  
ENGINEERING SCIENCE INC. (U) DELAWARE UNIV NEWARK  
M TAYA SEP 83 ARO-20222.1-EG-CF DAAG29-83-M-0258

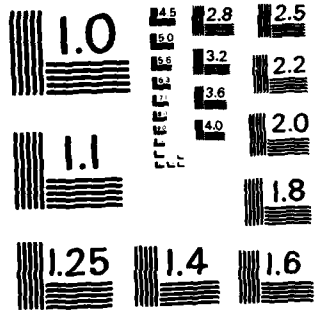
44

UNCLASSIFIED

F/G 5/1

NI

END
DATE
FORMED
3 84
DTIC



MICROCOPY RESOLUTION TEST CHART  
NATIONAL BUREAU OF STANDARDS-1963-A

ON THE BIFURCATION AND POSTBIFURCATION ANALYSIS OF RATE  
INDEPENDENT PLASTIC SOLIDS UNDER GENERAL PREBIFURCATION  
CONDITIONS

by

N. Triantafyllidis  
Department of Aerospace Engineering  
The University of Michigan  
Ann Arbor, Michigan 48109

Plastic buckling has been the object of intensive investigations over a long period of time. Major contributions to the field are due to Hill [1], [2] who placed the bifurcation analysis of elastic-plastic solids on a firm mathematical foundation. A fundamental assumption in Hill's theory is that the constitutive response of the body is hypoelastic at the onset of the bifurcation instability.

Interesting cases however exist where the behavior of the structure cannot be idealized as hypoelastic near the critical load. One such example is the presence of unloading in the prebifurcated solution of the body. Another example, applicable to structures with severe deviations from proportional loading, involves a class of recently developed rate independent corner theories of plasticity whose use have proven very fruitful in plastic buckling calculations.

Motivated by the aforementioned problems an attempt was made to study the bifurcation of elastic-plastic solids under unloading and consequently generalize the corresponding analysis in order to incorporate the most wide class of rate independent constitutive equations. A simple continuous model is considered in order to illustrate the different possibilities in the postbifurcation behavior of the elastic-plastic structures considered here. Next, the general three-dimensional analysis is presented. From the application standpoint, the most interesting result is that the bifurcation functional for the broad class of rate independent plasticity theories considered and for all possible prebifurcation paths, is a simple generalization of Hill's bifurcation functional. A completely different post-bifurcation analysis is needed however in the case where Hill's "hypoelastic comparison" solid concept is no longer applicable. It is shown that for this case, a "smooth" type bifurcation occurs, i.e., not only the perturbation of the solution  $\bar{u}$  tends to zero as the time-like parameter  $\lambda$  approaches its critical value  $\lambda_c$ , but the rate  $\bar{u} \rightarrow 0$  for  $\lambda \rightarrow \lambda_c$  as well. Finally, a recently completed application of the theory to puckering phenomena in sheet metal forming is briefly discussed.

[1] Hill, J. Mech. Physics Solids 4, 1956, p. 247.

[2] Hill, Ibid., 6, 1958, p. 236.

## THE EFFECTS OF RATE-DEPENDENT YIELD STRESS ON PLASTICITY THEORY

William H. Drysdale  
Ballistic Research Laboratory  
Aberdeen Proving Ground, MD 21005

The structural analysis of systems subjected to rapid or impulsive load application is a difficult task. The difficulty arises not only from the frequent necessity for a dynamic rather than static analyses, but also from the deviation of the materials of interest from classical elastic-plastic behavior under these conditions. It is well established that high rates of loading may lead to significant elevations of the apparent yield strength for many structural metals. For instance, the common titanium alloy Ti 6Al-4V has an increase in yield strength greater than 20% due to an increase of strain rate from  $10^{-2}$  to  $10^2$  per second. Clearly, a consistent model of the rate effect is required by the stress analyst.

The derivation is based on the simple extension of classical plasticity theory by the inclusion of a rate variable in the yield surface definition. The correct choice of rate variable is made by considering the physical deformation process within a metal crystal. Here, an increment of strain due to an increment of stress is composed of elastic and plastic parts. The elastic strain occurs essentially instantaneously. However, the plastic part must develop with time due to the finite velocity of dislocation motion, summed over all mobile dislocations, which contribute to this plastic strain. Hence, plastic strain rate is postulated as the correct quantity to serve as an internal variable in a rate-dependent formulation.

The specific form of classical plasticity chosen for modification consists of a VonMises yield surface with constant kinematic hardening (bilinear stress-strain response) and an associated flow rule. This form was chosen because of its modeling flexibility, ease of implementation in incremental FE codes, and conceptual simplicity due to isolation of the rate effect. Thus, the yield surface is

$$F(\sigma_{ij}, \epsilon_{ij}^p, \dot{\epsilon}_{ij}^p) = f(\sigma_{ij}, \epsilon_{ij}^p) - K(\dot{\epsilon}_{ij}^p) = 0 \quad (1)$$

where K contains the yield strength variation with rate. The basic concepts of plasticity theory are also retained, that is, in the stress subspace a load point which contacts the yield surface remains on the yield surface during plastic deformation. The increment of the yield function vanishes in the plastic state

$$dF = 0 = \frac{\partial f}{\partial \sigma_{ij}} d\sigma_{ij} + \frac{\partial f}{\partial \epsilon_{ij}^p} d\epsilon_{ij}^p - \frac{\partial K}{\partial \dot{\epsilon}_{ij}^p} d\dot{\epsilon}_{ij}^p \quad (2)$$

This relation may be interpreted as restricting the permissible variation of increments of stress, plastic strain, and plastic strain rate during plastic deformation. Equation (2) may be considered a linear first order differential equation for the increments of effective

plastic strain with constant coefficients in each increment. This equation may be solved to give

$$d\epsilon_{ij}^P = \left\{ \frac{1}{C\sigma_y} \frac{\partial f}{\partial \sigma_{kl}} d\sigma_{kl} + \left( \epsilon_o^P - \frac{1}{c\sigma_y} \frac{\partial f}{\partial \sigma_{kl}} \sigma_{kl} \right) dt \exp \left[ - \frac{3/2C}{\frac{\partial \sigma}{\partial y}} dt \right] \frac{\partial f}{\partial \sigma_{ij}} \right\} \frac{\partial f}{\partial \epsilon^P} \quad (3)$$

The first term in brackets is the classical rate-independent theory; the second term gives the correction for rate effects.

If the loading is restricted to uniaxial states of stress such as occur in material testing, a simplified equation of plastic state results. Assuming an empirically determined logarithmic dependence of yield stress on plastic strain rate and a piecewise linear loading history, Equation (2) may be integrated explicitly to give

$$\frac{1}{\epsilon_o + \epsilon^P} = \frac{1}{\epsilon_o + p} + C_1 \exp \left[ - \frac{\sigma + 3/2C\epsilon_o}{\sigma_o b} \right] \quad (4)$$

$$\epsilon^P = C_2 + pt - \frac{\sigma_o b}{3/2C} \ln (\epsilon_o + \epsilon^P)$$

The constants  $C_1$  and  $C_2$  in equation (4) are determined by requiring continuity of  $\epsilon^P$  and  $\dot{\epsilon}^P$  at the beginning of each piecewise linear loading interval.

In this theory yield occurs, i.e., the plastic state is entered, at the static yield strength. However, at this point the plastic strain rate is zero and may only increase in a continuous fashion, as indicated by Equation (4). The result is that the stress-strain curve continues to rise without apparent deviation from the elastic line, until a relatively abrupt transition to the plastic modulus occurs at a stress level corresponding to the applied loading rate. Back extrapolation or finite offset methods of measuring yield would indicate a rate-dependent yield stress.

By using equation (4), or a comparable solution for strain controlled loading, uniaxial material tests may be modeled. Many experimentally observed phenomena are included in the theory, creep and relaxation of metals above the yield point, differences in the shape of stress-strain curves in stress and strain controlled testing machines, etc. The incremental equation (3) may be readily adapted to a form compatible with incremental plastic finite element codes.

Stress Distributions in the Vicinity  
of a Necked Flat Sheet

by

P.P. Gillis and S.E. Jones  
College of Engineering  
University of Kentucky  
Lexington, Kentucky 40506

Consider a flat sheet which undergoes in-plane stretching with the normal strain in the width direction maintained at zero. Suppose that the plane of the sheet is the  $zy$ -plane and the sheet width is parallel to the  $y$ -direction. If the sheet is loaded in the  $z$ -direction, then the neck will form perpendicular to that direction (parallel to  $y$ ). Take the origin of the coordinate system at the minimum cross-section of neck.

Under fairly mild assumptions, in a region sufficiently close to the center of the neck, it can be shown that the normal stress component  $\sigma_z = \sigma_z(x, z)$  satisfies the simple wave equation

$$\frac{\partial^2 \sigma_z}{\partial x^2} = \frac{\partial^2 \sigma_z}{\partial z^2} \quad (1)$$

The boundary conditions for  $\sigma_z$  are:

$$\sigma_z(x, 0) = B(x), \quad \frac{\partial \sigma_z}{\partial x}(0, z) = 0 \quad (2)$$

where  $B(x) = B(-x)$  is the stress distribution at the center of the neck. Under these conditions,  $\sigma_z$  must take the form

$$\sigma_z = \frac{1}{2} [B(x+z) + B(x-z)] \quad (3)$$

Thus, it follows that the other stress components can be computed from (3) in terms of the distribution of normal stress  $B(x)$  at the minimum cross-section of the sheet.

As an application of the conclusion given in (3), the geometry of the neck can be estimated from:

$$\int_0^R \sigma_z dx = \frac{P}{2w} \quad (4)$$

where  $P$  is the load in the  $z$ -direction,  $w$  is the sheet width, and  $R = R(z)$  is the half-thickness of the sheet at the cross-section in question. Equation (4) provides a transcendental equation for the neck shape in terms of the stress distribution at the center of the neck. Several geometries and stress distributions are studied.

References

1. P.W. Bridgman, *Studies in Large Plastic Flow and Fracture* (McGraw-Hill, New York, 1952).
2. S.E. Jones, P.P. Gillis, and A.H. Shalaby, "Stress Distributions in the Vicinity of a Neck," *J. Appl. Phys.*, 50, (5) pp. 3168-3173 (1979).

A LARGE DEFORMATION PLASTICITY MODEL WITH RATE SENSITIVITY  
AND THERMAL SOFTENING

By

D.W. NICHOLSON AND K.C. KIDDY  
NAVAL SURFACE WEAPONS CENTER  
SILVER SPRING, MD 20910

A material instability known as adiabatic shear banding has been widely reported in steels, titanium, and several other materials [1]. It is thought to occur when thermal softening dominates strain hardening. In a recent paper [2] a small strain plasticity model with rate sensitivity and thermal softening was introduced and material stability criteria were developed on the basis of the reference quasistatic constitutive relation.

In this work, the previous model is extended to large strain. A generalization of isotropic hardening is introduced and the deformation rate tensor is assumed to be decomposable into elastic and flow parts. The elastic strain is governed by a generalization of Hooke's law while the flow strain observes a thermoviscoplastic relation. Stability criteria and flow thresholds are derived.

Temperature increases adiabatically according to

$$\dot{T} = \text{trace} (\sigma^T d^f) / \rho_0 c \quad (1)$$

where  $d^f$  is the flow part of the deformation rate tensor,  $\sigma$  is the symmetric Piola-Kirchhoff stress tensor,  $\rho_0$  is the initial mass density, and  $c$  is a thermodynamic constant defined carefully in the paper. By virtue of (1) the constitutive model embodies strong coupling of the thermal and mechanical fields.

The model is applied to rapid extension of a titanium strip (ignoring inertia). For imposed stresses several times the yield stress, it is predicted that the temperature will rise to the deleterious  $\beta$ -transus level (1600°F) in times on the order of  $10^{-2}$  sec. This result lends credibility to the model's potential for describing adiabatic shear.

[1] Rogers, H.C., "Adiabatic Shear Deformation", Annual Review of Materials Science, 9, 1979, p 283.

[2] Nicholson, D.W., and Kiddy, K.C., "Rate Sensitive Plasticity Model with Thermal Softening", in High Energy Rate Fabrication, PVP Vol 70, 1982, p 55.

Plastic Collapse of Short Thin-Walled Geometrically Imperfect  
Columns: Energy Absorption Considerations

David Hui\* and T. Wierzbicki\*\*  
Department of Ocean Engineering  
Massachusetts Institute of Technology  
Cambridge, Mass. 02139, U.S.A.

The present paper deals with the two-mode interaction between the anti-symmetric and the symmetric modes in the initial postbuckling study of short thin-walled columns under axial compression. The investigation was motivated by the experimental findings that the symmetric mode (which has a higher buckling load than the anti-symmetric mode and thus, it is not the most critical one) actually has a much higher energy absorption than the anti-symmetric mode as measured by the area under the curve of applied load versus end-shortening curves [1-2]. It appears that the mode shape of very large deflection (of the order of the length of the structure) of the structure in the plastic range is dictated by its initial elastic post-buckling behavior. Thus, an attempt is made to introduce initial geometric imperfection of specified magnitude in the symmetric mode so that the structure will follow the equilibrium path of this "beneficial" mode in the initial postbuckling as well as the very large deflection regimes, leading to the plastic collapse of the structure.

The analysis is studied using Koiter's multi-mode postbuckling theory [3]. The potential energy of a flat plate under axial compression can be written in the form (see [4])

$$P.E. = (1/2) \int_0^B \int_0^L [N_x \epsilon_x + N_y \epsilon_y + 2N_{xy} \epsilon_{xy} + M_x W_{,XX} + M_y W_{,YY} + 2M_{xy} W_{,XY}] dx dy$$

- work term (1)

Each rectangular plate is taken to be simply supported at the two loaded edges  $X=0$  and  $X=L$  and free at the edge  $Y=B$ . Two types of boundary conditions are considered at the line of attachment between the plates ( $Y=0$ ): simple support (anti-symmetric mode) and clamped support (symmetric mode). The buckling load and the corresponding mode shape for each type of boundary condition are obtained by solving the transcendental equation [5].

(20th SES Annual Meeting, August 22-24, 1983)

\* Graduate Student M.I.T.; now Assistant Professor, Dept.  
of Engineering Mechanics, The Ohio State University

\*\*Professor of Mechanics, M.I.T.

In the postbuckling analysis, the cubic terms of the potential energy vanish. Thus, the initial postbuckling behavior is governed by the quartic terms of the potential energy. In terms of the Budiansky-Hutchinson notation, the two-mode stability problem is specified by the two equilibrium equations [6],

$$\xi_1 [ b_1 (\xi_1)^2 + b_{12} (\xi_2)^2 + (1 - (\sigma/\sigma_1)) ] = (\sigma/\sigma_1) (\bar{\xi}_1) \quad (2)$$

$$\xi_2 [ b_2 (\xi_2)^2 + b_{21} (\xi_1)^2 + (1 - (\sigma/\sigma_2)) ] = (\sigma/\sigma_2) (\bar{\xi}_2)$$

where  $b_1$  and  $b_2$  are the "b" coefficients of the anti-symmetric and symmetric modes respectively and  $b_{12}$  and  $b_{21}$  are related to the coefficient of the interacting quartic term. Further,  $\sigma$  is the applied axial load,  $\sigma_1$  and  $\sigma_2$  refer to the anti-symmetric and symmetric classical buckling loads,  $\xi_1$  and  $\xi_2$  are the amplitude of the anti-symmetric and symmetric buckling modes and  $\bar{\xi}_1$  and  $\bar{\xi}_2$  are the amplitude of the geometric imperfections. The equilibrium path of a structure with a predominant geometric imperfection in the shape of the symmetric mode is examined followed by the plastic collapse analysis.

#### REFERENCES

1. Wierzbicki, T., Akerstrom, T. and Jernstrom, C., "Shape Optimization of Sheet Metal Structures Against Crash" Proc. of the 4th V.S.M. Conference, Detroit, Nov. 18-20, 1981.
2. Wierzbicki, T., "On the Formation and Growth of Folding Modes", Collapse: The Buckling of Structures in Theory and Practice, Proc. of IUTAM Symposium, Edited by Thompson, J.M.T. and Hunt, G.W., Aug. 1982, Cambridge University Press, 1983.
3. Koiter, W.T., "On the Stability of Elastic Equilibrium", Doctoral Thesis, Delft, Amsterdam, 1945; NASA-TT-F10-833, 1967 and AFFDL-TR-70-25, 1970.
4. Hui, D. and Hansen, J.S., "Two-Mode Buckling of an Elastically Supported Plate and its Relation to Catastrophe Theory", J. of Applied Mechanics, Vol. 47, Sept. 1980, pp. 607-612.
5. Timoshenko, S.P. and Gere, J.M., "Theory of Elastic Stability", McGraw-Hill, 1961.
6. Puskov, E. and Hutchinson, J.W., "Mode Interaction in Axially Stiffened Cylindrical Shells", AIAA Journal, Vol. 15, July, 1977, pp. 941-948.

Dynamic Plastic Analysis of Strain Rate Sensitive  
Rectangular Plates with Finite Deflections

David Hui\* and Joao G. de Oliveira  
Department of Ocean Engineering  
Massachusetts Institute of Technology

This paper deals with a theoretical investigation of the dynamic plastic behavior of thin rectangular plates made of strain rate sensitive materials undergoing finite deflections. The particular case of fully clamped plates under uniformly distributed lateral pressure pulse is examined.

The effects of finite displacements and material strain rate sensitivity on the dynamic behavior of simple rigid plastic structures have been extensively studied in the literature [1,2]. As reported in [1], the energy conservation analysis for rectangular plates with finite deflection proposed by Jones [3] was found to predict low but reasonable estimates of the maximum permanent lateral deflections for the strain rate sensitive mild steel rectangular plates tested in [4,5]. The strain rate effects for rectangular plates were examined by Wojewodzki and Wierzbicki [6] but the analysis is valid only for infinitesimal deformations. In the present study, the energy conservation analysis [3] is extended to include strain rate effects using the differential equation approach and the results are compared with the extended Hamilton's principle approach suggested by Taya and Mura [7]

The clamped rectangular plate is assumed to deform into a number of rigid regions separated by straight line plastic hinges each of length  $C_m$ . The empirical approximate constitutive equation [8]

$$\sigma/\sigma_0 = a + b(\dot{\epsilon}/D)^{1/p} \quad (1)$$

is employed such that  $a=1$ ,  $b=0$  corresponds to the rigid plastic case, while  $a=b=1$  corresponds to the well known Symonds-Cowper relation. Using the energy balance (see [3])

$$\int (p_3 - \mu \ddot{w}) \dot{w} \, dA = \sum_{m=1}^R \int_{C_m} (Nw - M) \theta_m \, dC_m \quad (2)$$

the respective governing nonlinear ordinary differential equation in time is derived for both the small and large

(20th SES Annual Meeting, August 22-24, 1983)

\* Graduate Student M.I.T.; now Assistant Professor, Dept. of Engineering Mechanics, The Ohio State University.

deflection regimes. After some algebra, the dissipation function  $(Nw-M)\dot{\delta}$  for the interior hinge  $D_h$  and the boundary hinge  $D_b$  expressions are obtained for the small deflection ( $W/H \leq 1$ ) as well as for the large deflection ( $W/H \geq 1$ ) regimes (see [8]). The nonlinear ordinary differential equation in time for the small deflection regime can be written in the form,

$$\ddot{(W/H)} + aC_1(W/H)^2 + b(\dot{W/H})^{1/p} (C_2 + C_3(W/H)^2) = C_0 \quad (3)$$

where the time independent coefficients  $C_1$ ,  $C_2$  and  $C_3$  are function of the aspect ratio and the coefficient  $p$  while  $C_0$  depends also on the lateral pressure. Finally, the nonlinear ODE for the large deflection regime is,

$$\begin{aligned} (W/H) \ddot{(W/H)} + Z_1(W/H) + aZ_2(W/H)^2 \\ + b(\dot{W/H})^{1/p} (Z_3 + Z_4(W/H)^{1/p} + Z_5(W/H)^{(1/p)+2}) = Z_0 \end{aligned} \quad (4)$$

where the time independent coefficients  $Z_0, Z_1, Z_2, Z_3, Z_4$  and  $Z_5$  are function of the aspect ratio and  $p$ . The initial valued problems are solved using Runge-Kutta formulas [9]. The maximum permanent deflection versus impulse parameter curves for mild steel plates are found to agree with the experiments [4,5].

ACKNOWLEDGEMENT: The authors wish to thank Prof. Norman Jones for his suggestion of the title problem and help.

#### REFERENCES

1. Jones, N., The Shock and Vibration Digest, Vol. 7(8), 1975, pp. 89-105.
2. Jones, N., The Shock and Vibration Digest, 10(9), pp.21-33 and 10(10), pp. 13-19, 1978, 13(10), pp.3-15, 1981.
3. Jones, N., "A Theoretical Study of the Dynamic Plastic Behavior of Beams and Plates with Finite Deflections", Int. J. of Solids and Struct., Vol. 7, 1971, pp.1007-1029.
4. Jones, N., Uran, T.O. and Tekin, S.A., Int. J. of Solids and Struct., Vol. 6, 1970, pp. 1499-1512.
5. Jones, N. and Baeder, R.A., Symposium on Plastic Analysis of Structures, Polytech. Inst. of Jassy, Rumania, Vol. 1, 1972, pp. 476-497.
6. Wojewodzki, W. and Wierzbicki, T., Archives of Mechanics, Vol. 24(4), 1972, pp. 587-604.
7. Faya, M. and Mura, T., Int. J. of Solids and Struct., Vol. 10, 1974, pp. 197-209.
8. Symonds, P.S. and Jones, N., "Impulsive Loading of Fully Clamped Beams with Finite Plastic Deflections and Strain-Rate Sensitivity", Int. J. of Mechanical Sciences, Vol. 14, 1972, pp. 49-69.
9. Hull, T.E., Enright, W.H. and Jackson, K.R., "User's Guide for DVERK- a Subroutine for Solving Non-Stiff ODE's", Dept. of Computer Science, University of Toronto, Technical Report No. 100, Oct. 1976, 36pp.

## THE EFFECT OF GRAIN SIZE ON THE PLASTIC BEHAVIOR OF METALS

by

G. J. Weng  
Department of Mechanics and Materials Science  
Rutgers University  
New Brunswick, New Jersey 08903

A micromechanical theory, taking into account the nature of crystallographic slip in each grain and grain interactions, is proposed to study the effect of grain size on the elastoplastic behavior of metals. First, based on the observations that dislocation pile-ups, formation of cell structures, and other inelastic activities influenced by the presence of grain boundary actually takes place trans-crystallinely, a grain-size dependent constitutive equation is derived for the deformation of slip systems. Using a mixed hardening law [1], this equation is extended to multi-slip. By means of Berveiller and Zaoui's [2] modification of Hill's [3] self-consistent relation, the local stress of a grain is calculated, and used in conjunction with this constitutive equation to evaluate the plastic strain of each constituent grain. The grain-size effect on the plastic flow of polycrystals is then determined by an averaging process. The present theory is finally applied to predict the stress-strain curves of a copper at various grain sizes. The obtained theoretical results were found to be in good agreement with Hansen and Ralph's experimental data [4].

References

1. Weng, G. J., "Dislocation Theory of Work Hardening and Yield Surface of Single Crystals," Acta Mech. 37, 1980, pp. 217-230.
2. Berveiller, M., and Zaoui, A., "An Extension of the Self-Consistent Scheme to Plastically-Flowing Polycrystals," J. Mech. Phys. Solids, 26, 1979, pp. 325-344.
3. Hill, R., "Continuum Micro-Mechanics of Elastoplastic Polycrystals," J. Mech. Phys. Solids, 13, 1965, pp. 89-101.
4. Hansen, N., and Ralph, B., "The Strain and Grain Size Dependence of The Flow Stress of Copper," Acta Metall. 30, 1982, pp. 411-417.

The Yield Surface of Textured Polycrystals, by U. F. Kocks\*, C. Tomé, G. R. Canova, and J. J. Jonas, Dept. of Mining and Metallurgical Engineering, McGill University, Montreal H3A 2A7, Canada.

The plastic anisotropy of polycrystalline materials is due to a nonrandom distribution of the crystallographic orientations of the constituent grains. Such "textures" often have orthorhombic symmetry; for this case, Hill has given a general description of the yield surface in terms of five independent parameters. When the current texture is a consequence of previous deformation, one may postulate that its orthorhombic axes coincide with the principal axes of stress or of strain or strain rate in this previous deformation (presuming these stayed constant). This is not always so. In particular, a study of torsion in materials of the face-centered cubic lattice structure has shown that the orthorhombic axes coincide with the radial, tangential, and axial directions; i.e., the fixed (but non-principal) directions of stress and of strain rate. Moreover, the symmetry is often close to cubic, requiring only 4 dimensions of stress space for a general description of the yield surface, and sometimes "fibrous" (i.e. isotropic perpendicular to one direction), requiring 3 dimensions only. Finally, the axes of higher-than-test symmetry need not coincide with the test axes themselves: the cubic axes for torsion textures are rotated around the axial direction by  $45^\circ$  (while the principal axes are rotated  $45^\circ$  around the radial direction). Some general suggestions for the construction of polycrystal yield surfaces will be given.

\*Visiting Professor, jointly supported by the U. S. Department of Energy. Permanent affiliation: The Center for Materials Science, Los Alamos National Laboratory, Los Alamos, NM 87545.

FINITE ELASTIC-PLASTIC DEFORMATION  
OF POLYCRYSTALLINE AGGREGATES\*

by

T. Iwakuma and S. Nemat-Nasser  
Department of Civil Engineering  
The Technological Institute  
Northwestern University  
Evanston, Illinois 60201

Beginning with the constitutive relations for single crystals at finite strains, and using a generalized self-consistent method in terms of the nominal stress rate and velocity gradient, overall moduli of polycrystalline aggregates are obtained for arbitrary elastoplastic deformations. An interesting feature of the solution is that the overall uniform deformation ceases to be supported by the polycrystal at a certain critical overall strain, leading to possible localized deformations. The results are illustrated in terms of two-dimensional sample problems.

References

1. Nemat-Nasser, S. and Iwakuma, T., "Finite Elastic-Plastic Deformation of Composites," Proc. IUTAM Symp. on Mechanics of Composite Materials, Blacksburg, VA, Aug. 16-19, 1982, Pergamon Press, 1983, to appear.
2. Iwakuma, T. and Nemat-Nasser, S., "Finite Elastic-Plastic Deformation of Polycrystalline Metals and Composites," Earthquake Research and Engineering Laboratory, Tech. Rept. No. 83-3-51, Dept. of Civil Engineering, Northwestern University, Evanston, IL, March 1983.

---

\*This work has been supported by the National Aeronautics and Space Administration under Grant No. NAG 3-134 to Northwestern University.

Large Plastic Deformations  
of a Simply-Supported Cracked Beam  
Under Impact Loading

by

H. J. Petroski and S. Kumar  
Department of Civil and Environmental Engineering  
Duke University  
Durham, North Carolina 27706

Dynamically-loaded beams with sizeable cracks need not fail by brittle fracture if the material is sufficiently tough, but they can fail to function due to excessive permanent lateral displacements. Such a possibility increases with increasing crack size, since the reduced net section will yield at decreasing load levels. This in turn can affect the entire subsequent deformation of the beam and can result in a final deformed configuration different not only in magnitude but also in shape from that expected of an uncracked beam under the same time-dependent loading.

A simple model for a cracked, simply-supported, rigid-perfectly plastic beam has been developed to study the effects of cracks on large plastic deformations resulting from impact loading. This model enables one to make quantitative as well as qualitative comparisons among beams with different size cracks in different locations and under different loading conditions. The presence of a crack not only causes plastic deformation to initiate earlier but also affects the distance through which plastic hinges will travel. This in turn affects the final deformed configuration and maximum displacement of the impacted beam.

As structures are designed to be more and more flaw-tolerant from the point of view of brittle fracture, the failure mode associated with excessive plastic deformation becomes increasingly important. Large cracks developed from fatigue or other mechanisms may have to be assumed present in structures analyzed under dynamic loading simulating accident or seismic circumstances. The questions asked in such analyses may not be whether the structure survives the event intact, but whether it remains in a configuration under which it can continue to be used or operated safely.

The results of preliminary analyses on simple models provide insight into the mechanics of the problem and provide solutions to bench-mark problems for guiding and checking the development of large computational models.

## NEW RESULTS ON THERMO-PLASTIC INSTABILITY IN SIMPLE SHEAR

T. J. Burns\*  
Sandia National Laboratories  
Albuquerque, New Mexico 87185

Several recent theoretical studies of dynamic thermo-plastic instability in simple shear have been based on a perturbation analysis which does not fully take into account the rapid time variation of the underlying deformation process.<sup>1-3</sup> In many problems of this type, appropriate scaling shows that some terms in the differential equations which govern the deformation process are much smaller than others, so that the asymptotic method of multiple time-scales can be used to include the rapid time variation of the simple shearing deformation in the study of its stability to small perturbations. An application is given of this approach to the analysis of the formation of adiabatic shear bands in mild steel, and new results pertaining to this phenomenon are presented.

\*This work performed at Sandia National Laboratories supported by the U. S. Department of Energy under contract number DE-AC04-76-DP00789.

1. Bai, Y. L., "Thermo-plastic Instability in Simple Shear," *J. Mech. Phys. Solids* **30**, 195-207 (1982).
2. Burns, T. J. and Trucano, T. G., "Instability in Simple Shear Deformations of Strain-Softening Materials," *Mechanics of Materials* **1**, (1982).
3. Grady, D. E., "Shock Deformation of Brittle Solids," *J. Geophys. Res.* **85**, 913-924 (1980).

## DYNAMIC BUCKLING OF A RIGID-PLASTIC SHELL:

## A SECOND ORDER DIFFERENTIAL EQUATION SUBJECT TO FOUR BOUNDARY CONDITIONS

E. Zak, U.S. Naval Academy, Annapolis, MD 21402  
 M. A. Veluswami, Indian Institute of Technology,  
 Madras 600036  
 G. Horvay, School of Engineering, University of  
 Massachusetts, Amherst, MA 01003

## SUMMARY

In the case of a Loss-Of-Coolant-Accident (LOCA) an impulsive pressure acts on the core-support-barrel within the nuclear reactor, and the danger arises that the out-of-round shell will buckle. The dimensionless equation governing the growth  $g(t)$  of initial imperfection  $g(\Omega t; n)$  is  $E \{g(t;n)\} g'' - pg' \operatorname{cosec} t - qg - r = 0$  as derived in Horvay-Veluswami [7]. Here  $g$  is amplification,  $t$  time,  $t_{\text{crit}}$  time to failure,  $\Omega$  natural frequency of membrane oscillation.  $t = \Omega(t_{\text{crit}} - t)$  is reversed time, i.e.  $\Omega t_{\text{crit}}$  represents the instant of initiating the impulse,  $t = 0$  the time of collapse.  $p(n)$ ,  $q(n)$ ,  $r(n)$  are functions of material properties, geometry (i.e., dimensions of the shell), and the buckling mode  $n$ ;  $r$  in addition depends also on the loading condition. The mathematical problem: to so solve  $E = 0$  that the boundary conditions be satisfied: (a)  $g(\Omega t_{\text{crit}}) = 1$  (normalization condition), (b)  $g'(\Omega t_{\text{crit}}) = 0$  (zero initial velocity), (c)  $g'(0) = 0$  (zero final velocity), (d)  $g(0) = \text{peak value}$  (solve the  $E = 0$  problem vs  $n$  and then select the value  $n_{\text{crit}}$  for which  $g$  reaches peak value). Note that conditions (c) and (d) are redundant, because when peak value is reached, the velocity is zero. Three methods of solution are considered: (A) Power series expansion (in conjunction with Pade approximants), exceedingly rapid convergence is observed; (B) Cosine series solution, and its pair obtained by the variation of parameters method; (C) Pseudo-Hill analysis. But only (A) is carried to completion, including a numerical confirmation that for the experimental aluminum shell of Vaughan-Florence [4] the results coincide with those of Horvay-Veluswami-Stockton [6] based on time-consuming (and expensive) numerical forward integration, which also requires a passage to  $\infty$  in the number  $N$  of integration steps. Because of the excellence of (A), the traditional method (B) is stopped short of numerical calculations. (C) is outlined in its principal features. While (C) constitutes a fascinating counterpart of the Hill-Mathieu theory, it would primarily reveal behavior of the solution of  $E = 0$  at large negative values of  $t$ , whereas the physical problem terminates at  $t = 0$ ; for this reason no effort was made to carry out the analysis (C), only its principal features are outlined.

This paper represents joint work of the authors while they were associated with the University of Massachusetts, Department of Mathematics, and Department of Civil Engineering, respectively.

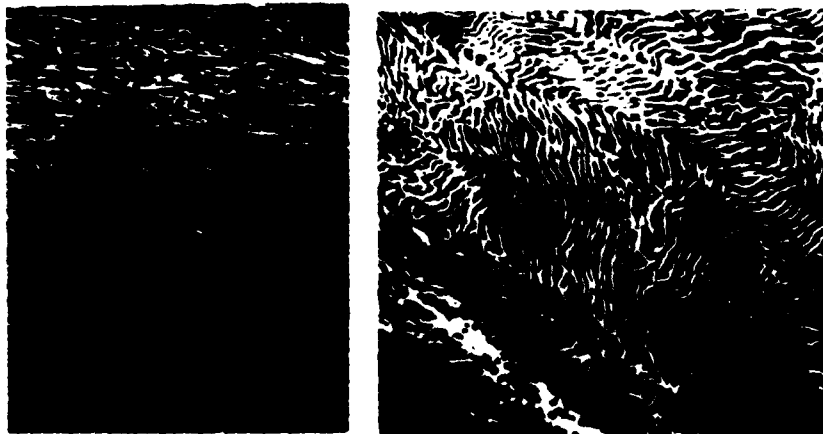
PLASTIC DEFORMATION AND FRACTURE OF THE NEAR  
SURFACE MICROSTRUCTURE

by

H. Ghonem  
Department of Mechanical Engineering  
University of Rhode Island  
Kingston, R.I. 02881

This paper is an attempt to characterize the plastic deformation aspects near surface microstructure of pearlitic rail steel subjected to heavy loading conditions. In the deformed zone of the rail head, aside from the compressive stress resulting from the normal force, the stress applied on the surface is basically of a different character than the one acting on the interior. In addition, the plastic flow of the subsurface layers being highly constrained in relation to that of the surface layer, these layers also possess different microstructures. Such differences manifest themselves in the degree of the severity of deformation pattern exhibited by these layers. In this study the deformed zone has been found to consist of two distinctive layers:

- 1) a fragmented layer having a thickness of 100  $\mu\text{m}$ -1mm consisting of heavily deformed broken "short" lamella, Fig. 1(a). Such a structure was found to consist of a cellular structure which develops during an initial break-in period of the rail surface. Rigney and Hirth [1] have observed that the thickness of this layer would vary with load by some power less than unity.
- 2) a plastically deformed subsurface layer with a thickness of 3-5 mm. This layer Fig. 1(b), under the effect of alternating shear, deforms in an "alternating" pattern while maintaining the integrity of its lamella structure.



(a)

(b)

Fig. 1 (a) Heavily Deformed layer and (b) Plastically Deformed layer

Based on this distinction an analytical work has been carried out to describe the net strain/cycle imposed on the surface layer as well as the effective stress intensity factor for cracks propagating in this layer. To achieve this several assumptions have been made: 1.) The average surface roughness would stabilize after the passage of the first few cycles and thus the magnitude of the coefficient of friction  $\mu$  is a constant. 2.) The extent of wheel material transfer to the rail surface would be extremely limited due to the hardening and the cold working effect of the surface. 3.) the work function of this surface would be in a level that no phase change would occur during the deformation process. When invoking these conditions, a steady state of plastic deformation is assumed to occur in the rail surface and the magnitude of strain,  $\epsilon_t$ , in this surface is considered to be the same for each cycle. This is evaluated as (see Refs. 1 and 2):

$$\epsilon_t = \frac{\mu N}{d \delta b} (\tau_0 + (K/\ell))^{-1} / \text{cycle}$$

where  $d, b$  are the layer thickness and width,  $N$  is the vertical load,  $\tau_0$  is average frictional stress,  $K$  is the Hall-Petch slope and  $\ell$  is the average of the cell size.

Furthermore in this layer and by considering the conditions of mixed loading (resulting from various maximum stresses) the maximum threshold stress intensity factor ( $K_{\max th}$ ) for crack propagation in the heavily deformed layer can be written as

$$K_{\max th} = 2\sigma \sqrt{a_{th}/\pi} + 0.8\tau \sqrt{\pi a_{th}}$$

where  $\sigma$  is the sum of longitudinal tensile stresses and  $\tau$  is the maximum shear stress. Experimental bi-axial tests are carried out to verify the above equations, for details see Ref.(2)

#### References

1. Rigney, D.A., and Hirth, J.P., "Plastic Deformation and Sliding Friction of Metals," *Wear*, 53, 1979.
2. Ghonem, H., and Kalousek, J., "Plastic Deformation and Fracture of Pearlitic Structure," *Journal of Material Science and Engineering*, to be published.

## INELASTIC BUCKLING OF SANDWICH PLATES

by

S.C. Shrivastava and Y.H. Wong

Department of Civil Engineering and Applied Mechanics  
817 Sherbrooke St. W.  
McGill University, Montreal, Que., Canada H3A 2K6

This paper deals with the buckling of flat rectangular solid core sandwich plates subjected to uniaxial compression beyond the elastic limits of the component materials. The analysis is based on the concept of bifurcation of equilibrium, and is done for material behaviour according to both the incremental and deformation theories of plasticity, assuming isotropic hardening and the von Mises yield condition. The moduli used in the inelastic range, when buckling occurs, are based on Shanley's concept of continued loading.

The formulation is based on kinematic assumptions [1], rather than on stress assumptions [2,3]. The approach is analytical and considers buckling of the plates with two cases of support conditions: (a) simple supports on all four sides, and (b) simple supports on three sides and no support on the fourth side. Furthermore, the investigation considers the two choices of what may be called simple support condition. These have not been previously investigated. It is shown that the alternative choices lead to important differences in the buckling loads of the sandwich plates supported on three sides.

Buckling charts, based on 24S-T5 aluminium alloy as facing plates and balsa wood as core material, are presented for design purposes. The analysis is also suitable for investigating elastic buckling of sandwich plates.

## REFERENCES

1. Shrivastava, S.C., "Inelastic Buckling of Plates Including Shear Effects," International Journal of Solids and Structures, Vol. 15, 1979, pp. 567-575.
2. Libove, C., and Batdorf, S.B., "A General Small Deflection Theory for Flat Sandwich Plates," NACA Report, No. 899, Sept. 1947.
3. Seide, P., and Stowell, E.2., "Elastic and Plastic Buckling of Simply Supported Solid-Core Sandwich Plates in Compression," NACA Report, No. 967, Dec. 1948.

## HYDRODYNAMIC MODELS OF FLUIDIZATION

by

Dimitri Gidaspow  
Department of Chemical Engineering  
Illinois Institute of Technology  
Chicago, IL 60616

ABSTRACT

Fluidized beds are ideal for gasifying coal due to high rates of heat and mass transfer and solids mobility. However, one of the largest concerns when using fluidized beds to commercialize many chemical processes, such as gasification of coal, in scale-up. We believe this is due to the absence of an experimentally verified hydrodynamic theory that can describe the complicated transient gas and solid motion in a fluid bed. During the past few years several organizations began to develop hydrodynamic computer models that promise to be predictive in many respects.

Our present computer calculates the pressure, the void fraction and the velocities of a single size solid and of the gas. Computed time averaged porosity distributions in two dimensional beds with a jet agreed with our measurements without the use of any fitted parameters. [1] Photographically determined bubble sizes compared well with the predicted sizes. [2] Calculated gas velocity distributions also agreed with the experimental values measured at Westinghouse in a semi-circular bed with a jet. [3] Our model also predicts the high values of the heat transfer coefficients in a fluidized bed without the use of any turbulence in the model. [4] Previous hydrodynamic theories of wall to bed heat transfer used mixing lengths theories as an additional transfer mechanism.

We are in the process of comparing several competing hydrodynamic two phase flow models and of extending one of the models to several particle sizes and to hot bed gasification conditions to better understand the transport processes. Preliminary results show a good comparison of computed gas compositions and those observed in the IGT U-GAS process. [5]

References Cited

1. Gidaspow, D. and B. Ettehadieh, "Fluidization in Two Dimensional Beds with a Jet. 2. Hydrodynamic Modeling" *I&EC Fundamentals* 22, 1983, pp. 193-201.
2. Gidaspow, D., Y.C. Seo and B. Ettehadieh, "Hydrodynamics of Fluidication: Experimental and Theoretical Bubble Sizes in a Two Dimensional Bed with a Jet" *Chem. Eng. Communications*, in press, 1983.
3. Ettehadieh, B., D. Gidaspow and R.W. Lyczkowski, "Hydrodynamics of Fluidization in a Semi-Circular Bed with a Jet" *AICHE Journal*, submitted (1982).

4. M. Syamlal and D. Gidaspow, "Hydrodynamics of Fluidization: Prediction of Wall to Bed Heat Transfer Coefficients" to be presented at the 21st ASME/AICHE National Heat Transfer Conference, Seattle, Wash., July 1983.
5. Institute of Gas Technology (IGT), "Technical Support Studies" Prepared for U.S. Department of Energy under contract No. ET-77-C-01-2582, November (1979).

#### ACKNOWLEDGEMENT

This work was supported by the National Science Foundation under grant No. CPE 8209290.

by

M. C. Roco  
 Department of Mechanical Engineering  
 University of Kentucky

The flow of the polydisperse systems can be modeled assuming either the continuum medium, separate component motion with interactions or applying volume averaging approach. In this paper, results obtained for liquid-solid flows using the last approach are presented and compared to experimental data in horizontal and inclined pipes.

The local volume-time averaging of the momentum and energy equations for turbulent two-phase flow yields specific terms caused by the spacial nonuniformities. The averaging volume was chosen as a stream tube of length equal to the local scale of turbulence [1]. The contributions of the new terms increase with the solid concentration and the ratio particle size/length scale of turbulence, as well as with the particle cluster grow in sheared suspensions. The effect of the random dispersion of the flow components in space on the volume averaging terms is analogous to the influence of the time nonuniformities on the Reynolds shear stresses.

The specific interactions between the solid particles in flowing suspensions (collisions, Coulombic contacts, mixing effects) are identified in the space/time averaged momentum equations. The corresponding terms can be related to the local turbulence parameters and computational procedures are derived based on experimental results. By supported load is defined the mass force of that fraction of solid particles which is supported through Coulombic contact with other solid particles or directly on a wall. The dispersive stress is defined as the normal repulsive stress between neighboring sheared layers of suspensions due to particle collisions. This stress is given by the composed average of the fluctuating concentration multiplied by the fluctuating kinetic energy,  $\sigma_{DS_i} = C' \cdot (U_{Si}^2/2)^{1/2}$  (where  $C'$  is the fluctuating concentration and  $U_{Si}$  the local instantaneous velocity of solids in the  $i$  direction). The experimental results show the dispersive and supported load stresses at any point are dependent on a modified Froude number,  $Fr_* = (\rho_L/\rho_M) \cdot V_*^2/a \cdot d \cdot (S-1)$  (where  $\rho_L$  and  $\rho_M$  are the liquid and mixture densities,  $V_*$  - friction velocity,  $a$  - specific mass force including the gravitational acceleration,  $d$  - particle diameter,  $S$  - solid specific density). The concept of the "equivalent length in fluid" is proposed to express the dynamic influence of solid particles on the local flow indices used in diffusion and convective terms.

A mixture of a newtonian fluid with a species of solid particles is initially considered for tests. The numerical

code is applied for horizontal pipes, as well as for pipes with positive and negative slopes. Experimental results performed with coal ( $S = 1.3$ ), ash ( $S = 2.3$ ), sand ( $S = 2.65$ ) and copper concentrates ( $S = 3.5$ ) in circular and rectangular slurry pipes were compared to the numerical model predictions. In Table I are illustrated the flow parameters of the experiments with water-sand mixture in circular pipes.

Table I. Experimental tests with water-sand mixtures in pipes

Particle diameter d (mm)	Pipe diameter D (mm)	Slope (-)	Concentration (% by vol.)	Velocity (m/s)
.165/.52	51.5/263/495	0	0-34.1	1.66-4.53
.36	80/100/152	$-\pi/6$ to $+\pi/6$	0-40.0	.5 - 3.9
13	158.5	0	0-35.0	2.0 - 4.2

The importance of the various interaction terms in the governing equations depends on the flow regime. For instance, at low velocities close to critical values the supported load is significant, and in flows with large shear stresses the dispersive stress become more important [2].

The local volume-time averaging of the conservation equations improves the accuracy of the polydisperse flow modeling compared to other commonly applied approaches. The shape and dimension of the averaging volume should be adapted to the modeled flow. In the case of a two-phase turbulent flow, the averaging should be made over a "macro-volume", which would include the specific macro-turbulent structures and the particle cluster formations.

#### References

1. Roco, M.C., "Space/Time Averaged Equations for Multi-component Turbulent Flows", Polyphase Forum, ASME, June 1983.
2. Roco, M.C. and Shook, C.A., "Modeling Slurry Flow for Different Particle Dimensions", Can. J. Chem. Engr., 1983 (in press).

#### Acknowledgements

The support received from National Science Foundation Grant CPE 8205217 is gratefully acknowledged.

PRACTICAL CONSEQUENCES OF ILL-POSED TWO-PHASE  
FLOW FIELD EQUATIONS

by

Robert. W. Lyczkowski  
Argonne National Laboratory  
Components Technology Division  
9700 South Cass Avenue  
Argonne, Illinois 60439

By now it is well appreciated that there are many two-phase flow models in the open literature<sup>(1)</sup>. Most of them are highly non-linear and thus must be solved by numerical methods<sup>(2)</sup>. There have been remarkably few attempts to verify these models by examining their basic physical character<sup>(3)</sup>. This process is necessary because, as it is now well-known, that with zero internal shear, many of the models possess complex characteristics in one dimension and are thus, by definition, ill-posed as initial-value problems<sup>(4)</sup>. The full implications are not completely agreed upon. To some, the question of ill-posedness may appear to be of mere academic interest, a subject to be debated extensively without full cognizance of the practical consequences<sup>(5)</sup>. The purpose of this paper is to clearly show through definite examples the connection between the stability of the field equations and the stability of the difference equations for a set of ill-posed two-phase flow equations. It is hoped that the demonstration of catastrophic numerical instability will convince theoreticians and those attempting to solve such equations by implicit and explicit numerical methods, that some remedies must be sought before two-phase flow becomes an exact science.

REFERENCES

1. R. W. Lyczkowski, Dimitri Gidasow, and C. W. Solbrig, "Multiphase Flow Models for Nuclear Fossil and Biomass Energy Conversion," in Advances in Transport Processes, Vol. 11., pp. 198-351, A. S. Mujumder and R. A. Mashelkar Eds., Wiley Eastern Ltd., New Delhi, 1982.
2. R. W. Lyczkowski, and W. T. Sha, "Foundations of Rational Multiphase Flow and Heat Transfer Field Equations," in Advances in Computer Methods for Partial Differential Equations - IV, pp. 160-167, R. Vichnevetsky and R. S. Stepleman, Eds., INACS, Rutgers University, New Brunswick, New Jersey, 1981.
3. W. H. Lee and R. W. Lyczkowski, "The Basic Character of Five Two-Phase Flow Model Equation Sets," in Advance in Mathematical Methods for the Solution of Nuclear Engineering Problems, pp. 489-511, American Nuclear Society, La Grange Park, IL., 1981.
4. R. W. Lyczkowski, D. Gidasow, C. W. Solbrig, and E. D. Hughes, "Characteristics and Stability Analyses of Transient One-Dimensional Two-Phase Flow Equations and their Finite Difference Approximations," Nucl. Sci. and Eng. 66, No. 3, pp. 378-396, June 1978.
5. Y. Zvirin and R. B. Duffey, Eds., EPRI Workshop Proceedings: Basic Two-Phase Flow Modeling in Reactor Safety and Performance, Electric Power Research Institute WS-78-143, Vols. I and II, Palo Alto, March 1980. Also Int. J. Multiphase Flow, 6, Nos. 1-2, 1980.

FRICION AND VOID FRACTION MEASUREMENTS IN  
TWO PHASE FLOW USING FREON RF114

by

P. F. Maeder, Professor of Engineering  
Brown University  
Providence, Rhode Island 02912

ABSTRACT

The new freon facility at Brown University is used to measure pressure, temperature and void fractions in Freon RF114 at speeds in the highly compressible range ( $.5 < M < 1$ ). The apparatus has a 5cm diameter test section, 8 meters long and can be oriented both horizontally and vertically. It is operated intermittently with running times of approximately 2 minutes and is instrumented for rapid measurements using a data acquisition system with a HP85 as controller/computer.

If one investigates the conditions of thermodynamic flow similarly between different substances in two phase flow, one finds that the latent heat of evaporation is the principal controlling parameter. Thus, a 5cm test section in two phase RF114, at room temperature, corresponds to a 30cm diameter pipe in water/steam at boiling conditions at reasonably high temperature such as encountered in industrial systems and geothermal wells.

Pressure loss measurements were performed by both pressure and temperature probes. The agreement was excellent, suggesting mechanical and thermal equilibrium across the test section; even though the slip between phases is considerable.

Void fraction (holdup) measurements were performed using two techniques. The conventional rapid closing valve method and a newly proposed method using the measurement of the average dynamic pressure by inserting cylindrical probes. Agreement with data in the published literature is acceptable.

Analysis by means of the two fluid model suggests that the coupling or interface term between phases is the important quantity and needs further detailed investigation. It is expected that this term will depend greatly on the Mach number, Froud number and Reynolds numbers of this highly compressible two phase flow, thus giving rise to the various flow patterns observed.

P. F. Maeder  
February 28, 1983

TPF-1 Upstream Flashing and Critical Flow in Nozzles:  
1 - Equilibrium View

by

Owen C. Jones, Jr.  
Professor of Nuclear Engineering

and

Tai-Sung Shin  
Graduate Student  
Rensselaer Polytechnic Institute  
Troy, New York 12181

Collins [1] examined choked two-phase flows in nozzles with subcooled inlet conditions (the term subcooled critical flow or SCF shall be used herein) from an isentropic homogeneous equilibrium (IHE) viewpoint, concluding that in some cases choking could occur with a liquid velocity at a quality of  $x = 0^-$  substantially greater than the sonic velocity immediately on the two-phase side of the saturation line,  $x = 0^+$ . Flashing inception superheat was later investigated by Alamgir and Lienhard [2] and by Jones [3]. Abuaf, Jones, and Wu [4,5] then demonstrated that these results could be used to accurately (within ~5%) predict SCF's. It is the purpose of this paper to show how the IHE model can be utilized to qualitatively predict the observed behavior and to evaluate the validity of Collins' theory.

Considering downstream two-phase expansion of SCF's, an obvious restriction is that there must be sufficient energy to allow the expansion to occur. Thus,

$$\left. \frac{\partial v}{\partial p} \right|_{s,E} > \left. \frac{\partial v}{\partial p} \right|_{s,C} \quad (1)$$

where E and C refer to energy and continuity, and s indicates the isentropic condition. Taking the energy equation as  $v = \sqrt{2(h_0 - h)}$  results in

$$\left. \frac{\partial v}{\partial p} \right|_{s,E} = - \frac{v}{c} \quad (2)$$

whereas with  $\dot{m} = \rho_p A v$  for the continuity equation one obtains

$$\left. \frac{\partial v}{\partial p} \right|_{s,C} = - \left[ \frac{\partial v}{c^2} + \frac{v}{A} \frac{dA}{dp} \right] \quad (3)$$

Here,  $v$  is velocity,  $A$  is area,  $h$  is enthalpy,  $p$  is pressure,  $s$  is entropy,  $v$  is specific volume, and  $c$  is defined in the usual manner. For compatibility, the equality in (1) must apply so that  $dv|_E = dv|_C$  and with  $M$  the Mach number defined as usual

$$\frac{dA}{dp} = \frac{vA}{v^2} [1 - M^2] \quad (4)$$

indicating exactly the behavior one expects in single-phase compressible flow. These results clearly indicate,

$v_{1\phi} \leq c_{2\phi}(x = 0+)$ , the equality indicating inception at the throat, the only single-phase throat condition allowing flashing expansion rather than pressure recovery to occur downstream, depending on the back pressure. This places restrictions on the combination of conditions which can be obtained between saturation, back and stagnation pressures. With decreasing inlet pressure the flashing inception moves upstream of the throat but the "sonic" condition remains squarely at the minimum area location. This decreases the critical flow rate. The flow rate parameter  $v^* = \dot{m} / \rho_c A^*$  is plotted against the location where flashing inception begins,  $A_f/A^*$  in Figure 1. The critical flow first decreases then becomes asymptotically a constant as  $A_f/A^*$  increases, the initial decrease being restricted to inception area ratios closer to unity as saturation pressure decreases. At any saturation pressure, then, there can be a range of possible "critical" flows depending on the combination of conditions. The saturation pressure is one additional variable not encountered in single-phase flow considerations.

In conclusion, it has been shown that in the IHE model, subcooled inlet flows are limited to those flows which, as in single phase flow, yield the sonic condition at the throat, and that a range of critical flows are thus achieved depending on the location of flashing inception. It has further been found that at low pressure (Figure 1), if the upstream stagnation pressure or subcooling is slowly decreased the flow rate would decrease by only a small amount with almost no change in the location of flashing inception. Then, a slight additional change would cause the inception point to jump almost immediately to the inlet. This is exactly what was encountered in practice [4,5].

#### References

- [1] Collins, R. L., "Choked Expansion of Subcooled Water and the I.H.E. Flow Model," Trans. ASME, J. Heat Trans., 100, pp. 275-280.
- [2] Alamgir, Md., and Lienhard, J. H., "Correlation of Pressure Undershoot During Hot Water Depressurization," Trans. ASME, J. Heat Trans., 103, pp. 52-55, 1981.
- [3] Jones, O. C., "Flashing Inception in Flowing Liquids," Trans. ASME, J. Heat Trans., 102, pp. 439-444, 1981.
- [4] Abuaf, N., Jones, O. C., and Wu, B. J. C., "Critical Flashing Flows in Nozzles with Subcooled Inlet Conditions," in Polyphase Flow and Transport Technology, R. A. Bajura, Ed., Proc. ASME Sym. on Polyphase Flow and Transport Technology, San Francisco, August 13-15, 1980.
- [5] ibid. Trans. ASME, J. Heat Transfer, in press.

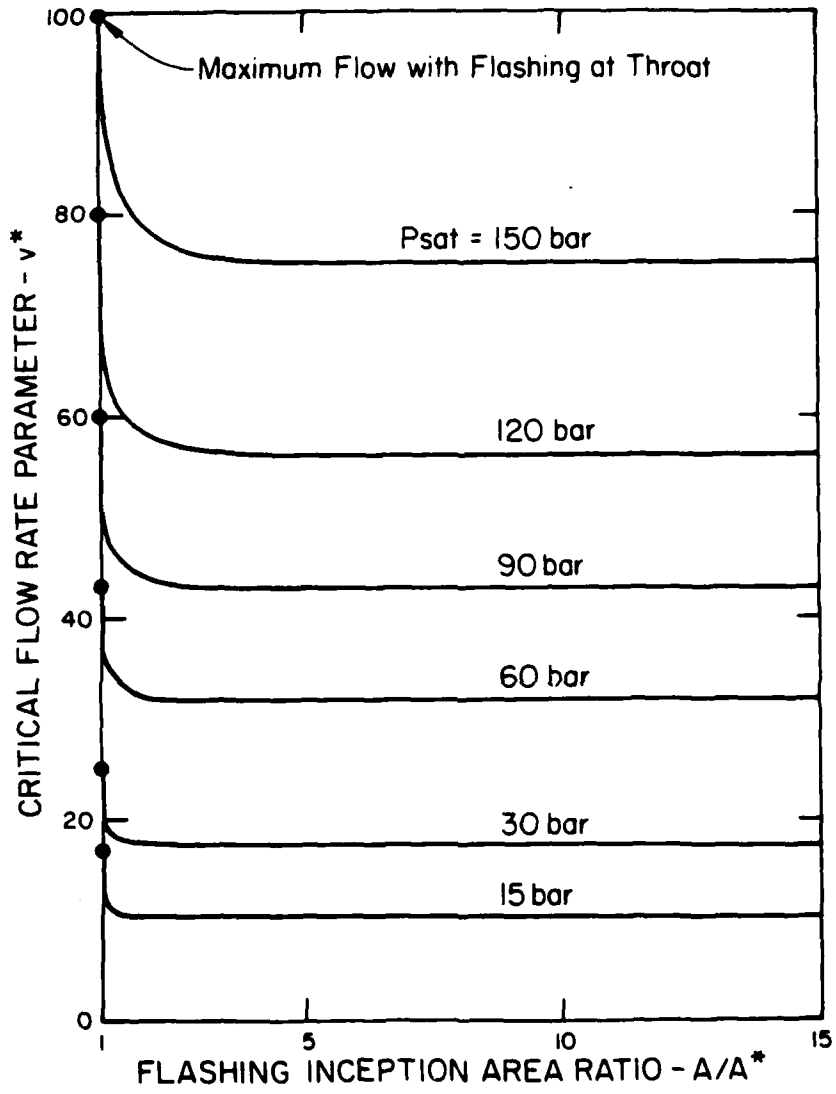


Figure 1. Behavior of Mass Flux in Two-Phase Critical Discharge of Water from Nozzles with Subcooled Inlets--IHE Model

Numerical Studies of Two-Phase Flow  
Instabilities in a Boiling System

by

Flavio Dobran  
Dept. of Mechanical Engineering  
Stevens Institute of Technology  
Hoboken, NJ 07030

Juan I. Ramos  
Dept. of Mechanical Engineering  
Carnegie-Mellon University  
Pittsburgh, PA 15213

A homogeneous two-phase flow model which accounts for inlet subcooling, thermal capacity of the heater wall, compressible capacities and exit pressure drop has been numerically studied in order to access the influence of inlet subcooling, mass flow-rate and heat flux on the steady state and dynamic characteristics of a single channel boiling system. The numerical scheme utilizes an explicit second order accurate predictor-corrector method which employs upwind differences for the convection terms in the predictor step and downwind differences in the corrector step. The numerical studies of single channel boiling system predict the pressure drop and density wave oscillations. Stable and unstable regions of these oscillations have been identified and the results are found to agree well with the experimental data and with the previous numerical study of Dogan, Kakac and Veziroglu [1] who used an explicit first order accurate finite difference algorithm.

References

1. T. Dogan, S. Kakac, and T.N. Veziroglu, Lumped Parameter Analysis of Two-Phase Flow Instabilities, Proc. 7th International Heat Transfer Conference, Vol. 5, Hemisphere, New York, 1982, pp. 213-218.

EXPERIMENTAL STUDY OF BOILING FLOW  
INSTABILITIES IN AUGMENTED SINGLE CHANNELS

A. Menteş<sup>†</sup>, O.T. Yıldırım, S. Kakaç, T.N. Veziroğlu  
and Long-quan Fu\*  
University of Miami  
Coral Gables, Florida 33124

The effect of different heat transfer augmentations on two-phase flow instabilities has been investigated in a single channel, forced convection, open loop, up-flow system. Freon-11 is used as the test fluid and six different heater tubes with various inside surface configurations have been tested at five different heat inputs. Two major modes of oscillations, namely density-wave and pressure-drop type oscillations, have been observed. Stable and unstable regions are determined on system pressure drop versus mass flow rate plots for various values of heat input rates. Comparison of different heater tubes is made by the use of the stability boundary maps and the plots of inlet throttling necessary to stabilize the system versus mass flow rate. The oscillations have also been recorded for various values of inlet temperature to study the effect on inlet subcooling on sustained instabilities with heat transfer augmentation. The experimental set-up shown in Fig. 1 consists of three basic parts: fluid supply section, test section and a fluid recovery section. Test section includes a surge tank, control valve, heater section and ends with a sharp-edged orifice. Heater section houses the heater tube in a vacuum jacket. All heater tubes are made of 7.493 mm inside, 9.525 mm outside diameter and 605 mm long Nichrome tubes. Tube A is a bare tube; tube B is internally threaded; C, D and E are inserted with springs of different wire diameters and pitches. The last tube, F, was coated with Union Carbide Linde High Flux Coating. Freon-11 is used as the test fluid. The whole boiling range, from single phase liquid to high qualities has been covered during the experiments. Pressure and temperature readings and recordings have been taken at different heat inputs and mass flow rates. Highspeed photography has also been used during some of the experiments. Graphs of system pressure drop versus inlet mass flow rate and additional inlet pressure drop necessary to stabilize the system versus inlet mass flow rate are used to examine the experimental results. Stability boundaries are shown on system pressure drop versus inlet mass flow rate plots and on graphs of heat input versus inlet mass flow rate. Heater tubes with internal springs have been found to be more stable than the other three tubes. The coated tube has been found more unstable over a wider range, however, the oscillations have been milder. Among the tubes with internal springs, stability increases with decreasing effective inside diameter, which is defined as  $\sqrt{4V/\pi L}$ , where V is the net inside volume and L is the length of the heater tube. Films taken during the oscil-

<sup>†</sup>On leave from the Middle East Technical University, Ankara, Turkey

\*On leave from Shanghai Electric Power Institute, Shanghai, China

lations show that flow regime has been changing from single phase liquid to mist flow during a cycle of pressure-drop oscillations, and annular flow and mist flow regimes have been dominant during the density-wave type oscillations and during the pressure-drop type oscillations with superimposed density-wave type oscillations[1].

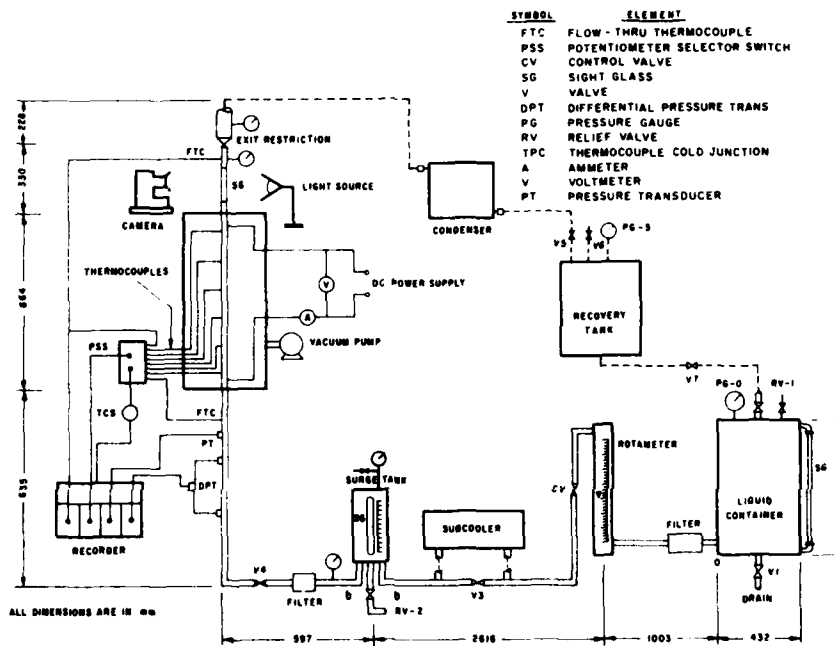


Figure 1 Schematic Drawing of the Experimental System

References

1. Veziroglu, T.N. and Kakac, S., Two Phase Flow Instabilities, Final Report, NSF Project CME 79-20018, 1983

TWO-PHASE FLOW INSTABILITIES IN BOILING FLOWS:  
SUMMARY REVIEW

by

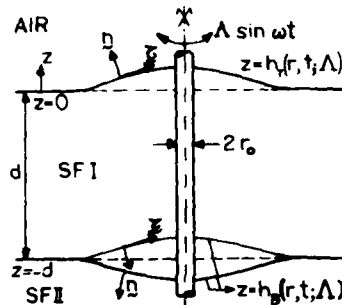
S. Kakaç  
University of Miami  
Coral Gables, Florida, U.S.A.

Boiling flow instability is a problem of great current interest in many heat transfer applications, ranging from nuclear reactors to refrigeration systems. Such an instability is detrimental to satisfactory operation of boiling flow systems. In this paper, the experimental and theoretical work carried out over a period of several years on single and parallel channel systems are summarized, demonstrating and explaining three different types of two-phase flow oscillations, namely, density-wave type, pressure-drop type oscillations and thermal oscillations, encountered in various boiling flow channel systems. Classification of two-phase flow instabilities is summarized first. Three distinct types of two-phase flow oscillations and their mechanisms are explained. Since 1950's with the beginning of commercialization of nuclear reactors, the interest in two-phase flow instability studies started to grow in the western countries followed by the Soviet Union and China. Hence, in this paper, the most available work to our knowledge is cited. The results of our experimental work on transient and sustained instabilities in single, double channel, cross-connected double channel, four parallel channel and four cross-connected parallel channel upflow systems are presented. The effects of heat flux variations, inlet subcooling, flow rate, inlet and exit restrictions are indicated. The effect of heat transfer augmentation on two-phase flow instabilities in a vertical single channel is also included. Numerical models which are based on the assumption of homogenous two-phase flow and thermodynamic equilibrium of the two phases to predict both the steady state and transient behavior of forced convection boiling upflow two-phase flow in a single channel are summarized and some of the results of these solutions are presented. Two different two-phase flow models, namely a constant-property homogeneous flow model and a variable property-flux model which are used for the prediction of the pressure-drop and density-wave instability thresholds in a single boiling channel upflow system are mentioned and some of the solution results are presented.

Aydeniz Siginer  
Department of Engineering Mechanics  
The University of Alabama  
University, Alabama 35486

This paper presents the results of an analytical investigation of the shapes of the free surface and the interface of two layers of non-Newtonian fluids set into time periodic motion driven by a vertical, cylindrical rod oscillating with amplitude  $\Lambda$  in a large vat. The results may be used in free surface viscometry to find the form of the material functions in order to specify the response of a simple fluid of integral type in all motions of small amplitude.

The analysis is set within the framework of Noll's concept of simple fluids. An algorithm developed by Joseph [1] for the computation of unsteady motions of a simple fluid is used together with the theory of domain perturbations which involves the simultaneous perturbation of the field equations and the unknown flow domain  $\mathcal{P}_\Lambda$ . The solution is supposed to be known in some known domain  $\mathcal{P}_0$  and the solution in the unknown physical domain  $\mathcal{P}_\Lambda$  is expressed as a series in  $\Lambda$  whose coefficients are the substantial derivatives evaluated in  $\mathcal{P}_0$ . The stress is expressed as a series of multiple integrals of polynomials in the histories of the motion. That representation becomes for a fluid of integral type of order two:



$$\underline{S} = \int_0^\infty \zeta(s) \underline{G}(s, \Lambda) ds + \int_0^\infty \int_0^\infty (\beta(s_1, s_2) \underline{G}(s_1, \Lambda) \underline{G}(s_2, \Lambda) + \alpha(s_1, s_2) [\text{tr} \underline{G}(s_1, \Lambda)] \underline{G}(s_2, \Lambda)) ds_1 ds_2,$$

The integral representation is assumed to be Fréchet differentiable and is expanded in a series in terms of the perturbation parameter  $\Lambda$ . The solution requires the computation of the canonical forms of the Fréchet stresses which arise at first and second orders. The inherent difficulty of the problem is the monitoring of the history of the deformation. The computation of the histories in the integral representation of the stress requires the substantial derivatives of the position vector of a given particle and of the Rivlin-Ericksen tensors evaluated at any past time.

The field equations which govern the motion are:

$$\rho_I (\underline{u}_t + \underline{u} \cdot \nabla \underline{u}) = -\nabla \phi_I + \nabla \cdot \underline{S}_I, \quad -d < z < h(r, t; \Lambda) \text{ in } \mathcal{P}_\Lambda,$$

$$\rho_{II} (\underline{u}_t + \underline{u} \cdot \nabla \underline{u}) = -\nabla \phi_{II} + \nabla \cdot \underline{S}_{II}, \quad -\infty < z < -d \text{ in } \mathcal{P}_\Lambda,$$

$$\mathcal{V}_\Lambda = \{r, z, t | r_0 \leq r < \infty, -\infty < z \leq h(r, t; \Lambda)\} .$$

Boundary and asymptotic conditions are:

$$u(r_0, z, t) = \Lambda r_0 \sin \omega t ,$$

$$\underline{u}(r, z, t; \Lambda), \underline{\phi}(r, z, t; \Lambda), \underline{S}(r, z, t; \Lambda) + \underline{u}(r, t; \Lambda), \underline{\phi}(r, t; \Lambda), \underline{S}(r, t; \Lambda) \text{ as } z \rightarrow -\infty ,$$

$$\underline{u}(r, z, t; \Lambda), \underline{S}(r, z, t; \Lambda) \rightarrow 0 \text{ as } r \rightarrow \infty .$$

Shear tractions  $S_{nT}, S_{n\theta}$  across the free surface and the interface are continuous,

$$S_{n\theta} = S_{z\theta} - h_{i,r} S_{r\theta} , \quad S_{nT} = h_{i,r} (S_{zz} - S_{rr}) + (1 - h_{i,r}^2) S_{rz} , \quad i=T, B$$

$$(S_{n\theta})_I = 0, \quad (S_{nT})_I = 0 \quad \text{on } h_T ,$$

$$(S_{n\theta})_I = (S_{n\theta})_{II}, \quad (S_{nT})_I = (S_{nT})_{II} \quad \text{on } h_B .$$

No fluid crosses the free surface or the interface,

$$w = h_{i,t} + u h_{i,r} = 0 \quad i=T, B .$$

The jump in the normal stress is balanced by surface tension,

$$-p_I + S_{Inn} + p_a = \frac{T_T}{r} (r h_{T,r} / \sqrt{1 + h_{T,r}^2})_{,r} \quad \text{on } h_T ,$$

$$-p_I + S_{Inn} - p_{II} - S_{IIInn} = -\frac{T_B}{r} (r h_{B,r} / \sqrt{1 + h_{B,r}^2})_{,r} \quad \text{on } h_B$$

The last two equations define the shape of the free surface and the interface. They may be solved, subject to contact angle boundary conditions, for the mean free surface or interface height if all the other variables are defined in terms of mean quantities independent of time.

The use of correct coupling conditions between the layers of immiscible, non-Newtonian fluids yield uncoupled flows in each layer at the 1st and 2nd orders of the perturbation analysis pivoted around the rest state. We find that at 1st order particles move in circles with no pressure field and height rise. At 2nd order, the motion is decomposed in each layer into a mean term and a time periodic term. There is no motion in the mean at the 2nd order and we find a non-trivial pressure field. The mean height rise at the free surface and the interface is determined in terms of the material functions. Further details of the analysis are given in (2).

(1) Joseph, D.D., Stability of Fluid Motions, Chap. XIII, Vol. I, Springer Tracts in Natural Philosophy, 1976.

(2) Siginer, A., Unconfined Flow of Two Layers of Simple Fluids Driven by an Oscillating Rod, forthcoming.

## ABSTRACT

Two-phase Flow Scaling Criteria and Its Application  
to Integral Test Facilities

by

M. Ishii, RAS, ANL  
G. Kocamustafaogullari, Univ. of Wisconsin at Milwaukee  
I. Kataoka, Institute of Atomic Energy, Kyoto Univ.

Scaling criteria for a forced and natural circulation loop under two-phase flow conditions are derived. The scaling laws for forced convection single phase flow have been well established and modeling using these criteria has long been an accepted practice. However, the similarity analysis for a natural circulation system particularly under two-phase flow conditions is much more complicated due to the coupling of the driving force and heat transfer as well as due to two-phase thermal-hydraulics. The flow condition can only be determined by the integral effects of heat transfer and flow processes along an entire loop. Therefore, in order to develop meaningful similarity criteria, it is necessary to consider these integral effects through some forms of simplified solutions to the balance equations.

For a single phase case the mass, integral momentum, and energy equations in one-dimensional area averaged forms are used in the present analysis. From this, geometrical similarity groups, friction number, and heat source number are obtained. The Biot number involves the heat transfer coefficient which may cause some difficulties in simulating the turbulent flow thermal boundary layer. For a two-phase flow case, the similarity groups are obtained from a perturbation analysis based on the one-dimensional drift-flux model. The physical significance of the resulting phase change number, subcooling number, drift-flux number, and friction number are discussed and conditions imposed by these groups are evaluated. The above similarity criteria are simplified to design purpose scaling laws for simulation experiments. These results are applied to some of the existing and planned large scale test facilities. Some preliminary conclusions on these facilities in terms of the proper scaling are obtained.

## ON WAVE PROPAGATION IN RANDOM PARTICULATE COMPOSITES

by

Abraham I. Beltzer  
Holon Technological Institute, P.O. Box 305, Holon 51802, IsraelCharles W. Bert and Alfred G. Striz  
School of AMNE, University of Oklahoma, Norman, OK 73019

A new method is presented for the analysis of wave propagation in random particulate viscoelastic composites. This method yields a convenient means for the extension of static results to the dynamic case. Previous approaches to the problem have included equating the scattered field in the composite to that due to a deformable sphere of the effective homogeneous material [1] or the use of the dynamic analog of the Reuss rule of mixtures [2]. The method systematically introduced in this paper incorporates losses due to scattering, viscoelastic losses, and the Kramers-Kronig relations valid for any causal linear system to compute the wave speed [3]. The basic equations for the general case of a viscoelastic composite are deduced and a viscoelastic matrix with the linear law of attenuation is considered. An advantage of the method is the possible incorporation of any theoretical or empirical value for the non-dispersive velocity. By accounting for the cut-off frequency effect, the theory is shown to give good agreement with experimental results [4, 5] for both wave attenuation and dispersion in a glass-filled epoxy composite.

- [1] Kligman, R.L., Madigosky, W.M., and Barlow, J.R., "Effective Dynamic Properties of Composite Viscoelastic Materials," J. Acoust. Soc. Am., 70, 1981, pp. 1437-1444.
- [2] Junger, M.C., "Dilatational Waves in an Elastic Solid Containing Lined, Gas-Filled, Spherical Cavities," J. Acoust. Soc. Am., 69, 1981, pp. 1573-1576.
- [3] O'Donnell, M., Jaynes, E.T., and Miller, J.G., "Kramers-Kronig Relationship Between Ultrasonic Attenuation and Phase Velocity," J. Acoust. Soc. Am., 69, 1981, pp. 696-701.
- [4] Kinra, V.K., Petraitis, M.S., and Datta, S.K., "Ultrasonic Wave Propagation in a Random Particulate Composite," Int. J. Solids Structures, 16, 1980, pp. 301-312.
- [5] Kinra, V.K. and Anand, A., "Wave Propagation in a Random Particulate Composite at Long and Short Wavelengths," Int. J. Solids Structures, 18, 1982, pp. 367-380.

A MONTE-CARLO/GEOMETRIC RAY TECHNIQUE  
FOR WAVE PROPAGATION IN PLATES

by

Davis M. Egle and Joseph Ewumi  
School of Aerospace, Mechanical and Nuclear Engineering  
The University of Oklahoma  
Norman, Oklahoma 73019

Interest in wave propagation in plates in recent years has been sparked by attempts to understand the relationship between detected acoustic emission signals and the nature of the sources causing the disturbances. A plate is the simplest geometry which is both amenable to theoretical analysis and suitable for experimental work. Although our long range goal is the development of a technique suitable for the analysis of acoustic emission events in more complicated geometries, the plate is a logical starting place.

Pao and associates [1-3] have been applying the generalized ray theory to the analysis of wave motion in plates with this objective in mind as well as applications in geophysics. As noted by Pao, the generalized ray technique involves evaluating rather complex integrals along all of the paths traced by the multiplicity of rays that may contribute to the disturbance. The technique is considered to be exact but is generally limited to near-field solutions because of the increasing number of complex integrals to be evaluated as the observation point moves away from the source.

It is our purpose here to present an alternative ray technique for computing the displacement response of a plate excited by a point source which has short time duration. The technique utilizes a geometric ray approach and incorporates the wave-front curvature transformations caused by mode conversions at the free surfaces of the plate. These transformations were apparently first developed by Chopra [4] for a layer problem but can be easily modified for the present case. The technique considers only the terms in the wavefront expansion which vary inversely with the distance from the source and hence is a far-field approximation.

The key to developing the wave-front curvature transformations is recognizing that for small deviations of the incident angle, the reflected mode converted rays will converge locally. This allows a simple computation of the curvature of the wavefront in the plane of reflection. The curvature of the wavefront normal to the plane of reflection does change. Knowing the radii of curvature of the wavefront allows the calculation of the amplitude within a tube of small solid angle based upon the conservation of energy. Plane wave reflection theory is used to compute the energy partition after reflection.

The approach allows the computation of the amplitude of a disturbance along particular ray path without the evaluation of the integrals encountered in the generalized ray theory. The displacement at a particular observation point

is determined by tracing all of the rays connecting the source to that point. Although the number of rays is relatively small and can be determined in other ways for the cases we are now considering, anticipation of more complex situations led us to incorporate a Monte Carlo technique for determining the ray paths. This approach has been used for wave propagation in fluids [5] but must be modified to account for the mode conversion encountered in solids. The modification consists of using a Russian roulette approach to selecting which of the reflected rays to follow.

Numerical results are being computed for the cases of a center of dilation buried within the plate and a single force applied at the surface of the plate. The computations are being compared to solutions generated by Pao [1,3] for the same geometry and loads.

#### References

- [1] Pao, Y-H, Gajewski, R.R., and Ceranoglu, A.N., "Acoustic Emission and Transient Waves in an Elastic Plate," Jour. Acous. Soc. Amer., Vol. 65, No. 1, 1979, pp. 96-105.
- [2] Pao, Y-H and Gajewski, R.R., "The Generalized Ray Theory and Transient Responses of Layered Elastic Solids," Physical Acoustics, Vol. 13, 1977, pp. 183-265.
- [3] Pao, Y-H, "Theory of Acoustic Emission," Elastic Waves and Nondestructive Testing, ASME, New York, 1978, pp. 107-128.
- [4] Chopra, S.D., "On the Equivalence of Saddle Point Approximations and Ray Theory in Elastic Wave Problems," Geophysical Journal, Royal Astronomical Society, Vol. 1, 1958, pp. 164-179.
- [5] Haviland, J.K. and Thanedar, B.D., "Monte Carlo Application to Acoustical Field Solutions," Jour. Acous. Soc. Amer., Vol. 54, No. 6, 1973, pp. 1442-1448.

THE EFFECT OF POISSON'S RATIO ON DILATATIONAL WAVE  
DISPERSION AND ATTENUATION IN POROUS ELASTIC SOLIDS

by

M. C. Junger  
Cambridge Acoustical Associates, Inc.  
54 Rindge Avenue Extension  
Cambridge, Massachusetts 02140

The reactance of the spherically symmetric mode of a cavity in an elastic medium is stiffness-controlled at all frequencies [1] if the Poisson's ratio  $\nu < 1/3$ . As  $\nu$  rises from  $1/3$  to  $1/2$ , the "breathing mode" natural frequency where this reactance changes sign drops from infinity to zero. If the cavity population in a porous solid is sparse, thereby making acoustic coupling unimportant, the single-cavity results can be incorporated in a long-wavelength elementary, physically suggestive mathematical model which predicts results substantially consistent with more rigorous analyses of porous solids [2].

In the elementary model, the solid matrix compressibility is, in electric-circuit parlance, in parallel with the cavity breathing mode admittance. If  $\nu > 1/3$ , the dispersion curve displays a negative slope in the stiffness controlled range below cavity resonance. In a broad range extending from the breathing mode resonance to an anti-resonance where the amplitude of the mass-controlled cavity admittance has dropped down to the solid matrix compressibility, the real component of the bulk modulus of the porous medium is negative, thus effectively preventing wave propagation. This conclusion is borne out by the large attenuations in gas-bearing marine sediments [3,4] and swarms of gas bubbles in water [5], and by a similar phenomenon in rubber waveguides embodying cylindrical cavities parallel to the waveguide axis [6]. Above this "dead zone", attenuation drops to the modest level of materials for which  $\nu < 1/3$ . The latter situation which has been extensively studied, is characterized by a long-wavelength dispersion curve displaying a positive slope [7] and monotonically increasing attenuation resulting from scattering and losses.

References:

- [1] Blake, Jr., F.G., "Spherical Wave Propagation in Solid Media," J. Acoust. Soc. Am., 24, 1952, pp. 211-215.
- [2] Kligman, R.L., W.M. Madigosky, and J.R. Barlow, "Effective Dynamic Properties of Composite Viscoelastic Materials," J. Acoust. Soc. Am., 70, 1981, pp. 1437-1444.
- [3] Anderson, A.L., and L. D. Hampton, "Acoustics of Gas-Bearing Sediments", J. Acoust. Soc. Am., 62, 1980, pp. 1865-1903.

- [4] Wood, A.B. and D.E. Weston, "The Propagation of Sound in Mud," Acustica, 14, 1968, pp. 156-162.
- [5] Silberman, E., "Sound Velocity in Bubbly Mixtures Measured in Standing Wave Tubes," J. Acoust. Soc. Am., 29, 1957, pp. 925-933.
- [6] Vovk, A.E. and V.V. Tyumekin, "On 'Superviscous' Longitudinal Waves in an Elastic Medium," Sov. Phys. - Acoustics, 7, 1961, pp. 201-202.
- [7] Beltzer, A.I., "Kramers-Kronig Relationship and Wave Propagation in Composites," J. Acoust. Soc. Am., 73, 1983, pp. 355-356.

Propagation and Scattering of Elastic Waves in  
Discrete Random Media

by

Vijay K. Varadan<sup>1</sup>, Vasundara V. Varadan<sup>1</sup> and Y. Ma<sup>1</sup>  
Wave Propagation Group  
Department of Engineering Mechanics  
The Ohio State University  
Columbus, OH 43210

Statistical theories and multiple scattering of elastic waves have been important tools in determining the frequency dependent properties of materials containing a distribution of pores and/or inclusions. They have important practical applications in fiber reinforced composites, particulate composites, poroelastic media, etc. The dynamic behavior of such materials depends on the concentration, type, size and distribution of the pores and inclusions. Such materials behave effectively like lossy materials due to geometric dispersion as well as real losses, if any, associated with the scatterers. A study of wave propagation in these materials is a convenient way to experimentally and theoretically predict the phase velocity, coherent attenuation, effective dynamic properties such as elastic moduli, etc.

We use a multiple scattering theory and a statistical averaging procedure for the random positions of the pair-correlated scatterers. The response of a single scatterer is described by a T-matrix. The formulation is well suited for numerical computations for wavelengths comparable to scatterer size, dense volume concentrations, arbitrary shaped scatterers and a statistical distribution of sizes. Numerical results and comparison with experimental results will be presented for both 2-D and 3-D scatterers.

---

<sup>1</sup>Present address: Department of Engineering Science and Mechanics, The Pennsylvania State University, University Park, PA 16802

WAVES DUE TO A MOVING LINE IMPULSE ON THE  
SURFACE OF A RUNNING STREAM OF FINITE DEPTH

by

Biman Ghosh and K.S. Chaudhuri

Department of Mathematics  
Jadavpur University  
Calcutta-700032  
INDIA.

ABSTRACT

We consider waves created in a channel of uniform depth  $h$ , which is flowing with uniform velocity  $U$  in the positive  $x$ -direction. The origin and the  $x$ -axis are taken on the undisturbed horizontal free surface of the channel while the  $y$ -axis is drawn vertically upwards. A wave motion is set up by the action of an initial impulse strip on the surface. An expression of the wave integral for a stationary line impulse is first obtained. Assuming that the impulse strip moves without disintegration on the free surface, the expression of the wave integral for a moving line impulse is next derived. The wave integral is then evaluated asymptotically for large times and distances with the help of Stationary Phase Principle. Some physical aspects of the wave motion are described. In the non-critical state of the transient motion, there exists a travelling wave on the upstream or downstream side depending on the values of some parameters. It is also seen that the steady-state wave motion consists of standing waves both on the upstream and downstream sides. The steady-state does not exist in the critical case. Actually, the critical case corresponds to wave motions of large amplitude and hence it cannot be dealt with the theory of waves of small amplitude.

STRESS WAVE PROPAGATION IN A PIEZOELECTRIC  
WITH NONLINEAR DIELECTRIC RELAXATION

by

W. T. Brown  
Computational Physics & Mechanics II  
Division 1533  
Sandia National Laboratories  
Albuquerque, New Mexico 87185

This work examines the electrical and mechanical response of a piezoelectric solid exhibiting nonlinear dielectric relaxation effects. The conditions of the problem are specialized to a one-dimensional mode in which a cylindrical disc of the material is electroded and subjected to a uniform, time dependent loading on one of its planar surfaces. The resulting piezoelectric polarization produces an electrical signal in an external circuit. If the material also exhibits nonlinear dielectric relaxation effects, then the resulting electrical output can be highly distorted. Such material behavior can be described in terms of a generalization of the normal piezoelectric equations, viz.,

$$E = -hS - \frac{1}{2} h_S S^2 + \beta^U D + \beta_S S D$$

$$+ \frac{1}{\tau} \int_0^\tau (\beta^R - \beta^U) \exp \left[ -\frac{(t-t')}{\tau} \right] D(t') dt'$$

$$T = CS + \frac{1}{2} C_S S^2 - hD - \frac{1}{2} h_S S D$$

These equations, to second-order in the uniaxial strain  $S$  and electric displacement  $D$ , incorporate a simple description of dielectric relaxation. The first and second order piezoelectric constants are  $h$  and  $h_S$ , respectively. First and second order values of the impermeability (inverse of the permittivity) are represented by  $\beta^U$  and  $\beta_S$ , respectively; the superscript  $U$  indicates an unrelaxed value and  $R$  indicates

a relaxed value. Relaxation of the impermeittivity from a value  $\beta^U$  to  $\beta^R$  occurs with a relaxation time  $\tau$  and the magnitude  $(\beta^R - \beta^U)$  can be a time dependent function of the electric displacement  $D(t)$ .

Finite-difference forms of these equations have been incorporated into a one-dimensional wavecode (WONDY) which integrates the conservation equations associated with stress wave propagation. Parameters representative of x-cut alpha quartz have been used to solve these equations. Special cases are considered in which the relaxation process may add to or detract from the usual piezoelectric response.

Interaction of a Rayleigh Wave with an Inclined  
Edge Crack in a Half-Space

by

Bien Q. Vu  
Naval Ocean Systems Center, Code 9322  
San Diego, CA 92152

and  
Vikram K. Kinra  
Aerospace Engineering Dept., Texas A & M University  
College Station, TX 77843

The scattered field generated by the interaction of a Rayleigh wave with an edge crack is believed to yield useful information about the crack geometry. In the area of non-destructive Testing and Evaluation (NDTE), one of the techniques is to solve the inverse problem, namely, to determine the crack size and orientation from its scattered field. Therefore, knowledge of the scattered field due to a known crack is a necessary prerequisite. For the case of the edge crack normal to the free surface, the exact theoretical solution of the scattered field has been recently obtained by Mendelson et al. The experimental investigation of the interaction for the incident Rayleigh wave was reported in reference 2. For the case of the inclined crack, Datta<sup>3</sup> used the technique of matched asymptotic expansion to obtain an approximate solution of the scattered field due to the incident SH-waves. However, his solution was confined to the long-wavelength limit.

In this paper we report the experimental results of the interaction of an incident Rayleigh wave with the inclined edge crack. The scattered field was obtained by subtracting the incident field received with the uncracked specimen from the total field received with the cracked specimen. The near field scattered field of one crack length, namely,  $z/\lambda_R = 0.61$  at two complementary inclinations, namely,  $66^\circ$  and  $114^\circ$ , was measured along the free surface. The results showed that the near field possesses a large number of peculiar features which can be used in the area of NDTE to distinguish between the inclined crack and the normal crack. The far field transmission and reflection coefficients  $A_T$  and  $A_R$  were obtained for three regimes of crack length, namely, crack length is small, equal and large compared to the wavelength. Measurements were performed for cracks at six inclinations, namely,  $23^\circ$ ,  $45^\circ$ ,  $66^\circ$ ,  $114^\circ$ ,  $135^\circ$  and  $157^\circ$ . In the short wavelength limit,  $A_R$  reaches asymptotically the reflection coefficient of an infinite corner wedge and was shown to agree very well with the early results of Viktorov<sup>4</sup> on the wedge. Over the whole range of crack lengths tested,  $A_T$  varies in an oscillating behavior with crack length; this is due to the resonance between the crack tip and the free surface. The uniform spacing of peaks and valleys of  $A_T$  was found to be  $2z/\lambda_R = 1$ . Furthermore,  $A_T$  was seen to be measurably identical for any two complementary cracks, namely of  $\theta$  and  $(\pi - \theta)$  inclinations. The scattering cross-

section,  $\gamma_N = 1 - A_T^2 - A_R^2$  was also plotted versus  $\theta$  for three crack lengths,  $l/\lambda_R = 0.5, 1.0,$  and infinity. For  $l/\lambda_R = 0.5$ ,  $\gamma_N$  was seen to be almost symmetric with respect to  $\theta = \pi/2$ . For any two complementary cracks,  $\gamma_N$  was found to be larger for the obtuse angled crack than for the acute angled crack.

References:

1. Mendelson, D. A., Achenbach, J. D., and Keer, L. M., "Scattering of Elastic Waves by a Surface-Breaking Crack", Wave Motion, 2, 1980, pp. 277-292.
2. Vu, B. O., and Kinra, V. K., "Diffraction of Rayleigh Waves in a Half-Space", CUMER Report, Department of Mechanical Engineering, University of Colorado, Boulder, CO 80309 (CUMER-81-7), August, 1981.
3. Datta, S. K., "Diffraction of SH-Waves by an Edge Crack". ASME J. of Appl. Mech., 46, 1979, pp. 101-106.
4. Viktorov, I. A., "Rayleigh Waves and Lamb Waves-Physical Theory and Application", Plenum Press, New York, 1967.

Abstract

The Signaling Problem For The Nonlinear  
Telegraph Equation

By E. Varley

Center for the Application of Mathematics  
Lehigh University  
Bethlehem, PA

In this lecture we describe a mathematical procedure that can be used to transform a certain nonlinear hyperbolic equation, that occurs naturally in the study of waves in highly nonlinear, hysteretic, materials, into the linear telegraph equation. This result is used to solve the signaling problem for the nonlinear equation. In particular, an exact representation is found describing the deformation that is produced by the passage of a large amplitude centered wave in a visco-elastic material. Such waves are produced during impact.

Abstract

## Exact Description of Waves in Stratified Materials

By B. R. Seymour

Department of Mathematics

University of British Columbia

Vancouver, British Columbia

In general it is only possible to obtain a detailed description of how waves propagate in a stratified (inhomogeneous) material in the high frequency, or short pulse width, limit when the stratification is varying slowly on a scale defined by wavelength. In this limit the expansion techniques of geometrical acoustics are applicable. When the stratification is not varying slowly, even an analysis of how low intensity waves propagate is extremely complex.

In this lecture it is shown that when the stratification can be curve-fitted by one of a *very general* class of laws, a simple representation can be found for any low intensity disturbance in the material. This representation is used to analyze the propagation of a stress pulse in a slab of elastic material whose impedance varies at an arbitrary rate with distance in the direction of pulse propagation. The representations that are obtained are exact.

A Nonlinear Evolution Equation Following Two Coalesced Waves.  
C.H. Su, Div. of Applied Mathematics, Brown University, Providence,  
R.I. 02912.

Abstract

Recently there is much interest in nonlinear partial differential equations of the dispersive type. This was largely stimulated by the successful solution of the Korteweg-deVries equation, which represents a class of weakly nonlinear, dispersive waves. The infinitesimal waves of this class are non-dispersive. Assuming that there is no degeneracy in wave speeds of these waves, one can select a frame of reference moving with one of these waves. The slow evolution of the wave field observed in such a frame, due to nonlinearities and dispersion is to be governed by the K-dV equation. We consider a situation where there are two linear waves having almost the same wave speed. This occurs in a two-layer fluid system which has the same thickness for both layers and the density of the bottom layer is much larger than the top one. We choose a frame of reference moving with these two waves and observe the long time evolution of these waves due to the nonlinear and dispersive effects. The resulting evolution equation is a system of two equations of the K-dV type. We study both analytically and numerically various types of solitary waves of this system. We shall also show that periodic as well as quasi-periodic waves also exist. Finally we shall present results on the interactions (collisions) of solitary waves of this system.

PLANE WAVES IN SIMPLE ELASTIC SOLIDS AND DISCONTINUOUS  
DEPENDENCE OF SOLUTION ON BOUNDARY CONDITIONS\*

Yongchi Li\* and T. C. T. Ting  
Department of Civil Engineering, Mechanics and Metallurgy  
University of Illinois at Chicago  
Box 4348, Chicago, Illinois 60680

Using stress as the dependent variable instead of the deformation gradient, plane waves of finite amplitude in simple elastic solids are studied. For isotropic materials there are two plane polarized simple waves as well as shock waves and one circularly polarized simple wave which can also be regarded as a shock wave. With the aid of the stress paths for simple waves and shock waves in the stress space introduced here, one can see clearly what combination of simple waves and/or shock waves is needed to satisfy the initial and boundary conditions. We use second order isotropic hyperelastic materials to illustrate the ideas. In one example we show that the solution requires as many as four simple waves. In another we show that depending on the boundary condition there are more than eight possible solutions to the problem. We also present an example in which the solution does not depend continuously on the boundary condition. This implies that in experiments if the applied load at the boundary is not properly controlled, any slight deviation in the applied load would result in a finite different response in the material.

---

\*To appear in Int. J. Solids Structures. This work is supported by the U. S. Army Research Office, through Grant DAAG 29-80-C-0093.

\*On leave (1981-83) from Department of Modern Mechanics, University of Science and Technology of China, Hefei, Anhui, The People's Republic of China.

Fully Nonlinear Waves in Vortices

by  
S. Leibovich  
Sibley School of Mechanical & Aerospace  
Engineering  
Cornell University  
Ithaca, N. Y. 14853  
and  
K. Stewartson  
Department of Mathematics  
University College, London

Abstract

Experimental evidence suggests the existence of large amplitude structures in vortices. To some extent, linear and weakly nonlinear wave theories describe features that are observed. The degree of success realized by the perturbation theories suggests that wave propagation of finite amplitude may be possible. In this paper, a class of special solutions representing axially symmetric, fully nonlinear, simple waves will be described. The waves have a modal structure determined by a two point boundary value problem singular at both ends, and wave breaking is typical.

NONLINEAR WAVES IN A ROD: EXACT RESULTS FOR  
INCOMPRESSIBLE MATERIALS

by T. W. Wright  
Ballistic Research Laboratory  
APG, MD 21005

A rod may be represented intrinsically as a stretching line endowed with structure. In the most elementary version of this idea one scalar internal variable can be used to simulate the effects of finite transverse dimensions in a straight cylindrical rod that undergoes only axisymmetric motions.

In a previous paper [1] some of the consequences of the theory were worked out for a material with strain energy that depends on axial strain, radial strain, and gradient of radial strain,  $W(\frac{\partial w}{\partial z}, u, \frac{\partial u}{\partial z})$ . In the terms of general continuum mechanics this is the energy density of any one-dimensional elastic continuum with one scalar, internal variable.

In the present paper, the restriction of incompressibility is added. The strain energy may now be written as  $\hat{W}(\frac{\partial w}{\partial z}, \frac{\partial u}{\partial z})$ . Hamilton's principle with a side constraint for incompressibility yields two coupled equations, one for axial motion and one for radial motion. These equations contain a Lagrange multiplier, which may be interpreted as a superimposed hydrostatic pressure.

Consideration of steady wave motions reduces the partial differential equations to ordinary differential equations for which two integrals of the motion may be found. Under the further restriction of small strain gradients, but arbitrary finite strains, a large variety of exact solutions exist. These include large amplitude periodic waves (which may contain shocks), solitary waves, and in some cases structured shock waves. Such solutions may be found for stress/strain curves that are concave up or down, that contain inflections, or what is even more remarkable, curves that represent phase changes.

[1] T. W. Wright, Nonlinear Waves in Rods, Proc. IUTAM Symp. on Finite Elasticity, Nijhoff Publ. The Hague 1981.

ELASTODYNAMIC BOUNDARY INTEGRAL  
EQUATION SOLUTIONS TO THE HALF SPACE PROBLEM  
USING A TIME DEPENDENT GREEN'S FUNCTION: SH-WAVES

by

J. M. Rice and M. H. Sadd  
Mechanical Engineering and Applied Mechanics  
University of Rhode Island  
Kingston, R.I. 02881

The Boundary Integral Equation (B.I.E.) Method is applied to the integral representation of the Navier equations of motion for linear elastodynamics. The geometry of the problem presented is the half space with arbitrary and multiple cavities. Possible boundary conditions on the problem are a stress free bounding surface and arbitrary tractions and/or displacements over the cavity surfaces.

Previous work in this area by Cole [1] has had success with the B.I.E. method for elastodynamics using an infinite-space, time-dependent Green's function. Other relevant work includes Telles and Brebbia [2] in which a half space Green's function was successfully employed for half space static elasticity problems. The present work has combined these two ideas to employ a half-space, time-dependent Green's function technique.

The research was conducted by numerically solving the following integral representation of the Navier equation of motion (Wheeler and Sternberg [3]).

$$\underline{u}(r, t) = \int_{t_0}^{\infty} \int_{\partial B} \underline{G} \cdot \underline{\tau}(r_0, t_0) - \underline{u}(r_0, t_0) \cdot \underline{K} \cdot \underline{n} \, dS_0 dt,$$

where  $\underline{G}$  is the half-space Green's function,  $\underline{K}$  is the stress field associated with  $\underline{G}$ ,  $\underline{\tau}$  and  $\underline{u}$  are the surface tractions and displacements on the boundary,  $r_0$  and  $t_0$  are the space and time positions of the source, and  $\underline{n}$  is the unit normal vector to the surface.

Results will be presented for the SH-wave case, and numerical data will be shown for several problem types.

#### References

- [1] Cole, D. M. (1980) "A Numerical Boundary Integral Equation Method for Transient Motions". Thesis, California Institute of Technology, Pasadena, California.
- [2] Telles, J. C. F. and Brebbia, C. A. (1981) "Boundary Element Solution for Half-Plane Problems", Int. J. Solids Str., Vol. 17, No. 12, pp. 1149-1158.
- [3] Wheeler, L. T. and Sternberg, E. (1968) "Some Theorems in Classical Elastodynamics", Arch. Rat. Mech. Anal., Vol. 31, pp. 51-90.

## AUTHOR INDEX

- Aaronson, H. I., 274-275  
 Aboudi, J., 39  
 Adler, M., 17  
 Aggarwala, B. D., 233  
 Ahmadi, N., 135  
 Ali, M. M., 95-96  
 Al-Khadhra, O. H., 97-98  
 Al-Tayyib, A. J., 97-98  
 Ariel, P. D., 233  
 Asano, N., 140, 264  
 Asay, J. R., 176  
 Atluri, S. N., 254  
 Aung, W., 223-224  
 Azad, A. K., 97-98  
 Bahar, L. Y., 74  
 Baker, A. J., 110-111, 255  
 Baluch, M. H., 97-98  
 Bapat, C., 126-127  
 Barber, J. R., 136  
 Batra, R. C., 126-127  
 Bau, H. H., 216  
 Beatty, M. F., 77  
 Beltzer, A. I., 315  
 Bert, C. W., 44-45, 315  
 Bertazzoli, R., 9-10  
 Blythe, P. A., 214-215  
 Bodner, S. R., 183  
 Bowen, R. M., 217  
 Brahma, C. S., 174-175  
 Brenner, H., 17  
 Brock, L. M., 133-134  
 Brody, H. D., 5  
 Brown, R. L., 158  
 Brown, W. T., 322-323  
 Burch, J. N., 221-222  
 Burns, T. J., 294  
 Bussolari, S. R., 29-30  
 Canova, G. R., 291  
 Catton, I., 204-205  
 Cavendish, J. C., 244  
 Chan, C., 6-7  
 Chan, S. W., 166-167  
 Chaney, R. C., 156-157, 206-207  
 Chang, F.-K., 136  
 Chang, L. P., 260-261  
 Chang, T., 270-271  
 Chaturvedi, S. K., 63  
 Chaudhuri, K. S., 321  
 Chavez, P. F., 262-263  
 Chen, J. L. S., 231-232  
 Chen, M. M., 6-7  
 Chen, T. S., 218-219  
 Chen, W. F., 166-167  
 Chen, Y., 90  
 Cheng, H. S., 143, 148  
 Cheng, P., 210-211  
 Chiang, C. R., 42  
 Chidambarrso, D., 99-100  
 Chou, T.-W., 35-36  
 Chun, Y. W., 235  
 Clifton, R. J., 181-182  
 Comninou, M., 136  
 Cupini, N. L., 12-13  
 Dandu, M. R., 70-71  
 Delale, F., 50  
 DeOliveira, J. G., 288-289  
 Dhir, V. K., 212  
 Dobran, F., 308  
 Doraivelu, S. M., 192-193  
 Douglas, A. S., 187-188

- Drysdale., W. H., 282-283  
Duffy, J., 177  
Dundurs, J., 124, 137  
Dung, N. L., 18  
Dunn, J. C., 198-199  
Dunn, J. E., 106  
Dybbs, A., 202-203  
Eckert, E. R. G., 196-197  
Edwards, R. V., 202-203  
Egle, D. M., 316-317  
Elber, W., 57  
Epstein, J. S., 61  
Evans, B., 168  
Evans, J. C., 156-157  
Ewumi, J., 316-317  
Fabrikant, V. I., 128  
Failmezger, R. A., 156-157  
Fang, H. Y., 156-157, 206-207  
Farouk, B., 229-230  
Fosdick, R. L., 84  
Freudenstein, F., 64-65  
Fu, L., 309-310  
Gandhi, M., 83  
Garcia, A., 9-10  
Gause, L. W., 53-54  
Gautesen, A. K., 124, 137  
Ghoneim, H., 90  
Ghonem, H., 296-297  
Ghosh, B., 321  
Gidaspow, D., 299-300  
Gillis, P. P., 284  
Gilpin, R. R., 11  
Giron, A., 117-119  
Glockner, P. G., 101-102  
Golden, J. M., 123  
Goodman, L. E., 139  
Googerdy, A., 241  
Gopinathan, V., 192-193  
Gordaninejad, F., 44-45  
Graham, G. A. C., 123  
Good, E. S., 19-20  
Gunzberger, M. D., 243  
Hall, I., 195  
Hamilton, G. M., 139  
Hamrock, B. J., 141-142  
Harding, J., 178-179  
Hayes, D. B., 190  
Hefzy, M. S., 19-20  
Hendricks, R. C., 227-228  
Hetnarski, R. B., 47  
Hikami, F., 35-36  
Ho, C. T., 8  
Hoenig, A., 129-130  
Horii, H., 169-170  
Horvay, G., 295  
Hsaio, G. C., 250  
Hsu, C.-T. T., 91-92, 99-100  
Hu, L. W., 75-76  
Huffington, N. J. Jr., 191  
Hui, D., 93-94, 286-287, 288-289  
Inman, D. J., 78  
Ishii, M., 314  
Ishikawa, H., 40-41, 48-49  
Iwakuma, T., 292  
Jenkins, J. T., 159  
Johnson, B., 28  
Johnson, R. E., 151-152  
Jonas, J. J., 291  
Jones, O. C. Jr., 305-307  
Jones, S. E., 284  
Joseph, D. D., 108  
Joseph, K. P., 31-32  
Jungfer, M. C., 318-319  
Kakac, S., 309-310, 311  
Kamegaya, H., 264  
Kandadai, R. D., 19-20

- Kataoka, I., 314  
Kaufman, H. N., 114-116, 117-119  
Kaufman, R. E., 70-71  
Kaviany, M., 213  
Kawata, K., 180  
Kearsley, E. A., 107  
Keer, L. M., 135, 148  
Kennedy, K. J., 225-226  
Kerr, A. D., 88-89  
Kiddy, K. C., 285  
Kikuchi, N., 268-269  
Kimura, H., 40-41  
Kincaid, D. R., 267  
Kinra, V. K., 55, 324-325  
Kipp, M. E., 190  
Kocamustafaogullari, G., 314  
Kocks, U. F., 291  
Koert, D. N., 229-230  
Koh, S. L., 166-167  
Koppula, S. D., 236-237  
Krausz, A. S., 14, 131  
Krausz, K., 14, 131  
Krishnamurthy, L., 247-248  
Krishnamurthy, R., 15-16  
Kulacki, F. A., 200-201  
Kumar, K., 132  
Kumar, S., 293  
Kuo, A. Y., 125  
Kwatny, H. G., 74  
Labbe, F., 114, 116  
Lakhanpal, S. K., 81-82  
Lambert, A., 28  
Lebowitz, J. L., 277-278  
Lee, C.-C., 1-2  
Lee, T. W., 68-69  
Leibovich, S., 330  
Levinson, M., 86-87  
Li, V. C., 153  
Li, Y., 329  
Liu, M. C., 99-100  
Llorens, R. E., 53-54  
Lindholm, U. S., 183  
Lukasiewicz, S., 101-102  
Lyczkowski, R. W., 303  
Ma, Y., 320  
MacSithigh, G. P., 84  
Maeder, P. F., 304  
Mahrenholtz, O., 18  
Malvern, L. E., 184-185  
Mazumder, J., 6-7  
McMeeking, R. M., 151-152  
McLaughlin, P. V. Jr., 58-59  
McTigue, D. F., 109, 161  
Melosh, H. J., 160  
Mentes, A., 309-310  
Mikata, Y., 85  
Miller, G. R., 148  
Mirchandani, M. G., 58-59  
Montor, K., 28  
Moss, G. L., 189  
Müller, I., 279  
Muller, M. R., 221-222  
Mura, T., 135  
Natarajan, R., 15-16  
Nemat-Nasser, S., 169-170, 292  
Nicholas, T., 186  
Nicholson, D. W., 285  
Nomura, S., 37-38  
Noor, A. K., 257-258  
Nunziato, J. W., 190  
Oden, J. T., 259  
Olaosebikan, O., 61  
Orabi, I., 78  
Oreper, G. M., 3-4  
Owen, W. S., 276  
Pan, X. C., 75-76

- Passman, S. L., 161  
Patterson, W. G., 56  
Paul, B., 66, 138  
Peddieson, J. Jr., 241  
Peterson, J. S., 249  
Petroski, H. J., 293  
Pipes, R. B., 60  
Podowski, M., 234  
Porsching, T. A., 242  
Prasad, V., 200-201  
Prevost, J. H., 171  
Pritchard, D. S., 194, 195  
Rajagopal, K. R., 83, 106, 251  
Ramanjaneya, G., 206-207  
Ramos, J. I., 308  
Rao, K. P., 192-193  
Ray, H., 43  
Reed, K. W., 254  
Rice, J. M., 332  
Rinaldo, J. M., 29-30  
Rivlin, R. S., 103-105  
Robert, M. H., 12-13  
Roco, M. C., 301-302  
Ruina, A., 150  
Sadd, M. H., 332  
Sadegh, A. M., 251  
Sadeh, W. Z., 112-113  
Saharon, D. B., 112-113  
Samaría, N. K., 239-240  
Sankar, B. V., 51-52  
Sankar, T. S., 128  
Sasaki, Y. K., 260-261  
Schneider, S. J., 114-116, 117-119  
Schor, A. L., 245-246  
Schultz, A. B., 21  
Seering, W. P., 67  
Seymour, B. R., 327  
Snahinpoor, M., 164-165, 172-173  
Shakespeare, W. J., 225-226  
Shanebrook, J. R., 29-30  
Shapira, Y., 272-273  
Sharma, M. G., 23-24  
Shen, H. H., 159, 162-163  
Shin, T.-S., 305-307  
Shrivastava, S. C., 298  
Shukla, A., 132  
Sigíner, A., 121-122, 252-253,  
312-313  
Simpkins, P. G., 214-215  
Singh, B., 11  
Singh, J. G., 154-155  
Singh, M., 31-32  
Singh, S., 138  
Singh, V. P., 239-240  
Smith, C. W., 61  
Somerton, C., 204-205  
Spanos, P. D., 73  
Speziale, C. G., 120  
Stewart, W. E. Jr., 208-209  
Stewartson, K., 330  
Stoehr, R. A., 5  
Stout, M. G., 280  
Striz, G., 315  
Su, C. H., 328  
Sullivan, P. P., 112-113  
Sun, C. T., 51-52, 63  
Szekely, J., 3-4  
Szeri, A. Z., 114-116, 117-119  
Tanimoto, T., 40-41, 48-49  
Taya, M., 56, 85, 195  
Ting, T. C. T., 329  
Todreas, N. E., 245-246  
Tomé, C., 291  
Torzilli, P. A., 25  
Triantafyllidis, N., 281  
Tucker, C. L. III, 1-2

Upadhyay, P. C., 154-155, 239-240  
Updike, D. P., 46  
Vaishnav, M. P., 26-27  
Vaishnav, R. N., 26-27  
Varadan, V. K., 320  
Varadan, V. V., 320  
Varley, E., 326  
Veluswami, M. A., 295  
Veziroglu, T. N., 309-310  
Vinson, J. R., 62  
Vossoughi, J., 26-27  
Vu, B. Q., 324-325  
Walsh, J. B., 149  
Walters, R. A., 265-266  
Waltz, T. L., 62  
Wang, A. S. D., 33  
Wang, S. S., 34, 125  
Wedeven, L. D., 146-147  
Weng, C. I., 8  
Weng, G. J., 42, 290  
Westerling, C., 18  
Wierzbicki, T., 286-287  
Wineman, A. S., 83  
Winer, W. O., 144-145  
Wisniewski, H. L., 191  
Wong, Y. H., 298  
Worku, G., 223-224  
Wright, T. M., 22  
Wright, T. W., 331  
Wu, C., 238  
Xirouchakis, P. C., 93-94  
Xistris, G. D., 128  
Yamazaki, K., 268-269  
Yang, C.-T., 254  
Yang, C. Y., 79-80  
Yao, L. S., 220  
Yildirim, O. T., 309-310  
Yoon, H. S., 195  
Yost, B. A., 60  
Young, M. I., 72  
Yuceoglu, U., 46  
Zak, E., 295  
Zhou, G. Q., 90

ATE  
MED  
8